

CYCLOTRON RADIATION FROM ELECTRON STREAMS GYRATING
IN THE JOVIAN MAGNETOSPHERE, THE TERRESTRIAL
EXOSPHERE AND THE SOLAR ACTIVE CORONA

by

Peter Chin Wan Fung, B.Sc. (Hons.)

A thesis submitted in fulfillment of
the requirements for the Degree of
Doctor of Philosophy
in the
University of Tasmania

HOBART

April, 1966

CONTENTS

| Chapter | | Page |
|---------|---|------|
| I | INTRODUCTION | 1 |
| | (A) Plasma | 1 |
| | (B) The Dispersion Equation | 3 |
| | (C) The Basic Equations of the Kinetic Approach | 4 |
| | (D) Macroscopic Description of the Response of a Plasma to Electromagnetic Disturbance | 7 |
| | (E) Different Modes of Electromagnetic Disturbance in a Plasma | 8 |
| | (F) Identification of the Four Modes in the Graphical Presentation of the Dispersion Equation | 10 |
| | (G) Generation of High Frequency Waves in a Plasma | 13 |
| | (H) Emissions from the Sun and Planets | 20 |
| | (I) Two Common Features in the Observational Data of the Sun, Jupiter and Earth | 22 |
| II | EXCITATION OF ELECTROMAGNETIC WAVES IN A STREAM-PLASMA SYSTEM | 25 |

| | | |
|-----|---|----|
| (A) | Introduction | 25 |
| (B) | Formulation of Radiative Instability Theory in a Helical-Stream-Plasma System | 29 |
| (C) | Instability Theory of a Stream-Plasma- System when the Temperature Effects in the Stream have been Included | 39 |
| (D) | The "Negative-Absorption" Approach in Solving the Instability Problem | 54 |
| (E) | Two Types of Instability | 57 |
| (F) | Conclusions | 59 |
| III | AMPLIFICATION OF FORWARD-SHIFTED CYCLOTRON RADIATION IN THE EXTRAORDINARY-MODE AND ITS APPLICATION TO JUPITER'S DECAHETRIC EMISSIONS | 61 |
| (A) | Introduction | 61 |
| (B) | Theory and Analysis | 63 |
| (C) | Discussions | 68 |
| IV | THE ORIGIN OF VLF DISCRETE EMISSIONS IN THE TERRESTRIAL EXOSPHERE | 84 |
| (A) | Review | 84 |
| (B) | Excitation of Backward Doppler-shifted Cyclotron Radiation in a Magnetoactive Plasma by a Helical Electron Stream ... | 87 |
| (C) | Discussions | 91 |

| | | |
|------|--|-----|
| V | A REVIEW OF THE PHENOMENUM OF SOLAR | |
| | TYPE I NOISE STORM | 110 |
| | (A) Solar Radio Emissions | 110 |
| | (B) Characteristics of Type I Noise Storms . | 111 |
| | (C) Existing Theories of Type I Noise | |
| | Storms | 131 |
| VI | MODEL OF THE SOLAR CORONA | 137 |
| | (A) Radial Distribution of Electron Density | |
| | in the Corona | 137 |
| | (B) Models of Spot-field Configurations ... | 140 |
| VII | COUPLING CONDITIONS IN THE SOLAR CORONA | 151 |
| | (A) Introduction | 151 |
| | (B) Transformation of Plasma Waves to Radio | |
| | Waves through Rayleigh Scattering and | |
| | Combination Scattering | 152 |
| | (C) Coupling of Characteristic Waves in the | |
| | Solar Corona | 154 |
| VIII | CYCLOTRON RADIATION FROM ELECTRON STREAMS | |
| | GYRATING IN SPOT-FIELD CONFIGURATIONS | 167 |
| | (A) Emitted Frequency Range from Electrons . | 167 |
| | (B) Power Spectrum of a Single Electron ... | 173 |
| | (C) Amplification of Electromagnetic Waves | |
| | in a Stream-Plasma System | 186 |
| | (D) Resonance Absorption at the First Three | |
| | Harmonies | 203 |

| | | |
|------------|--|-----|
| | (E) Reflection Levels and Escape Conditions for the Two Characteristic Waves | 212 |
| | (F) Predictions of the Theory | 227 |
| IX | THEORETICAL DYNAMIC SPECTRA OF STORM BURSTS | |
| | (A) Ray Tracing in the Corona | 233 |
| | (B) Theoretical Dynamic Spectra of Storm Bursts | 239 |
| X | CONCLUDING REMARKS ON THE INTERPRETATION OF SOLAR TYPE I NOISE STORMS | 249 |
| XI | CONCLUSIONS | 260 |
| | (A) General Concluding Remarks | 260 |
| | (B) Suggestions for Further Research | 263 |
| Appendix A | DERIVATION OF THE VLASOV EQUATION | 265 |
| Appendix B | THE TRANSPORT EQUATIONS IN THE MACROSCOPIC APPROACH OF DESCRIBING WAVE PROPAGATION IN A PLASMA | 272 |
| Appendix C | DISPERSION EQUATION OF PLANE WAVES PROPAGATING IN A WARM, COLLISIONLESS, MAGNETOACTIVE PLASMA | 274 |
| Appendix D | TWO METHODS OF SOLVING THE RADIATIVE INSTABILITY PROBLEM OF A STREAM-PLASMA SYSTEM WITHIN THE KINETIC REGIME | 277 |

| | | |
|-------------------------|-------|-----|
| Acknowledgements | | 283 |
| Publication | | 284 |
| References | | 286 |
| Symbols | | 296 |

CHAPTER I

INTRODUCTION

All identified radio sources, except for line emissions, are regions of plasma, and the study of radio astronomy is, therefore, inherently linked up with the study of behaviour of waves in a plasma. In this chapter, we will thus firstly outline some basic concepts concerning the description of a plasma and its response to electromagnetic disturbances (sections (A) to (G)). An introduction to the problems attacked in this thesis is then given in sections (H) and (I). Gaussian units will be used in this thesis.

(A) Plasma (Smerd, 1965)

A plasma is a gas which is macroscopically neutral and microscopically ionized. When a static external magnetic field is present, the plasma is said to be magnetoactive. The behaviour of a plasma is controlled mainly by the electrostatic forces between its constituent charged particles. The effect of the electric field on the behaviour of a plasma differs in a qualitative manner at distances and wavelengths which are larger or smaller than the "radius", called the Debye length of the space charge around the positive ions. This length is

$$D = (\kappa T / 4 \pi N e^2)^{1/2}$$

where $k =$ Boltzman's constant.

$T =$ kinetic temperature.

$N =$ particle density of electron.

$e =$ charge of an electron.

For distances and wavelengths $\lambda < D$, the electrostatic force of individual ions dominates while for $\lambda > D$, the electrostatic force is the cumulative long-range effect due to many ions, and this gives the plasma its macroscopic properties, i.e. coherent motions of electrons and the corresponding wave-particle interactions which allow energy exchange between particles and waves in the plasma. When the plasma is magnetoactive, the situation is complicated by the presence of the $\vec{v} \times \vec{H}_0$ term ($\vec{v} =$ velocity of charged particle and $\vec{H}_0 =$ magnetic intensity of the static magnetic field) of the Lorentz force. If \vec{H}_0 is large and the temperature of the charged particles not too high, the predominant macroscopic motion of the particles will ^{be} the helical motion along the static magnetic field.

For radio frequencies, we specify a plasma macroscopically by several basic quantities: its particle density N , kinetic temperature T , and external magnetic field intensity \vec{H}_0 (if it exists). The following quantities which are expressed in terms of the mentioned basic ones are normally employed in the study of a plasma:

electron plasma frequency $f_p = \omega_p / 2\pi = (Ne^2 / m_0 \pi)^{1/2}$, where m_0 = rest mass of electron.

electron gyro-frequency $f = \omega_H / 2\pi = eH_0 / (2\pi m_0 c)$,

where c = speed of light in vacuum.

electron-ion collision frequency

$$\nu = \frac{Z^2 e^4}{3} \left[\frac{8\pi}{m_0 (\chi T)^3} \right]^{1/2} N_i \left[\ln \frac{8(\chi T)^3}{m_0 (\pi Z e^2 f)^2} - 5 \gamma \right]$$

where Z = degree of ionization, f = wave frequency,

$\gamma = 0.577 \dots$ is Euler's constant, and N_i = particle density of ions.

root mean square value of the thermal velocity of electrons

$$v_{th} = (3 \chi T / m_0)^{1/2}$$

(B) The Dispersion Equation

Wave of angular frequency $\tilde{\omega}$ propagation in z in the z direction in a plasma are normally assumed to take the form of monochromatic plane waves, the electrostatic field E of which being specified by

$$E = E_0 e^{i(\tilde{k}z - \tilde{\omega}t)} e^{(-\delta z + \delta t)} \quad (1.1)$$

where $\tilde{k} = 2\pi / \lambda = \frac{\tilde{\omega} n_j}{c}$ is the real part of wave number

λ = wavelength

n_j = refractive index (real part)

and q, δ are the imaginary parts of the complex quantities

k, ω respectively (i.e. $k = \tilde{k} + iq, \quad \omega = \tilde{\omega} + i\delta$).

The phase velocity, group velocity for plane waves described by (1.1) are $v_{ph} = \tilde{\omega}/\tilde{k}, \quad v_g = d\omega/dk$ respectively.

To study the propagation of plane waves in a plasma, generally two approaches are taken to arrive at an equation, called the dispersion equation, relating ω and k * :

- (i) The kinetic or microscopic approach.
- (ii) The transport or macroscopic approach.

We will discuss the derivation of the dispersion equation by these two approaches in sections (C) and (D); in particular, the kinetic approach is considered in more detail.

(C) The Basic Equations of the Kinetic Approach

The propagation of a wave in a plasma may be regarded as a perturbation on the parameters specifying the plasma by the passage of the wave. The electromagnetic field associated with the wave is due to current and space charge which themselves represent the response of the plasma to the wave field. Hence, the derivation of the physically

*The dispersion equation may take either the form $\omega = \omega(k)$ or $k = k(\omega)$.

existing wave modes in a plasma is a self-consistent electromagnetic field problem.

The response of an ensemble of particles of different species j , mass m_j , charge e_j , radius vector \vec{r} and velocity \vec{v} to an external force \vec{F} can be described in a kinetic approach by the Boltzman equation:

$$\frac{\partial f_j}{\partial t} + \vec{v} \cdot \frac{\partial f_j}{\partial \vec{r}} + \frac{\vec{F}}{m_j} \cdot \frac{\partial f_j}{\partial \vec{v}} = \left(\frac{df_j}{dt} \right)_{\text{collision}} \quad (1.2)$$

where f is the particle density in phase space. In our case the external force is

$$\vec{F} = e_j \left[\vec{E} + \frac{1}{c} \vec{v} \times (\vec{B}_0 + \vec{B}) \right] \quad (1.3)$$

where \vec{B}_0 is the static magnetic induction of the magnetoactive plasma. The electromagnetic wave field \vec{E} and \vec{B} is related to the macroscopic charge density ρ and current density \vec{j} through the well known Maxwell equations:

$$\begin{aligned} \nabla \times \vec{B} &= \frac{4\pi}{c} \vec{j} + \frac{1}{c} \frac{\partial \vec{E}}{\partial t} \\ \nabla \times \vec{E} &= - \frac{1}{c} \frac{\partial \vec{B}}{\partial t} \\ \nabla \cdot \vec{B} &= 0 \end{aligned} \quad (1.4)$$

$$\nabla \cdot \vec{E} = 4\pi\rho$$

while ρ and \vec{j} are given by

$$\begin{aligned} \rho &= \sum_j e_j \int f_j d\vec{v} \\ \vec{j} &= \sum_j e_j \int \vec{v} f_j d\vec{v} \end{aligned} \quad (1.5)$$

In most astrophysical problems the changes in the

distribution function due to collisions are much slower than those due to the wave electromagnetic field, and the term $(\frac{df}{dt})_{\text{collision}}$ is usually neglected in (1.2) in practice.

With the external force \vec{F} described by (1.3), the wave field satisfying the Maxwell equations, together with ρ and \vec{J} given by (1.5), the collision-free Boltzman equation is called the Vlasov equation. Vlasov pointed out that the Boltzman equation itself is an approximation to a many-body problem and one of the assumption taken in the derivation of the equation is that the interaction between particles consists only of binary interaction. This assumption clearly does not apply to the Coulomb force between many charged particles. A rigorous derivation of the Vlasov equation is reviewed in Appendix A.

When the wave disturbance in the plasma is small, the particle distribution function f can be written in the form

$$f = f_0 + f_p \quad (1.6)$$

where f_0 is the unperturbed distribution function and f_p is the perturbation term due to the presence of the wave. In this presentation if the effect of f_p on f_0 is small such that the perturbation theory is valid, the Vlasov equation (with f given by (1.6)) is said to be linearized. From the linearized Vlasov equation, the dispersion equation which

describes the behaviour of waves in a plasma can be derived. However, in a number of problems in astrophysics, the description of the plasma can be simplified further if the macroscopic approach is employed.

(D) Macroscopic Description of the Response of a Plasma to Electromagnetic Disturbance

The relevant macroscopic quantities describing a plasma are obtained as moments of the microscopic distribution functions. The plasma can then be treated as a fluid and the changes of states are specified by the hydrodynamic equations which can be obtained as successive moments of the first BBGKY equation (equation (A5); see Delcroix, chapter, 1963, for detail discussion). These hydrodynamic equations may be called transport equations and two transport equations together with the Maxwell equations are essential in the derivation of the dispersion equation. A brief discussion on two transport equations is given in Appendix B.

The macroscopic approach is used more often in practice to describe electromagnetic phenomena in a plasma because the mathematics involved is more simple. However, it must be pointed out that some phenomena are masked theoretically by this approach if the occurrences of such phenomena

depend on the microscopic distribution of the particle velocity. Two well known examples are the Landau damping and the cyclotron damping. Some discussions on these two damping mechanisms have been given by Ginzburg (1964) and Stix (1962) and the cyclotron damping process will be considered in more detail in the later part of this thesis.

(E) Different Modes of Electromagnetic Disturbance in a Plasma

A study of the dispersion equation indicates that, in general, there are four distinct modes of electromagnetic disturbance capable of propagating in a warm magnetoactive plasma (Astron, 1950; Piddington, 1955). Two of the four modes tend to be longitudinal or pressure waves and they arise only if the plasma is not at absolute zero temperature. The existence of these two modes depend partly on the occurrence of elastic forces due to compression of the plasma.

One of these longitudinal mode, called the ion mode or magnetic sound mode, appears when thermal motions of the heavy plasma particles, both ions and atoms, are included such that the whole plasma has a finite pressure. The plasma motion of the disturbance is the longitudinal type and the velocity of disturbance is of the order of the velocity of sound. When the propagation of the wave

is along the external static magnetic field, the wave is almost a pure sound wave, having an associated electric field only.

The second longitudinal mode, called the electron mode or p-mode, appears when electron thermal motion and electron gas pressure are taken into account. When the external static magnetic field exists and the electron pressure is finite, the electron wave or p wave becomes a travelling electromagnetic wave. If the p wave propagates along the static magnetic field, it becomes a pure electric wave and is quite independent of the other two transverse modes. The p wave changes its physical character from a pure longitudinal wave (refractive index $\gg 1$) to a transverse electromagnetic wave extraordinary mode, refractive index $\lesssim 1$) (Wild, Smerd and Weiss, p. 342, 1963).

The two transverse modes are termed the ordinary mode (o-mode) and extraordinary mode (x-mode). The polarization of the transverse waves is in general elliptical (Ratcliffe, 1959). The two ellipses correspond to the two modes are identical in shape, but with the major and minor axes interchanged and with opposite senses of rotation. When the o and x waves are propagating along the static magnetic field of a magnetoactive plasma, the waves are circularly polarized; the sense of the x-mode is the sense of rotation of an electron in the same

magnetic field. When the phase velocities propagate in directions transverse to the static magnetic field, the polarization of the two modes tend to be linear polarized.

At low frequencies where the motion of the ions is important, the phase velocities of the ion mode and the two transverse modes remain almost constant for change of plasma density (see Figure 1.1(a)) and the waves of these three modes are grouped together as hydromagnetic waves.

In the case of transverse waves the plasma acts as a dielectric medium and it changes the propagation constant or the refractive index only. For longitudinal waves the plasma takes part in the wave motion itself and the waves cannot exist outside the plasma. When the static magnetic field is absent, the ordinary and extraordinary modes are purely transverse electromagnetic waves while the electron and ion modes are purely longitudinal waves. An external static magnetic field provides coupling between transverse and longitudinal field vectors of the disturbances.

(F) Identification of the Four Modes in the Graphical Presentation of the Dispersion Equation

Using the linearized macroscopic treatment, Denisse and Delcroix (1963) derived the dispersion equation for plane waves in a warm collisionless magnetoactive plasma.

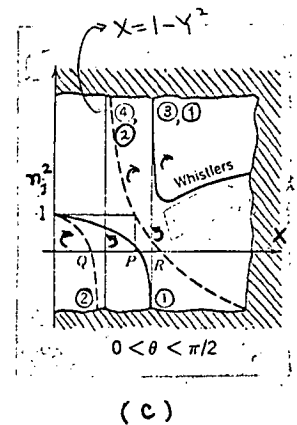
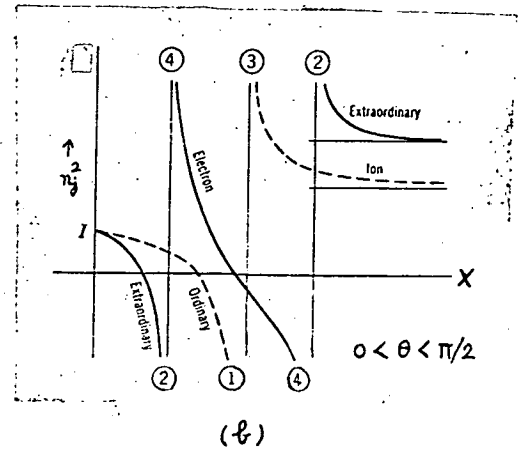
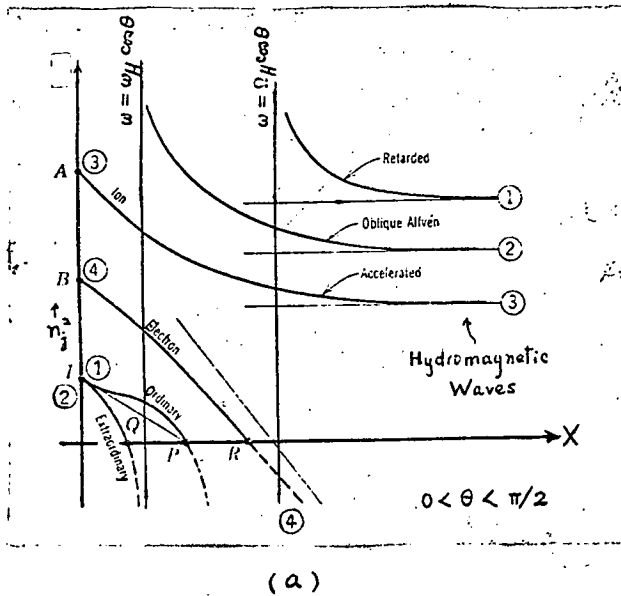


Fig.1.1 The four modes of propagation in a collisionless magnetoactive plasma when

- (a) the plasma is warm
- (b) the plasma is cold
- (c) the plasma is cold and the wave

frequency is high such that the effects of the ions' motion are negligible. In this case the Appleton-Hartree approximation of the dispersion equation is valid within the unshaded region. The arrows indicate the sense of polarization for different branches.

(Denisse and Delcroix, 1963, with modifications)

The complete form of the equation is given in Appendix C.

To analyse the propagation properties of different modes in a plasma, one can plot the refractive index squared n_j against the quantity $X = \frac{\omega_p^2}{\omega^2} + \frac{\omega_{pe}^2}{\omega^2}$ with $A^* = \omega_p^2/\omega_H^2 + \omega_{pe}^2/\omega_H^2 = \text{constant}$.

Fig.1.1(a) shows such a graph for a warm collisionless magnetoactive plasma. The two transverse modes, i.e. ordinary mode and extraordinary mode, are referred to as modes number 1 and 2 respectively while mode 3 (ion mode) and 4 (electron mode) represent the two longitudinal modes. When the plasma is cold, the dispersion diagram takes the form of Fig.1.1(b).

When the wave frequency considered is high such that the effects of the ions can be neglected, the dispersion equation for waves in a cold collisionless magnetoactive plasma will be approximated to the well known Appleton-Hartree equation. In this high frequency cold plasma regime, modes 2 and 4 group together to form the transverse extraordinary mode 2 of the branch of refractive index curve intersecting the x-axis at R, where R represents the point $X = 1 + Y$ ($Y = |\omega_H/\omega|$). The mode 3, on the other hand, will be transformed to the transverse "Whistler" mode in the Appleton-Hartree approximation. According to the Appleton-Hartree dispersion equation, the whistler mode can be identified as mode 1. It should be remarked that each mode does not represent a particular sense of polarization (left hand or right hand). For $n_j > 1$, mode 3 and part of mode 4 have the same sense of polarization. As

mode 4 transits through the point $n_j = 1$, its sense of polarization reverses. In Figure 1.1(c), the states of polarization in various branches are indicated by the arrows.

So far we have considered the propagation of waves in a plasma. Since only high frequency waves (i.e. effects of ions can be neglected) are studied in this thesis, we will discuss briefly in the next section the physical pictures of the basic generating mechanisms in the high frequency regime.

(G) Generation of High Frequency Waves in a Plasma

Due to various momentum distributions of charged particles and different types of motion of particles in the plasma, various waves can be generated.

When two charged particles in a plasma approach close to each other on account of thermal motion (speed = $\beta_T = \frac{v_T}{c}$), the energy lost in particles deceleration is emitted in the form of electromagnetic wave disturbance — this type of radiation in a plasma is called Bremsstrahlung radiation. In fact, this radiation is emitted in "close" or binary encounters as well as in "distant" or multiple encounters, where each ion interacts with an electron as in a binary encounter (Scheuer, 1960). Since the motion of the charged

particles is of random nature (due to thermal agitation), the observed radiation radiation will be unpolarized.

If a charged particle is moving through a medium containing neutral atoms in a certain direction with velocity \bar{v} , the so called Čerenkov waves, which are transverse waves, are emitted on the surface of a cone if the velocity of the particle is greater than the phase velocity of quanta in this medium; the unpolarized radiation is observed only at a particular value of wave-normal angle θ (with respect to \bar{v}) such that

$$\cos \theta = \frac{c}{vn_j} \quad (1.7)$$

where n_j = refractive index in the medium and c = speed of light in vacuum (Jelley, 1958). When the medium is a plasma, the Čerenkov effect (i.e. $\cos \theta = \frac{c}{vn_j}$) may be satisfied also if the refractive index n is greater than 1. This condition is satisfied for modes 3 and 4 (see Fig. 1) and the "Čerenkov Plasma waves" are in general longitudinal waves, in contrast to the transverse waves emitted in a microscopically neutral medium. An unusual feature of the wave disturbance emitted by the Čerenkov effect is that waves of a given frequency are propagated only at a particular angle θ which defines the emission cone. Cohen (1961) has calculated the intensity of waves emitted by this process.

In the presence of a significant magnetic field with intensity H_0 in a plasma, an electron of charge e and rest mass m_0 will gyrate in a helix in general, where the gyration frequency is given by $f_H = \frac{eH_0(1 - \beta_T^2)}{2\pi m_0 c} = \frac{eH_0}{2\pi m_0 c}$, for normalized thermal velocity $\beta_T = \frac{v_T}{c} \ll 1$. In a helical trajectory, since a charged particle is undergoing acceleration at all instants on the plane perpendicular to the external magnetic field where the motion is circular, the particle radiates electromagnetic energy as it gyrates along.

First of all, we will consider the emission from an electron rotating about a static magnetic field in a vacuum. When the speed $\beta = v/c$ of the electron is nonrelativistic ($\beta \sim 0$), the electric field of the wave disturbance $E(t)$ received by an observer at the orbital plane shows the form of a simple harmonic wave. The spectrum of the received radiation is the Fourier transform of the simple harmonic wave (Fig.2.2(a)) and the radiated frequency is confined to the gyrofrequency f_H only. At mildly relativistic speeds ($\beta \lesssim 1$), the wave form of the electric wave field is distorted and the Fourier transform of $E(t)$ indicates that the received energy is significant at the first few harmonics of the relativistic gyrofrequency γf_H , where $\gamma = (1 - \beta^2)^{-1/2}$.

(Fig. 2.1(b)). The radiation from such a rotating electron (or in general an electron gyrating in a helical path) with nonrelativistic or mildly relativistic speeds is called cyclotron radiation.

At highly relativistic speeds ($1 - \beta^2 \ll 1$, or energy of electron > 1 Mev.), the classical equations which describe the distant field radiated by an accelerating electron indicate that the emission is sharply beamed along the direction of the particle's motion (see, for example, Jackson, chapter 14, 1962), and is highly polarized with the electric vector of the wave perpendicular to the external magnetic line of force. Hence, an observer at the orbital plane receives the radiated energy not in the form of a simple harmonic wave but in short sharp packets at the instant when the particle's velocity is directed towards him. The spectrum of the received radiation is then the Fourier transform of the regular pulse train; its form is that a long series of harmonics of the frequency γf_H , all contained within an envelope defined by the Fourier transform of an individual pulse (Wild, Smerd and Weiss, p. 353, 1963). The higher the energy of electrons, the greater the number of harmonics and closer is their spacing. The individual harmonics in the spectrum due to an assemblage of electrons are broadened by various effects, with the result that the spectrum being

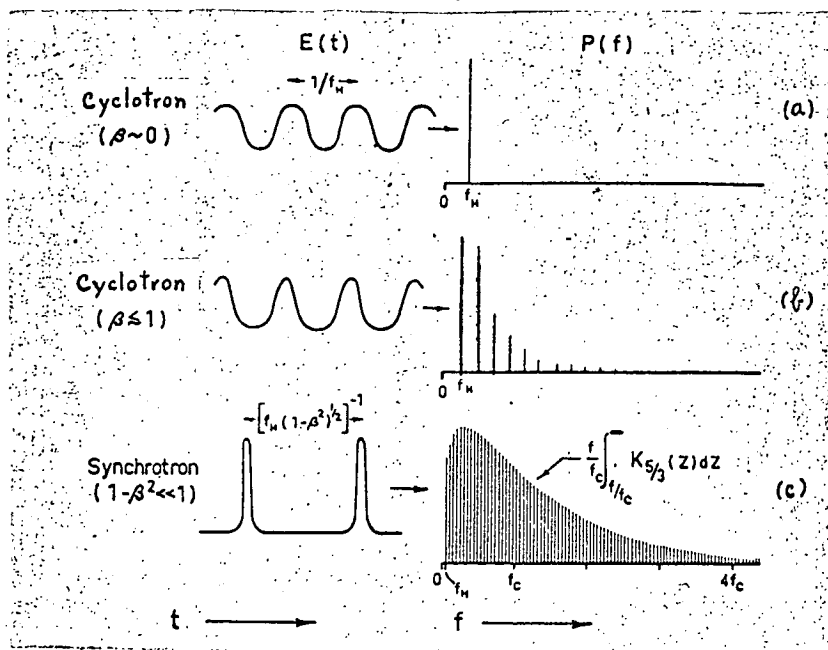


Fig.2.2 Diagram illustrating the origin of cyclotron and synchrotron radiation. $E(t)$ represents the electric field at a stationary observer in the orbital plane of an electron rotating at velocity βc . The emission spectrum $P(f)$ is the Fourier transform of $E(t)$. The critical frequency, which is a measure of the duration of the pulses, is given by $f_c = \frac{3e}{4\pi m_0 c} H_0 \left(\frac{E}{m_0 c^2} \right)^2$, where E is the energy of the electron in ergs.

(Wild, Smerd and Weiss, p.352, 1963)

smearred into a continuum. This type of radiation is called synchrotron radiation (Fig.2.2(c)).

In the general case, the motion of the electron is helical and the medium of interest is a plasma. By virtue of the Doppler effect, the frequency of radiation as received by an observer in a reference system fixed in the plasma is given by the Doppler equation:

$$f = \frac{s \gamma f_H}{|1 - \beta_{||} n_j \cos \theta|} \quad (1.8)$$

If the condition

$$\beta_{||} n_j \cos \theta < 1 \quad (1.9)$$

is satisfied, the Doppler effect is said to be normal.

Using the quantum treatment, Ginzburg and Frank (1947) have shown that the radiation of a quantum in the normal Doppler effect is accompanied by a change of the electron to a state with a smaller value of transverse momentum p_{\perp} ; here the direction perpendicular to the static magnetic field is assigned the transverse direction. In this case, the observed frequency may be higher or lower than the frequency $s \gamma f_H$, depending on whether the electron is moving towards ($0 \leq \theta < \frac{\pi}{2}$) or away ($\frac{\pi}{2} < \theta \leq \pi$) from the observer:

When

$$\beta_{||} n_j \cos \theta > 1 \quad (1.10)$$

holds, the Doppler effect is said to be anomalous. In this

case, the component of $v_{||}$ in the direction of the emitted wave is larger than the phase velocity v_{ph} of this wave and the electron leaves a polarized wake which radiates electromagnetic energy into the forward hemisphere. When a quantum is emitted with a frequency corresponding to the anomalous Doppler effect, the radiating electron is changed into a state with a larger transverse momentum p_{\perp} (see, for example, Ginzburg, Zheleznyakov and Eidman, 1962). It is clear from (1.9) that for radiation corresponding to the anomalous Doppler effect, we must have $n_j > 1$ and the waves can only propagate in the whistler mode and some part of the electron mode.

In the case of synchrotron radiation, the refractive index is close to 1 for most plasmas of interest and the radiation characteristics are the same as in vacuum. The intensity of this radiation has been calculated by Schwinger (1949). For cyclotron radiation, the refractive index can be far away from 1 and the mathematics involved in the study of radiation properties is much more complicated. A detailed study of the cyclotron process under various conditions will be made in the later chapters.

We will consider only the frequency range from the order of Kc/s to the order of 100 Mc/s in this thesis and the only relevant generation mechanisms for such frequencies are the ones described briefly above. All these processes can occur

in a plasma, depending on different physical conditions of the radiators and background medium. For example, in a magnetoactive plasma there may be the case when the temperature of the particles is so high that before a particle has a chance of gyrating once along the external magnetic field and radiate cyclotron radiation, it has already collided with another particle. In such circumstance, the only significant radiation will be the Bremsstrahlung radiation. On the other hand, if the temperature of the background magnetoactive plasma is low and highly relativistic charged particles streams are present, the synchrotron mechanism will predominate. Consequently, the investigation of the generating mechanism for waves coming from a radio source requires the knowledge of the physical conditions of the generating region. Conversely, postulating the correct theory of emission will lead us to understand the physical situations of the region where the radiators reside. Hence, the theoretical study of plausible generating mechanisms is a very important part of radio astronomy.

(H) Emissions from the Sun and Planets

Most planets have no remarkable internal source of

energy and are, thus, weak radio sources in general. On account of the impingement of sunlight, the atmospheres of the planets are being heated up to several hundred degrees Kelvin, and all planets emit weak thermal radiation in the microwave range. However, among them Mercury and Venus emit more radio power at some ranges of frequencies than would otherwise be observed from Bremsstrahlung radiation due to simple heating of the planets by the incident solar rays. More surprisingly still, Jupiter has been discovered lately to be a very strong source of radio waves in the decametric range. A good review on the emissions from the planets was given by Roberts (1963). Intense VLF and ELF electromagnetic waves, which are believed to be generated in the terrestrial magnetosphere, have been received on Earth (for example, Ellis, 1959 and Mainstone and McNicol, 1962). One or more generating mechanisms rather than the Bremsstrahlung radiation must be responsible for these abnormally high intensity radiations from the two planets. The Sun has been known for a long time as a very active radio source for waves of wavelengths ranging from centimetre to decametre. Up to the observed data of the present day, therefore, the most interesting objects in the solar system, according to a radio astronomer, are the Sun, Jupiter and the Earth.

(I) Two Common Features in the Observational Data of the Sun, Jupiter and Earth

Because of the difference in generating mechanism, the variation in physical conditions of the source region, and the difference in propagation conditions, the observed characteristics of various types of emissions from the three ^{planets} ~~stars~~ show a large variety of forms. However, among all the observed features of various radiations from these three objects, the following two features are common and have presented difficulties to radio astronomer:

- (i) very narrow-banded emissions are observed _____
Solar type I noise bursts, VLF discrete emissions from terrestrial magnetosphere, and Jupiter's Decametric bursts radiation;
- (ii) all these narrow-banded emissions are associated with much intensive power than would otherwise be obtained from incoherent radiation of all the listed generating mechanisms except synchrotron radiation, which is not a likely generating process because the bandwidth of emission from this radiation is wide.

These two existing problems stimulate my interest in studying the plausible generating mechanisms for the three

types of narrow-band emissions stated, and thus, to look for a solution. Seeing the theory of cyclotron radiation from electron bunches has been applied to explain VLF discrete emissions (Dowden, 1962a & b) and Jupiter's Decametric bursts radiation (Ellis, 1965) successfully in several important aspects, the author examines the conditions under which the two mentioned features will appear; the solution to these problems is also a strong test to the cyclotron theory.

In solving the first problem, one has to know the power spectrum of the radiating system. It is well known that in the cyclotron mechanism one electron will radiate a wide range of frequencies in almost all directions. Thus, one must know what range of frequency is associated with the majority of the electromagnetic power before one can estimate the bandwidth of emission. Lidman's equation (1958), corrected by Liemohn (1964), gives cyclotron radiation power spectra from single electrons. This equation has not been well explored yet. Moreover, when the gyrating, radiating particles form a stream or bunch, some particles may radiate in phase gradually, so that, waves in the radiating system are perceived to grow according to an observer outside the system, and the resulting power spectrum will be different

from that of single electrons. When one considers this effect one is led to the problem of radiative instability of a stream-plasma system. Hence, the author starts off to investigate the conditions of instability in a stream-plasma system in chapter II. When the collective power spectrum is obtained, the two stated problems may be solved consequently.

In chapters III and IV, the instability theory is applied to solved the mentioned two problems in Jupiter's Decametric Burst radiation and terrestrial VLF discrete emissions respectively. In considering solar type I noise storms radiation, the first proposal of the theory of cyclotron radiation in the ordinary mode is made and the theory is investigated in detail (chapters V to X). It is found that not only the two features can be accounted for by the cyclotron mechanism and the instability theory, many other important observed characteristics of both Burst radiation and Continuum radiation can be explained.

The last chapter concludes the thesis and gives suggestions for further research.

CHAPTER II

EXCITATION OF ELECTROMAGNETIC WAVES IN A STREAM-PLASMA SYSTEM

(A) Introduction

Using the classical kinetic approach (chapter I), the radiative instability problem of a stream-plasma system has been studied by a number of authors. The main features of these investigations vary according to the form of momentum distribution taken for the stream, the wave-normal angle assumed, the frequency domain chosen and the types of waves excited (longitudinal or transverse electromagnetic waves). The momentum distribution functions of the charged particle stream considered are chiefly of four types:

- (a) The mean longitudinal momentum $p_{||}$ of the stream is finite and the transverse momentum p_{\perp} of each particle is zero, i.e., the stream is not gyrating. Here we assign the direction parallel to the static magnetic field to be the longitudinal direction and the one perpendicular to it the transverse direction^{*}.

^{*}In case the plasma is not magnetoactive, the longitudinal direction is referred to the direction where the stream is travelling.

- (b) A delta distribution in momentum space for both components of momentum p_{\perp} and p_{\parallel} where $p_{\perp} \neq 0$ and $p_{\parallel} \neq 0$. A stream of this distribution is called "helical".
- (c) A distribution function where there is dispersion of particles over the longitudinal and transverse momenta and $p_{\perp}^{\circ} = 0$ whereas p_{\parallel}° is non-zero — p_{\perp}° , p_{\parallel}° are values of momenta where the distribution curve shows the maximum.
- (d) In case (c) where $p_{\perp}^{\circ} \neq 0$.

The homogeneous background plasma is usually assumed either to be cold, or cold and magnetoactive. We refer to the treatments where the wave frequency is very much higher than, and of the order of the ion gyro-frequency as the high frequency treatment and low frequency treatment respectively. The wave-normal angle θ assumed generally fall into three classes:

- (α) strictly longitudinal propagation, i.e. $\theta = 0^{\circ}$ or 180°
- (β) θ close to 0° or 180°
- (γ) general θ

With above specifications, the characteristics of various treatments are summarized in Table 2.1:

Table 2.1

| Momentum Distribution of Stream | Background Plasma | Frequency Domain | Nature of Waves Excited | θ Assumed | Authors* |
|---------------------------------|---------------------------|------------------------|--------------------------------------|---|---------------------------------|
| (a) | cold plasma | high frequency | longitudinal e.m. waves | $0^\circ, 180^\circ$ | Akhiezer & Fainberg, 1949 |
| (b) | cold magnetoactive plasma | " | transverse e.m. waves | $0^\circ, 180^\circ$ | Zheleznyakov, 1960a |
| (d) | " | " | " | " | Zheleznyakov, 1960b |
| (c) | " | low frequency | longitudinal & transverse e.m. waves | general | Kovner, 1961a & 1961b |
| (c) | " | high frequency | " | general θ for Cerenkov instability small θ but $\neq 0$ for cyclotron instability | Stepanov & Kitsenko, 1961 |
| (a) | " | " | longitudinal e.m. waves | general | Bokhan'kov, 1964 |
| (b) | " | " | transverse e.m. waves | $0^\circ, 180^\circ$ | Bell & Buneman 1964 |
| (b) | " | high & low frequencies | " | $0^\circ, 180^\circ$ | Neufeld & Wright, 1964a & 1964b |

*The reference is by no means complete; we have given some typical publications only.

It is obvious that with type (a) distribution function of the stream, cyclotron waves cannot be excited. When the distribution function of the stream is as type (c), most nonthermal particles in the system acquire zero or very small values of p_{\perp} , hence, the excitation of cyclotron waves will not be important in such a system. On the other hand, the excitation of longitudinal plasma waves will be pronounced in a system with a stream of type (a) or (c). As far as excitation of cyclotron waves is concerned, distribution function types (b) and (d) of the stream are more important, in particular the latter, for it is most likely the realistic case. With these two distribution functions, it is clear from Table 2.1 that only the case of longitudinal propagation ($\theta = 0^{\circ}, 180^{\circ}$) has been investigated. Since cyclotron radiation is emitted in all directions by a gyrating charged particle, the instability theory for general θ is therefore highly desirable and it is only when such a theory is available that we can estimate the frequency spectrum of radiation emitted by a gyrating stream. Hence, to start off, we will derive the dispersion equation for general θ and, thus, the expression for the growth rate in time (excitation coefficient) for a "helical stream-magnetoactive plasma" system in section (B). This is the limiting situation for the case where the stream has a narrow spread in momentum distribution and will be found to

be important in application. When the temperature of the stream is included, i.e. taking into account the spread in momentum distribution of the stream, the dispersion equation for the stream-plasma system is then derived in section (C). In this chapter, we will give the essential mathematical expressions only. The numerical analysis of the radiative unstable system is achieved in chapters III, IV, and VIII, where the instability theory is applied to various particular cases of interest in radio astronomy.

(B) Formulation of Radiative Instability Theory in a Helical-Stream-Plasma System

In the investigation of this section, the more general case of a helical electron stream is considered, i.e. each electron in the stream moves with the same non-zero transverse velocity $\beta_{\perp} = v_{\perp}/c$ and the same longitudinal velocity $\beta_{\parallel} = v_{\parallel}/c$; the direction along the static magnetic field is assigned the longitudinal direction. The particle density in the stream is assumed to be very small compared with that in the background plasma and the stream-plasma system is assumed to be electrically neutral.

The dispersion equation for an electromagnetic wave specified by $e^{i(\vec{k} \cdot \vec{r} - \omega)t}$ propagating in a medium

with dielectric tensor $\epsilon_{ik}(\omega, \mathbf{k})$ is given by

$$\det[n^2 \delta_{ik} - n_i n_k - \epsilon_{ik}(\omega, \mathbf{k})] = 0 \quad (2.1)$$

where $\bar{n} = ck/\omega$, \mathbf{k} = wave vector, ω = angular frequency of the electromagnetic wave, and c = speed of light in vacuum. δ_{ik} is Kronecker delta.

For cyclotron radiation from a charged particle gyrating about a static magnetic field line, the wave vector \mathbf{k} gyrates with the gyrating radiator and \mathbf{k} forms a cone for one complete gyration of the charged particle. If the static magnetic field is along the z direction, on account of symmetry, we can, thus, let $k_y = 0$. The dispersion equation, namely equation (2.1), in matrix form becomes

$$\begin{pmatrix} -n_z^2 + \epsilon_{xx} & \epsilon_{xy} & n_x n_z + \epsilon_{xz} \\ \epsilon_{yx} & -n_x^2 - n_z^2 + \epsilon_{yy} & \epsilon_{yz} \\ n_x n_z + \epsilon_{zx} & \epsilon_{zy} & -n_x^2 + \epsilon_{zz} \end{pmatrix} \begin{pmatrix} E_x \\ E_y \\ E_z \end{pmatrix} = 0 \quad (2.2)$$

The dielectric tensor for a growing electromagnetic wave in a plasma permeated by a static magnetic field, specified by an unperturbed distribution function f_0 , is of the form (Stepanov and Kitsenko, 1961)*.

*In this study, relativistic effects have been included.

$$\epsilon_{xx} = 1 + 2\pi \frac{\omega_0^2}{\omega^2} \int \frac{T}{k_{\perp}^2} s^2 J_s^2 \omega_H^2 m_0^2 dp_{\perp} dp_{\parallel}$$

$$\epsilon_{yy} = 1 + 2\pi \frac{\omega_0^2}{\omega^2} \int T J_s'^2 p_{\perp}^2 dp_{\perp} dp_{\parallel}$$

$$\epsilon_{zz} = 1 - \frac{\omega_0^2}{\omega^2} \left\{ 1 + 2\pi \int \frac{\partial f_0}{\partial p_{\perp}} p_{\parallel}^2 dp_{\perp} dp_{\parallel} - 2\pi \int T J_s^2 p_{\parallel}^2 dp_{\perp} dp_{\parallel} \right\}$$

$$\epsilon_{xy} = i \frac{2\pi \omega_0^2}{\omega^2} \int \frac{T}{k_{\perp}} s J_s J_s' \omega_H m_0 p_{\perp} dp_{\perp} dp_{\parallel} \quad (2.3)$$

$$\epsilon_{xz} = 2\pi \frac{\omega_0^2}{\omega^2} \int \frac{T}{k_{\perp}} s J_s^2 p_{\parallel} \omega_H m_0 dp_{\perp} dp_{\parallel}$$

$$\epsilon_{yz} = -i \frac{2\pi \omega_0^2}{\omega^2} \int T J_s J_s' p_{\perp} p_{\parallel} dp_{\perp} dp_{\parallel}$$

$$\epsilon_{yx} = -\epsilon_{xy}$$

$$\epsilon_{zx} = \epsilon_{xz}$$

$$\epsilon_{zy} = -\epsilon_{yz}$$

where $T = \left[(\omega m - k_{\parallel} p_{\parallel}) \frac{\partial f_0}{\partial p_{\perp}} + k_{\parallel} p_{\perp} \frac{\partial f_0}{\partial p_{\parallel}} \right] \frac{1}{(\omega m - k_{\parallel} p_{\parallel} - s \omega_H m_0)}$

$$\omega_0 = \left(\frac{4\pi N e^2}{m_0} \right)^{1/2} = \text{angular plasma frequency, } N = \text{particle density}$$

ω = angular wave frequency

k_{\parallel}, k_{\perp} = components of wave vector along and perpendicular to the direction of the static magnetic field respectively

p_{\parallel}, p_{\perp} = corresponding momenta of particle

$m = (m_0^2 + p_{||}^2/c^2 + p_{\perp}^2/c^2)^{1/2}$, is the relativistic mass of a charged particle of rest mass m_0 in the plasma

ω_H = angular gyro-frequency and negative for negatively charged particles

n = harmonic number

J_n and J_n' are Bessel's function and its derivative; the argument being

$$a = \frac{k_{\perp} p_{\perp}}{\omega_H m_0}$$

It should be noted that expression (2.3) can be obtained from the general expression for ϵ_{ik} which was derived (by Shafranov, 1958) under the condition that the part of the distribution function $f(\bar{p}, \bar{r}, t)$, which is connected with the electromagnetic disturbance, tends to zero with $t \rightarrow -\infty$. Evidently, this means that the wave disturbance grows with time.

Now suppose the radiators constitute a helical stream; the unperturbed distribution function takes the form

$$f_0(\bar{p}) d\bar{p} = \frac{1}{2\pi p_{\perp}^0} \delta(p_{\perp} - p_{\perp}^0) \delta(p_{||} - p_{||}^0) d\bar{p} \quad (2.4)$$

We can simplify (2.3) through integration by parts, assuming f_0 tends to zero sufficiently quickly with p_{\perp} and $|p_{||}|$ tending to infinity. With a delta function distribution as in expression (2.4), the dielectric tensor becomes:

- 6 -

$$\epsilon_{xx} = 1 - \sum_{s=-\infty}^{\infty} \left\{ \frac{2\omega_0^2 s^2 J_s J_s' (\omega - k_{||} v_{||}) \gamma \omega_H}{\omega^2 k_{\perp} v_{\perp} R} + \frac{\omega_0^2 \gamma^2 \omega_H^2 s^2 J_s^2 (k_{\perp}^2 - \omega^2 / c^2)}{\omega^2 k_{\perp}^2 R^2} \right\}$$

$$\epsilon_{yy} = 1 - \sum_{s=-\infty}^{\infty} \left\{ \frac{2\omega_0^2 J_s'^2 (\omega - k_{||} v_{||})}{\omega^2 R} + \frac{2\omega_0^2 J_s' J_s'' v_{\perp} k_{\perp}}{\omega^2 \gamma \omega_H R} + \frac{\omega_0^2 J_s'^2 v_{\perp}^2 (k_{\perp}^2 - \omega^2 / c^2)}{\omega^2 R^2} \right\}$$

$$\epsilon_{zz} = 1 - \frac{\omega_0^2}{\omega^2} - \sum_{s=-\infty}^{\infty} \left\{ \frac{2\omega_0^2 J_s J_s' v_{||}^2 k_{\perp} (\omega - k_{||} v_{||})}{\omega^2 v_{\perp} \gamma \omega_H R} + \frac{\omega_0^2 J_s^2 v_{||} (2k_{||} + \omega v_{||} / mc^2)}{\omega^2 R} + \frac{\omega_0^2 J_s^2 v_{||}^2 (k_{||}^2 - \omega^2 / c^2)}{\omega^2 R^2} \right\}$$

(2.5)

$$\epsilon_{xy} = -i \frac{\omega_0^2}{\omega^2} \sum_{s=-\infty}^{\infty} \left\{ \frac{s J_s J_s' \gamma \omega_H (\omega - k_{||} v_{||} + \omega v_{\perp}^2 / mc^2)}{v_{\perp} k_{\perp} R} + \frac{s J_s'^2 (\omega - k_{||} v_{||})}{R} + \frac{s J_s J_s'' (\omega - k_{||} v_{||})}{R} + \frac{s J_s J_s' \gamma \omega_H v_{\perp} (k_{\perp}^2 - \omega^2 / c^2)}{k_{\perp} R^2} \right\}$$

$$\epsilon_{xz} = - \sum_{s=-\infty}^{\infty} \left\{ \frac{2\omega_0^2 s J_s J_s' v_{||} (\omega - k_{||} v_{||})}{\omega^2 v_{\perp} R} + \frac{\omega_0^2 s J_s^2 v_{||} \gamma \omega_H (k_{\perp}^2 - \omega^2 / c^2)}{\omega^2 k_{\perp} R^2} \right\}$$

$$\epsilon_{yz} = i \frac{\omega_0^2}{\omega^2} \sum_{s=-\infty}^{\infty} \left\{ \frac{(\omega - k_{||} v_{||}) v_{||} J_s J_s'}{R} + \frac{k_{\perp} v_{||} (\omega - k_{||} v_{||}) (J_s'^2 + J_s J_s'')}{\gamma \omega_H R} + \frac{J_s J_s' v_{\perp} v_{||} (k_{\perp}^2 - \omega^2 / c^2)}{R^2} \right\}$$

$$\epsilon_{yx} = - \epsilon_{xy}$$

$$\epsilon_{zx} = \epsilon_{xz}$$

$$\epsilon_{zy} = - \epsilon_{yz}$$

For a non-trivial solution, equation (2.2) can be written as

$$A n_s^4 + B n_s^2 + C = 0$$

$$\text{where } A = \sin^2 \theta \epsilon_{xx} + \cos^2 \theta \epsilon_{zz} + 2 \sin \theta \cos \theta \epsilon_{xz}$$

$$B = 2 \sin \theta \cos \theta (\epsilon_{xy} \epsilon_{yz} - \epsilon_{yy} \epsilon_{xz}) + \epsilon_{xz}^2 - \epsilon_{xx} \epsilon_{zz} \\ - \cos^2 \theta (\epsilon_{yy} \epsilon_{zz} + \epsilon_{yz}^2) - \sin^2 \theta (\epsilon_{xx} \epsilon_{yy} + \epsilon_{xy}^2)$$

$$C = \epsilon_{zz} (\epsilon_{xx} \epsilon_{yy} + \epsilon_{xy}^2) + \epsilon_{xx} \epsilon_{yz}^2 + 2 \epsilon_{xy} \epsilon_{yz} \epsilon_{xz} - \epsilon_{yy} \epsilon_{xz}^2$$

Solving for n_s^2 :

$$n_s^2 = \frac{-B \pm \sqrt{B^2 - 4AC}}{2A} = 1 - F \quad (2.6)$$

here we use the subscript s to indicate that n_s^2 is the square of the refractive index for the "stream static magnetic field" system. In (2.6)

$$F = F(\theta, p_{\perp}, p_{\parallel}, k, \omega, \omega_H, \omega_0)$$

So far we have not yet considered the ambient plasma.

Since we have assumed the density of the stream to be very much smaller than that of the ambient plasma, n_s^2 can be considered as a perturbation term in the overall refractive index expression for the stream-magnetoactive-plasma system. Following Zheleznyakov (1960a), we assume:

$$n^2 = n_j^2 + n_s^2 - 1 \quad (2.7)$$

where n = overall refractive index

n_j = refractive index of the ambient plasma

The validity of the above assumption is discussed in Appendix D.

Equation (2.6) can then be written as:

$$F_p + F' = 0 \quad (2.8)$$

$$\text{where } F_p = c^2 k^2 - \omega^2 n_j^2, \quad (2.8a)$$

$$F' = \omega^2 F$$

We employ the real- k method, i.e. we assume the wave vector to be real and the frequency complex in order to find the growth of the electromagnetic wave in time. We let

$$\omega = \tilde{\omega} + \delta \quad (2.9)$$

where $\tilde{\omega}$, the "characteristic frequency", is real and δ being complex, assuming

$$|\omega| \gg |\delta| \quad (2.9a)$$

With above approximation, one has (Zheleznyakov, 1960a; Neufeld and Wright, 1964)

$$\left(\frac{\partial F_p}{\partial \omega} \right)_{\tilde{\omega}} \delta + (F_p)_{\tilde{\omega}} + F' = 0 \quad (2.10)$$

The equation $(F_p)_{\tilde{\omega}} = 0$ in fact gives the dispersion equation for electromagnetic wave of frequency $\tilde{\omega}$ in the ambient plasma alone. With a thin stream as assumed, we have

$$(F_p)_{\tilde{\omega}} \doteq 0$$

$$\text{hence we can take } \left(\frac{\partial F_p}{\partial \omega} \right)_{\tilde{\omega}} \delta + F' = 0 \quad (2.10a)$$

We now refer back to equation (2.5). Since we are considering an electron stream, ω_H will be negative. Physically, for a non-zero harmonic number, the only possible non-thermal radiation from a gyrating charged particle is gyro-radiation. In the frame of reference where the radiator is at rest, the frequency radiated is equal to the gyro-frequency of the radiator. For an observer in a system fixed to the background medium, the radiated frequency will be Doppler-shifted to a frequency higher than $|s\gamma\omega_H|$ in the forward direction and Doppler-shifted to a frequency lower than $|s\gamma\omega_H|$ in the backward direction. For gyro-radiation from a single particle, the Doppler equation gives $(\tilde{\omega} - k_{||} v_{||} - s\gamma\omega_H) = 0$. In case of electrons where ω_H is taken to be negative, negative integers of s represent normal cyclotron radiation, while a positive integer of s represents the s^{th} harmonic of the anomalous cyclotron radiation. For the whole system, as ω_o^2 is assumed to be small (thin stream), we can see that unless the term $(\omega - k_{||} v_{||} - s\gamma\omega_H)$ is small,

$$\epsilon_{xx} = \epsilon_{yy} = \epsilon_{zz} \doteq 1, \quad \epsilon_{xy} = \epsilon_{xz} = \epsilon_{yz} = \epsilon_{yx} = \epsilon_{zx} = \epsilon_{zy} \approx 0$$

and $n_g^2 \doteq 1$, implying that the stream has a negligible effect on the refractive index of the system. We let $\tilde{\omega} - k_{||} v_{||} - s\gamma\omega_H$

= 0, hence, from (2.9)

$$\omega - k_{||} v_{||} - s \gamma \omega_H = \delta \quad (2.11)$$

From relation (2.9a), the largest terms in (2.5) are the terms which contain

$$\frac{1}{(\omega - k_{||} v_{||} - s \gamma \omega_H)^2}$$

and the number 1. Expression (2.5) now reads:

$$\epsilon_{xx} = 1 - s^2 Q J_s^2 K$$

$$\epsilon_{yy} = 1 - J_s^2 v_{\perp}^2 K$$

$$\epsilon_{zz} = 1 - J_s^2 v_{||}^2 K$$

$$\epsilon_{xy} = \frac{1 J_s J_s' s \gamma |\omega_H| v_{\perp} K}{k_{\perp}} \quad (2.12)$$

$$\epsilon_{xz} = s J_s^2 |\sqrt{Q}| v_{||} K$$

$$\epsilon_{yz} = 1 J_s J_s' v_{\perp} v_{||} K$$

$$\epsilon_{yx} = -\epsilon_{xy}, \quad \epsilon_{zx} = \epsilon_{xz}, \quad \epsilon_{zy} = -\epsilon_{yz}$$

where $Q = \frac{\gamma^2 \omega_H^2}{k_{\perp}^2}$ $K = \frac{\omega_0^2 (s^2 k_{||}^2 - \omega^2)}{\omega^2 s^2 \delta^2} = \frac{\omega_0^2 (s^2 k_{||}^2 - \tilde{\omega}^2)}{\tilde{\omega}^2 s^2 \delta^2}$

The coefficients A, B, C in equation (2.6) then become

$$A = 1 - J_s^2 P^2 K$$

$$B = -2 + J_s^2 K (P^2 + s^2 Q + v_{||}^2) + J_s^2 v_{\perp}^2 \quad (2.13)$$

$$C = 1 - J_s'^2 K Q - J_s'^2 K v_{||}^2 - J_s'^2 v_{\perp}^2$$

$$\text{where } p^2 = v_{||}^2 \cos^2 \theta \frac{\xi^2}{(\xi + s\gamma)^2}, \quad \xi = \frac{\tilde{\omega}}{|\omega_H|}$$

$$\text{and } K = \frac{\omega_0^2}{c^2 \gamma^2} \left(\frac{(\xi + s\gamma)^2}{\xi^2 \beta_{||}^2} - 1 \right)$$

The perturbation term F' on the dispersion equation (2.10a) can be calculated:

$$F' = \tilde{\omega}^2 \frac{J_s'^2 K v_{\perp}^2 + J_s'^2 K \frac{v_{||}^2 (s\gamma + \xi \sin^2 \theta)^2}{\sin^2 \theta (\xi + s\gamma)^2}}{1 + \frac{s J_s'^2 K v_{||}^2 \cos^2 \theta \xi^2}{(\xi + s\gamma)^2}} \quad (2.14)$$

With the definition of F' given by expression (2.14), and the definition of F_p given by relation (2.8a), equation (2.10a), therefore, gives the complete form of the dispersion equation in a helical-stream-plasma system. Here, n_j^2 and thus F_p and $\frac{\partial F_p}{\partial \omega}$ are left in the most general form. The expression for n_j^2 depends on the type of ambient plasma under consideration and will be written in chapters III and IV when we discuss different particular cases of application of the theory.

(C) Instability Theory of a Stream-plasma System when the Temperature Effects in the Stream have been Included

Instead of a strictly "monoenergetic" charged particle stream, we consider a stream having momentum spread in both components p_{\perp} , p_{\parallel} . p_{\perp}^0 and p_{\parallel}^0 are supposed to be the values of momentum components where the distribution curve reaches its maximum. More precisely, the unperturbed particle distribution function $f_0(\bar{p})$ of the stream is given by

$$f_0(\bar{p}) d\bar{p} = \frac{1}{A} e^{\left[-\frac{(p_{\parallel} - p_{\parallel}^0)^2}{a_{\parallel}^2} - \frac{(p_{\perp} - p_{\perp}^0)^2}{a_{\perp}^2} \right]} d\bar{p} \quad (2.15)$$

where $A = 2\pi^{3/2} a_{\perp}^2 a_{\parallel} G_0$ is the normalization constant of f_0 .

$$a_{\perp}^2 = 2 m_0 \kappa T_{\perp}$$

$$a_{\parallel}^2 = 2 m_0 \kappa T_{\parallel}$$

m_0 = rest mass of radiating particle⁺

κ = Boltzmann constant

T_{\perp} , T_{\parallel} = transverse and longitudinal temperatures respectively

⁺For simplicity, we consider one species of radiating particles only.

and $\mathcal{S} = \frac{p_{\perp}}{a_{\perp}}$

with $\mathcal{S}_0 = \frac{p_{\perp}^0}{a_{\perp}}$

Leaving the expression for the ambient plasma refractive index unspecified, we will now derive the dispersion equation for electromagnetic waves in a stream-plasma system when the distribution function of the radiating particles is given by relation (2.15). The method employed here follows that in section (B) of this chapter and the work of Zheleznyakov (1960b).

Before using expressions (2.3) and (2.15) to derive the relations of the dielectric tensor components, we have to define several quantities:

Let $\xi' = \frac{(p_{\parallel} - p_{\parallel}^0)^*}{a_{\parallel}}$

$$\beta_j = \frac{\omega \tilde{m} - k_{\parallel} p_{\parallel}^0 - s \gamma \omega_H m}{k_{\parallel} a_{\parallel}} \quad (2.16)$$

$$\delta(p_{\perp}, p_{\parallel}) = \delta(S, \xi') = - \frac{\omega m - \omega \tilde{m} - k_{\parallel} (p_{\parallel} - p_{\parallel}^0)}{k_{\parallel} a_{\parallel}}$$

where the sign \sim indicates that the corresponding value

*Our quantity ξ' is equivalent to the quantity ξ defined by Zheleznyakov, in order to distinguish it from the normalized frequency $\xi = \omega/|\omega_H|$ which will be introduced later.

is taken at the point $p_1 = p_1^0$, $p_{||} = p_{||}^0$

Let us now consider an integral of the form

$$I(\xi, \beta_j) = \int_{\text{contour}} \frac{g(\xi', \xi) e^{-\xi'^2}}{\beta_j - \delta(\xi', \xi)} d\xi' \quad (2.17)$$

The contour of integration runs along the real axis of $p_{||}$ from $-\infty$ to $+\infty$, by-passing from above or below the singularities of the integrand.

The integrand of the above integral will have singularities at two points specified by $\xi'_{1,2}$ such that

$$\left. \begin{aligned} \beta_j - \delta(\xi'_{1,2}, \xi) &= 0 \\ \text{or } \omega \sqrt{m_0^2 + \frac{p_{||}^2}{c^2} + \frac{p_{\perp}^2}{c^2}} - k_{||} p_{||} - s \gamma \omega_H &= 0 \end{aligned} \right\} \quad (2.18)$$

We note that we have changed the variables in expression (2.16) in order to deal with the denominator in relation (2.3); in fact, equation (2.18) is equivalent to $k_{||} = 0$, which is the Doppler equation.

It has been pointed out by Zheleznyakov that

$$\left. \begin{array}{l} \text{when } |\xi'| \lesssim 1 \quad \text{and} \quad |S - S_0| \lesssim 1 \\ \\ \text{we have } |\beta_j| \gg |\delta(\xi, S)|; \quad |\xi_{1,2}| \gg |\xi'| \end{array} \right\} \quad (2.19)$$

and the integral (2.17) can be simplified to

$$I(S, \beta_j) \approx \frac{1}{\beta_j} \int_{-\infty}^{\infty} g(\xi') e^{-\xi'^2} d\xi' + \frac{1}{\beta_j^2} \int_{-\infty}^{\infty} g(\xi') \delta(\xi') e^{-\xi'^2} d\xi' - i\pi \sum_{l=1,2} \delta_l g(\xi_l') e^{-\xi_l'^2} \left(\frac{\partial \delta}{\partial \xi'} \right)_l \quad (2.20)$$

with an accuracy up to terms of order $\frac{1}{\beta_j^2}$

where $\delta_l = +1$ if the contour of integration in (2.17) by-passes the singularity ξ_l from below and $\delta_l = -1$ if the contour by-passes the singularity ξ_l from above.

The mass of the radiating particle can be expressed in terms of ξ' , β as:

$$m(\xi', \beta) = \tilde{m} \sqrt{1 + \frac{2a_{||}p_{||}^0}{\tilde{m}^2 c^2} \xi' + \frac{a_{||}^2}{\tilde{m}^2 c^2} \xi'^2 + \frac{2a_{\perp}^2 \beta_0}{\tilde{m}^2 c^2} (\beta - \beta_0) + \frac{a_{\perp}^2}{\tilde{m}^2 c^2} (\beta - \beta_0)^2} \quad (2.21)$$

Let us assume that $m(\xi', \beta)$ changes little in the range $|\xi'| \lesssim 1$, $|\beta - \beta_0| \lesssim 1$. We can now express $m(\xi', \beta)$ in the form:

$$m(\xi', \beta) \simeq \tilde{m} \left[1 + \frac{a_{||}p_{||}^0}{\tilde{m}^2 c^2} \xi' + \frac{a_{||}^2}{2\tilde{m}^2 c^2} \xi'^2 + \frac{a_{\perp}^2 \beta_0}{\tilde{m}^2 c^2} (\beta - \beta_0) + \frac{a_{\perp}^2}{2\tilde{m}^2 c^2} (\beta - \beta_0)^2 \right] \quad (2.22)$$

It is easy to see that the angular plasma frequency can be written as:

$$\omega_0^2(\xi', \beta) \simeq \tilde{\omega}_0^2 \left[1 - \frac{a_{||}p_{||}^0}{\tilde{m}^2 c^2} \xi' - \frac{a_{||}^2}{2\tilde{m}^2 c^2} \xi'^2 - \frac{a_{\perp}^2 \beta_0}{\tilde{m}^2 c^2} (\beta - \beta_0) - \frac{a_{\perp}^2}{2\tilde{m}^2 c^2} (\beta - \beta_0)^2 \right] \quad (2.23)$$

In writing down expressions (2.22) and (2.23), we have taken:

$$\left| \frac{a_{||}p_{||}^0}{\tilde{m}^2 c^2} \right| \ll 1; \quad \left| \frac{a_{||}^2}{\tilde{m}^2 c^2} \right| \ll 1; \quad \left| \frac{a_{\perp}^2 \beta_0}{\tilde{m}^2 c^2} \right| \ll 1; \quad \left| \frac{a_{\perp}^2}{\tilde{m}^2 c^2} \right| \ll 1 \quad (2.24)$$

Since the denominator $\omega m - k_{||}p_{||} - sm_0\omega_H$ in expression (2.3) can be written as $k_{||}a_{||}[\beta_j - \delta(\xi', \beta)]$ and the quantities ω_0 , m are expressed as functions of ξ'

(given in (2.22), (2.23)), all the integrals in (2.3) fall into the type specified by (2.17), when integration is carried out with respect to ξ' . Let us note that on account of the inequalities given in (2.19), the integral $I(\xi, \beta_j)$ can be approximated to

$$I(\xi, \beta_j) \simeq \frac{1}{\beta_j} \int_{-\infty}^{\infty} g(\xi') e^{-\xi'^2} d\xi' \quad (2.25)$$

We now substitute relations (2.16), (2.17), (2.22), (2.23) and (2.25) into the expression for dielectric tensor components (expression (2.3)) and perform the integration with respect to ξ' . It has been pointed out in section (B) that the largest terms in the dielectric tensor components are the ones containing $1/(\omega m - k_{\parallel} p_{\parallel} - s m_0 \omega_H)^2$ and the number 1.

Confining ourselves to this approximation, we have:

$$\begin{aligned} \epsilon_{xx} &= 1 - \frac{s^2 \tilde{\gamma}^2 \omega_H^2 W}{k_{\perp}^2 D^2 G_0} \left\{ R_1 \int_0^{\infty} J_s^2 S e^{-(S-S_0)^2} dS - R_2 \int_0^{\infty} J_s^2 S (S-S_0) e^{-(S-S_0)^2} dS - R_3 \int_0^{\infty} J_s^2 S (S-S_0)^2 e^{-(S-S_0)^2} dS \right\} \\ \epsilon_{yy} &= 1 - \frac{a_{\perp}^2 W}{m^2 D^2 G_0} \left\{ R_1 \int_0^{\infty} J_s^2 S^3 e^{-(S-S_0)^2} dS - R_2 \int_0^{\infty} J_s^2 S^3 (S-S_0) e^{-(S-S_0)^2} dS - R_3 \int_0^{\infty} J_s^2 S^3 (S-S_0)^2 e^{-(S-S_0)^2} dS \right\} \\ \epsilon_{xy} &= -\frac{i s m_0 \omega_H a_{\perp} W}{k_{\perp} m^2 D^2 G_0} \left\{ R_1 \int_0^{\infty} J_s J_s' S^2 e^{-(S-S_0)^2} dS - R_2 \int_0^{\infty} J_s J_s' S^2 (S-S_0) e^{-(S-S_0)^2} dS \right. \\ &\quad \left. - R_3 \int_0^{\infty} J_s J_s' S^2 (S-S_0)^2 e^{-(S-S_0)^2} dS \right\} \\ \epsilon_{zz} &= 1 - \frac{a_{\parallel}^2 W}{m^2 D^2 G_0} \left\{ R_4 \int_0^{\infty} J_s^2 S e^{-(S-S_0)^2} dS - S_0 R_5 \int_0^{\infty} J_s^2 S (S-S_0) e^{-(S-S_0)^2} dS \right. \\ &\quad \left. - \frac{R_5}{2} \int_0^{\infty} J_s^2 S (S-S_0)^2 e^{-(S-S_0)^2} dS \right\} \end{aligned} \quad (2.26)$$

$$\begin{aligned} \epsilon_{xz} = & -\frac{S m_0 \omega_H p_{||}^0 W}{k_{\perp} \tilde{m}^2 D^2 G_0} \left\{ \left(R_1 - \frac{a_{||}^2}{2 \tilde{m}^2 c^2} \right) \int_0^{\infty} J_s^2 S e^{-(S-S_0)^2} dS \right. \\ & \left. - R_2 \int_0^{\infty} J_s^2 S (S-S_0) e^{-(S-S_0)^2} dS - R_3 \int_0^{\infty} J_s^2 S (S-S_0)^2 e^{-(S-S_0)^2} dS \right\} \\ \epsilon_{yz} = & \frac{i a_{\perp} p_{||} W}{\tilde{m}^2 D^2 G_0} \left\{ \left(R_1 - \frac{a_{||}^2}{2 \tilde{m}^2 c^2} \right) \int_0^{\infty} J_s J_s' S^2 e^{-(S-S_0)^2} dS \right. \\ & \left. - R_2 \int_0^{\infty} J_s J_s' S^2 (S-S_0) e^{-(S-S_0)^2} dS - R_3 \int_0^{\infty} J_s J_s' S^2 (S-S_0)^2 e^{-(S-S_0)^2} dS \right\} \end{aligned}$$

As the argument of the Bessel's function and its derivative is $a = \frac{k_{\perp} p_{\perp}}{m_0 \omega_H} = \frac{k_{\perp} S}{a_{\perp} m_0 \omega_H}$ is a function of S , all the J_s , J_s' , and J_s'' have to be kept inside the integrals. In (2.26), we define

$$\begin{aligned} W &= \frac{\tilde{\omega}_0^2 (c^2 k_{||}^2 - \omega^2)}{\omega^2 c^2} \\ D &= \omega - k_{||} v_{||} - s \gamma \omega_H \\ R_1 &= 1 - \frac{a_{||}^2}{4 \tilde{m}^2 c^2} \\ R_2 &= \frac{a_{\perp}^2 S_0}{\tilde{m}^2 c^2} \\ R_3 &= \frac{a_{\perp}^2}{2 \tilde{m}^2 c^2} \\ R_4 &= \frac{1}{2} - \frac{3 a_{||}^2}{8 \tilde{m}^2 c^2} - \frac{5 p_{||}^{02}}{4 \tilde{m}^2 c^2} + \frac{p_{||}^{02}}{a_{||}^2} \\ R_5 &= \frac{a_{\perp}^2}{\tilde{m}^2 c^2} \left(\frac{1}{2} + \frac{p_{||}^{02}}{a_{||}^2} \right) \end{aligned} \quad (2.27)$$

Following the method employed in section (B), the dispersion equation for electromagnetic cyclotron waves in the stream-magnetoactive plasma system can be expressed as

$$A \left(\frac{c^2 k^2}{\omega^2} - n_j^2 + 1 \right)^2 + \left(\frac{c^2 k^2}{\omega^2} - n_j^2 + 1 \right) B + C = 0 \quad (2.28)$$

where

$$A = \sin^2 \theta \epsilon_{xx} + \cos^2 \theta \epsilon_{zz} + 2 \sin \theta \cos \theta \epsilon_{xz}$$

$$B = 2 \sin \theta \cos \theta (\epsilon_{xy} \epsilon_{yz} - \epsilon_{yy} \epsilon_{xz}) + \epsilon_{xz}^2 - \epsilon_{xx} \epsilon_{zz} - \cos^2 \theta (\epsilon_{yy} \epsilon_{zz} + \epsilon_{yz}^2) - \sin^2 \theta (\epsilon_{xx} \epsilon_{yy} + \epsilon_{xy}^2)$$

$$C = \epsilon_{zz} (\epsilon_{xx} \epsilon_{yy} + \epsilon_{xy}^2) + \epsilon_{xx} \epsilon_{yz}^2 + 2 \epsilon_{xy} \epsilon_{yz} \epsilon_{xz} - \epsilon_{yy} \epsilon_{xz}^2$$

and ϵ_{ik} are given by (2.26).

Employing the real-k approach, we write

$$\left. \begin{aligned} \omega &= \tilde{\omega} + \delta \\ |\omega| &\gg |\delta| \end{aligned} \right\} \quad (2.29)$$

with

where $\tilde{\omega}$, the "characteristic frequency", is real and δ is complex; the imaginary part of δ gives us the growth rate. Let us define

$$\delta' = \frac{\delta}{\tilde{\omega}} \quad (2.30)$$

After some lengthy calculation, the coefficients in (2.28) are found to be

$$A = 1 - \frac{u_1}{\delta^2}$$

$$B = -2 + \frac{u_2}{\delta^2} + \frac{u_3}{\delta^4}$$

$$C = 1 - \frac{u_4}{\delta^2} + \frac{u_5}{\delta^4} + \frac{u_6}{\delta^8} \quad (2.31)$$

where $U_1 = T_2 + 2 \sin \theta \cos \theta T_1 - \cos^2 \theta T_5 - \sin^2 \theta T_7$

$$U_2 = T_3 + 2 \sin \theta \cos \theta T_8 + \cos^2 \theta T_4 + \sin^2 \theta T_6$$

$$U_3 = \sin^2 \theta E_{xx} + \cos^2 \theta E_{zz} + 2 \sin \theta \cos \theta T_9$$

$$U_4 = T_6 + E_{zz}$$

$$U_5 = T_7 + T_6 E_{zz}$$

$$U_6 = T_7 E_{zz}$$

$$U_7 = U_5 + E'_{yz} - T_8^2$$

$$U_8 = -U_6 - E_{xx} E'_{yz} + 2 T_8 E_{xyz} R_6 R_6'$$

and $T_1 = E_{xyz} (R_6 R_6' - R_7 R_8')$

$$T_2 = E_{xz}^2$$

$$T_3 = E_{xx} + E_{zz}$$

$$T_4 = E_{yy} + E_{zz}$$

$$T_5 = E_{yy} E_{zz} + E'_{yz}$$

$$T_6 = E_{xx} + E_{yy}$$

$$T_7 = E_{xx} E_{yy} + E'_{xy}$$

$$T_8 = E_{xz}$$

with $E_{xx} = \frac{s^2 \tilde{\gamma}^2 \beta_{||}^2 W'}{\tan^2 \theta (\xi + \tilde{\gamma}_s)^2} R_9$

$$E_{yy} = \frac{a_1^2 W'}{\tilde{m}^2 c^2} R_7$$

$$E_{zz} = \frac{W'}{\tilde{m}^2 c^2} R_9$$

$$E'_{xy} = - \frac{s^2 \tilde{\gamma}^2 a_1^2 \beta_{||}^2 W'^2 R_6^2}{\tilde{m}^2 c^2 \tan^2 \theta (\xi + \tilde{\gamma}_s)^2}$$

$$E_{yz}' = - \frac{a_{\perp}^2 \beta_{\parallel}^{\circ 2} W'^2 R_6'}{\tilde{m}^2 c^2}$$

$$E_{xz}' = \frac{s \tilde{\gamma} \beta_{\parallel}^{\circ 2} W' R_8'}{\tan \theta (\xi + \tilde{\gamma} s)}$$

$$E_{xyz}' = \frac{s \tilde{\gamma} a_{\perp}^2 \beta_{\parallel}^{\circ 2} W'^2}{\tilde{m}^2 c^2 \tan \theta (\xi + \tilde{\gamma} s)}$$

$$W' = \frac{\sigma A (c^2 k_{\parallel}^2 / \omega^2 - 1)}{\xi^2} = \frac{\sigma A \left[\frac{(\xi + s \tilde{\gamma})^2}{\xi^2 \beta_{\parallel}^2} - 1 \right]}{\xi^2}$$

σ = density of stream/density of ambient plasma

$$A = \omega_p^2 / \omega_H^2$$

$$\xi = \omega / |\omega_H|$$

$$\tilde{\gamma} = (1 - \beta_{\parallel}^{\circ 2} - \beta_{\perp}^{\circ 2})^{1/2}$$

$$\beta_{\parallel}^{\circ}, \beta_{\perp}^{\circ} = p_{\parallel}^{\circ} / \tilde{m} c, p_{\perp}^{\circ} / \tilde{m} c \quad \text{respectively}$$

c = speed of light in vacuum

and

$$R_6 = R_1 R_7 - R_2 R_8 - R_3 R_9$$

$$R_6' = R_6 - \frac{a_{\parallel}^2}{2 \tilde{m}^2 c^2} G_7$$

$$R_7 = R_1 G_4 - R_2 G_5 - R_3 G_6$$

$$R_8 = R_1 G_1 - R_2 G_2 - R_3 G_3$$

$$R_8' = R_8 - \frac{a_{\parallel}^2}{2 \tilde{m}^2 c^2} G_1$$

$$R_9 = R_4 G_1 - \frac{1}{2} R_5 G_2 - \frac{1}{2} R_5 G_3$$

where

$$G_1 = \frac{1}{G_0} \int_0^{\infty} J_s^2 s e^{-(s-s_0)^2} ds$$

$$G_2 = \frac{1}{G_0} \int_0^{\infty} J_s^2 s (s-s_0) e^{-(s-s_0)^2} ds$$

$$G_3 = \frac{1}{G_0} \int_0^{\infty} J_s^2 s (s-s_0)^2 e^{-(s-s_0)^2} ds$$

$$G_4 = \frac{1}{G_0} \int_0^{\infty} J_s'^2 s^3 e^{-(s-s_0)^2} ds$$

$$G_5 = \frac{1}{G_0} \int_0^{\infty} J_s'^2 s^3 (s-s_0) e^{-(s-s_0)^2} ds$$

$$G_6 = \frac{1}{G_0} \int_0^{\infty} J_s'^2 s^3 (s-s_0)^2 e^{-(s-s_0)^2} ds$$

$$G_7 = \frac{1}{G_0} \int_0^{\infty} J_s J_s' s^2 e^{-(s-s_0)^2} ds$$

$$G_8 = \frac{1}{G_0} \int_0^{\infty} J_s J_s' s^2 (s-s_0) e^{-(s-s_0)^2} ds$$

$$G_9 = \frac{1}{G_0} \int_0^{\infty} J_s J_s' s^2 (s-s_0)^2 e^{-(s-s_0)^2} ds$$

The dispersion equation for electromagnetic waves in the ambient plasma alone is given by

$$(F_p)_{\tilde{\omega}} = c^2 k^2 - \tilde{\omega}^2 n_j^2(\tilde{\omega}) = 0$$

Expanding $(F_p)_{\omega}$ in Taylor series about $\tilde{\omega}$, we have

$$(F_p)_{\omega} \approx \left(\frac{\partial F_p}{\partial \omega} \right)_{\tilde{\omega}} \delta + (F_p)_{\tilde{\omega}}$$

$$= \left(\frac{\partial F_p}{\partial \omega} \right)_{\tilde{\omega}} \delta$$

(2.32)

Writing $P = \frac{1}{\tilde{\omega}} \left(\frac{\partial F_p}{\partial \omega} \right)_{\tilde{\omega}}$ (dimensionless) (2.33)

we can simplify equation (2.28) into the following form:

$$W_1 \delta'^8 + W_2 \delta'^6 + W_3 \delta'^5 + W_4 \delta'^4 + W_5 \delta'^3 + W_6 \delta'^2 + W_7 = 0 \quad (2.34)$$

where

$$\begin{aligned} W_1 &= P^2 \\ W_2 &= P^2 U_3 \\ W_3 &= P(U_2 - 2U_3) \\ W_4 &= U_2 - U_3 - U_4 \\ W_5 &= PU_1 \\ W_6 &= U_1 + U_7 \\ W_7 &= U_8 \end{aligned}$$

Solving equation (2.34) for complex $\delta = \tilde{\omega} \delta'$, one can calculate the growth rate $|\Im_m(\delta)|$

Taking only terms containing $1/(\omega m - k_{||} \rho_{||} - sm_0 \omega_H)^2$ and the number 1 in the dielectric tensor components and other assumptions as stated, the dispersion equation has been derived (equation (2.28)). Using perturbation theory, we have expressed the dispersion equation as a polynomial in $\delta' = \frac{\delta}{\tilde{\omega}}$ (equation (2.34)), where $\delta = \omega - \tilde{\omega}$, is complex. The remaining work, therefore, is to solve equation (2.34).

Before attempting to solve (2.34) which is complicated as it stands we consider the case of strictly longitudinal propagation, i.e. $\theta = 0^\circ$ or 180° . Moreover, we confine ourselves to the first harmonic only, so that $s^2 = 1$. It

is found that when $\sin \theta = 0$, $W_2 = W_4 = W_5 = W_6 = W_7 = 0$,

while $W_3 = P(U_2 - 2U_3)$

$$= \frac{Pa_{\perp}^2 W^0}{2G_0 \tilde{m}^2 c^2} (R_1 G_4^* - R_2 G_5^* - R_3 G_6^*) \quad (2.35)$$

where

$$G_4' = \int_0^{\infty} \xi^3 e^{-(\xi - \xi_0)^2} d\xi$$

$$G_5' = \int_0^{\infty} \xi^3 (\xi - \xi_0) e^{-(\xi - \xi_0)^2} d\xi$$

$$G_6' = \int_0^{\infty} \xi^3 (\xi - \xi_0)^2 e^{-(\xi - \xi_0)^2} d\xi$$

The dispersion equation now reads

$$\xi^3 + \frac{a_{\perp}^2 W^0}{2PG_0 \tilde{m}^2 c^2} (R_1 G_4^* - R_2 G_5^* - R_3 G_6^*) = 0 \quad (2.36)$$

After some simple manipulation, one realizes that equation (2.36) agrees with Zheleznyakov's result (equation (2.12)) if the following assumptions or approximations hold:

- (i) $a_{\perp}^2 G_4^*/G_0 \gg a_{\parallel}^2$
- (ii) $G_4^*/G_0 \gg |(R_1 - 1) G_4^*/G_0 - R_2 G_5^*/G_0 - R_3 G_6^*/G_0|$
- (iii) terms containing $e^{-\xi_0^2}$ are negligible.
- (iv) The terms containing $1/(\omega \tilde{m} - k_{\parallel} \rho_{\parallel}^0 - s \tilde{\omega}_{\mu} \tilde{m})$ are small in comparison to the terms containing $1/(\omega \tilde{m} - k_{\parallel} \rho_{\parallel}^0 - s \tilde{\omega}_{\mu} \tilde{m})^2$.

We consider the validity of the above four approximations now. If the spread in p_{\perp} (specified by a_{\perp}^2) is of the order of the spread in p_{\parallel} (specified by a_{\parallel}^2), we have $G_4^2/G_0 \gg 1$ in cases when the spread in p_{\perp} is not too large. More precisely, we want $S_0 = \frac{p_{\perp}^0}{a_{\perp}} > 1$ (the least value of S_0 should be about 3) in order that (1) is valid. Approximations (ii) and (iii) are taken also by Zheleznyakov and approximation (iv) is the well known assumption in radiative instability problem of a stream-plasma system if the growth rate be small (i.e. $|\omega| \gg |\delta|$).

For another example, we consider the stream to be cold, i.e. $a_{\perp} = a_{\parallel} = 0$, and we have a delta momentum distribution for the particles in the stream. In this case, where the wave-normal angle assumes general values, one has in equation (2.34):

$$W_4 = W_5 = W_6 = W_7 = 0$$

therefore, equation (2.34) reads

$$\delta'^3 + \frac{W_2}{W_1} \delta' + \frac{W_3}{W_1} = 0 \quad (2.37)$$

$$\text{In this particular case } W_2/W_1 = \frac{s J_s^2 \sigma A \beta_{\parallel}^{\circ 2} \cos^2 \theta \left[(s\tilde{\gamma} + \xi)^2 - 1 \right]}{(\xi + \tilde{\gamma}s)^2 \left[\beta_{\parallel}^{\circ 2} \xi^2 \right]}$$

$$\text{and } W_3/W_1 = \frac{\sigma A \left[(s\tilde{\gamma} + \xi)^2 - 1 \right]}{\xi^2 \left[\beta_{\parallel}^{\circ 2} \xi^2 \right]} \left[\frac{J_s'^2 \beta_{\perp}^{\circ 2} + J_s^2 \beta_{\parallel}^{\circ 2} \frac{(s\tilde{\gamma} + \sin^2 \theta \xi)^2}{\sin^2 \theta (s\tilde{\gamma} + \xi)^2}}{P} \right]$$

One sees that this equation is, in fact, exactly the

equation derived in section (B) (equation (2.10a) with the definition of (2.14)). We may, thus, conclude that the dispersion equation derived in this investigation agrees with that obtained by Zheleznyakov on transition from general θ to $\theta = 0^\circ$ or 180° (under the approximations stated), and when the temperature of the stream is taken to zero, the dispersion equation (2.34) is simplified to the one derived in section (B).

Evaluating the coefficients of the dispersion equation (2.34) in the case of VLF emission in the terrestrial magnetosphere indicate that only the first three terms are significant, i.e. the dispersion equation can be approximated to

$$\delta^3 + \frac{W_2}{W_1} \delta + \frac{W_3}{W_1} = 0 \quad (2.38)$$

This is of the same form as the dispersion equation for the case of a strictly helical stream in a magnetoactive plasma as derived in section (B). Hence, if the dispersion equation of the system can be approximated in the form as in equation (2.38), one can have an exact solution for readily by Cardan's method; otherwise, one has to take equation (2.34) and work for complex numerical solutions.

Under different conditions, electromagnetic waves generated by normal or anomalous cyclotron radiation processes by particles in the stream may grow in the stream-magneto-active-plasma system and the power of the waves may be

amplified enormously. This radiative instability may in fact happen in many natural radio emissions in radio astronomy. The study of such instability problem will help to understand various phenomena in plasma radiation.

As far as cyclotron radiation is concerned, the distribution function of the stream considered in section (C) seems to be a realistic and important one. However, when "almost mono-energetic streams" are present as in the case of VLF emissions in the terrestrial magnetosphere, distribution of electron stream described by relation (2.4) becomes more convenient in application on account of the simplicity in the corresponding dispersion equation. The general qualitative behaviour of the stream-plasma system is the same if the spread in momentum distribution of the stream is not too wide⁺.

(D) The "Negative-Absorption" Approach in Solving the Instability Problem

The discussions in the previous sections are based on the classical kinetic treatment. We will consider below the

⁺When the momentum spread is wide, the bandwidth of emission will be broad and the harmonics may not be resolved.

general deductions from another approach.

Twiss (1958) employed the quantum formulation for deriving the macroscopic radio absorption coefficient⁺ and indicated that amplification of waves occur when the absorption coefficient is negative. The conditions for negative absorption are given in terms of energy distribution $F(\epsilon)$ of the source electrons and the mean electron emissivity $Q(\epsilon)$ for the effective radiating mechanism in concern. Here $Q(\epsilon)$ is defined as the mean power delivered by each electron of energy ϵ per unit time per unit frequency interval in one polarization per unit solid angle into any direction.

Smerd (1963) then developed the theory and derived the general expression for the absorption coefficient K in an anisotropic medium. Defining $g(\epsilon) d\epsilon$ as the statistical weight of energy levels, Smerd obtained two necessary conditions for amplification to occur:

- (i) A positive gradient in the electron energy distribution $F(\epsilon)$.
- (ii) A negative gradient in $g(\epsilon) Q(\epsilon)$.

Assuming that the refractive index is equal to 1, the above

⁺A quantity defined as the difference between the total stimulated absorption and the total stimulated emissions.

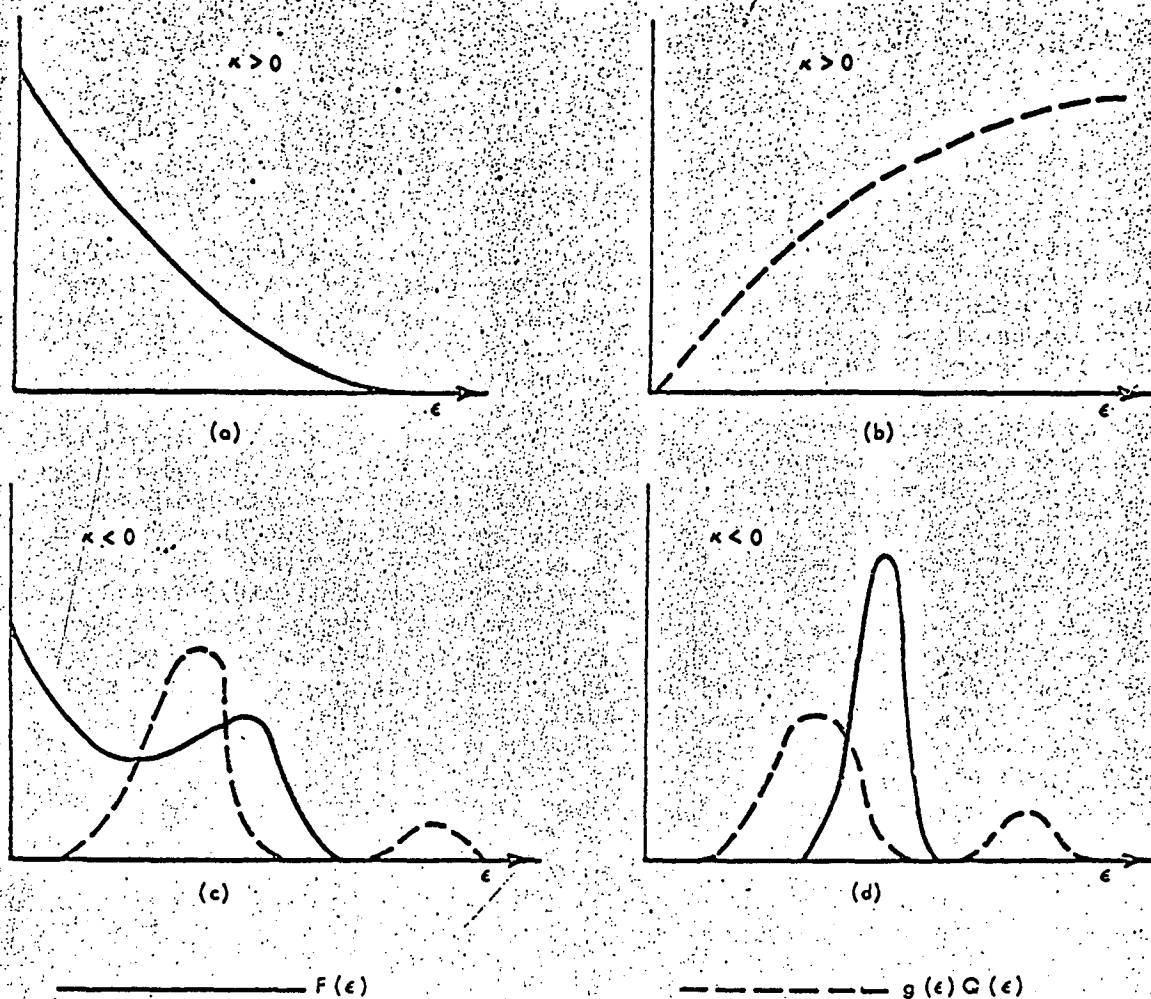
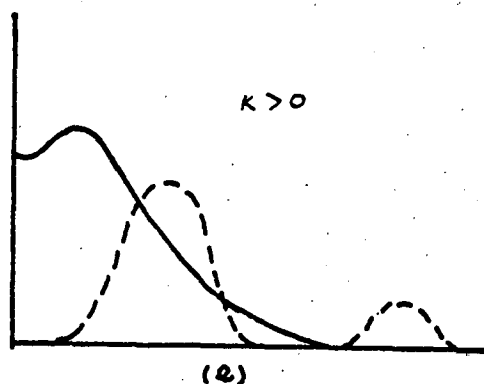


FIGURE 2.1 Examples of electron energy distributions $F(\epsilon)$, the product of statistical weight $g(\epsilon)$, and electron emissivity, $Q_F(\epsilon)$, which lead to positive and negative absorption. (a) Positive absorption when $dF/d\epsilon$ is negative; a thermal source of radiation is an example. (b) Positive absorption when $(d/d\epsilon) [g(\epsilon) Q_F(\epsilon)]$ is positive; bremsstrahlung is an example. (c) and (d) Two situations which lead to negative absorption where $dF/d\epsilon$ is positive and $(d/d\epsilon) [g(\epsilon) Q_F(\epsilon)]$ is negative as in conditions (a) and (b); this can apply to gyro-radiation.

(Smerd, 1963). (e) Positive absorption for gyro-radiation (harmonic resonance absorption).



idea about the conditions for negative absorption is illustrated in Fig. 2.1(a) - (d). Note that in Fig. 2.1(c), the electron energy distribution can be considered to be composed of a Maxwellian background plasma and a stream with quite wide momentum spread. If $F(\epsilon)$ and $g(\epsilon)$ $Q(\epsilon)$ vary with ϵ as in Fig. 2.1(e), positive absorption will result. We see, therefore, that either amplification or absorption can take place for a particular type of generating mechanism, depending on the distribution function of the system. Whereas a stream gyrating in a cold magnetoactive plasma can give rise to cyclotron instability and amplification as discussed in sections (B) and (C), transverse electromagnetic waves can be absorbed in a Maxwellian or cold magnetoactive plasma due to the fact that the total stimulated absorption exceeds the total stimulated emission. This collisionless absorption is called harmonic resonance absorption and will be discussed again in chapter VIII.

(E) Two Types of Instability

Twiss (1952) pointed out that the general conclusions of instability from studying the dispersion equation could be misleading; for instance, it may not be possible to distinguish an apparent wave growth in one direction from an actual damping of the reflected wave in the opposite direction without introducing the appropriate initial and

boundary conditions. To overcome the above difficulty, Sturrock (1958) put forward an elegant method by which it is possible to distinguish amplifying from evanescent waves by investigation of the dispersion equation alone.

In discussing simple dynamical systems, one interprets the existence of a normal mode which grows exponentially in time as signifying that the system cannot persist in a quiescent state, since arbitrarily small initial disturbances will lead to the generation of large scale disturbances. Theoretical analysis of the travelling-wave or two-stream amplifier (Pierce, 1950) shows the existence of time growing modes, but we know experimentally that such systems can persist in a quiescent state. The backward-wave oscillator (Bech, 1958), on the other hand, will not remain in a quiescent state. Based on the above ideas, Sturrock (1958) went on to study the kinematics of a growing system and found that in general there are two types of instability:

(i) Convective Instability

If a propagating system exhibits convective instability, a finite length of the system may persist in a quiescent state, even in the presence of small random disturbances, since these disturbances, although amplified, are carried away from the region in which they originate. Such systems may be used as amplifiers.

(ii) Nonconvective or Absolute Instability

If a propagating system exhibits nonconvective instability, an arbitrary perturbation of the system will give rise to a disturbance which grows in amplitude at the point at which the perturbation originated; we also expect that the disturbance will spread until it extends over an arbitrary large region of the system. Such system may be used as oscillators.

Assuming $\theta = 0^\circ$ or 180° , it has been found by Sturrock's method that the Cerenkov, anomalous cyclotron and forward cyclotron ($\theta < 90^\circ$) instabilities are convective whereas the backward cyclotron ($\theta > 90^\circ$) instability is nonconvective.

(F) Conclusions

Even though the instability theory of a stream-plasma has been solved for general θ , it is by no means the end of our study on this subject. It will be fruitful in the future to carry out research on the correspondence between the kinetic approach and the negative-absorption approach. In the kinetic treatment we have assign the boundary conditions for growing waves: $f_1(\bar{p}, \bar{r}, t) \rightarrow 0$ as $t \rightarrow -\infty$. Now if we have the reverse boundary conditions, i.e.

$f_1(\bar{p}, \bar{r}, t) \longrightarrow 0$ as $t \longrightarrow \infty$ for the dielectric tensor, we are looking for a damping wave and it will be interesting to calculate the damping coefficient to see whether it is of any significant value compared to the excitation coefficient, for the purpose of checking our theory. Moreover, we have employed the linearized theory so far, i.e. the distribution function associated with the electromagnetic disturbance $f_1(\bar{p}, \bar{r}, t)$ is assumed to be small compared to the unperturbed distribution function $f_0(\bar{r}, \bar{p})$. This assumption holds only when the growth or damping is small, so that, the energy of the electrons in the stream remain practically constant. Therefore, strictly speaking, the linearized theory is valid at the onset of the excitation process only. The nonlinear instability theory for general θ for various radiating systems will be a challenging problem in plasma physics. In fact, pioneering work in this topic has been started a few years ago (e.g. Shapiro and Shevchenko, 1962; Engel, 1965; Shapiro, 1963; Fainberg and Shapiro, 1965).

It should be remarked that a radiative instability is in fact in the macroscopic sense a tendency to coherent radiation, i.e. more and more particles in the system will radiate in phase. In a birefringent medium like a magneto-active plasma, it is, thus, possible that both the o- and x-mode waves are excited at the same time.

CHAPTER III

AMPLIFICATION OF FORWARD-SHIFTED CYCLOTRON RADIATION IN THE EXTRAORDINARY-MODE AND ITS APPLICATION TO JUPITER'S DECAMETRIC EMISSIONS

(A) Introduction

Since most planets are radio inactive, intense emissions in the decametric range from Jupiter have aroused great excitement in the late years (Shain, 1956; Gardner and Shain, 1958; Smith and Douglas, 1959; Warwick, 1961; Carr et al, 1961; Barrow, 1962; Ellis, 1962a). The dynamic spectra of the decametric emissions show the form of bursts with a duration of about 0.2 sec. onwards, with a minimum bandwidth of about 1 Mc/s. The centre frequency of an event changes in time in the upward sense (frequency increases in the course of time) or downward sense, and the frequency range extends from a few Mc/s to more than 35 Mc/s. Among the proposed theories to explain this phenomenon (Gardner and Shain, 1958; Zheleznyakov, 1958; Warwick, 1963), the cyclotron theory put forward by Ellis (1962) is the most plausible one. This theory was studied in detail later by Ellis (1963), and Ellis and McCulloch (1963); very good agreements between observations and theoretical predictions are found. By that time, a

stream-plasma system has already found to be unstable, but the instability theory for general emission angle has not been derived. Eidman derived the expression for the power spectrum radiated by a single electron in a magnetoactive plasma in 1958^{*}, hence, the only existing knowledge concerning radiation from gyrating electron bunches or electron streams was the radiation spectrum from a single electron. Ellis and McCulloch used the property of the radiation pattern from a single electron, together with the focussing effects in the magnetoactive plasma, to explain the existence of an emission cone which is necessary to explain what is observed. If we assume all the electrons radiate incoherently, we are forced to assume that there^{are} about 10^5 electrons per cm^3 in the radiating bunch. Comparing to electron stream density of the order of 10^{-4} el/ cm^3 observed in the terrestrial magnetosphere, it is, thus, not probable to have such dense electron bunches existing in an exospheric ionized medium which is taken to be similar to that of the Earth. We are led to the conclusion that in order to explain the observed high intensity, at least some of the electrons must be radiating coherently. When some particles are radiating coherently, the emitted wave may induce other particles to radiate in phase, so that, more particles are

^{*}The equation derived by Eidman was found later to contain a few errors by Liemohn (1965).

radiating coherently. For an observer outside the stream-plasma system, the amplitude of the wave is observed to be growing; the system is radiatively unstable. A mathematical treatment of the instability theory has been given in chapter II. It is found that waves emitted by the cyclotron radiation mechanism can be unstable in a stream-plasma system if the momentum spread of the stream is not too wide. In order to study the significance of the growing process and to investigate the behaviour of the growth with respect to emission direction, we will evaluate the growth rate for parameters appropriate to Jovian decametric bursts emission in this chapter. The mode of wave considered in this chapter is a x-mode wave the frequency of which is Doppler-shifted in the forward direction, as suggested by Ellis.

(D) Theory and Analysis

Ellis and McCulloch assume that due to disturbances near the outer boundary of the Jovian exosphere, bunches or streams of electrons are accelerated and, thereafter, travel down the high-latitude field lines. Those electrons travel at almost the same velocity and pitch angle will form a stream having a small spread in momentum distribution. Since very narrow-

band emissions ($\Delta f/f \sim 0.1$) are observed in many cases, the spread in momentum distribution of the streams must be very narrow in these circumstances. For simplicity in calculation, and without loss of generality in behaviour, we will assume the radiators to form a helical electron stream. In the case we are considering, the wave and ray are moving in the forward direction. In the kinematics terminology of a radiative unstable system, the instability of normal cyclotron waves in the forward direction is convective (e.g. Neufeld and Wright, 1964a): the amplitude of the electromagnetic disturbance increases as it is carried along the system and the amplitude remains finite at each point. Hence, both the concept of growth in time (excitation) and the concept of growth in distance (amplification) have real physical meaning.

The Jovian exospheric plasma is assumed to be cold and magnetoactive. Neglecting the effects of heavy positive ions, the refractive index for an electromagnetic wave in the background plasma alone is given by the Appleton-Hartree relation:

$$n_j^2 = 1 - \frac{X(1-X)}{1-X - \frac{1}{2}\sin^2\theta Y^2 \mp \sqrt{\frac{\sin^4\theta}{4} Y^4 + (1-X)^2 \cos^2\theta Y^2}}$$

where $X = \omega_p^2/\omega^2$ $Y = |\omega_H|/\omega$

ω_p = angular plasma frequency

ω = angular wave frequency

ω_H = angular plasma gyro-frequency

Taking the negative sign before the discriminant, one has the refractive index expression for the x-mode.

With the definition of n_j given by (3.1), we have in equation (2.10a)

$$\left(\frac{\partial F_p}{\partial \omega}\right)_{\tilde{\omega}} = -2\tilde{\omega} + \frac{\omega_p^2 L}{\tilde{\omega}} \quad (3.2)$$

where
$$L = \frac{\frac{2A}{\xi^2} D - \left(1 - \frac{A}{\xi^2}\right) \left\{ \frac{2A}{\xi^2} + \frac{\sin^2 \theta}{\xi^2} - B^{-1/2} \left[-\frac{\sin^4 \theta}{\xi^4} + \frac{4A \cos^2 \theta}{\xi^4} \left(1 - \frac{A}{\xi^2}\right) - \frac{2 \cos^2 \theta}{\xi^2} \left(1 - \frac{A}{\xi^2}\right)^2 \right] \right\}}{D^2}$$

$$D = 1 - \frac{A}{\xi^2} - \frac{\sin^2 \theta}{2\xi^2} - B^{\frac{1}{2}}$$

$$B = \frac{\sin^4 \theta}{4\xi^4} + \left(1 - \frac{A}{\xi^2}\right)^2 \frac{\cos^2 \theta}{\xi^2}$$

Using relations (3.2) and (2.14), after some manipulation, equation (2.10a) is re-arranged into:

$$\left(\frac{\delta}{\tilde{\omega}}\right)^3 + b \left(\frac{\delta}{\tilde{\omega}}\right) + d = 0 \quad (3.3)$$

where $b = -\sigma A J_s^2 \left[\frac{(s\gamma - \xi)^2}{\beta_{||}^2 \xi^2} - 1 \right] \frac{\beta_{||}^2 \cos^2 \theta}{(\xi - s\gamma)^2}$

and $d = \sigma A \left[\frac{(s\gamma - \xi)^2}{\beta_{||}^2 \xi^2} - 1 \right] \frac{\left[J_s'^2 \beta_{\perp}^2 + J_s^2 \beta_{||}^2 \frac{(s\gamma - \sin^2 \theta \xi)^2}{\sin^2 \theta (s\gamma - \xi)^2} \right]}{(AL - 2\xi^2)}$

with $\sigma = \omega_o^2 / \omega_p^2$ = density of stream/density of ambient plasma

We note here that the harmonic number s and the argument of Bessel's function a have been transformed into positive numbers.

The quantity $\Lambda = \omega_p^2 / \omega_H^2$ describes the relative importance of the plasma frequency and the gyro-frequency in a magnetoactive plasma. Following the model of Jovian exosphere as proposed by Ellis (1962), a typical value of Λ at the source region is 0.03. Before solving for the imaginary part of angular wave frequency $\Im_m \delta$, we must find the characteristic angular frequency $\tilde{\omega}$, which is real. This is done by solving the Doppler equation

$$\tilde{\omega} - k_{||} v_{||} - s\gamma |\omega_H| = 0 \quad (3.4)$$

and relation (3.1) simultaneously. In doing so for $s = 1$, for small values of $\Lambda (< 0.2)$, there exists a cut-off angle θ_c greater than which no real solution can be found for $\tilde{\omega}$ (Ellis, 1962; Ellis and McCulloch, 1963). The angle θ_c ,

therefore, forms the surface of a solid cone within which radiation in the fundamental harmonic is allowed. For higher harmonics, i.e. $s \geq 2$, this restriction need not exist. One example of the frequency-wave-normal angle plot appropriate to the Jovian magnetosphere is given in Fig. 3.1.

The growth rate can then be calculated from equation (3.3):

$$\Im_m\left(\frac{\delta}{\tilde{\omega}}\right) = \pm \frac{\sqrt{3}}{2} (M^{1/3} - C^{1/3}) \quad (3.5)$$

where

$$M = -\frac{d}{2} + \sqrt{\frac{d^2}{4} + \frac{b^3}{27}}$$

$$C = -\frac{d}{2} - \sqrt{\frac{d^2}{4} + \frac{b^3}{27}}$$

We can also take the quantity

$$\left| \frac{\Im_m \delta}{\omega_H} \right| = \xi \left| \frac{\Im_m \delta}{\tilde{\omega}} \right|$$

to specify the growth rate. Fig. 3.2 gives graphs of the quantity $\left| \frac{\Im_m \delta}{\omega_H} \right|$ vs wave-normal θ for different values of energies and pitch angles of the electron stream appropriate to the theory suggested by Ellis (1963), where the Jovian magnetosphere is specified by the quantity $A = 0.03$, and the density of the stream is specified by $\sigma = \text{density of stream} / \text{density of ambient plasma} = 10^{-7}$. If P_0 be the power of the electromagnetic wave at time $t = 0$ and P be the

power after 1 msec., we can calculate the db power gain ($= 10 \log_{10}(P/P_0)$) as a function of wave-normal angle θ , taking the electron gyro-frequency to be $|\omega_H| = |\omega_H|/2\pi = 5 \text{ Mc/s}$; Fig. 3.3 show these graphs. The relation of the angle of maximum growth rate θ_m and the pitch angle of the stream ϕ for the fundamental harmonic is shown in Fig. 3.4 for $\beta_{\perp} = 0.1, 0.2$. To indicate how the pitch angle ϕ and the angle of maximum growth rate θ_m behave with respect to change of cut-off angle θ_c for the fundamental harmonic, we have Fig. 3.5 and 3.6. The relation of $(\theta_c - \theta_m)$ and pitch angle ϕ is shown in Fig. 3.7 indicating the fact that for a constant value of β_{\perp} , the growth rate maximizes at an angle close to the cut-off angle when the pitch angle is small. To illustrate how the growth rate and power gain varies with the normalized frequency $\xi = \frac{\tilde{\omega}}{|\omega_H|}$ and hence, to estimate the band width of emission, we have Fig. 3.8 and 3.9.

(C) Discussions

It has been assumed in the cyclotron theory that the electron density in the Jovian exosphere is nearly proportional to magnetic intensity H , so that planes of

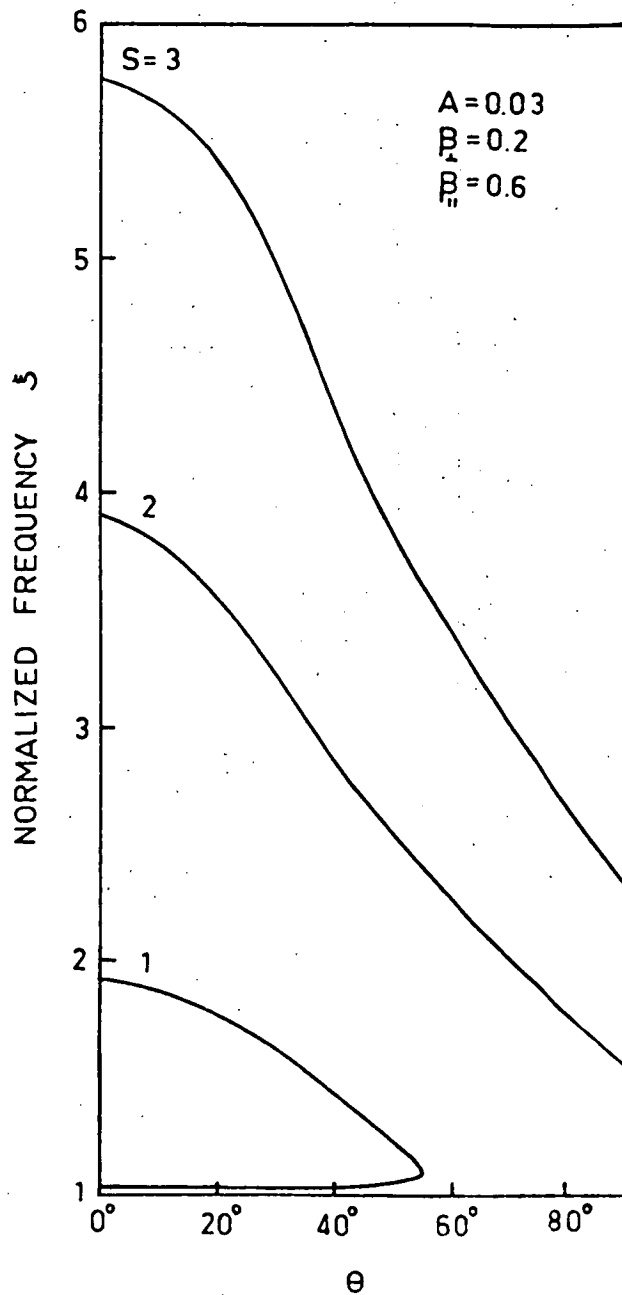


FIG 3.1 NORMALIZED FREQUENCY VS WAVE-NORMAL ANGLE θ

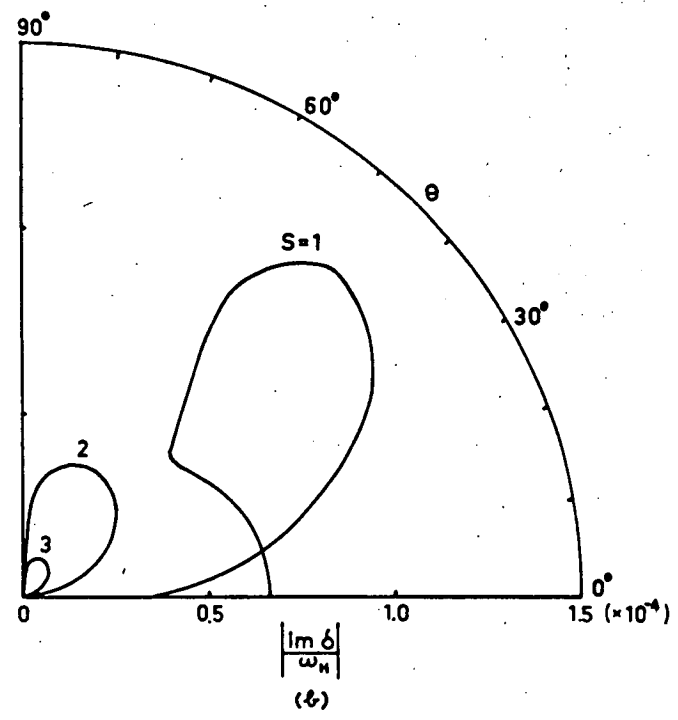
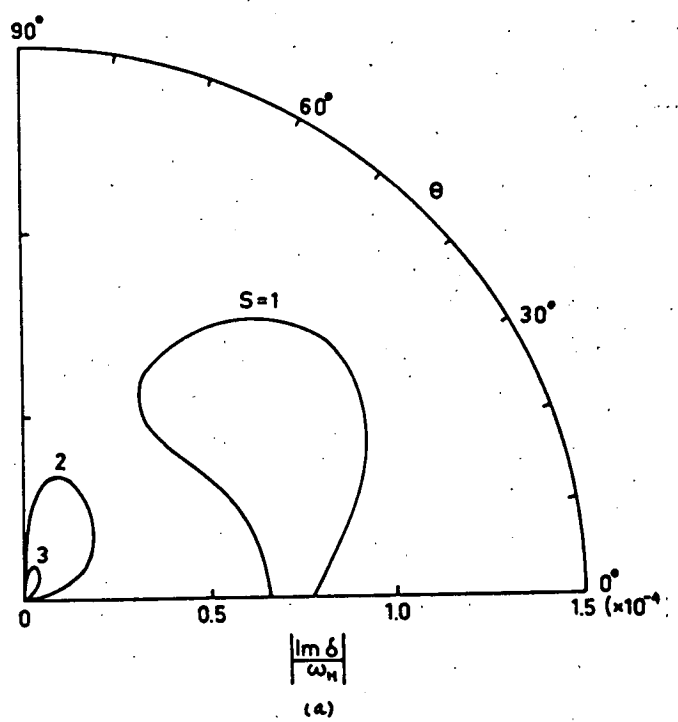


FIG. 3.2 THE DEPENDENCE OF THE GROWTH RATE $\frac{|\text{Im } \delta|}{\omega_H}$ ON WAVE-NORMAL ANGLE θ FOR $A = \omega_p^2/\omega_H^2 = 0.03$, $\sigma = \omega_o^2/\omega_p^2 = 10^{-7}$, HARMONIC $S = 1, 2, 3$, AND (a) $\beta_\perp = 0.1$, $\beta_\parallel = 0.2$ (ENERGY $E = 13.5 \text{ KeV}$, PITCH ANGLE $\phi = 26^\circ 36'$) (b) $\beta_\perp = 0.1$, $\beta_\parallel = 0.5$ (ENERGY $E = 82.5 \text{ KeV}$, PITCH ANGLE $\phi = 11^\circ 18'$).

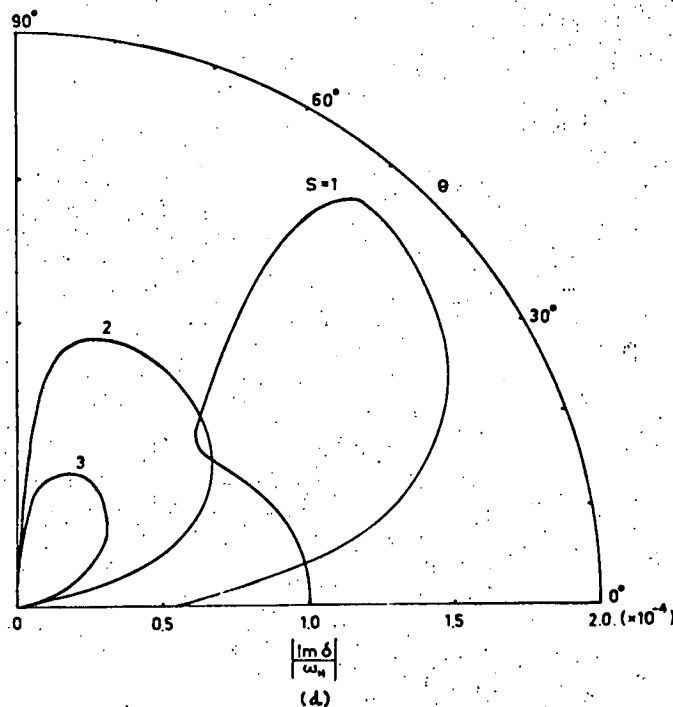
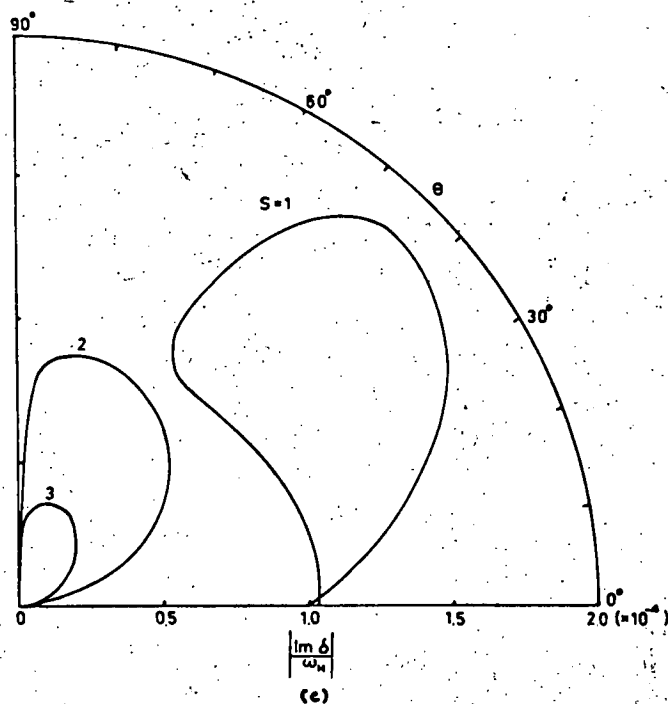


FIG 3.2 THE DEPENDENCE OF THE GROWTH RATE $\frac{|\text{Im } \delta|}{\omega_M}$ ON WAVE-NORMAL ANGLE θ FOR $A = \omega_p^2/\omega_M^2 = 0.03$, $\sigma = \omega_c^2/\omega_p^2 = 10^{-1}$, HARMONIC $s = 1, 2, 3$, AND
 (c) $\beta_{\perp} = 0.2$, $\beta_{\parallel} = 0.35$ (ENERGY $E = 47$ Kev, PITCH ANGLE $\Phi = 29^\circ 46'$)
 (d) $\beta_{\perp} = 0.2$, $\beta_{\parallel} = 0.6$ (ENERGY $E = 150$ Kev, PITCH ANGLE $\Phi = 18^\circ 26'$)

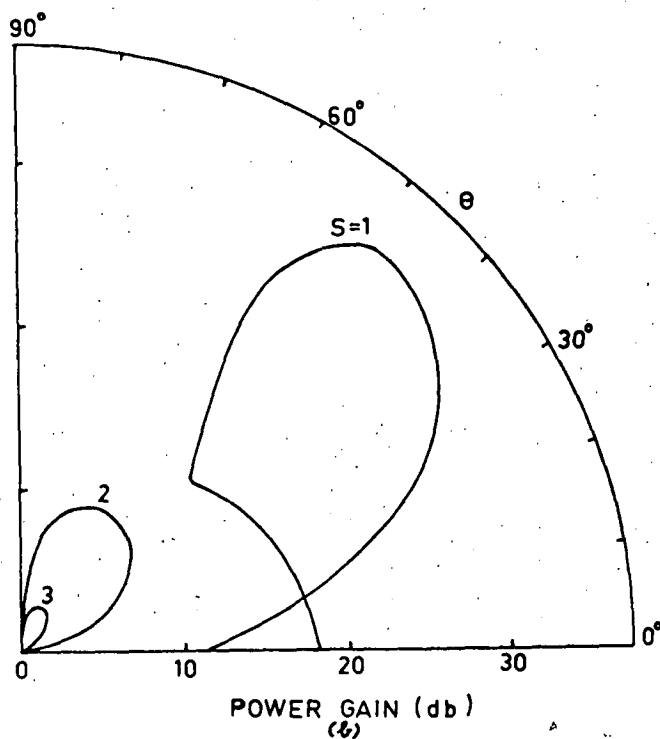
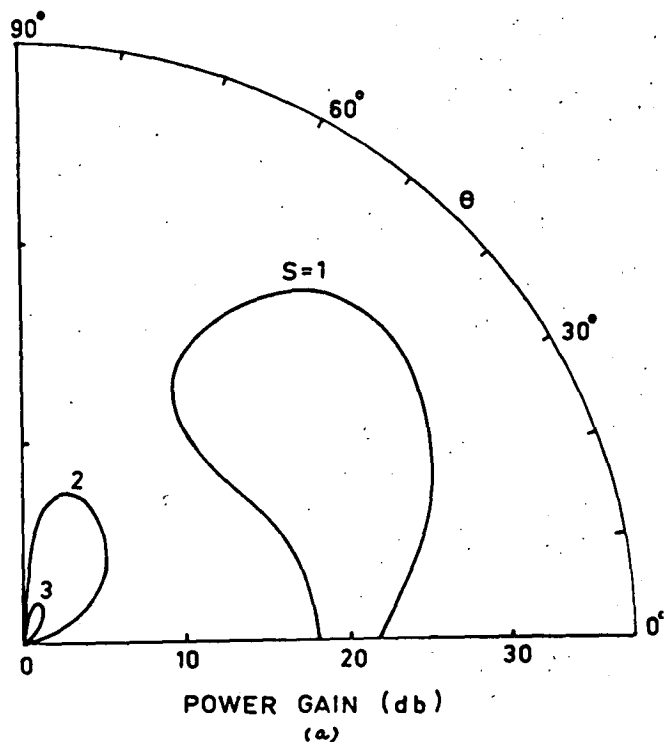


FIG 3.3 THE DEPENDENCE OF POWER GAIN IN db AFTER 1 msec ON WAVE-NORMAL ANGLE θ FOR $A = \omega_p^2/\omega_n^2 = 0.03$, $\sigma = \omega_0^2/\omega_p^2 = 10^{-7}$, HARMONIC $s = 1, 2, 3$, GYRO-FREQUENCY $|\omega_n| = 5 M\omega_p$, AND
 (a) $\beta_\perp = 0.1$, $\beta_\parallel = 0.2$ (b) $\beta_\perp = 0.1$, $\beta_\parallel = 0.5$.

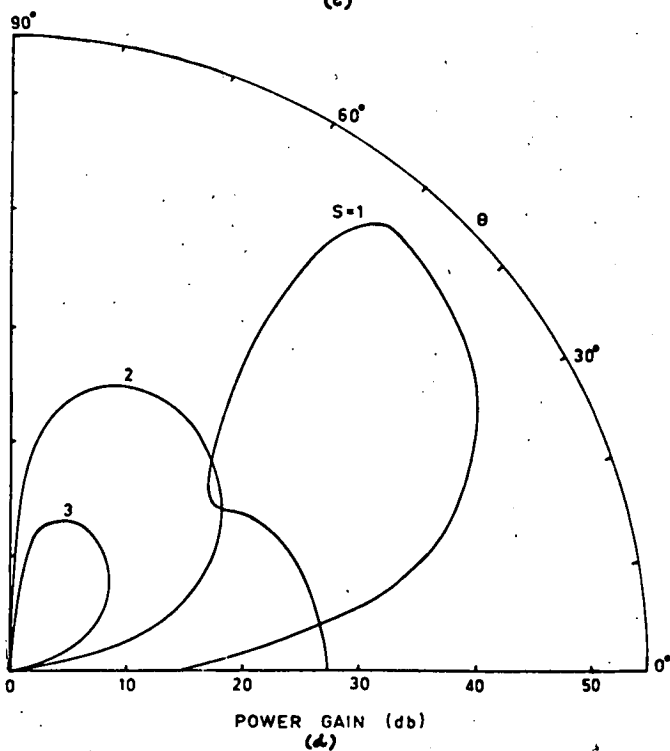
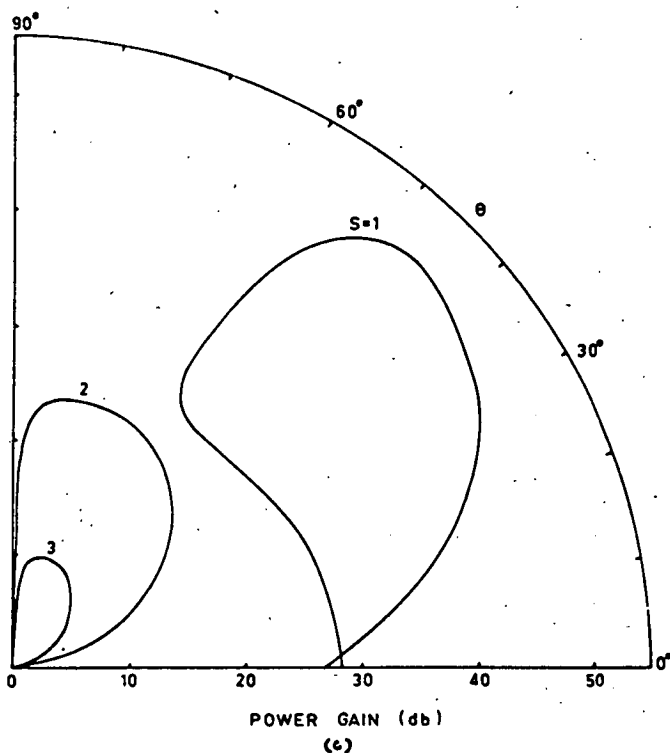


FIG 3.3 THE DEPENDENCE OF POWER GAIN IN db AFTER 1 msec ON WAVE-NORMAL ANGLE θ FOR $A = \omega_p^2/\omega_n^2 = 0.03$, $\sigma = \omega_0^2/\omega_p^2 = 10^{-7}$, HARMONIC $s = 1, 2, 3$, GYRO-FREQUENCY $|f_n| = 5 \text{ Mc/s}$, AND
 (c) $\beta_1 = 0.2$, $\beta_{11} = 0.35$ (d) $\beta_1 = 0.2$, $\beta_{11} = 0.6$.

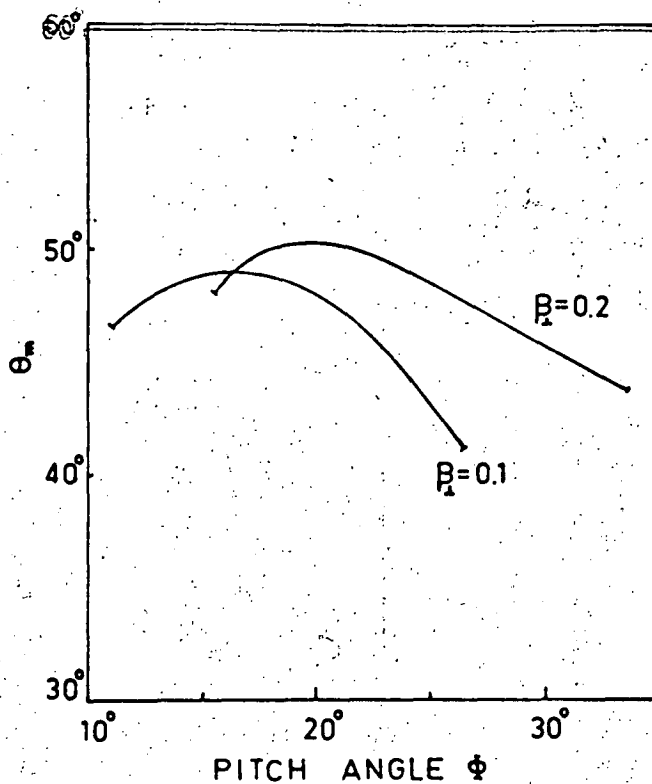


FIG 3.4 THE RELATION OF THE ANGLE OF MAXIMUM GROWTH RATE Θ_m AND THE PITCH ANGLE OF THE STREAM Φ FOR THE FUNDAMENTAL HARMONIC, $A = 0.03$, $\sigma = 10^{-7}$, $\beta_1 = 0.1, 0.2$.

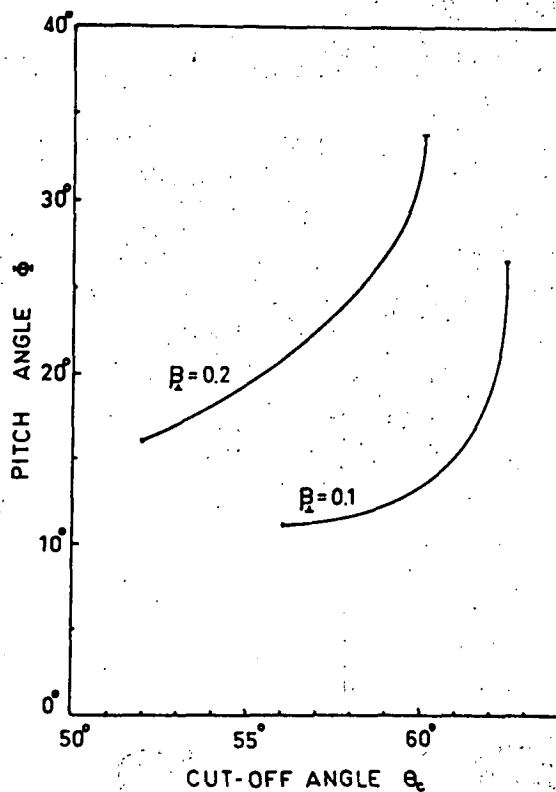


FIG 3.5 THE RELATION OF THE PITCH ANGLE OF THE STREAM Φ AND THE CUT-OFF ANGLE Θ_c FOR THE FUNDAMENTAL HARMONIC, $A = 0.03$, $\beta_1 = 0.1, 0.2$.

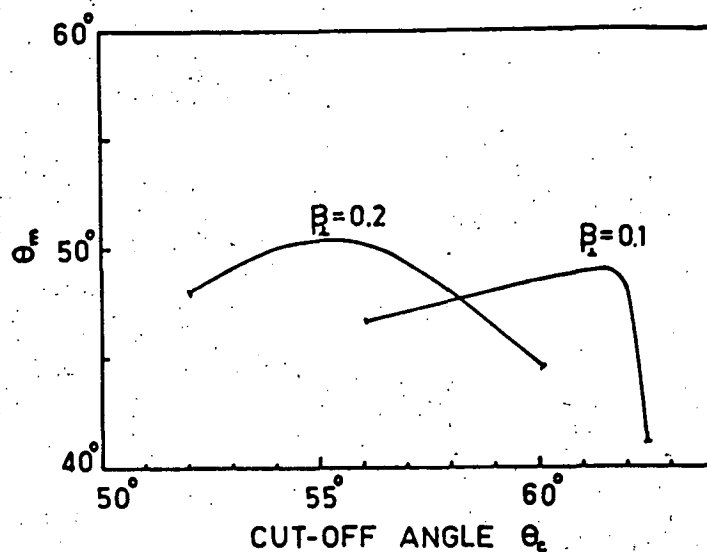


FIG 3.6 THE RELATION OF THE ANGLE OF MAXIMUM GROWTH RATE θ_m AND THE CUT-OFF ANGLE θ_c FOR $s = 1$, $A = 0.03$, AND $\beta_1 = 0.1, 0.2$.

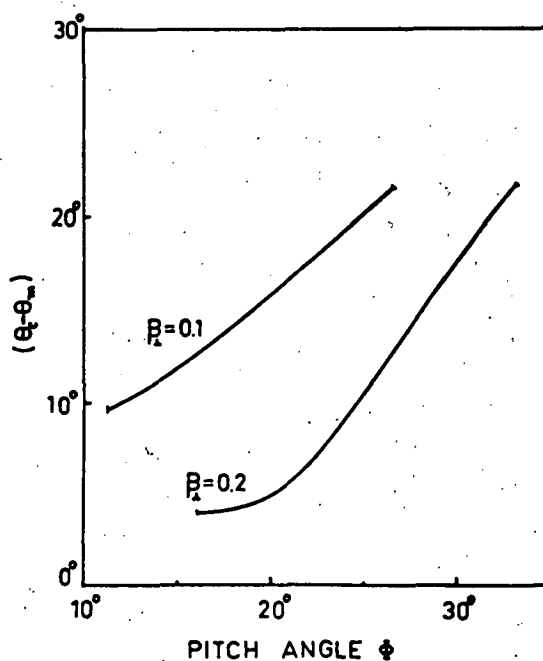


FIG 3.7 THE DEPENDENCE OF THE QUANTITY $(\theta_c - \theta_m)$ ON THE PITCH ANGLE OF THE STREAM ϕ FOR $A = 0.03$, $\beta_1 = 0.1, 0.2$.

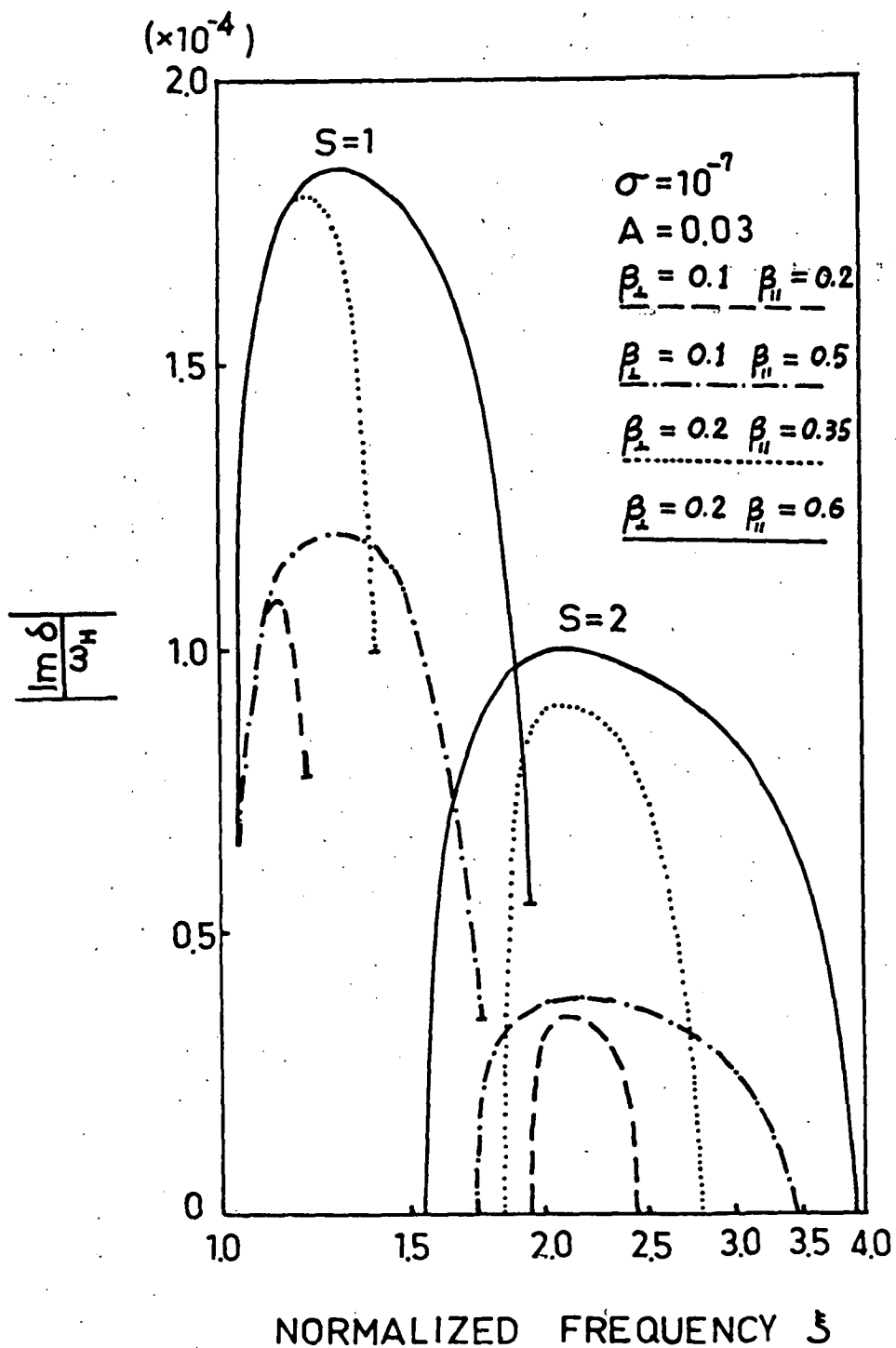


FIG. 3.8 GROWTH RATE $|\text{Im } \delta|/\omega_H$ VS NORMALIZED FREQUENCY ξ FOR $A = 0.03$, $\sigma = 10^{-7}$, HARMONIC $s = 1, 2$ AND $\beta_{\perp} = 0.1, \beta_{||} = 0.2$; $\beta_{\perp} = 0.1, \beta_{||} = 0.5$; $\beta_{\perp} = 0.2, \beta_{||} = 0.35$; $\beta_{\perp} = 0.2, \beta_{||} = 0.6$.

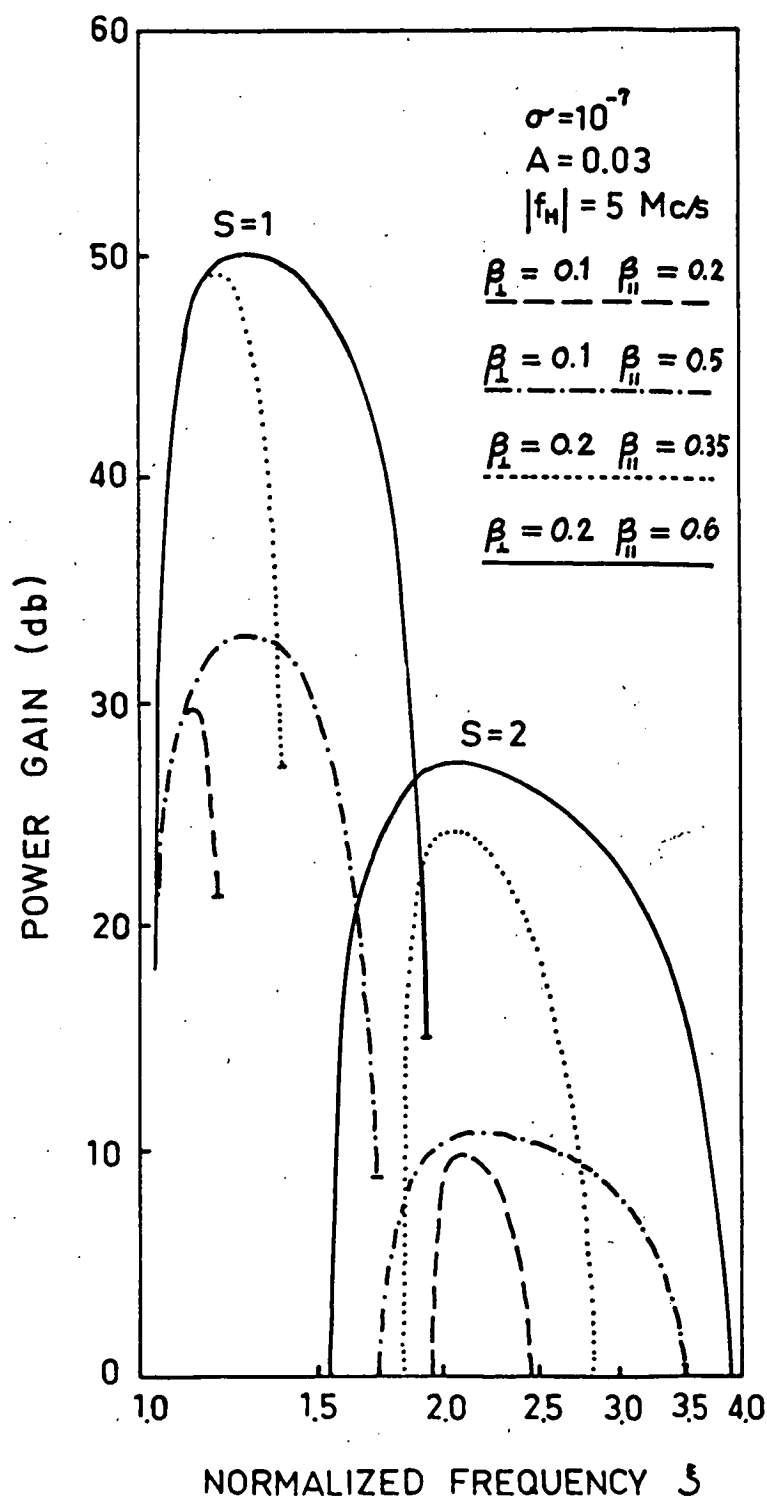


FIG 3.9 POWER GAIN IN db AFTER 1 msec VS NORMALIZED FREQUENCY ξ FOR $A = 0.03$, $\sigma = 10^{-7}$, GYRO-FREQUENCY $|f_H| = 5 \text{ Mc/s}$, HARMONIC $s = 1, 2$ AND DIFFERENT VELOCITIES AS INDICATED.

constant refractive index will be normal to H vector and the final direction of the radiation after refraction is approximately given by

$$\sin \alpha = n_j \sin \theta \quad (3.6)$$

where α is the wave-normal angle after refraction. Consequently, the initially power $W(\theta)$ radiated by a single electron will be modified by refraction and focussing effects in the magnetoactive plasma and the final distribution of power $W(\alpha)$ will be given by

$$W(\theta) d\theta = W(\alpha) d\alpha \quad (3.7)$$

From the relation of α and θ , it occurs that $(\frac{d\alpha}{d\theta})_{\alpha_{max}} \sim 0$ for a range of θ so that the radiation within this range of θ ($\sim 15^\circ$) will be confined to a direction $\alpha = \alpha_{max}$ after refraction. It was assumed that the greatest amount of power per unit solid angle is emitted at $\alpha = \alpha_{max}$ and for other directions there is negligible radiation. However, we note that the polar diagram of radiation considered was that for a single electron. When there is a bunch or stream radiates, it absorbs radiation, and re-radiates, so that, the polar plot of radiation may have a different appearance than that

calculated for single electron.

In this chapter, we have found that for the fundamental harmonic the growth rate maximises at θ_m where θ_m ranges from about 40° to 50° for values of pitch angle, energy and model of Jovian magnetosphere appropriate to that suggested by Ellis. In fact, θ_m has been found to occur close to α_{max} , so that, after refraction almost all the radiated energy is concentrated at α_{max} . That is, the angular distribution of the radiation used by Ellis would appear to be justified by the results of the present investigation.

From Fig. 3.9, we observe that the half-power bandwidth before refraction ranges from about 0.08ξ to 0.45ξ , for the first harmonic. This result is consistent with the observed bandwidth. The corresponding bandwidth for the second harmonic is in general a few times larger. It should be remarked that in Fig. 3.8 and 3.9 the range of frequency excited corresponds to different directions. However, as waves in a cone of about 15° centred at θ_m initially will be confined to almost one direction (α_{max}) after refraction in the Jovian magnetosphere, the above estimated bandwidth is the bandwidth that would be received.

Among the higher harmonics, the growth rate of the second harmonic can assume significant values only when the energy of the electron is high. (It should be noted

that we consider energy greater than 100 Kev. to be high in this context. When the energy is greater than several hundred Kev. synchrotron radiation occurs and the situation will be different.) Thus, for a more energetic stream, we may have two bands of frequencies excited simultaneously, the ratio of the two centre-frequencies being always less than 2 (~ 1.6) and the second harmonic carries less energy and broader bandwidth. The growth rate for the third harmonic is seen to be negligible.

Under the above formulation, the growing factor is $e^{|S_m \delta| t}$. It is well known that in an anisotropic medium (e.g. magnetoactive plasma) the directions of the phase velocity of the wave and the group velocity of the wave packet do not, in general, coincide. A wave packet grows in the course of time as $e^{|S_m \delta| t}$ is moving in space along the direction of the group v_{gp} , say, the z' direction, and will be growing in space as $e^{|S_m \delta| z' / v_{gp}}$. Along the direction of the wave vector \vec{k} (z direction) the growing factor is

$$e^{qz} = e^{|S_m \delta| z / [v_{gp} \cos(\vec{k}, \vec{v}_{gp})]} \quad (3.8)$$

where q is the growth rate in space. It can be shown that (Ginzburg, 1964)

$$\frac{1}{v_{gp} \cos(\vec{k}, \vec{v}_{gp})} = \frac{1}{c} \cdot \frac{d(\omega n_z)}{d\omega} \quad (3.9)$$

One then finds that

$$q = \frac{|g_m \delta|}{c} \left\{ n_j + \frac{A}{n_j \xi^2} \left[\frac{2(1 - \frac{2A}{\xi^2})D + (1 - \frac{A}{\xi^2}) \left(\frac{2A}{\xi^2} + \frac{\sin^2 \theta}{\xi^2} - \frac{E}{2B^{1/2}} \right)}{D^2} \right] \right\} \quad (3.10)$$

where n_j is given by relation (3.1), D , B as defined under equation (3.2), and E is given by

$$E = - \frac{\sin^4 \theta}{\xi^4} - 2 \frac{\cos^2 \theta}{\xi^2} \left(1 - \frac{2A}{\xi^2} \right) \left(1 - \frac{3A}{\xi^2} \right)$$

Knowing the growth rate in time, we can thus calculate the growth in space readily.

If we assume that the density of the helical electron stream causing Jupiter's burst radiation is the same as that observed in the terrestrial magnetosphere, namely, $10^{-4}/\text{cm}^3$, and the density of the background plasma to be of the order of $10^3/\text{cm}^3$ as estimated by Ellis and McCulloch, we can then estimate roughly what magnitude of power gain is needed in order to account for the high flux intensity observed on the Earth — 10^{-21} watts $\text{m}^{-2}/(\text{c/s})$, for frequency $\sim 5 \text{ Mc/s}$.

Let us suppose that for a particular frequency the radiating part of the stream has a cross-sectional area of 10^5 Km^2 and a length of 600 Km. Total number of electrons radiating is then 6×10^{18} . With the knowledge of the order of magnitude of $\left| \frac{g_m \delta}{\omega_H} \right|$, the maximum power gain after an interaction length of 600 Km. can be calculated from relation

(3.10) and it is found to be of the order of 10^{10} . The maximum power radiated by a single electron for a frequency of 5 Mc/s in the forward x-mode is about 4×10^{-23} watts/sterad. Confining radiation to a solid cone of 15° , the total power radiated by the stream for a particular frequency after amplification is about 6×10^{15} watts. It has been pointed out that the power radiated initially in a range of 15° will be confined to about 1° after focussing in the ionized medium. For a frequency ~ 5 Mc/s, the theoretical flux density received on the Earth will be of the order of 10^{-21} watts $M^{-2}/(c/s)$.

The above estimate indicates that in order to produce the observed high intensity of radiation, the interaction distance needed is ~ 600 Km. or alternatively the interaction time needed is < 10 msec.

Finally, we note that with a model of Jovian magnetosphere as set out by Ellis (A ranges from 1.6×10^{-3} to 9×10^{-2}), the value of K at the source region is small for the fundamental harmonic radiation ($f \sim f_H$):

$$K = \frac{f_p^2}{f^2}$$

$$\sim \frac{f_p^2}{f_H^2}$$

$$= A$$

$$\sim 1.6 \times 10^3 \text{ --- } 9 \times 10^{-2}$$

With such small values of X , the harmonic resonance absorption⁺ for the x-mode is small unless θ is very large ($\theta > 70^\circ$, say), while that for the o-mode is entirely negligible (Gershman, 1960). Since the radiation power for the x-mode is about one to two orders of magnitude larger than that of the o-mode, the radiation received will be predominant in the x-mode in this case. Here, of course, the source position for a particular frequency must be situated above the reflection level $X = 1 - Y$ in order that the radiation may escape.

⁺The basic concept of harmonic resonance absorption is discussed in chapters I and VIII.

CHAPTER IV

THE ORIGIN OF VLF DISCRETE EMISSIONS IN THE TERRESTRIAL EXOSPHERE

(A) Review

Very Low Frequency emissions which are believed to be generated in the terrestrial exosphere, have caused great excitement in the past ten years (e.g. Watts, 1957; Gallet, 1959; Ellis, 1960; Helliwell and Carpenter, 1961; Dowden, 1962^c; Harang and Larsen, 1965)⁺. These emissions are generally classified into two main types, the quasi-continuous or continuous type which is wide-band noise lasting for hours and the discrete emissions which are short-lived (with a duration of about one second), narrow-banded and have reproducible frequency-time variations. The study in this chapter will be centred on the discrete type.

Dowden (1962a, 1962b) suggested that discrete emissions, in particular the "Hooks", are produced by backward Doppler-shifted cyclotron radiation from electron

⁺These papers describe observations of VLF emissions only.

bunches travelling along field lines in the terrestrial exosphere. On the assumption of strict longitudinal emission ($\theta = 180^\circ$), Dowden calculated dynamic spectra which showed good agreement with those observed. Later, Hansen (1963) investigated Dowden's theory and found that the calculated theoretical dynamic spectra of Hooks can generally explain the observed frequency-time shape. However, she pointed out that many Hooks are triggered by whistlers and produced an interaction mechanism to explain the triggering process. The discrepancies between observed and theoretical dynamic spectra are also accounted for qualitatively by the resonance mechanism. Another similar resonance process to explain triggered emissions is produced by Brice (1963). Helliwell (1963) observed whistler-triggered periodic VLF emissions in several stations. He found from the observational data that a sequence of emissions is initiated, or triggered by a whistler and the period between emissions is the same as the whistler-mode echoing period at some frequency within the range of the emission. To explain these results it is proposed that the triggering of the emissions is controlled by packets of electromagnetic waves echoing in the whistler mode. In this triggering hypothesis it is supposed that the wave packets act to organize temporarily the particles in existing streams of charge, so that, their radiation is coherent. Brice (1964) studied the fundamentals of the wave-electron interaction process and found that

energy can be transferred between a wave-packet and an electron gyrating in resonance with the wave when they propagate in opposite directions[†]. Even though the non-triggered emissions may be caused by cyclotron radiation from helical streams or small bunches and that the triggered emissions may be explained by the interaction or resonance process, three problems still remain unsolved:

- (i) In all the existing radiation and interaction theories for explaining VLF emissions, it has been assumed, without any justification, that the emission angle is 180° . Since a gyrating electron emits cyclotron radiation in all directions and the wave-particle interaction process does not necessarily occur only along the field line direction, we need to investigate the validity of the longitudinal propagation assumption.
- (ii) Since a wide range of Doppler frequencies is radiated by a single electron at any instant, a process which has a frequency selective effect must exist, in order to explain the very narrow band structure of discrete emissions.

[†]However, he did not clarify the direction of the process, i.e. under what conditions energy is transferred from wave to particle and vice versa.

(iii) The quantitative explanation of the high intensity received ($\sim 10^{-10}$ watts $m^{-2}/(c/s)$ at the base of the exosphere).

Before we solve these three problems, we will first of all analyse numerically the excitation process of normal backward Doppler-shifted cyclotron waves in a stream-plasma system for general θ which has been derived in the last chapter II. Since the bandwidth of discrete emissions is so narrow, the radiating stream must be very close to helical. For simplicity in calculation, the discussion in section (B) is carried out under the assumption that the stream is strictly helical.

It should be remarked that besides the three mentioned problems, the explanations for the origin of triggered emissions given by Helliwell (1964), Brice (1964), and, Bell and Buneman (1964) have been incomplete and sometimes confusing; this respect will be discussed in section (C).

(B) Excitation of Backward Doppler-shifted Cyclotron Radiation in a Magnetoactive Plasma by a Helical Electron Stream

In this investigation the particle density in the stream is assumed to be very small compared with that in the background plasma and only the fundamental

harmonic is considered⁺. The collisionless Appleton-Hartree equation for the whistler mode is assumed to be applicable to the propagation of electromagnetic waves in the background plasma alone:

$$n_j^2 = 1 + \frac{A}{(|\cos \theta| - \xi)} \quad (4.1)$$

With the definition of n_j^2 given by (4.1), relation (3.2) is simplified into

$$\left(\frac{\partial F_p}{\partial \omega} \right)_{\tilde{\omega}} = -2\tilde{\omega} - \frac{|\cos \theta| \omega_p^2 / \omega_H}{(|\cos \theta| - \xi)^2} \quad (4.2)$$

The dispersion equation for the helical-stream-plasma system now reads

$$\left(\frac{\delta}{\tilde{\omega}} \right)^3 + b \left(\frac{\delta}{\tilde{\omega}} \right) + d = 0 \quad (4.3)$$

where
$$b = - \frac{\sigma J_1^2 A \beta_{||}^2 \cos^2 \theta}{(\gamma - \xi)^2} \left[\frac{(\gamma - \xi)^2}{\xi^2 \beta_{||}^2} - 1 \right]$$

⁺This assumption is valid due to (i) The radiated frequency must be smaller than $|f_H|$ so that the wave will not be trapped at the resonance region $f \approx |f_H|$ (ii) For high harmonic number, the growth factor is found to be small.

$$d = - \frac{\sigma \left[\frac{(\gamma - \xi)^2}{\xi^2 \beta_{\parallel}^2} - 1 \right] \left[J_1'^2 \beta_{\perp}^2 + \frac{J_1^2 \beta_{\parallel}^2 (\gamma - \xi \sin^2 \theta)^2}{\sin^2 \theta (\gamma - \xi)^2} \right] (|\cos \theta| - \xi)^2}{|\cos \theta| \xi}$$

with $\sigma = \omega_0^2 / \omega_p^2$

It should be noted that in the expression for d we have neglected the term $\tilde{\omega} / \omega_p^2$. This approximation is valid in case of VLF emissions in the terrestrial upper atmosphere. The rate of growth, being represented by the dimensionless quantity $\Im_m(\frac{\delta}{\tilde{\omega}})$, can readily be solved from (4.3):

$$\Im_m \left(\frac{\delta}{\tilde{\omega}} \right) = \pm \frac{\sqrt{3}}{2} \left[(M)^{1/3} (C)^{1/3} \right] \quad (4.4)$$

where $M = -\frac{a}{2} + \sqrt{\frac{a^2}{4} + \frac{b^3}{27}}$

and $C = -\frac{a}{2} - \sqrt{\frac{a^2}{4} + \frac{b^3}{27}}$

In the particular case $\theta = 180^\circ$, $b = 0$, $d = \frac{1}{2} \cdot \frac{\omega_0^2 \beta_{\perp}^2 (c^2 k^2 - \tilde{\omega}^2)}{(\partial F_p / \partial \omega) \tilde{\omega}}$

and we get $\left| \Im_m \delta \right| = \frac{\sqrt{3}}{2} \sigma^{1/3} \left| \frac{\omega_p^2 \beta_{\perp}^2 (c^2 k^2 - \tilde{\omega}^2)}{2 (\partial F_p / \partial \omega) \tilde{\omega}} \right|^{1/3} \quad (4.5)$

This result agree with that found by Zheleznyakov (1960a) for this case.

We now evaluate the growth rate for general θ , for parameters appropriate to VLF emissions in the terrestrial exosphere.

To solve for the characteristic frequency $\tilde{\omega}$, we have to solve Appleton-Hartree equation (i.e. equation (4.1)) and Doppler equation $\tilde{\omega} - k_{\parallel} v_{\parallel} - \gamma |\omega_H| = 0$ simultaneously. Fig. 4.1 gives an example of the graph $\xi = \tilde{\omega}/|\omega_H|$ against wave-normal angle θ . The parameter is transverse velocity β_{\perp} and each line represents a particular value of longitudinal velocity β_{\parallel} ; we repeat this for two values of $\Lambda = \omega_p^2/\omega_H^2 = 25, 100$ which may be considered as a quantity specifying the ambient plasma. We can also take the quantity $|\Im m(\delta/\omega_H)|$ to specify the growth rate. $|\Im m(\delta/\omega_H)|$ is plotted against wave-normal angle θ in Fig. 4.2 for $\sigma = \text{density of stream/density of ambient plasma} = 1 \times 10^{-7}$, for various values of Λ , β_{\perp} and β_{\parallel} . Let P_0 be the power of the electromagnetic wave at time $t = 0$, and P be the power after 0.016 second. Fig. 4.3 shows graphs of the power gain in 0.016 second against wave-normal angle θ for growth rates shown in Fig. 4.2. The electron gyro-frequency is taken to be $|f_H| = |\omega_H|/2\pi = 10 \text{ Kc/s}$. Corresponding to Fig. 4.3, the power gain after 0.016 second is also plotted against the excited frequency normalized to the gyro-frequency in Fig. 4.4. As the growth rate maximizes at $\theta = 180^\circ$, the "open end" point of each curve in Fig. 4.4 gives us the

frequency excited and the power gain of the electromagnetic wave when the wave-normal angle is 180° . The small circle on each curve indicates the frequency and power gain for $\theta = 150^\circ$. The narrow bandwidth of the radiation implied by Fig. 4.4 is illustrated more clearly in Fig. 4.5.

From the analysis of the dispersion equation for whistler-mode waves, we observe that:

- (i) The growth rate maximizes at $\theta = 180^\circ$.
- (ii) Since the frequency is almost constant for a range of wave-normal angles (about $180^\circ - 150^\circ$) in most cases, in particular for large pitch angles, the excitation theory indicates that for large pitch angles, the very narrow band of frequencies (theoretical bandwidth $< 0.01\omega$ when one considers the half-power bandwidth in Fig. 4.5) emitted with θ between about 180° and 150° may be excited to a much greater extent than other frequencies, resulting in a frequency selective effect.
- (iii) For constant energy of radiating electron, the larger the pitch angle, the greater the radiation power.

(C) Discussions

We have obtained the radiation characteristics of a stream-plasma system. It is interesting to compare this result with the power spectrum radiated by a single electron. Lienohn (1965) has corrected Lidman's equation (Lidman, 1958)

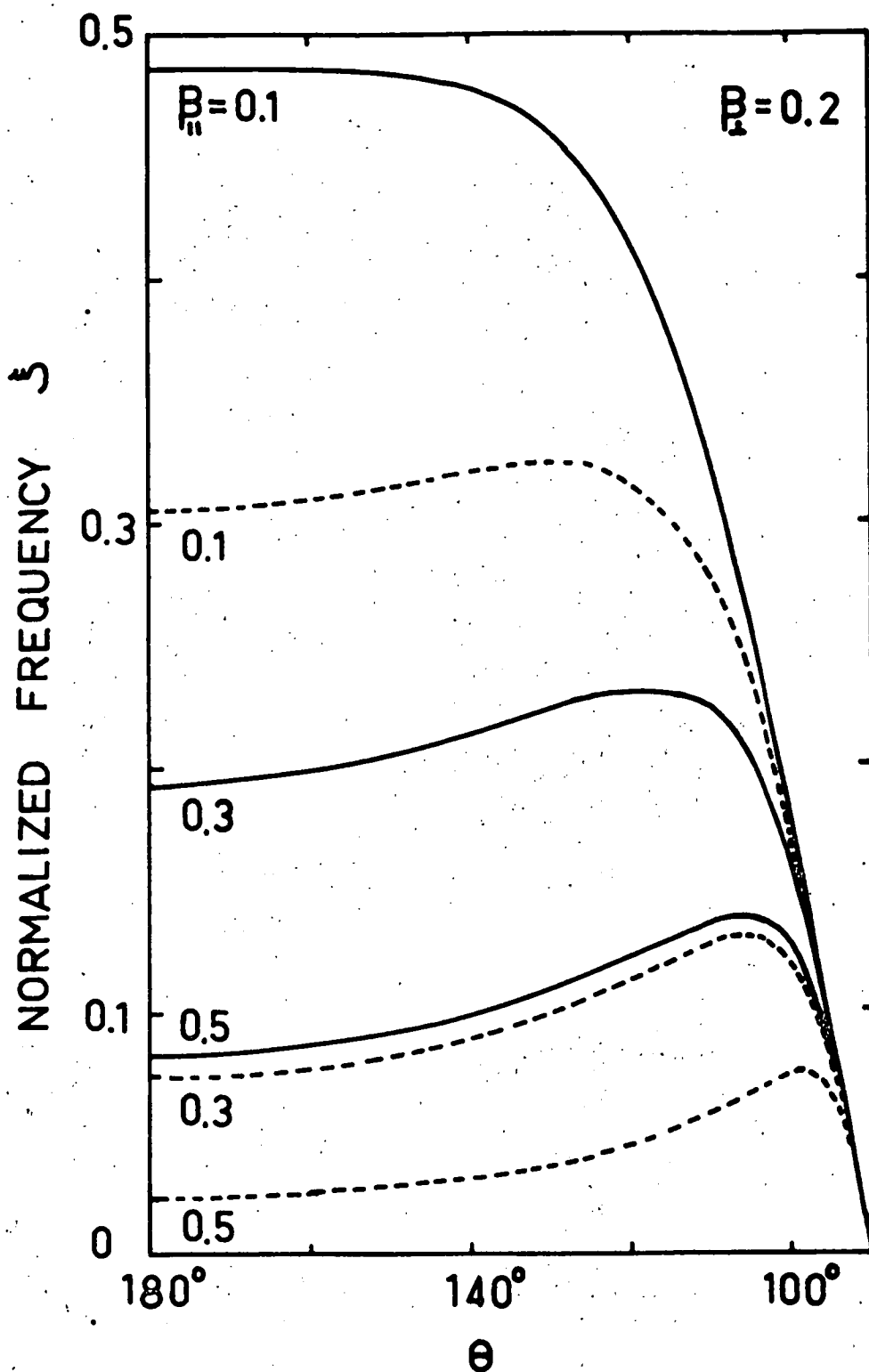


Fig. 4.1 Normalized wave frequency ξ vs wave-normal angle θ , with β_1 as parameter for two cases: $A = 25, 100$.

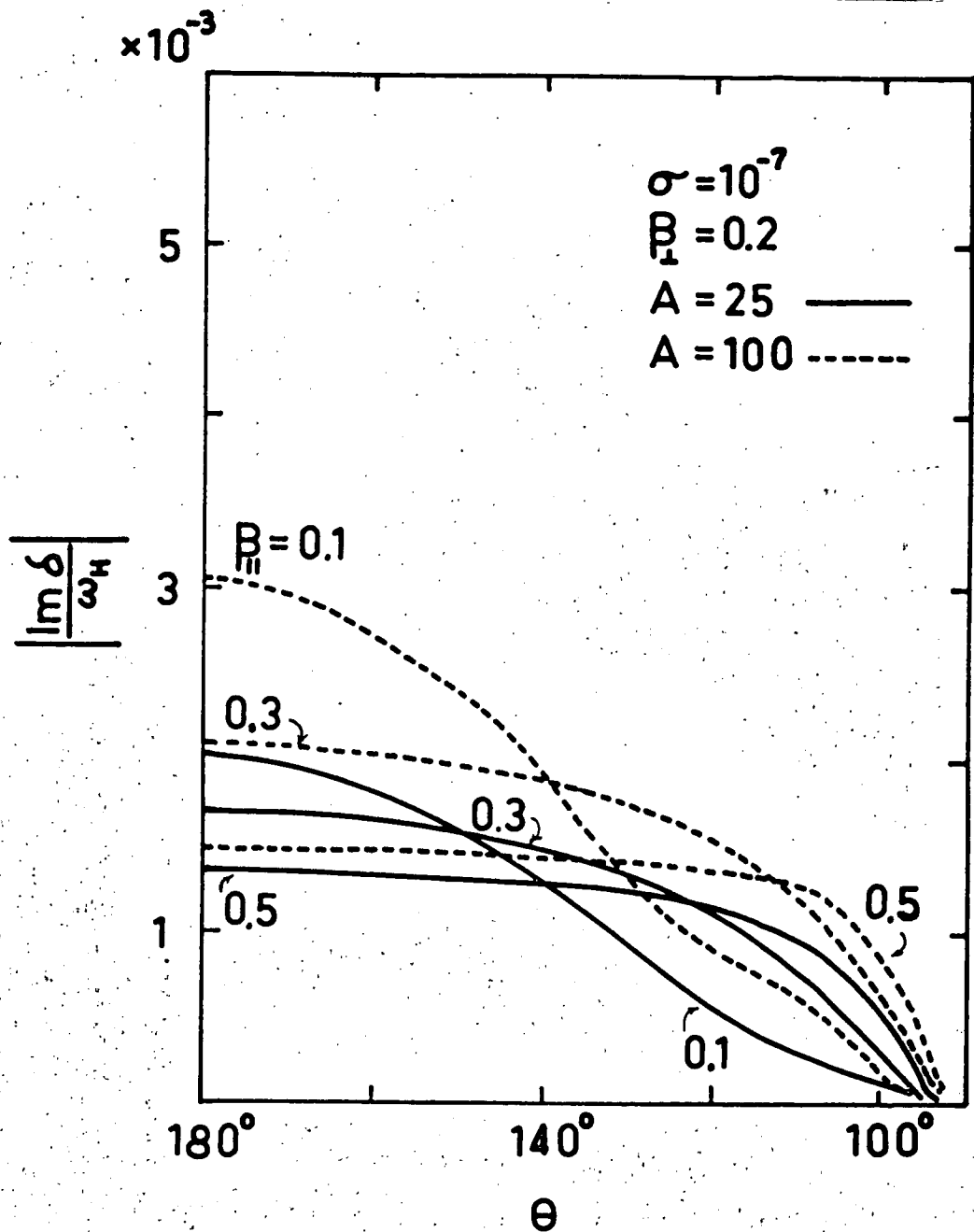


Fig. 4.2 Dependence of the growth rate $|\text{Im } \delta|/\omega_H$ on wave-normal angle θ for $\sigma = 10^{-7}$, $A = 25, 100$ and
 (a) $\beta_L = 0.2$; $\beta_{||} = 0.1, 0.3, 0.5$
 (b) $\beta_L = 0.4$; $\beta_{||} = 0.1, 0.3, 0.5$
 (c) $\beta_L = 0.6$; $\beta_{||} = 0.1, 0.3$.

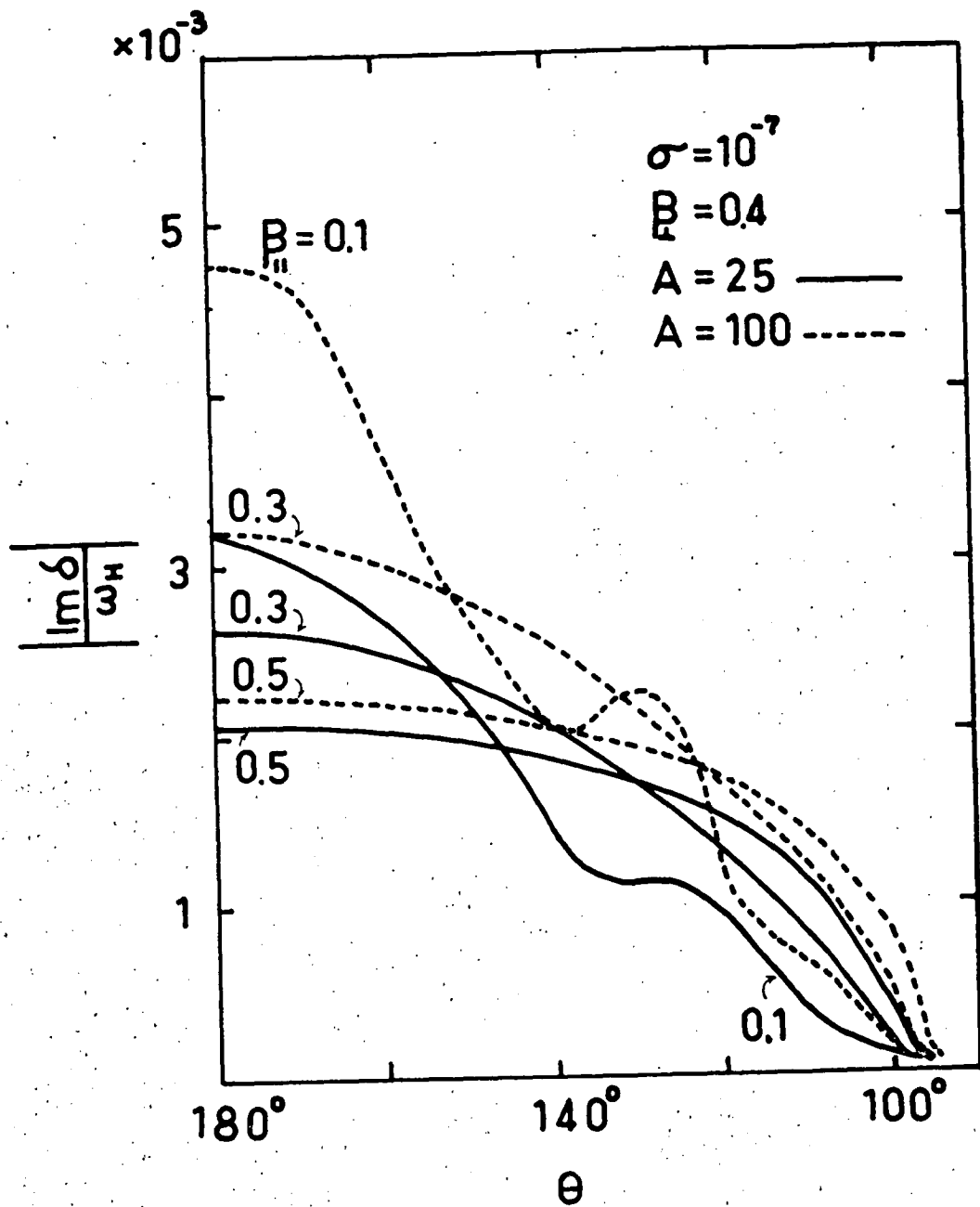


Fig. 4.2 (b)

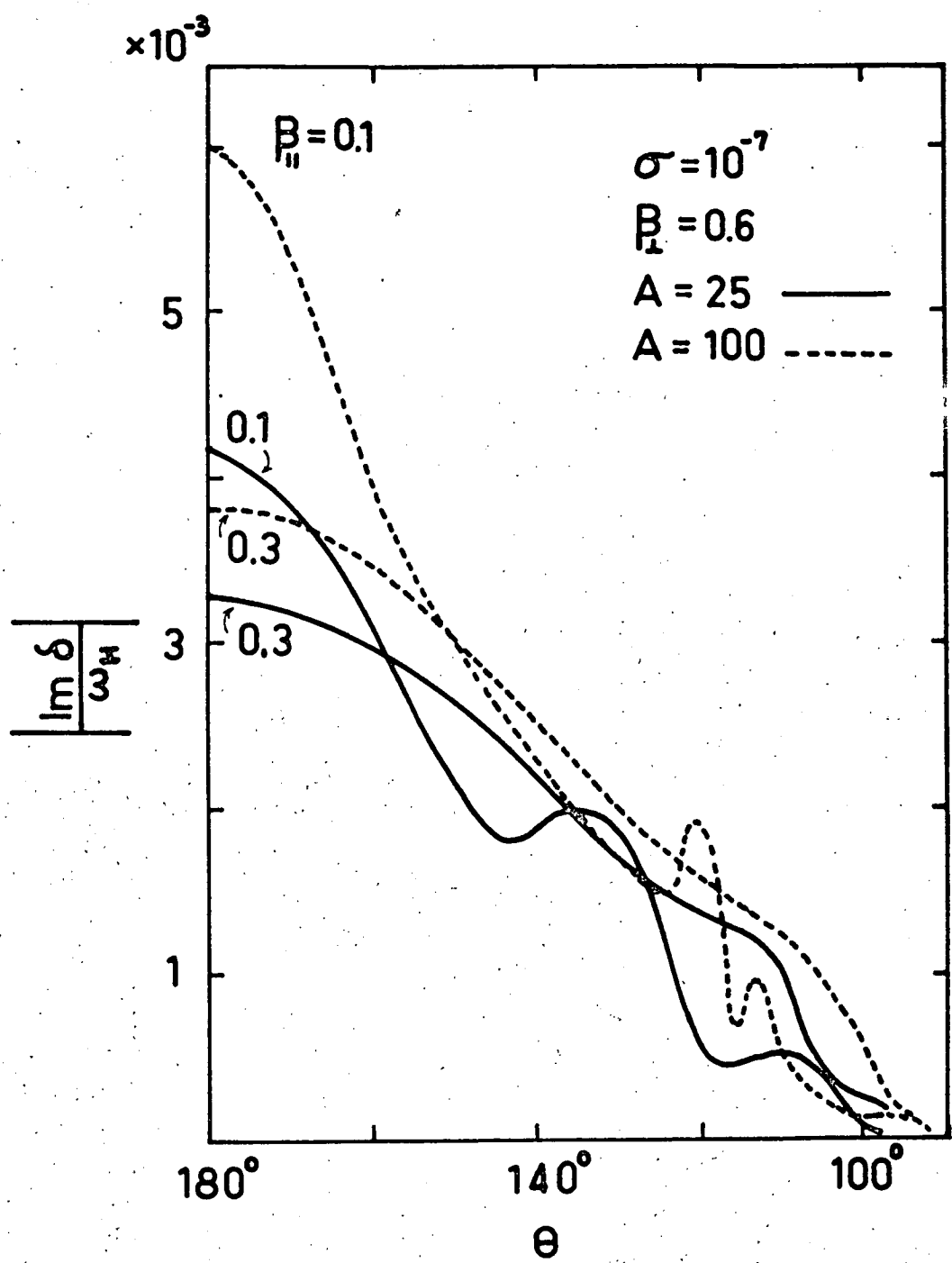
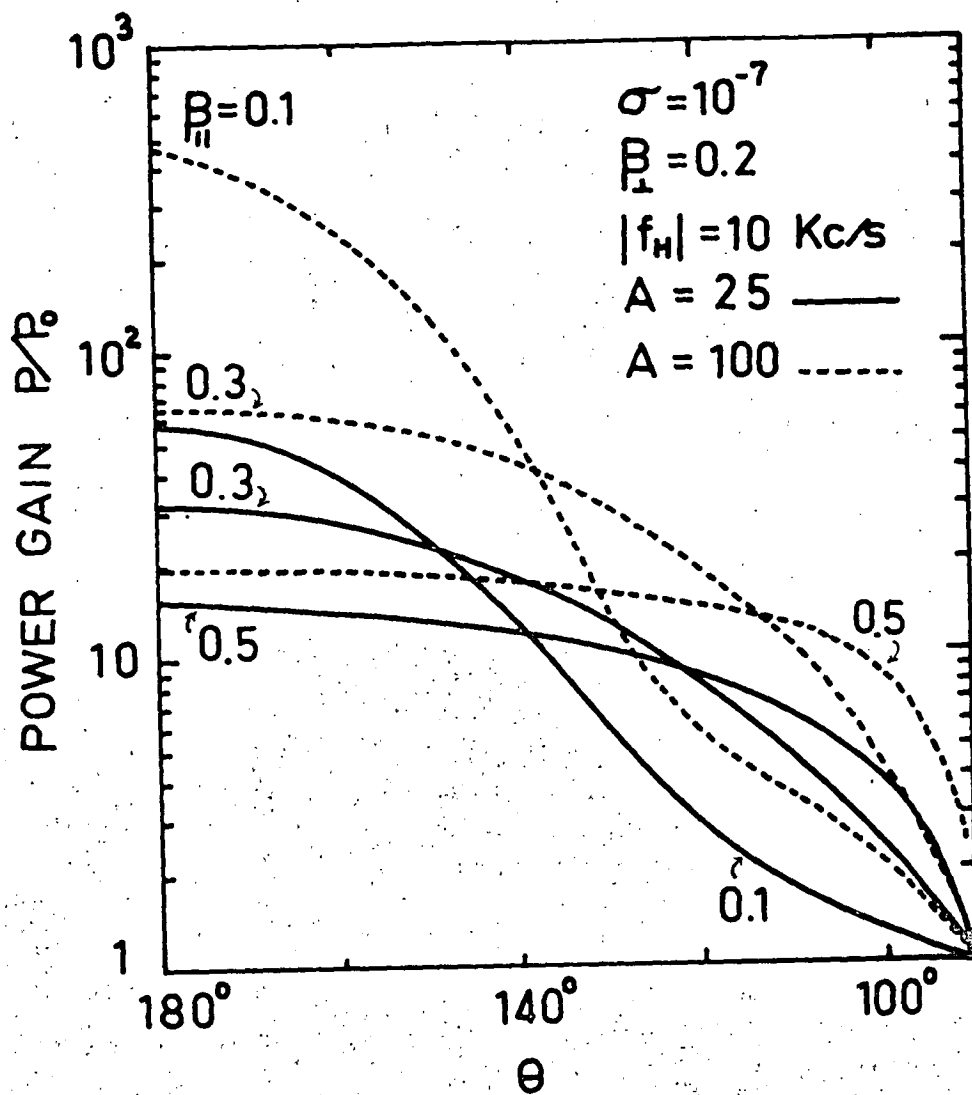


Fig. 4. 2(c)



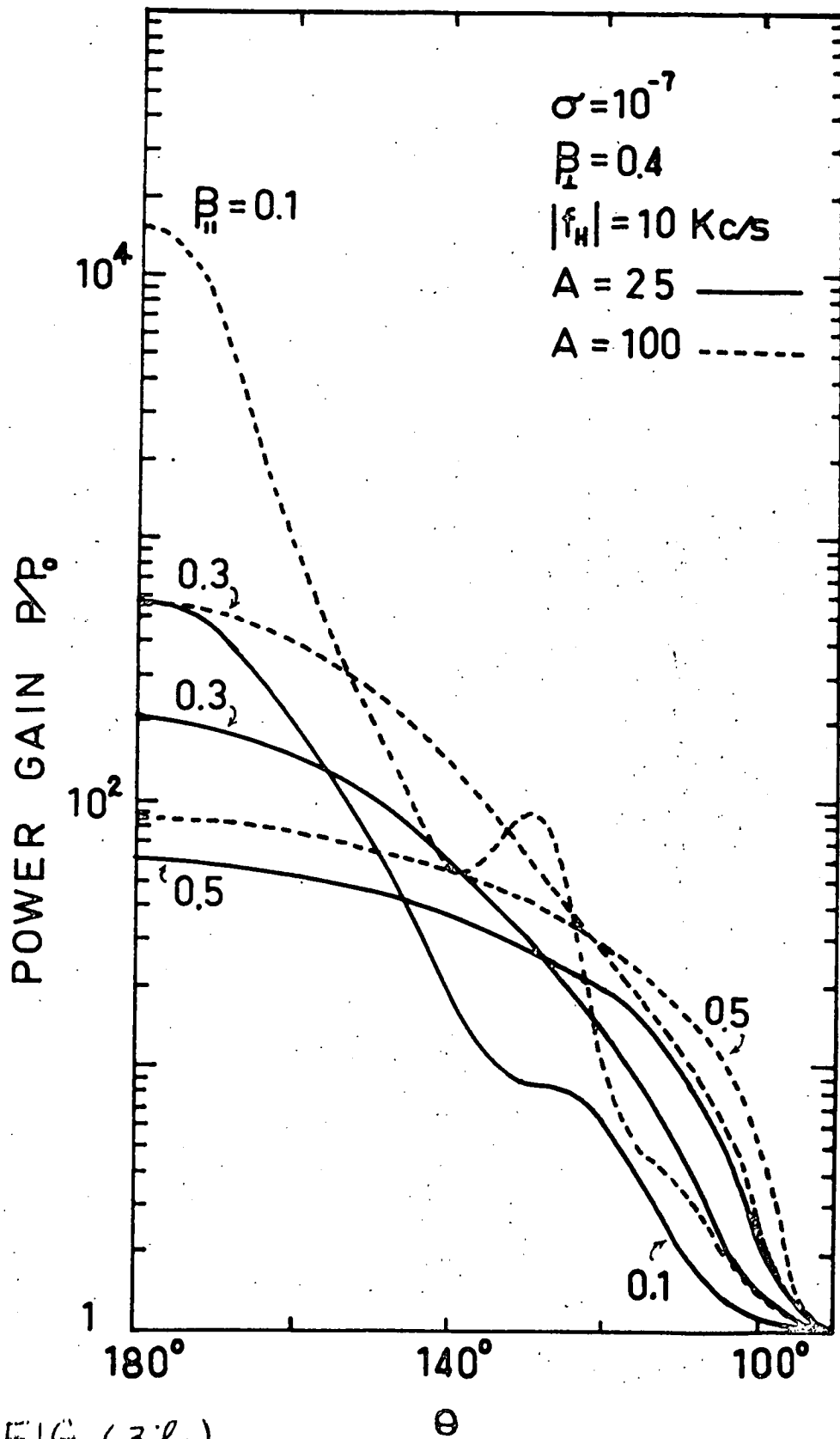
(a)

Fig. 4.3 Dependence of the power gain P/P_0 after 0.016 sec. on wave-normal angle θ for $\sigma = 10^{-7}$, $|f_H| = 10$ Kc/s, $A = 25, 100$ and

(a) $\beta_{\perp} = 0.2$; $\beta_{\parallel} = 0.1, 0.3, 0.5$

(b) $\beta_{\perp} = 0.4$; $\beta_{\parallel} = 0.1, 0.3, 0.5$

(c) $\beta_{\perp} = 0.6$; $\beta_{\parallel} = 0.1, 0.3$.



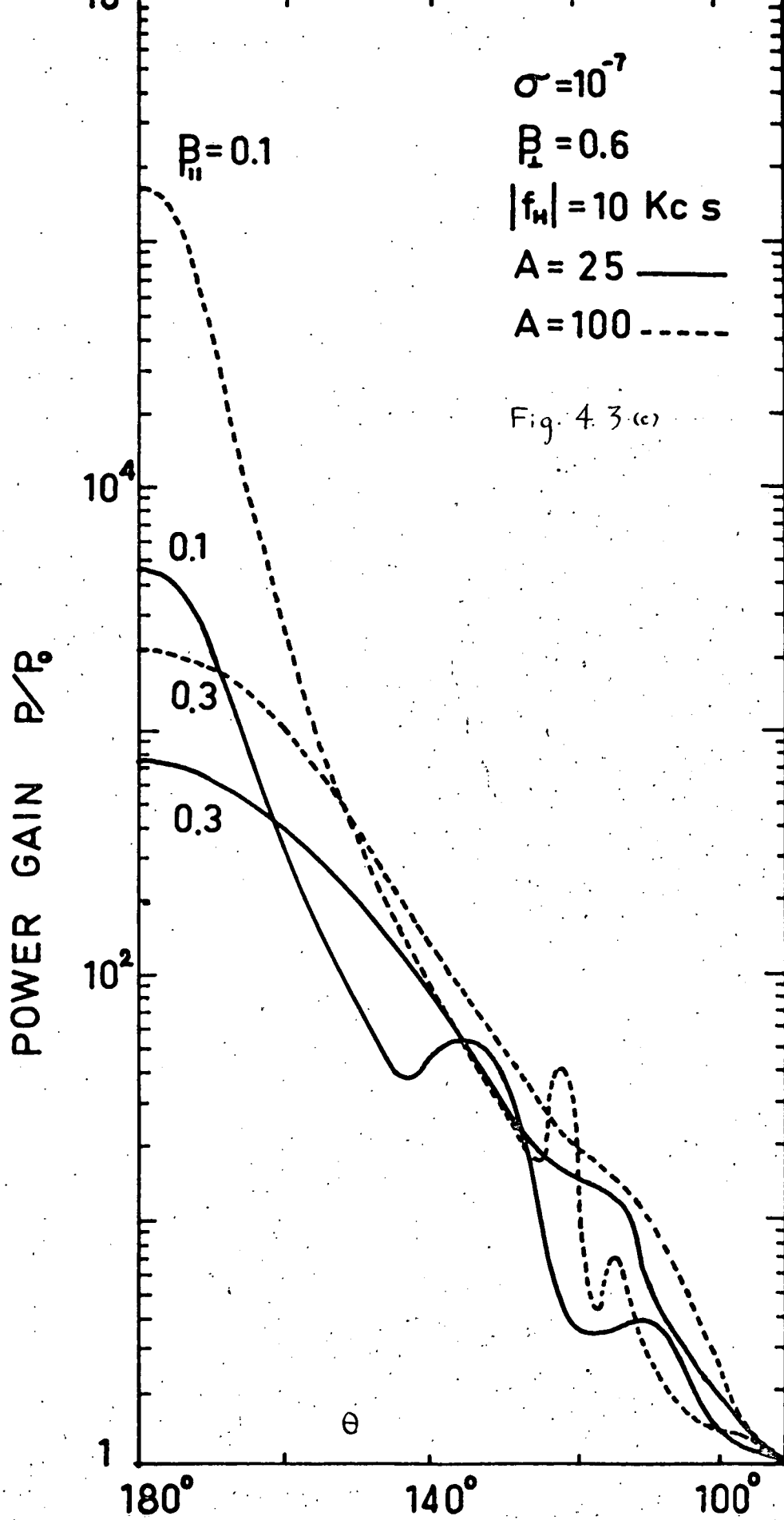


Fig. 4.3(c)

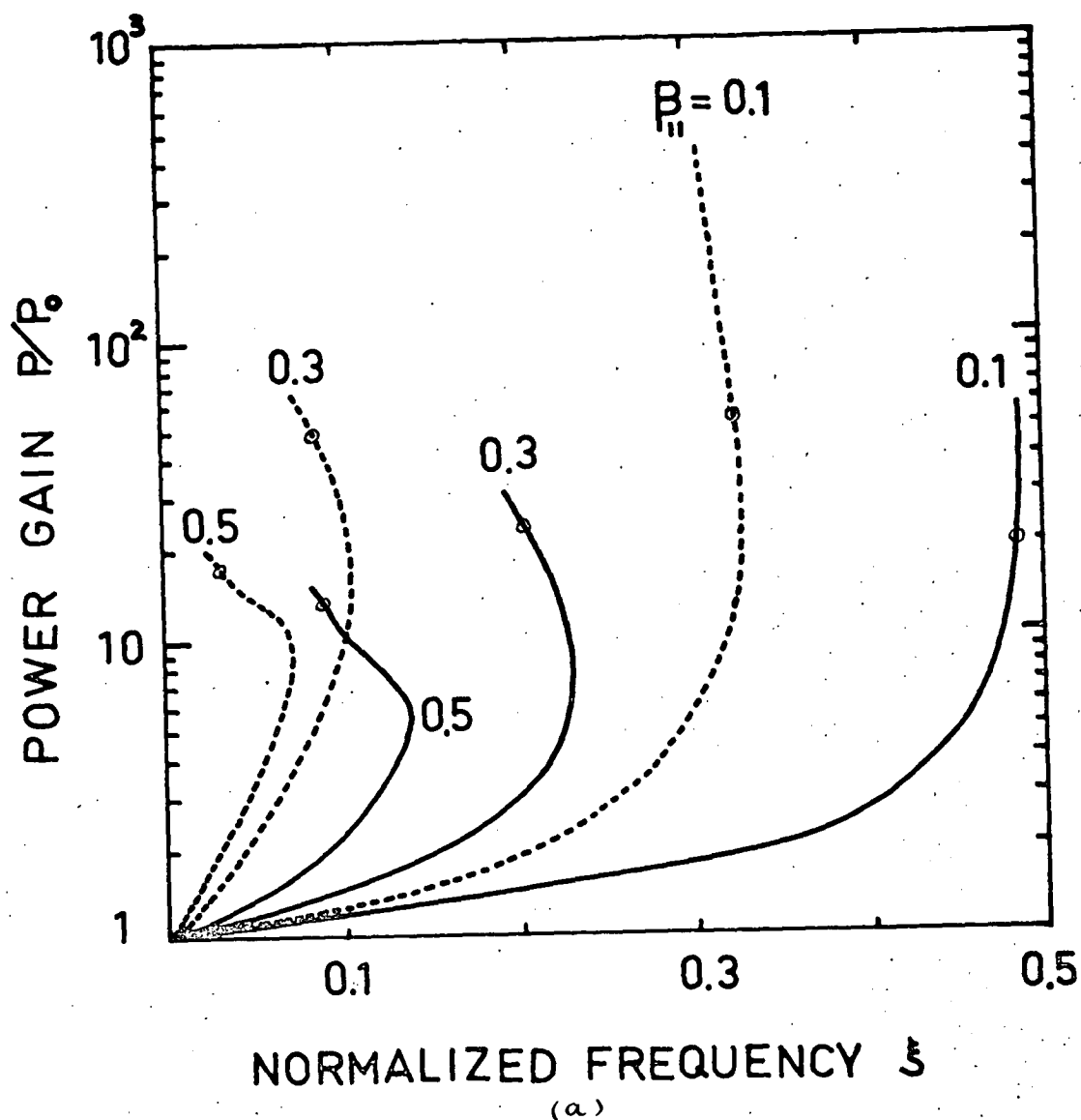


Fig. 4.4 Power gain P/P_0 after 0.016 sec. vs normalized wave frequency ξ for $\sigma = 10^{-7}$, $|f_H| = 10$ Kc/s, $A = 25, 100$ and

- (a) $\beta_{\perp} = 0.2$; $\beta_{\parallel} = 0.1, 0.3, 0.5$
- (b) $\beta_{\perp} = 0.4$; $\beta_{\parallel} = 0.1, 0.3, 0.5$
- (c) $\beta_{\perp} = 0.6$; $\beta_{\parallel} = 0.1, 0.3$.

The little circle on each curve indicates the frequency emitted at $\theta = 150^\circ$.

Fig. 4.4 (b)

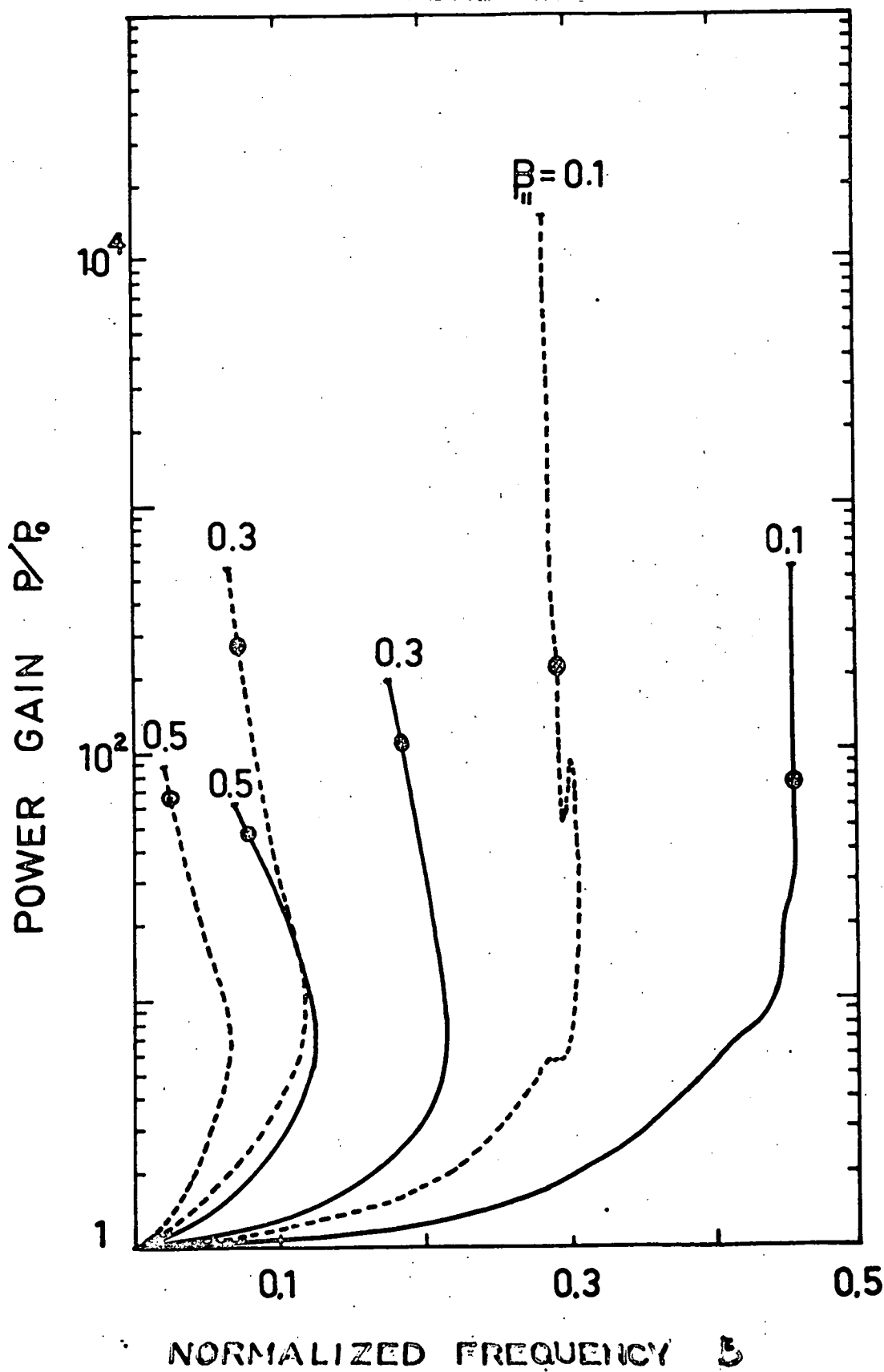
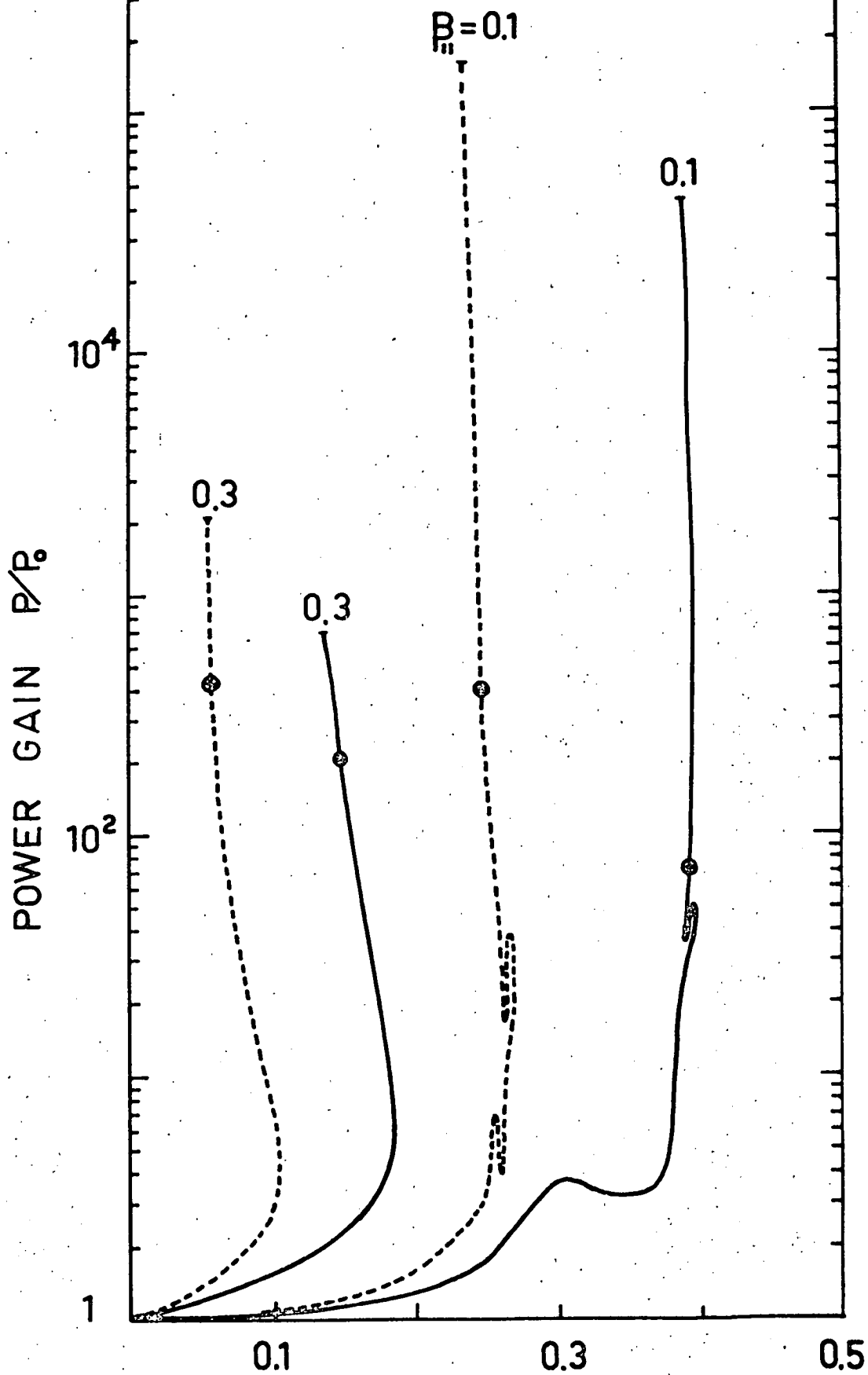


Fig. 4.4 (cc)



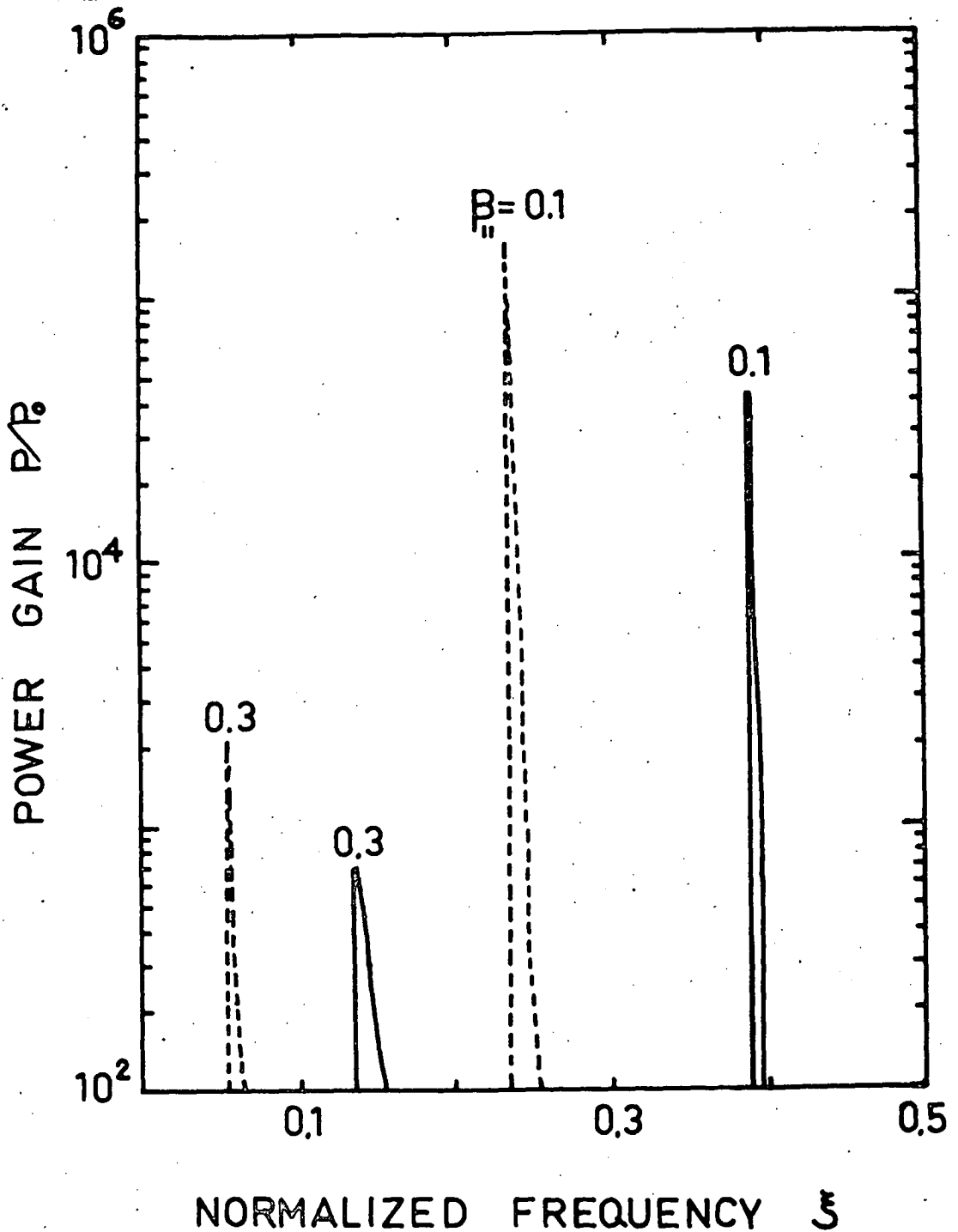


Fig. 4.5 Power gain P/P_0 after 0.016 sec. as a function of normalized wave frequency ξ , indicating the narrow band structure of the growing wave. The parameters are the same as in Fig. 4.4(c).

(which gives the power spectrum radiated a single electron gyrating in a magnetocactive plasma) and evaluated the radiation pattern from a single electron (energy = 10 Kev. and 1,000 Kev.) for parameters appropriate to the lower exosphere ($A \approx 5$). His result indicates that the maximum power occurs at about 110° and the wave propagating along the field line carries minimum power. However, it should be pointed out that Liemohn has taken a pitch angle of 30° ($\phi = \arctan \frac{\beta_\perp}{\beta_\parallel}$) for the radiating electron whereas Dowden (1962d) measured from experimental data that the pitch angle of the source electrons generating a Hock is generally large, being greater than 60° in most cases. Using the appropriate value of A in the exosphere ($A = 25$) and fixing β_\perp for the helical stream to be 0.4, we show in Fig. 4.6 the power spectrum radiated by a single electron for different values of β_\parallel . We observe that for large value of $\beta_\perp/\beta_\parallel$ and, hence, large pitch angle ϕ , the power is large and maximizes at 180° . As the pitch angle decreases, the emission angle corresponding to maximum power shifts rapidly away from the field line.

The result of the instability theory, together with the radiation pattern of single electron, indicates that the assumption of longitudinal propagation (as taken by previous VLF workers) is fortunately correct, and thus the first problem is solved.

The frequency selective effect has been explained by the

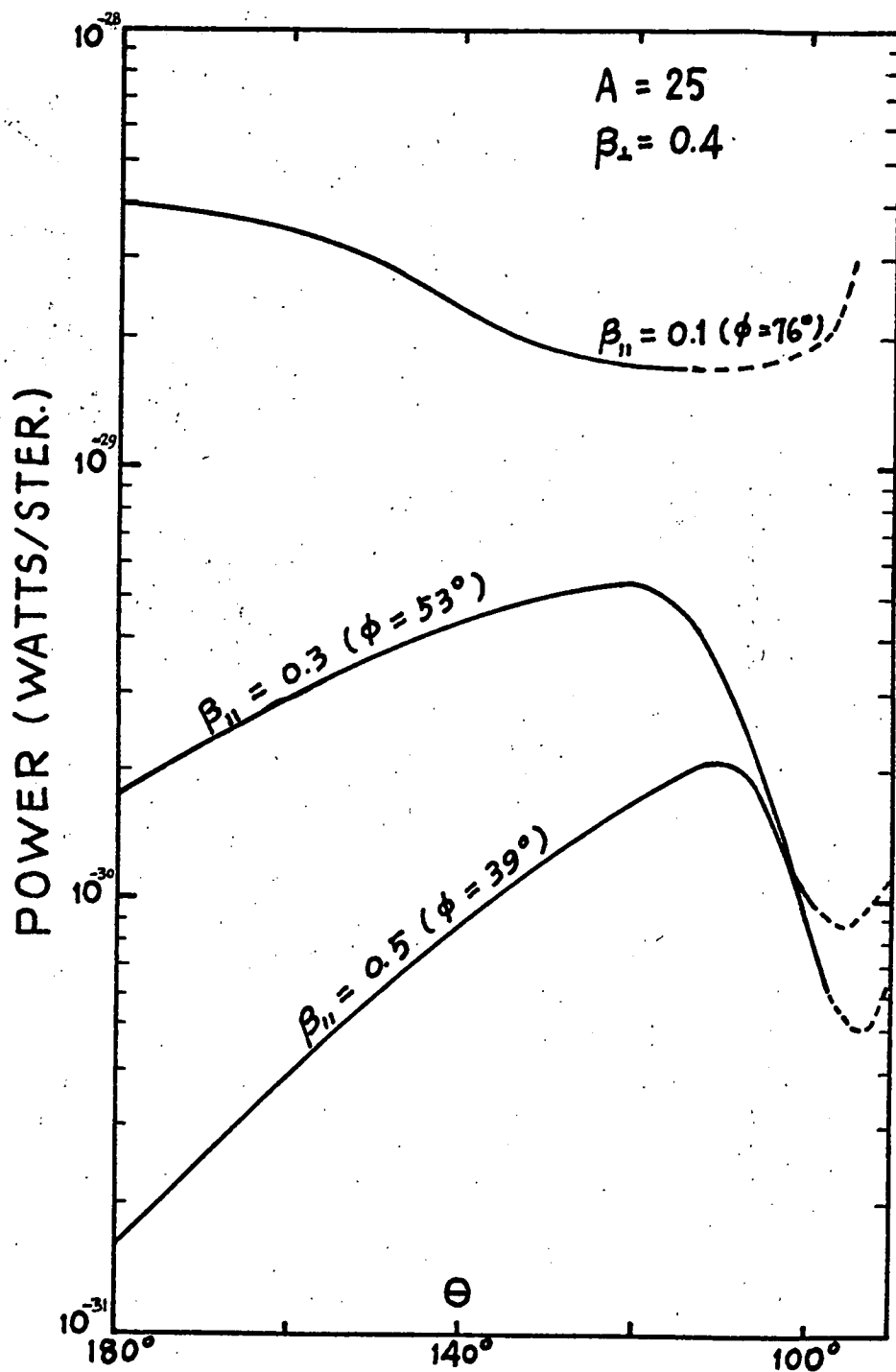


Fig. 4.6 Power spectrum radiated by a single electron for various values of energy (specified by β_{\perp} , $\beta_{||}$) and pitch angle ϕ for $A = \omega_p^2 / \omega_H^2 = 25$. The dotted parts indicate that the refractive index is greater than 20.

result in section (B). Assuming a strict helical stream, the theory shows that a bandwidth smaller than $0.01 f$ is possible. This result, which is consistent with observation, suggests that the radiating stream is in fact very much close to helical. The existence of a small finite temperature in the stream will result a relatively broader bandwidth, which is observed in rare cases. The second problem, hence, has been accounted for.

Assume the cross-sectional area of the stream and the ionized column to be

$$A \sim 10^2 \text{ Km}^2 \quad (4.6)$$

at the equatorial plane. Suppose the length of the part of the stream radiating a particular frequency (in this case the minimum frequency of a Hook f_0) to be

$$L \sim 6 \times 10^2 \text{ Km} \quad (4.7)$$

Let the particle density of the stream to be 10^{-4} el/cm^3 and that of the background plasma to be 100 el/cm^3 , giving $\sigma = 10^{-6}$. Then the number of radiating electrons in a volume bounded by area A and length L is

$$N \sim 6 \times 10^{15} \quad (4.8)$$

It has been found that in the ionosphere and exosphere the ray direction of a whistler mode wave is guided along the field line (e.g. Budden, 1961). We may, therefore, assume

that all the electromagnetic energy radiated in the ionized column ^{is concentrated at the base of the ionized column} (Liemohn, 1965). The cross-sectional area of the ionized tube at the base of the magnetosphere is estimated to be $\frac{1}{100}$ that at the equatorial plane (expression (4.6)). Now if each radiating electron emits a power of 10^{-30} watts/(c/s) (Liemohn, 1965), the power flux received at the base of the magnetosphere is

$$P \sim 6 \times 10^{-21} \text{ watts m}^{-2}/(\text{c/s}) \quad (4.9)$$

Since the observed value of power flux at the base of the magnetosphere is of the order of 10^{-10} watts $\text{m}^{-2}/(\text{c/s})$ (Dowden, 1962c), we need a power gain of the order

$$\frac{P}{P_0} \sim 10^{10} \quad (4.10)$$

Using the method as described in section (B), the interaction time needed for this value of power gain is ~ 25 msec., if the pitch angle of the stream is greater than 50° and the energy of each electron is of the order of 100 Kev. We note that for longitudinal propagation, the wave and ray directions coincide. If the refractive index for the whistler wave is taken to be 15, the wave will take 30 msec. to travel a distance of 6×10^2 Km. We will, thus, conclude that with the assumed values of stream density and interaction time, the high intensity of VLF emissions can readily be explained quantitatively with the result of the instability theory — the third problem has been dealt with.

From the existing interaction theories, it seems that it has not been realized that in fact there are two interaction processes taking place in steps. We can understand the above statement readily with the knowledge of chapter II.

We have discussed briefly the possibility of excitation and damping of cyclotron waves; the controlling factor is the distribution function of the electron stream. When the electron stream has a very wide momentum spread or when the stream is absent (leaving a Maxwellian background plasma), part of the energy of the propagating electromagnetic waves are absorbed by the medium and particles are accelerated. This process is called harmonic resonance absorption (section (D) of chapter II). Consequently, when an electron stream of high temperature encounters a strong whistler signal (either a whistler or an artificial whistler-mode code signal), the macroscopic absorption is positive and in average, energy is fed from the wave to the particles such that some particles will gyrate in phase with the wave; this process is in fact the harmonic resonance absorption mechanism. The affected particles, being organized, form a stream which is close to helical. The particles in this stream emit cyclotron radiation continuously as they have always been, but now the stream-plasma system becomes radiatively unstable and the waves radiated by the cyclotron mechanism will grow as a

function of time (absorption is negative). After some interaction time, the waves acquiring sufficiently large amplitude, are received as triggered VLF emissions. As the stream radiates, the interaction process sustains for some time, while the energy of the electrons is decreasing (causing an increase in $\beta_{||}$ and a larger decrease in β_{\perp}), until the distribution function of the stream is far from helical and the radiation is insignificant to be observed. When the echo of the previous triggering whistler signal encounters the stream again, the two interaction processes repeat and we may receive triggered periodic VLF emissions.

It has been found that VLF discrete emissions can readily be triggered by artificial whistler-mode signals of single frequency when the signal is long enough⁺ (Helliwell, 1964). In average, the time interval between the leading edge of the transmitted signal and the commencement of a triggered emission is 100 msec. Based on our previous estimated interaction time for the excitation process (~ 25 msec.), we see that the interaction time for the organising process (harmonic resonance absorption) is

⁺When the duration of the transmitted signal is 45 msec. (a dot) no triggered emissions are observed. If the transmitted signal lasts for 145 msec. (a dash), VLF discrete emission are triggered in most cases.

is ~ 75 msec. We must note that our estimation has been crude and our instability theory is a linearized one. When nonlinear effects come into being (which will be the realistic case⁺), the growth rate will be smaller and the interaction time needed will be larger than our previously calculated values. We can only state here that the interaction times for both processes are of the same order of magnitude, being equal to several tens of msec.

During magnetic disturbed periods, energetic electrons are dumped from the radiation belts to the exosphere. Those electrons travelling with about the same velocity and same direction will form a stream with very narrow momentum spread. Non-triggered VLF discrete emissions will be radiated and excited in the same manner as described before in such a stream-plasma system.

With the results of the investigation in this chapter, we conclude here that the three existing problems mentioned are solved and the origins of both non-triggered and triggered emissions are explained.

⁺Since the received intensity is almost constant during the duration of an event (a Hook, say), the unstable stream-plasma system must have come to an equilibrium situation; this will be the case only when nonlinear effects occur.

CHAPTER V

A REVIEW OF THE PHENOMENON OF SOLAR TYPE I NOISE STORM

(A) Solar Radio Emissions (e.g. Kundu, 1964)

Radio emissions from the Sun come from both thermal and nonthermal sources. The thermal emission can be separated into two components:

- (1) The quiet Sun component which originates from the solar atmosphere at temperatures of the order of 10^4 ° K (chromosphere) and 10^6 ° K (corona) and is the radiation which still occurs in the absence of localized sources in the atmosphere of the Sun.
- (2) The slowly varying component which arises in high density regions of the corona (called condensations) with temperature of about 2×10^6 ° K; these regions exist over sunspots and plage regions.

The nonthermal emissions, which consist of wide-band and narrow-band radio bursts, are generally associated with solar flares or sunspots. They originate from all levels of the solar atmosphere between the lower chromosphere (millimetre and centimetre waves) and the outer corona to heights of several solar radii (metre and decametric waves). The equivalent brightness temperature of the

source in these emissions can be as high as 10^{12} ° K. Such nonthermal burst emissions on metre waves are characterized by great variety and complexity; based on their spectral characteristics, they are classified as types I, II, III, IV and V. Wild, Smerd and Weiss (1963) have summarized their characteristics, geophysical associations and probable mechanisms of generation (Table 5.1).

(B) Characteristics of Type I Noise Storms

During solar disturbed periods, the most common radio events on metre waves are the occurrences of type I radio emissions or type I "noise storms". This type of radiation consists of a slowly varying, broadband emission (called "background continuum") lasting even up to hours or days, on which are superimposed series of intense, narrow-band, short-lived bursts (called "storm bursts"). Some examples of dynamic spectra and single-frequency records of noise storms are shown in Fig. 5.1. The radiation is usually strongly circularly polarized and its occurrence is always associated with a sunspot group. Even though this common nonthermal radiation has been observed since 1942 (e.g. Hey, 1946; Ryle and Vonberg, 1946; Martyn, 1946; Pawsey, 1950), the

Table 5.1

CHARACTERISTICS OF METRE-WAVE BURSTS (Wild, Smerd & Weiss, 1963)

| Type of burst | Circular polarization | Tentative identification of mode | Duration | Variability | Apparent angular size (min of arc) | Height of source above photosphere | Cone of emission | Tentative identification | | Relationship with other phenomena |
|---------------------------------|-----------------------|----------------------------------|---|--|---|--|------------------|--|----------------------|-----------------------------------|
| | | | | | | | | Exciting agency | Emission process | |
| II | None | — | 5–30 min | Complex | 6–12 | $0.2\text{--}1.0 R_{\odot}^a$ | Wide | Ascending shock front vel $\sim 10^3$ km/sec | Plasma | Solar protons, geomagnetic storms |
| III | None or partial | ? | Burst: ~ 10 s Group: ~ 1 min | Group of simple bursts | $3\text{--}12^a$ | $0.2\text{--}2.0 R_{\odot}^a$ | Wide | Ascending electron stream vel $\sim c/2$ | Plasma | Initial expansion of flare |
| V | Weak | ? | ~ 1 min | Smooth | Similar to III | Similar to III | Wide? | Same as III | ? | Same as III |
| IV mA (moving) | Weak | Extraordinary | 10 min–2 hr | Smooth | 6–12 | $0.5\text{--}5 R_{\odot}$ ascending at speeds $\sim 10^3$ km/sec | Wide | Electrons trapped in expelled plasma | Synchrotron | Solar protons, geomagnetic storms |
| IV mB ^b (stationary) | Strong | Ordinary | Few hrs to days | Slow variations with some fine structure | $3\text{--}6^a$ | $0.2\text{--}1.0 R_{\odot}^a$ | Narrow | Descending electron stream trapped in field | Plasma Synchrotron? | |
| I | Strong | Ordinary | Burst: ~ 1 s Storm: few hrs to days | Slow | Burst: 1–6 Storm centre $5\text{--}10^a$ | $0.2\text{--}1.0 R_{\odot}^a$ | Narrow? | ? | Plasma? Synchrotron? | |

^a Increase with λ .^b Includes continuum storms.

Fig. 5.1

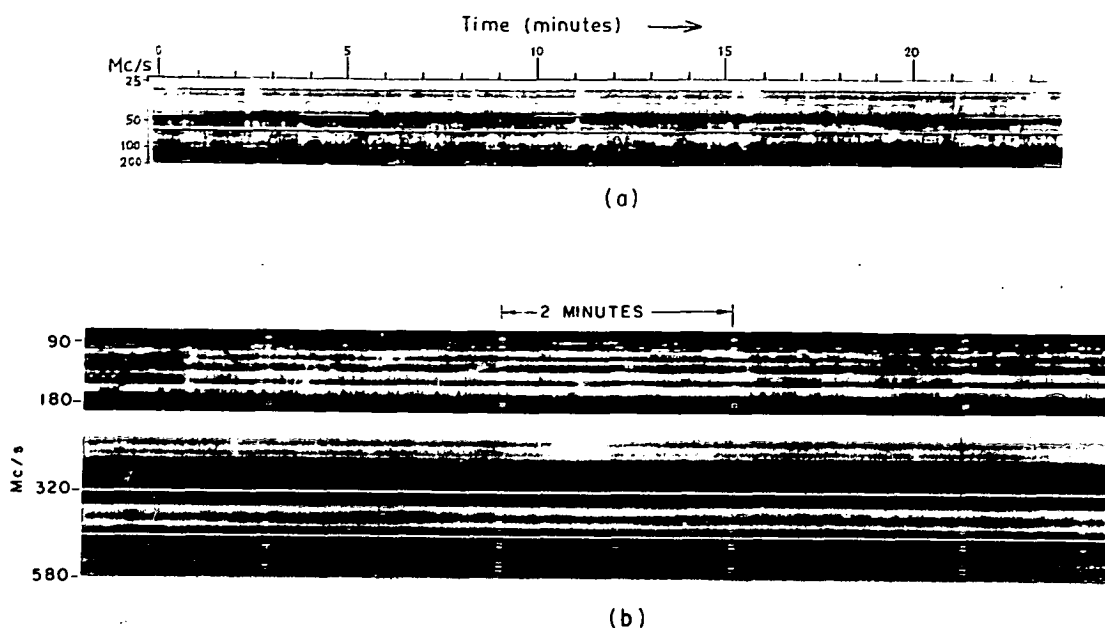
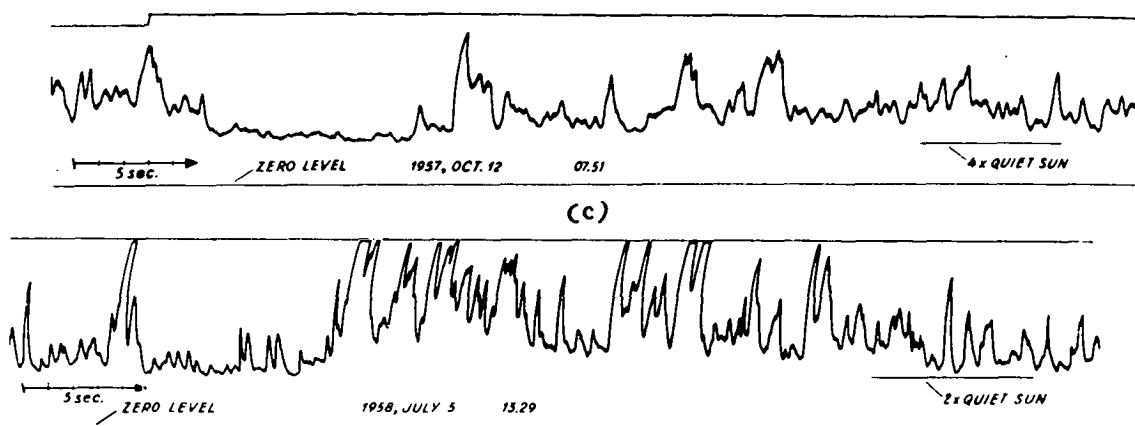


Fig. 5.1 Some dynamic spectrum records of storm bursts (a) in the 25–210 Mc/s range (Wild et al, 1963) and (b) in the 100–580 Mc/s range (Kundu, 1964).



(c) Examples of high-speed single frequency record at 200 Mc/s (Fokker, 1961).

theoretical interpretations of this complex phenomenon so far published have been unsatisfactory. Before we put forward a theory to explain this type of solar emission, we will summarize the important observed features below:

(1) Frequency Range

Normally the frequency range lies between 50 Mc/s and 300 Mc/s for background continuum radiation, but for bursts, it is shorter. However, a frequency as low as 6 Mc/s and as high as 400 Mc/s has been observed in rare cases (e.g. Fokker, 1961; Kundu, 1964).

(2) Bandwidth

The bandwidth of background continuum radiation usually extends to 100 Mc/s while that of a burst is very narrow, typically around 4 Mc/s (Payne-Scott, Yabsley and Bolton, 1947; Ryle and Vonberg, 1948; Wild, 1951; Elgaroy, 1961; see Fig. 5.2). However, wide-band bursts having bandwidths up to 35 Mc/s have been observed less frequently (Vitkevich and Gorelova, 1961).

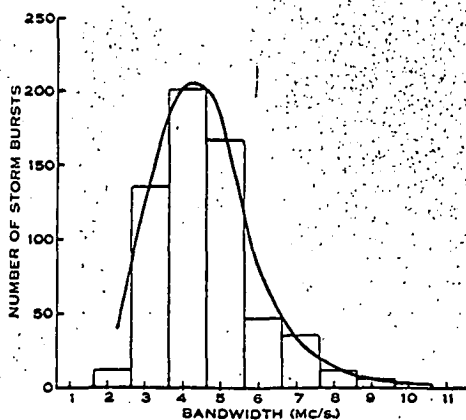
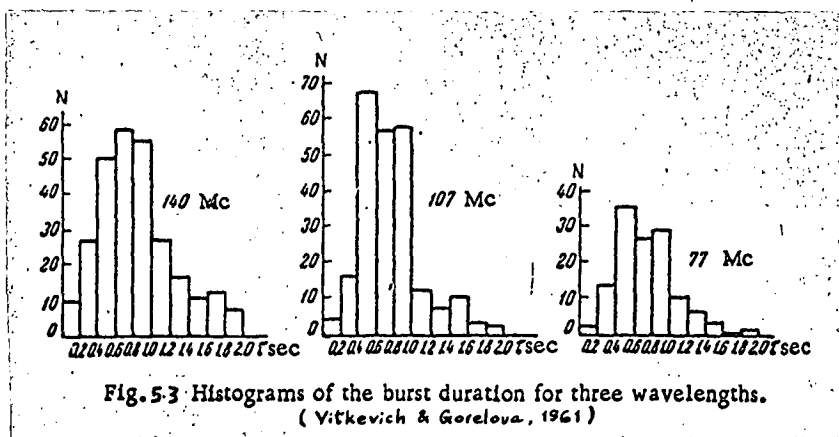
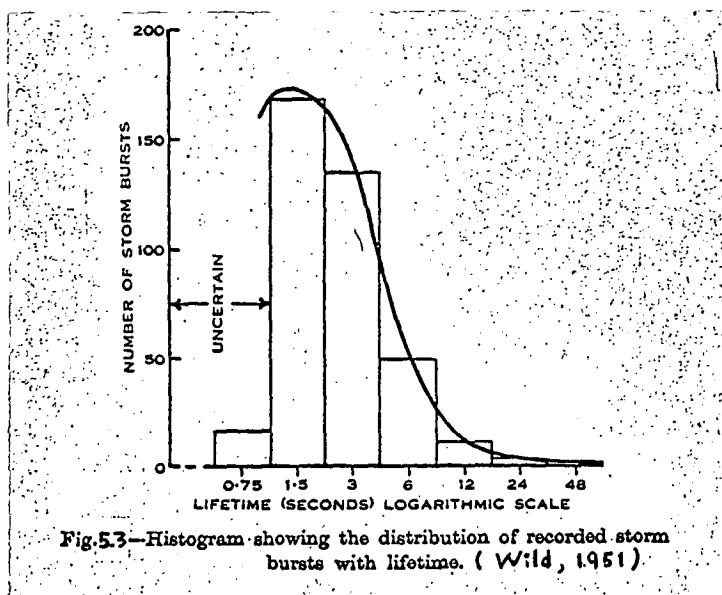


Fig. 5.2—Histogram showing the distribution of recorded storm bursts with bandwidth. (Wild, 1951)



(3) Duration

When a noise storm is in progress, the spectrum shows a slowly varying wide-band steady level lasting for hours or days. Above this continuum emission, short-lived bursts appear; the duration ranges from some tenths of a second to several seconds (Fig. 5.3).

(4) Frequency Drift of Bursts

In most cases, the mid-frequency of a burst stays constant (Wild, 1951; Vitkevich and Gorelova, 1961; Fig. 5.4). However, high speed sweep-frequency records of Elgaroy (1961) indicates that sometimes the frequency of a burst can increase or decrease in the course of time and the drift velocities range from 1 Mc/s per second up to tens of Mc/s per second (see also work of Vitkevich and Gorelova, 1961). Moreover, some "U-bursts" (in a event of a burst the frequency firstly decreases and then increases or vice versa) occur at times.*

Fig. 5.5 gives some examples of such events.

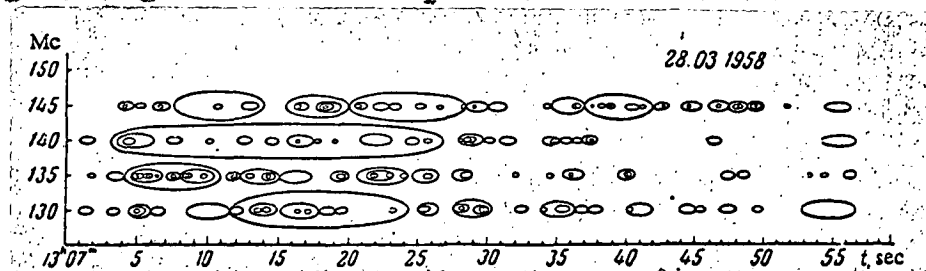


Fig. 5.4 Dynamic spectrum of narrow-band and wide-band bursts. (Vitkevich and Gorelova, 1961).

*There is also the possibility that the U-bursts are some particular cases of type III bursts.

Fig. 5.5 Some sweep-frequency records of storm bursts in the 190-215 Mc/s range (Elgaroy, 1961).

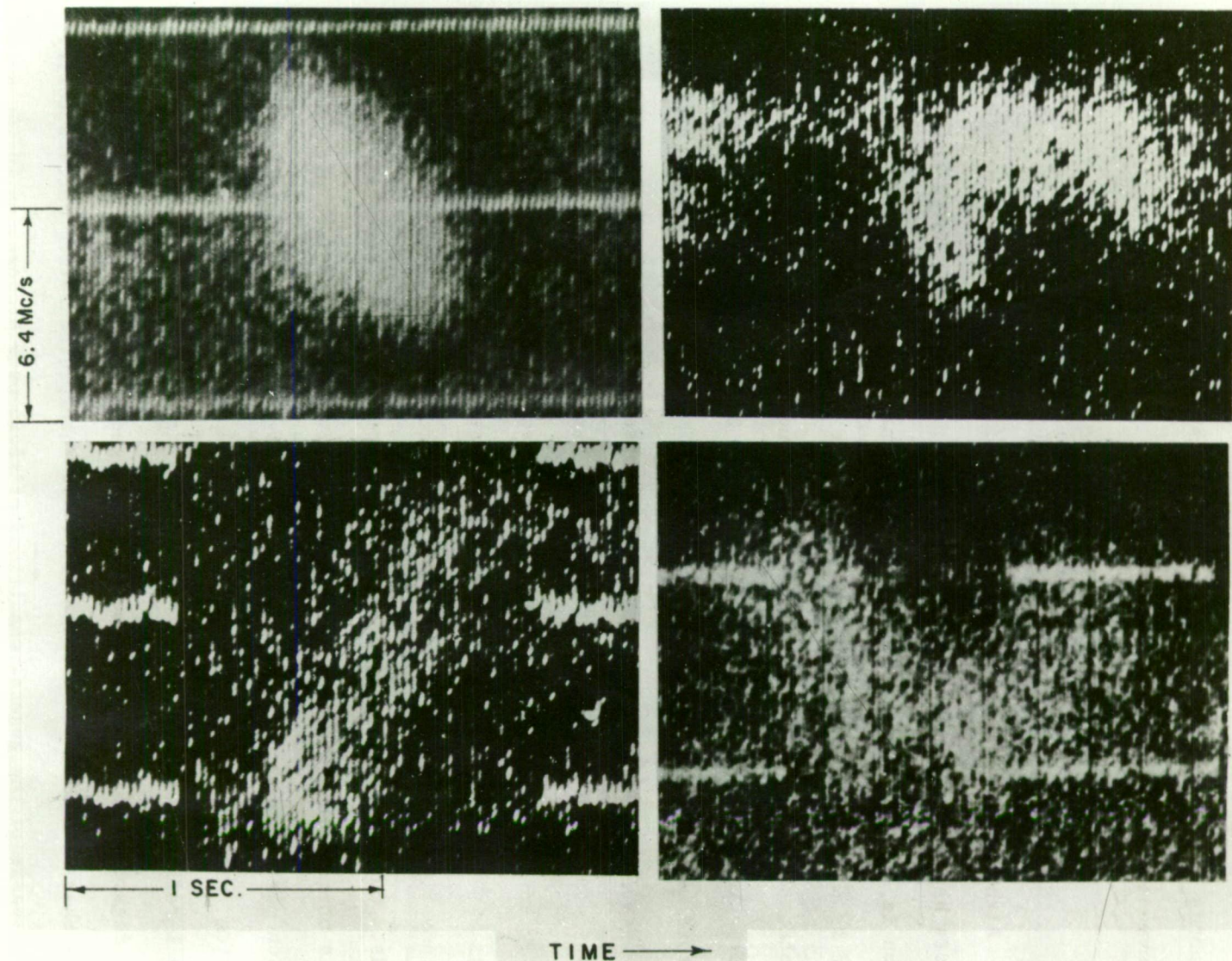


FIG. 12-55

(5) Relation between the Occurrence of Background Continuum and that of Storm Bursts

(i) There is good general daily correlation between the occurrences of the two components (Fokker, 1961).

However, during some periods a strong continuum radiation is detected with no appreciable burst emission, and vice versa (Wild, 1951).

(ii) There is no apparent correspondence between the integrated spectrum of bursts and the observed spectrum of continuum radiation (Wild, 1951; Fokker, 1961). However, as pointed out by Wild, by postulating a suitable amplitude distribution of the bursts (i.e. a suitable relationship between the amplitude A^+ of individual bursts and the occurrence probability of a burst of amplitude between A and $A + dA$ occurring in unit time), with the shape of the distribution being allowed to change slowly with time, the integrated spectrum of bursts may approach the observed spectrum of continuum radiation.

(6) Polarization (Suzuki, 1961; Kai, 1962)

(i) Referring to the magnetic polarity of the stronger

* A denotes the maximum amplitude reached at a particular frequency by an individual burst.

member (normally the preceeding spot) of a sunspot group, in most cases, the polarization of both background continuum and bursts corresponds to the ordinary mode radiation in the magneto-ionic theory. The sense of polarization of both storm bursts and background continuum at an instant during a noise storm are the same.

- (11) The majority of storm bursts are close to one hundred per cent circularly polarized. However, sometimes there are noise storms being composed of partially polarized, mixed polarized, or completely unpolarized bursts. A partially polarized storm may occur sporadically near the solar disk centre between days of completely polarized storm, but it occurs very often near the limb. This situation is indicated in Fig. 5.6. There is also a tendency that the percentage polarisation of the storm correlating to one spot group decreases rather suddenly at the limb. Fig. 5.7 shows some single-frequency records for various degrees of polarization. Note that there are three sources (situated at 0.1E, 0.6E and 1.3W radii on the solar disc) in the event observed by Kai.

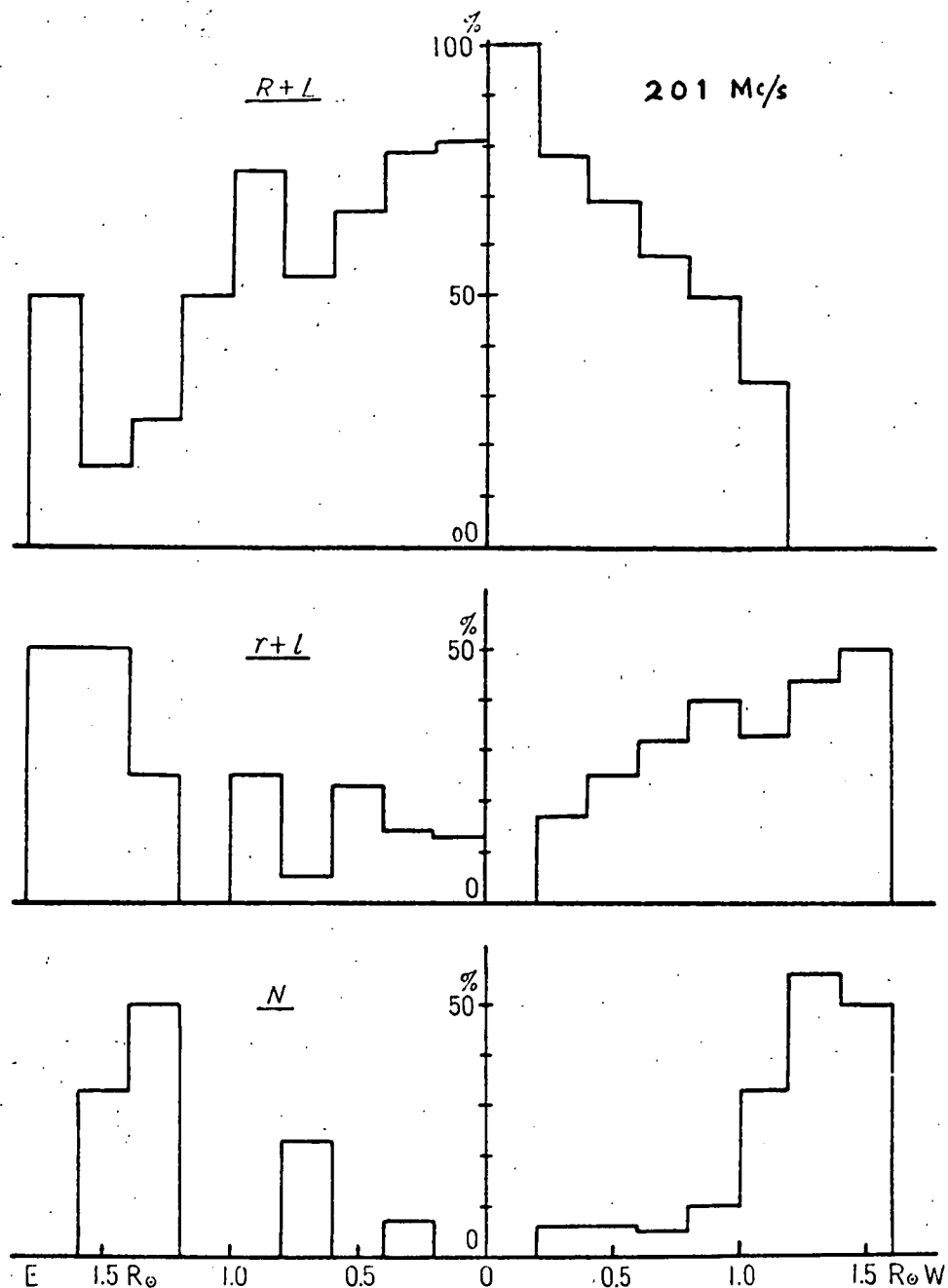


Fig.5.6 Distribution of the polarized noise storms on the solar surface. Three groups of noise storms are given according to the degree of polarization.

R, L — Strongly righthand, lefthand circularly polarized respectively

r, l — partially righthand, lefthand circularly polarized respectively

N — un-polarized

(Suzuki, 1961)

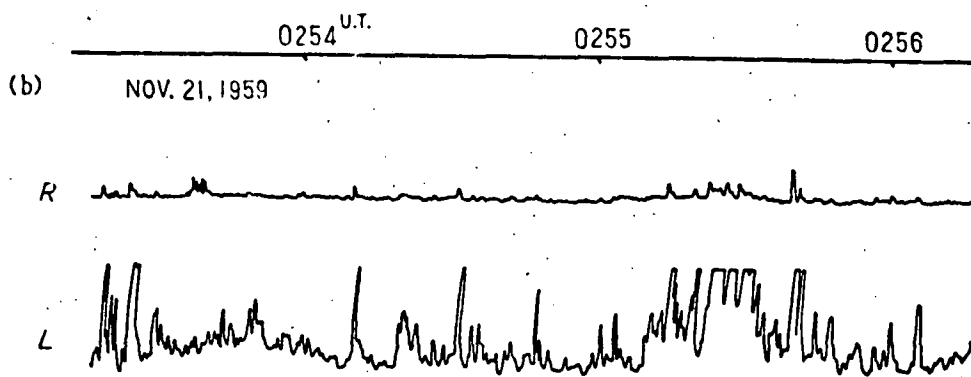
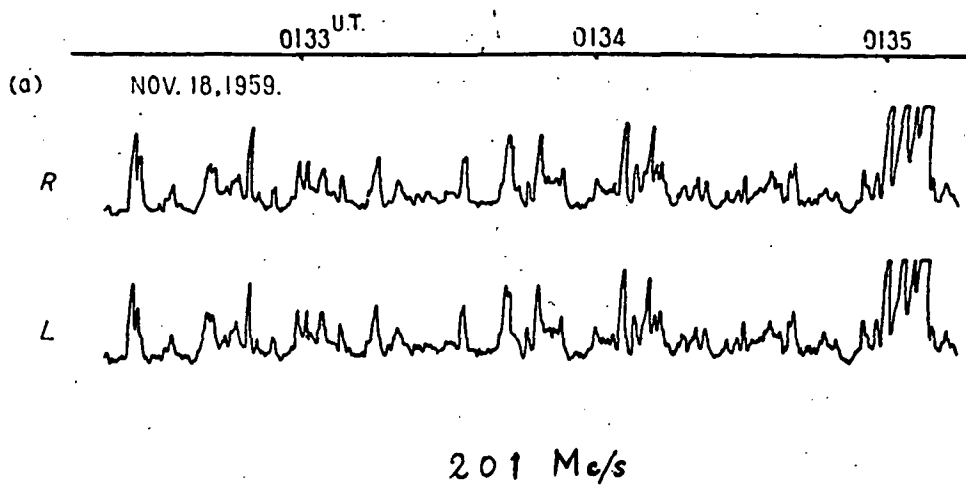


Fig. 5.7 Records for the unpolarized and polarized storm bursts on Nov. 18 and 21, 1959.
(Suzuki, 1961)

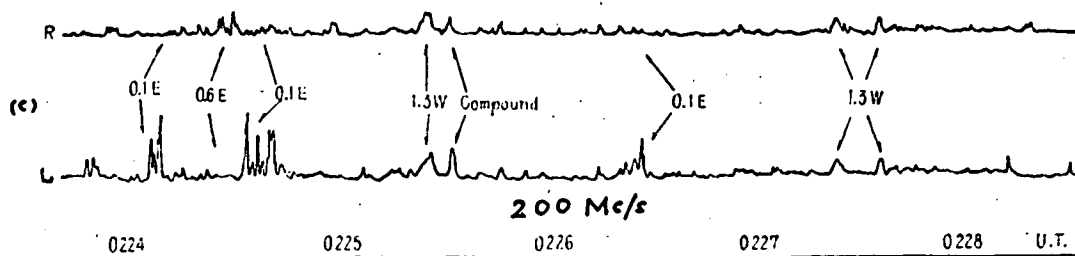
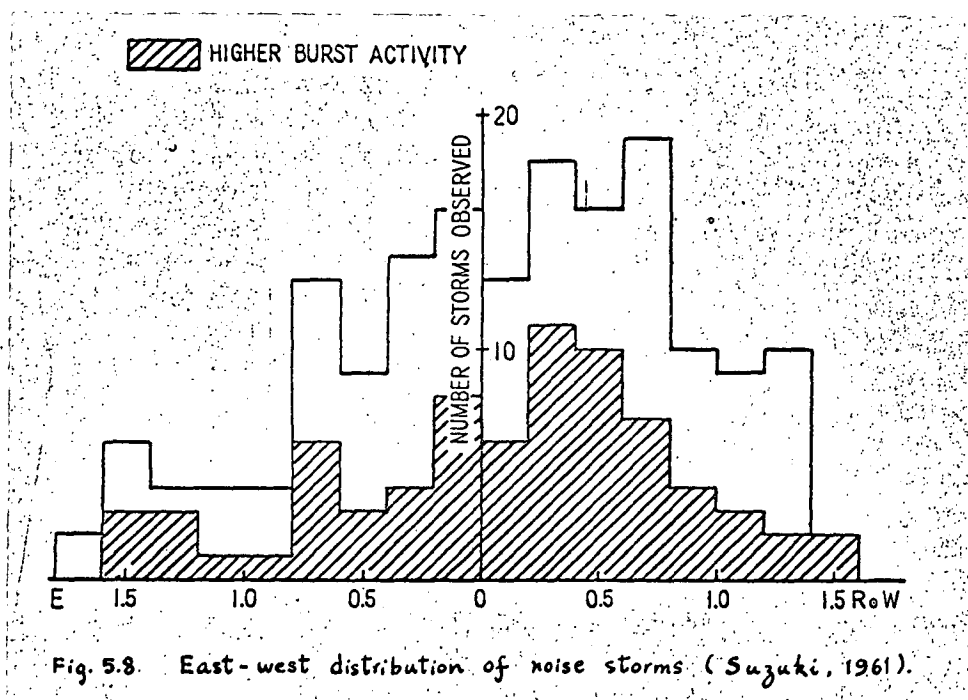


FIG. 5.7 An example of a limb event (Mar. 23, 1959). The upper record is the right-handed polarized component, and the lower one the left-handed component. The number indicates the position of a source.
(Kai, 1962)

(7) Apparent Source Positions (Suzuki, 1961; Fokker, 1961; Kai, 1962)

The experimental result on apparent storm centres, as observed on earth with respect to the position on the solar disc, indicates that the number of occurrence of noise storms decreases from the central meridian towards the limb (Fig. 5.8). This means that the storm radiation



has a narrow directivity. Moreover, the concentration of the noise storms is biased to the west, in contrast to the east predominancy of type III bursts (Wild, Sheridan and Neylan, 1959). During a storm both bursts and background continuum are normally observed to come

from the same source which has the size of a sunspot. To measure positions of bursts, Suzuki (1961) and Kai (1962) used multiphase interferometers whose accuracy in absolute position measurement is about $1''$ arc. One of such records is shown in Fig. 5.9 where the positions of sunspots and the instantaneous positions (circles) of storm bursts on 200 Mc/s in the course of a noise storm are indicated. The dotted line gives the centroid position of the background continuum and the line marked "transit" indicates the true local noon time.

From interferometric observations, Fokker (1961) measured the source positions of 255 and 169 Mc/s near the limb and found that the source position for 169 Mc/s is situated systematically higher than the source for 255 Mc/s (Fig. 5.10). The source positions for the two frequencies near the centre of the disc were found, however, to be more or less coincide. Since the source has a finite size, this result is understandable when one considers the difference in visibility. In general, the observed frequency of a noise storm decreases with increasing apparent source height.

Morimoto and Kai (1961) investigated statistically the heights of type I bursts on 200 Mc/s from a comparison of the apparent positions of bursts with those of the corresponding optical phenomena (sunspots). The mean height

of the source was found to be about $0.2 R_0$ (R_0 = solar radius) above the photosphere near the centre of the disc and to increase towards the limb (Fig. 5.11). A number of workers (e.g. Kundu, 1964) have suggested that this effect may be due to the fact that the height of the reflection level increases from centre to limb.

Most storm centres are not situated exactly radially with respect to the optical centres of the leading spots, but are not far away from them (Malinge, 1963).

The average altitude of the apparent source for a particular frequency is observed to be higher for the unpolarized storms than that of the polarized ones.

Perhaps the most interesting result in position observation is that storm centres are located near, but slightly above, the corresponding plasma levels (Kundu, 1964; Weiss, 1965).

(8) Association of Occurrence of Noise Storms with Solar Flare and Sunspots

- (1) Most noise storms are received within two hours after the occurrence of a flare and the most probable delay time between noise storms and flares is found to be approximately 30 min. (Fig. 5.12). However, simultaneous occurrence of a noise storm and a flare

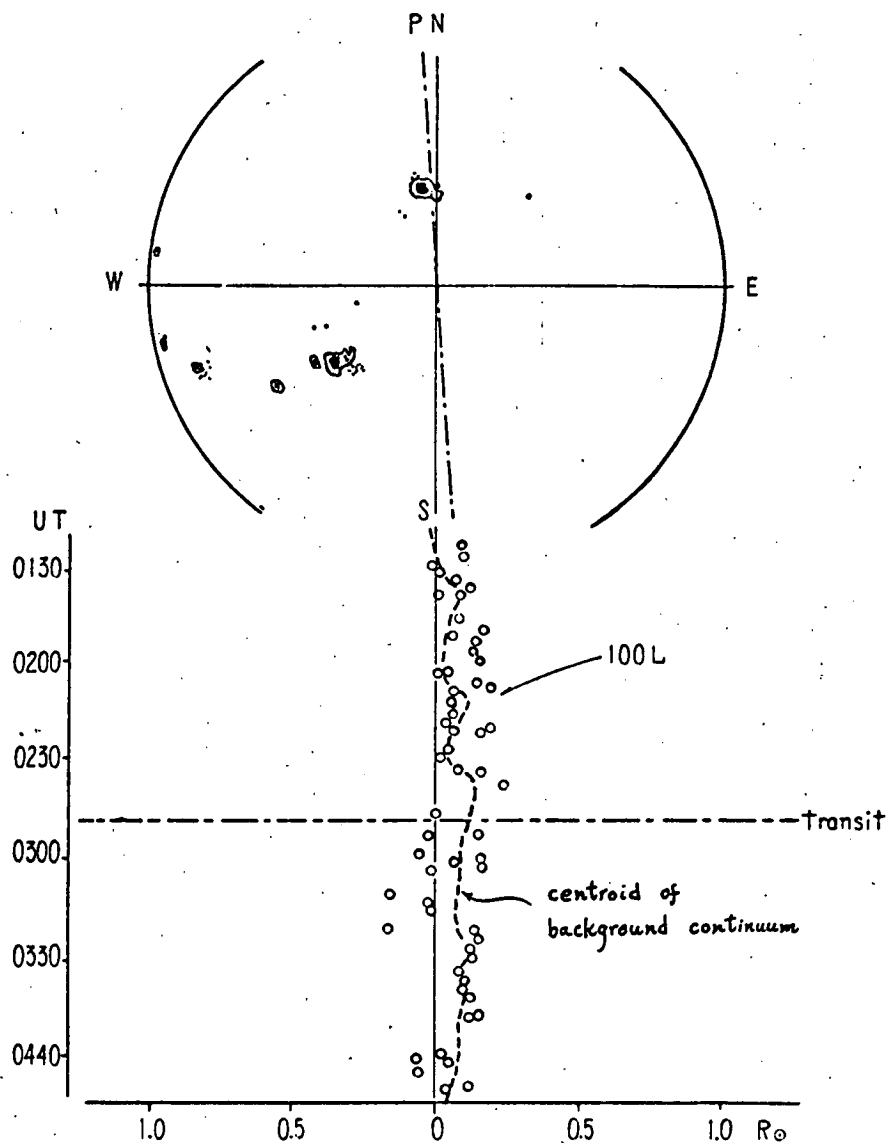


FIG. 5.9 Jan. 12, 1960. Each circle represents a instantaneous position of type I burst, and broken line represents that of the associating continuum. Individual bursts are completely polarized, while the continuum is partially polarized (80~90 %). The sense of polarization is the same both for burst and continuum. (Kai, 1962)

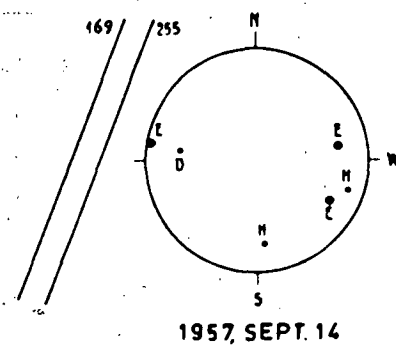
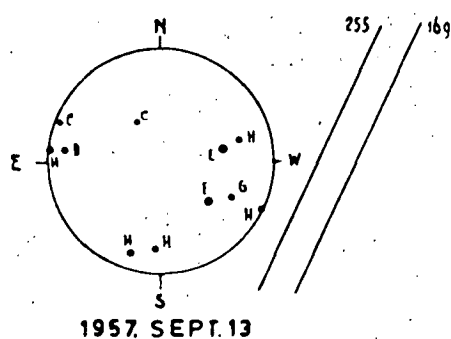
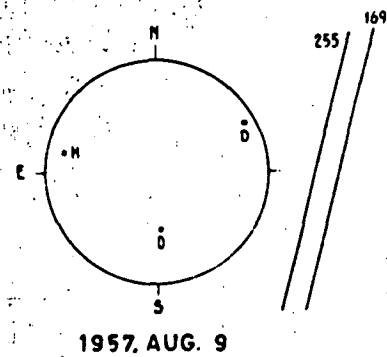
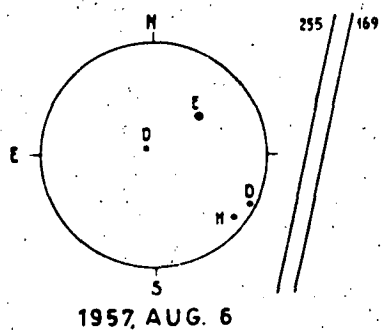
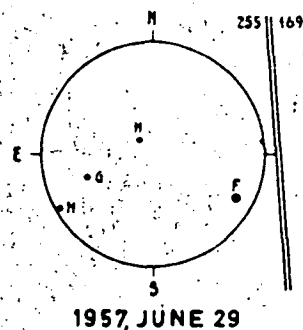
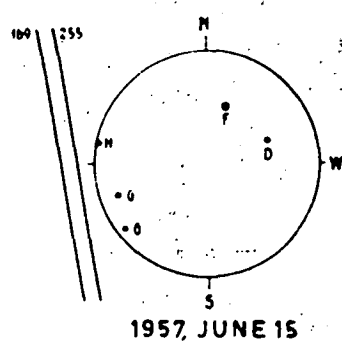


Fig. 5.10. Source positions of 255 and 169 M/s radiation near the limb. The straight lines indicate the source positions and the dots represent the positions of sunspot groups appearing at the time. (Fokker, 1961)

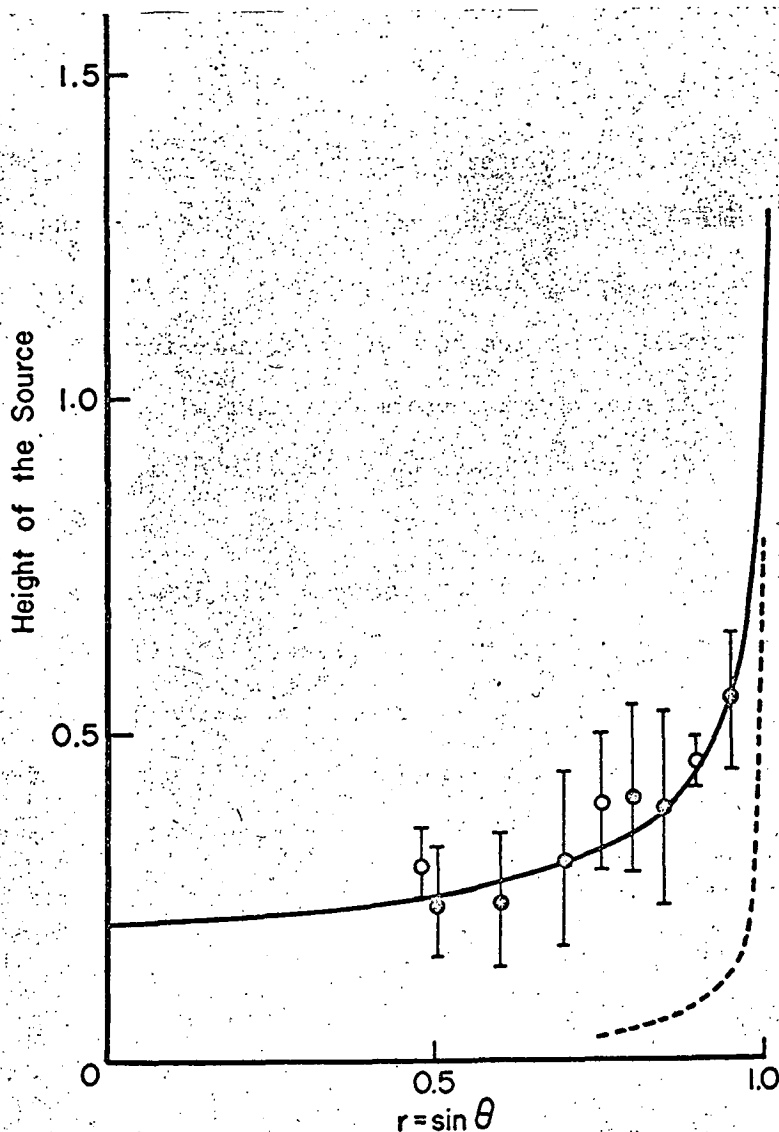


Fig. 5.11 Centre-to-limb variation of average height of type I bursts. Dots and circles correspond to type I and type III bursts respectively. Dashed curve represents the computed variation of height of turning point (reflection point) on 200 Mc/s for the Baumbach-Allen corona. Solid curve represents the same for a model with ten times the electron density given by the Baumbach-Allen model (Morimoto and Kai, 1961).

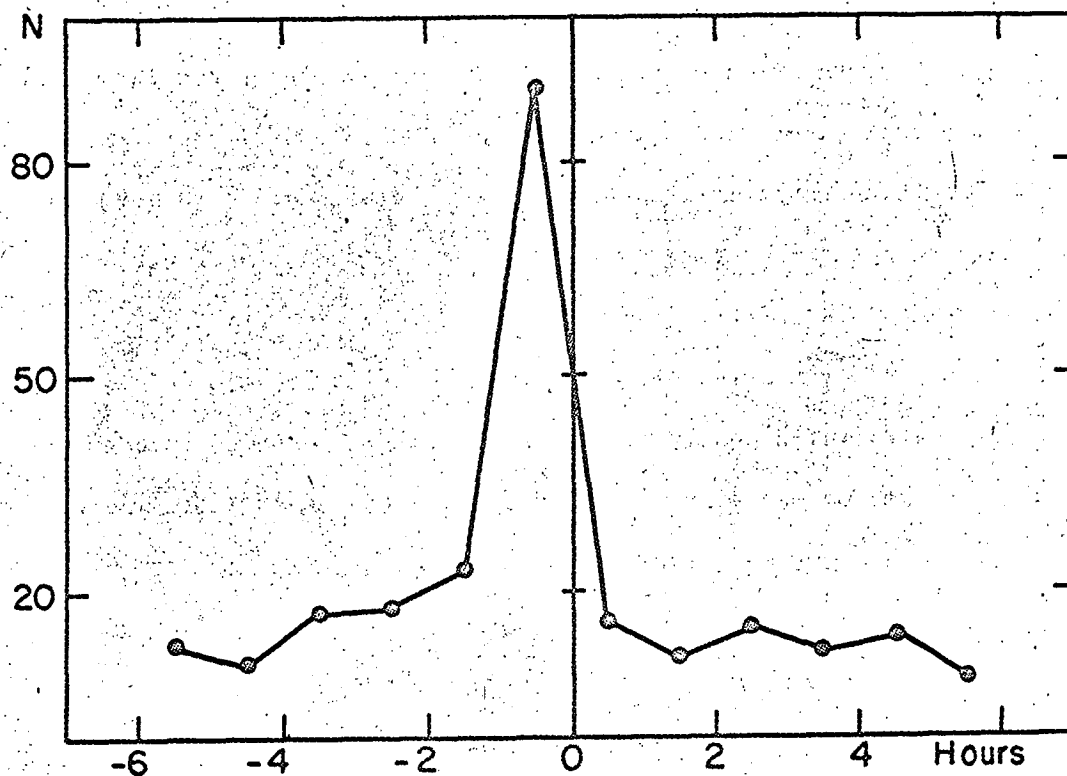


Fig. 5.12 Superposed-epoch diagram of the start of noise storms with respect to the start of optical flares (Malinge, 1963).

has been observed (Fokker, 1961; Wild, 1951; see Fig. 5.13).

- (ii) Noise storms are always associated with sun spots-group when the maximum area of the group is greater than about 6×10^{-4} of the solar disc and when the maximum area of the largest spot in the group is greater than about 4×10^{-4} of the solar disc. For sunspots of areas greater than 7.5×10^{-4} of the solar disc, the probability of association between the occurrence of noise storms and sunspots increases with the maximum magnetic field strength associated with the spots (Malinge, 1963; Payn-Scott and Little, 1951).

(9) Angular Size of Apparent Storm Centres

- (i) Using two-element interferometers, Tchickachev (1956) and Fokker (1961) observed that the storm centres on 200 Mc/s occupy diameters between $4'$ and $7'$ arc while storm centres on 150 Mc/s have an average size of $8'$ arc. The fact that the average source size of a noise storm decreases with increasing frequency has also been observed by Wild and Sheridan (1958).
- (ii) The angular sizes of storm bursts were found to be much smaller than those of storm centres, being less

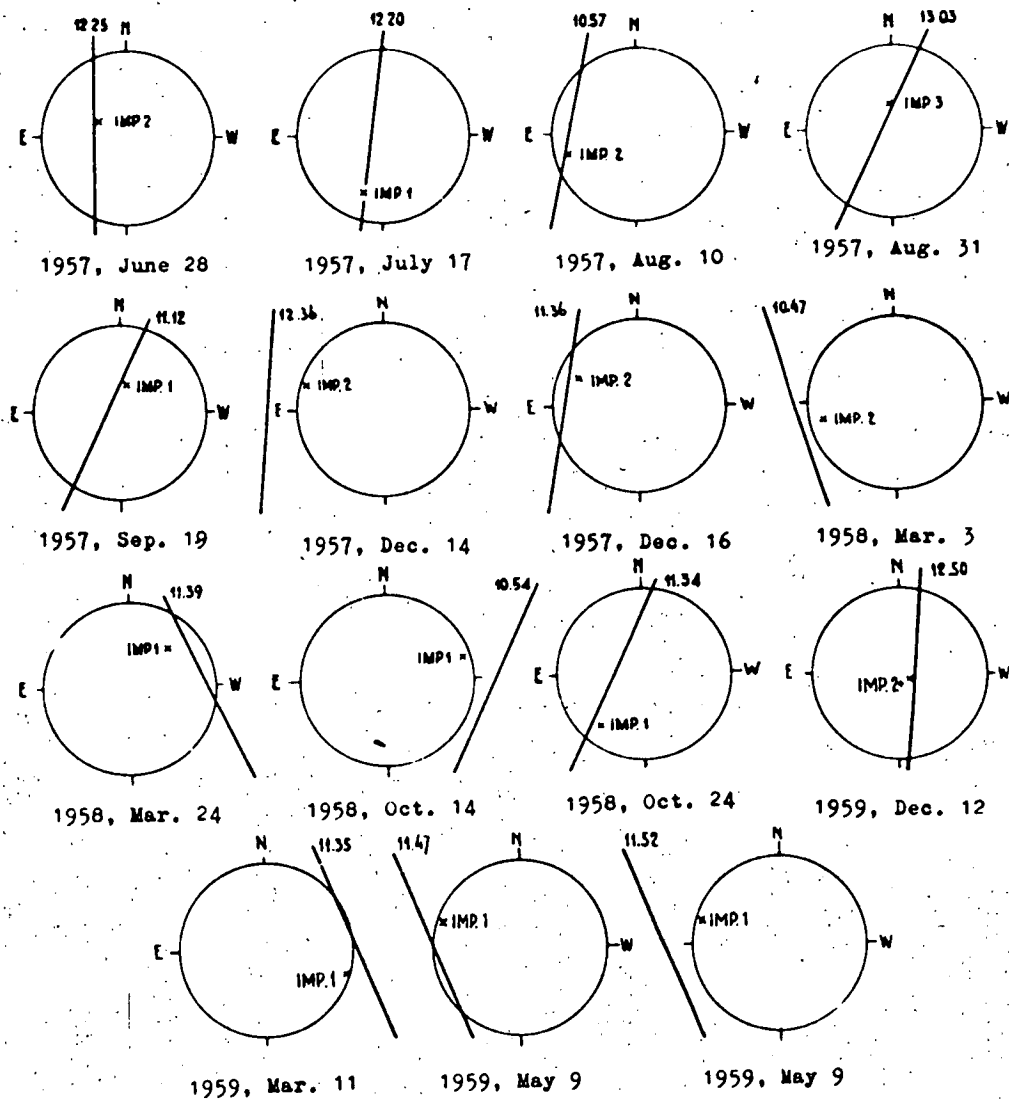


Fig. 5.13

Positions of flare-associated outbursts, 255 M₄₅.
The cross indicates the position of the flare (Fokker, 1961).

than 1'6 arc on 105-140 Mc/s (Goldstein, 1959).

(iii) The size of the background continuum in a noise storm has been found to be the same as the scattering range of the individual bursts (Kai, 1962).

(iv) The mean apparent source size of bursts which are partially or unpolarized is generally larger than that of strongly polarized bursts (Suzuki, 1961).

However, the finite source size as observed may mainly be due to scattering.

(10) Flux Density Received

The peak flux density of a noise storm received on Earth ranges from about $10^{-22} \text{ Wm}^{-2}/(\text{c/s})$ to $10^{-20} \text{ Wm}^{-2}/(\text{c/s})$ (e.g. Fokker, 1961).

A detailed study of many observed features of type I noise storms is given by Fokker (1961). A very comprehensive review of the subject (both observed characteristics and interpretations) has been contributed by Kundu (1964).

(C) Existing Theories of Type I Noise Storms

To explain part of the listed observed properties, a number of theories concerning the generating mechanism and

propagation condition has been proposed. The theory of cyclotron radiation from fast electrons in the corona (relativistic or mildly relativistic) has been investigated by Kiepenheuer (1946), Kruse, Marshall and Flatt (1956), Takakura (1956) and Twiss and Roberts (1958). However, all these theories are qualitative only and none of them explains why the o-mode waves is observed, instead of the x-mode wave which carries more power according to Eidman's equation[†].

Ginzburg and Zheleznyakov (1959) suggested that the background continuum radiation would be caused by coherent radiation from the coronal plasma permeated by a magnetic field $H > 1$ gauss, mainly in the o-mode. The burst are thought to be generated during the damping of free oscillation in the corona.

Denise (1960a, 1960b) suggested that the charged particles, which have been trapped in some magnetic field configuration in the active region, diffuse along the solar streamer slowly towards the Sun and excite plasma waves which then couples to electromagnetic waves in the ordinary mode.

[†]This equation gives the power radiated in both modes by a single electron in a magnetoactive plasma. The equation was later rederived by Liemohn (1965) who corrected a few errors in Eidman's work.

Ginzburg and Zheleznyakov (1961) re-examined the possible generating mechanisms for sporadic solar emissions in light of emission power consideration and they concluded that incoherent cyclotron radiation from weakly relativistic electrons (energy $\sim 10^2 - 10^3$ Kev. and density ~ 1 electron/cm³) might be responsible for the background continuum radiation, while storm bursts cannot be related to incoherent emission from either cyclotron, synchrotron or Cerenkov radiation.

According to Malinge's theory (1963), for a storm centre situating above the plasma level, the continuum radiation arrives on earth directly from the source whereas the type I bursts radiation arrives indirectly after reflection at a reflection level which is lower than the generating position. The reflection stated is assumed to occur at density inhomogeneities which do not have a stable form in time and a small change in the configuration of such inhomogeneities could account for the large fluctuation of intensity and change in position of type I bursts.

Recently, Takakura (1963) employed the "combination scattering" theory (Rayleigh ^{type} scattering of coherent plasma waves) put forward by Ginzburg and Zheleznyakov (applied to type III bursts) to explain type I bursts. According to his theory, the coherent plasma waves are excited by a stream of electrons with a group velocity which is a few times the

electron mean thermal velocity. The electron stream is supposed to be created and accelerated at a collision of two Alfvén wave packets travelling in opposite directions.

So far, all the theories proposed have been speculative only. Each theory is successful in explaining a few aspects of the observed properties. To put forward a successful theory, one has to study the theory in great detail, in a quantitative way.

From radiation power consideration, the Bremsstrahlung process is out of the way. Since plasma waves cannot exist outside the plasma, any plasma wave hypothesis necessitates the existence of an efficient coupling mechanism (from plasma waves to transverse electromagnetic waves). After setting up some models for density distribution and spot-field configuration in the active corona (chapter VI), we, therefore, study the coupling conditions in the possible source region (chapter VII). The result indicates that in the corona, the two possible coupling mechanisms^{*} are inefficient, i.e. only a very small fraction of the energy associated with plasma waves is transferred to the transverse electromagnetic

^{*}One of these mechanisms is the transfer of plasma waves into electromagnetic waves through Rayleigh^{type} scattering. The other process is the coupling of characteristic modes (o-mode and x-mode).

energy. This result, together with polarization observations, suggests that the cyclotron mechanism is beyond doubt the more plausible generating process. Indeed, among all types of solar emissions, type I noise storms occur most frequently during solar active periods. Understanding the generating mechanism and propagation will lead to a better realization of the physical conditions in the solar corona, particularly during the active periods. We intend, hence, to investigate the cyclotron radiation theory and the propagation of the subsequent electromagnetic waves in detail.

We suggest that electron streams travelling in spot-field configurations are the cause of both the background continuum and burst radiation. In chapter VIII, we study the possible emitted range of frequencies for x- and o-modes by assuming some pitch angles and kinetic energies of the electron stream spiralling in the spot-field. The Eidman's equation is employed to find out the power spectrum radiated by a single electron in a magnetoactive plasma (corona) for both modes. From the radiative instability theory developed in chapter II, the growth rate for the radiated electromagnetic waves in both modes in the stream-plasma system is evaluated for some typical cases in the source region. Subsequently, the propagation conditions (the escape conditions through the corona) for both modes are investigated: this includes the study of

reflection levels and the first three harmonic resonance absorption levels. To end that chapter, we list the important predictions from the cyclotron theory. The ray tracing problem and theoretical dynamic spectra of storm bursts are investigated in chapter IX. Chapter X concludes the interpretation of solar type I noise storms.

CHAPTER VI

MODEL OF THE SOLAR CORONA

In order to investigate the coupling conditions as well as to study a plausible generating mechanism and the subsequent propagation conditions in a quantitative way, we need some models for the electron density distribution and spot-field configurations in the corona. In the source region, the Sun's general magnetic field is very much smaller than the sunspot field and we will neglect the effects of the general field.

(A) Radial Distribution of Electron Density in the Corona

Allen (1947) modified the formula given by Baumbach (1947) for the radial distribution of electron density in the corona:

$$N = 10^8 (1.55 \rho^{-6} + 2.99 \rho^{-16}) \text{ els/cm} \quad (6.1)$$

where $\rho = R/R_0$, R = distance from centre of the Sun.

Corresponding to electron density N , the electron plasma frequency is given by $f_p = \sqrt{Ne^2/(\pi m_0)}$. The Baumbach-Allen model is the well known conventional one for the background or normal corona.

Situated above an optical centre of activity (sunspots and plages), there is a region of enhanced plasma

density permeated by the sunspot magnetic field. Such a region in the corona is called an "active region".

From radio observations of the positions for type II and type III bursts, the electron densities in the source regions are found to be around ten times over the values given by the Baumbach-Allen model (Weiss, 1963; Shain and Higgins, 1959; Wild, Sheridan and Neylan, 1959; Morimoto and Kai, 1962). The required model for the source regions of type II and type III bursts agrees with that deduced for typical coronal streamers⁺, which have been observed optically (Newkirk, 1959). This result suggests that type II and type III disturbances may travel outwards along coronal streamers (Fig. 6.1). Note that between the altitudes $0.2 - 0.5 R_{\odot}$ (most noise storm are observed to occur within this region), the electron densities given by Newkirk's model are about five times that of Baumbach-Allen's model. For the purpose of numerical calculation, Newkirk's model within the region $0.2 - 0.5 R_{\odot}$ may be assumed to be:

$$N = 5 \times 10^8 (1.55 \rho^{-6} + 2.99 \rho^{-16}) \text{ els/cm} \quad (6.2)$$

⁺Corona streamers are formations of plasma emerging slowly, almost radially from the Sun in the active regions.

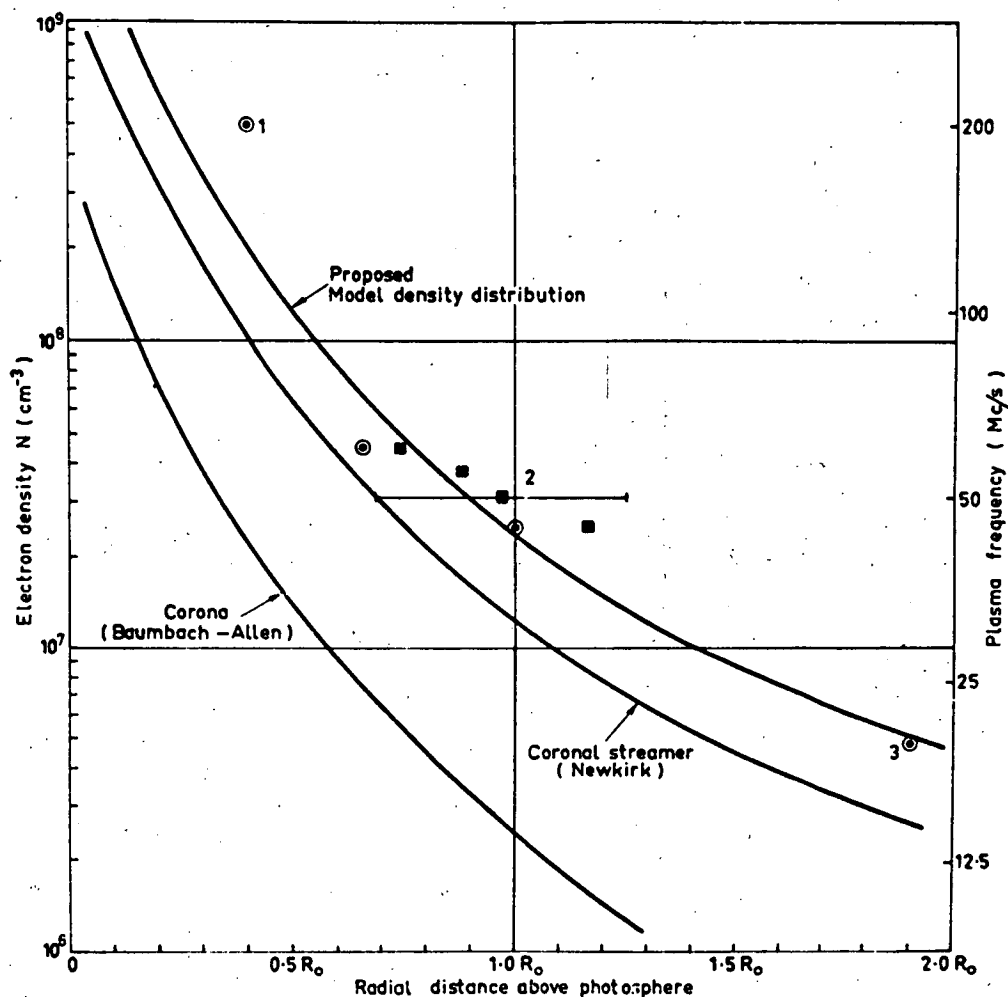


FIG. 6.1 Average electron densities in the corona as a function of height. The plotted points give the measured height of origin of type II and type III bursts. \odot —type III bursts (Morimoto; Wild, Sheridan & Neylan; Shain & Higgins). \blacksquare —type II bursts (Weiss); the bar represents the probable error of the 50 Mc/s point and is typical of the errors in all four points for type II bursts. The full curves represent model electron density distributions (the standard Baumbach-Allen corona, the density of the average coronal streamer as given by Newkirk (1959), and a streamer with twice the density given by Newkirk). The results suggest that type II and type III disturbances may travel outwards along coronal streamers [Weiss 1963]

(Wild, Smerd & Weiss, 1963)

(B) Models of Spot-field Configurations

Before we set up our theoretical models for the spot-field configurations which turn out to be necessary in our later investigations, we will outline briefly some observed data about sunspots.

Sunspots are regions of intense magnetic field from the visible surface of the sun. As a result of the extensive observations of Hale and his collaborators at Mt. Wilson, we have a classical picture of the magnetic field configuration inside the surface of a regular, single spot:

- (i) The spot is circular in area on the Sun's surface and the field is symmetrical around the axis of the spot.
- (ii) The field line of force is maximum at the centre of the umbra and it is almost perpendicular to the solar surface at this point.
- (iii) Away from the centre of the umbra the field becomes smaller and inclined to the vertical; an inclination of about 70° being attained at the outer border of the penumbra.

All sunspots have detectable magnetic field strength and the maximum field strength of the spot is directly proportional to the spot area. The maximum field strength

on the photosphere is found to be about 4,000 gauss for the largest spots and is of the order of 100 gauss for the small spots (Hale and Nicholson, 1938).

A systematic attempt has been made (von Klüber, 1948) experimentally to investigate the variations in field strength as well as brightness across spots. A typical example of the variation of light intensity and magnetic field strength along a diameter through a sunspot is given in Fig. 6.2.

Sunspots occur as individuals or in groups of two or more. Many spots tend to appear in associated pairs, with the polarities of the two poles being of opposite signs. The single spot is known as unipolar sunspot while an associated pair is referred to as bipolar sunspots group. During every solar cycle, spots appear firstly at a solar latitude of about 30° north and south, then the zones where the spots occur are slowly displaced towards the equator. The number of spots attains a maximum value when the zones reach 10° north and 15° south latitudes. In such action of a bipolar group, the member which "leads" the way is termed the "leading spot", whereas the other member is called the "following spot". Usually, the leading spot is the magnetically stronger one in the associated pair.

The unipolar and bipolar sunspots are the simplest types. It has been pointed out (Bray and Loughhead, 1962, 1964) that

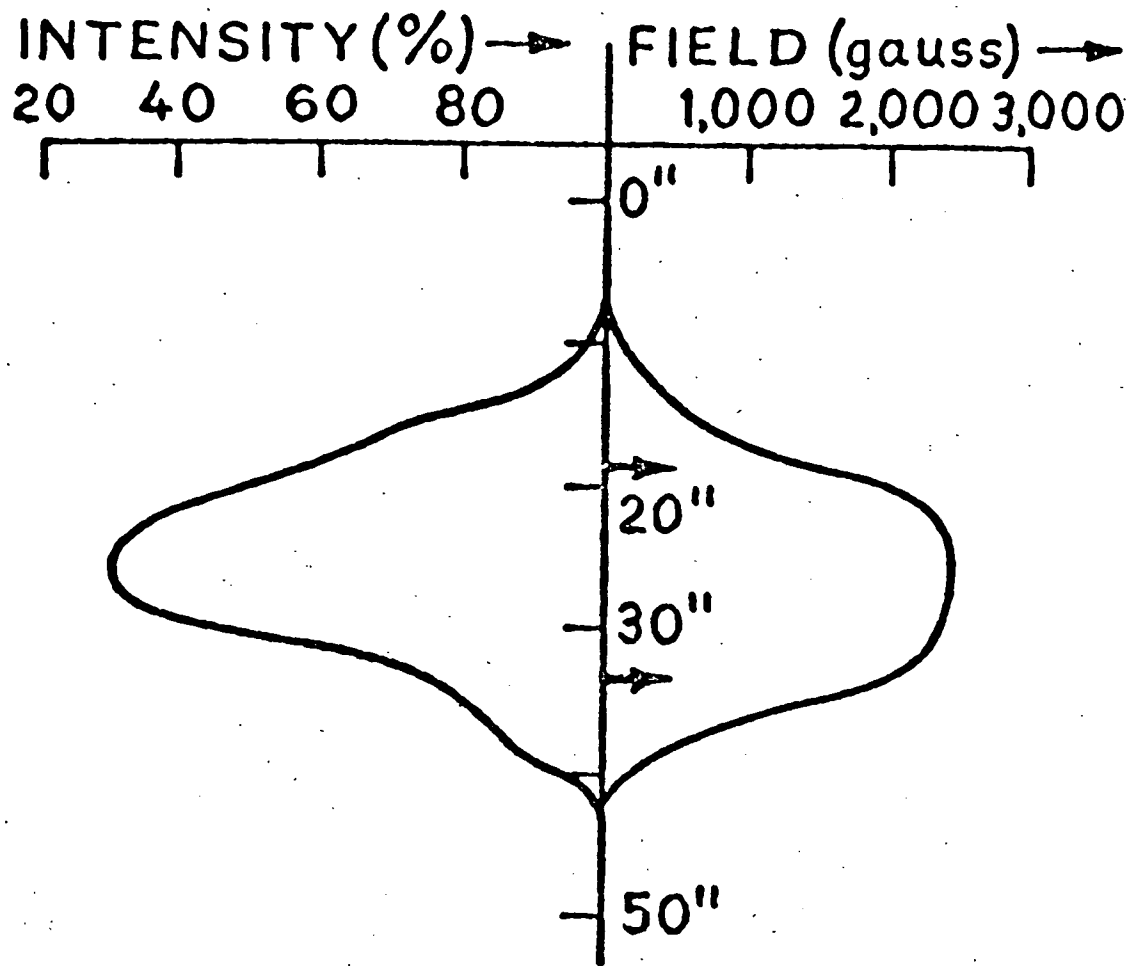


Fig. 6.2 Variation of light intensity and magnetic field strength along a line through a sunspot. The arrows indicate the approximate limits of the umbra. (von Klüber, 1948)

experimental results have indicated that regions of opposite polarity may frequently appear even within a single isolated spot. No matter how complicated the structure of the spot's field is, the field line can only either stretch straight into the corona as coming from a unipolar spot, or go up and bend down to join a region of opposite polarity which can be the following spot in a bipolar spot-group or a region in some spot near by, or in the leading spot itself. Consequently, if we take that the electron stream (which is supposed to be responsible for the noise storm emissions) is trapped in the strongest field line of a magnetic field structure which is either of the unipolar nature or belongs to a bipolar character, the description of the generating mechanism and escape conditions will be physically meaningful. We will devote the rest of this chapter to setting up two models for spot-field configurations. It must be pointed out here that up to the present, there is no experimental result giving the magnitude and the exact nature of spot magnetic fields above the photosphere. Our models, therefore, are empirical only.

Referring to Fig. 6.3, we assume an imaginary dipole situated at a point P , at a distance PE below the photosphere. Some lines of force originating from this dipole emerge from a circular area a (spot area) on the Sun's surface. By choosing a suitable orientation of the imaginary dipole with respect to the radius of the Sun and the distance PE , one can obtain a situation where the field intensity at the point

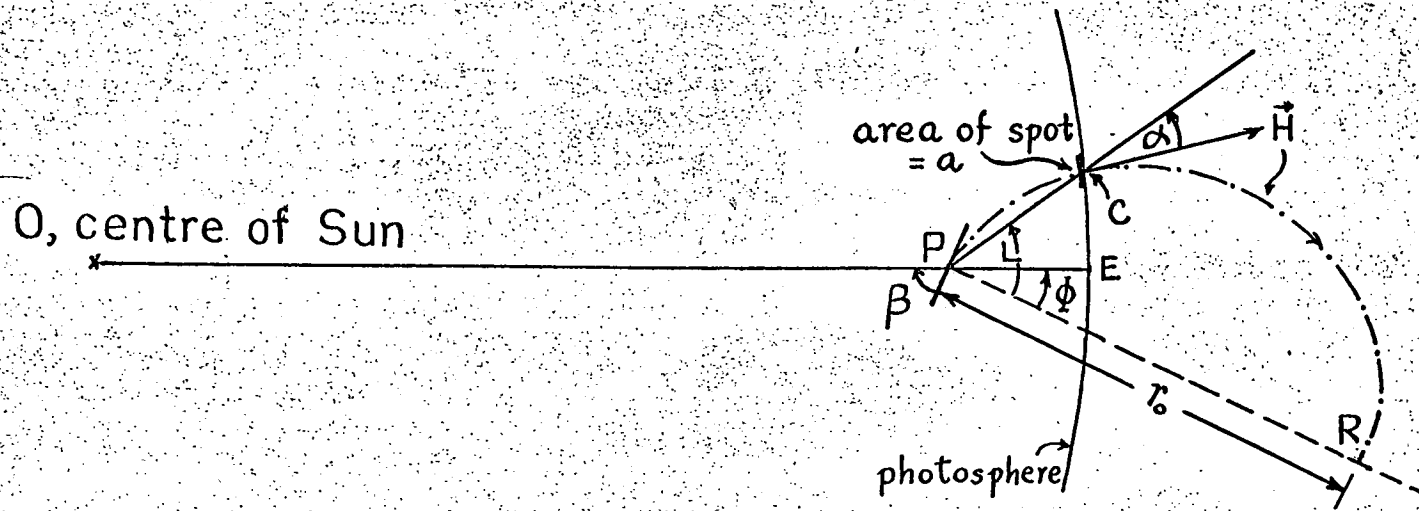


Fig.6.3 Geometry showing the calculation of a theoretical bipolar spot-field configuration.

O is the centre of the Sun and P is the mid-point of the imaginary dipole. The line $-----$ represents the field line passing through the centre C of the leading spot of area a .

PR is perpendicular to the axis of the dipole.

C which is the centre of the spot, is the strongest in comparison to the intensity at any other point on a. It should be remarked that for a fixed value of β , we can vary the distance PE in order to achieve this condition. With PR perpendicular to the dipole, angle $l' = L$ will be the latitude angle for the field line at the point C ($l' =$ latitude angle with respect to PR). If, considering a particular field line, $r = r_0 \cos^2 l'$, where $r =$ radius vector at a point of the field line, $r_0 =$ distance between the middle point of the dipole axis and the point of minimum field strength along the line, the dipole field equation gives

$$H = \frac{M}{r^3} (1 + 3 \sin^2 l')^{\frac{1}{2}} \quad (6.3)$$

where M is a constant depending on the pole strength of the dipole.

If we now let $PE = 0.1 R_0$ ($R_0 =$ solar radius), $\beta = 70^\circ$, $L = 60^\circ$ and $\phi = 20^\circ$ in our present case, and we let the field intensity at C to be 2,500 gauss, one finds that the field strength of the field line passing through C to be specified by

$$H = \frac{8.4}{r^3} (1 + 3 \sin^2 l')^{\frac{1}{2}} \quad (6.4)$$

and $r = 0.63 \cos^2 l'$

The field direction at any point along the field line is given by

$$\tan \alpha = \frac{1}{2} \cot l' \quad (6.5)$$

where α = angle between the field line and the radius vector passing through the point in question. From geometry, it is elementary to show that at the point C, the field line is making an angle of 22.7° with the solar radius vector passing through C.

Following the same method one can calculate the field intensity (equation similar to (6.4)) and the direction of the field vector \vec{H} of any point along all the field lines emerging from the spot area a . These lines will terminate on the other spot of the associated sunspot pair. It is found that with this model, the field intensity on the spot area follows a very similar pattern as observed experimentally by von Klüber (Fig. 6.2). However, we note here that although the field intensity at the centre of the spot on the photosphere is maximum, the field line passing through this point may not be the strongest field line emerging through the spot. We note here that a very similar magnetic field model, like the one described above, was introduced by Takakura (1961).

When we consider a unipolar spot, we will assume the axis of the imaginary dipole is along a radius vector of

the Sun, and only some lines of force from the pole nearer to the photosphere will emerge through an area (spot area) on the surface. These field lines are supposed to be straight, extending to the corona and the line passing through the centre of the spot will be the strongest line, whose magnetic intensity at a height ($\rho - 1$) being specified by (Gingburg, p. 413, 1964):

$$H = H_S \left(1 - \frac{\rho - 1}{\sqrt{(\rho - 1)^2 + b^2}} \right) \quad (6.6)$$

where b is the radius of sunspot in units of solar radii and H_S is the maximum field intensity of the spot.

Following Gingburg, we take b to be 0.05.

Some examples of theoretical spot-field configurations and electron density distributions are indicated in Fig. 6.4.

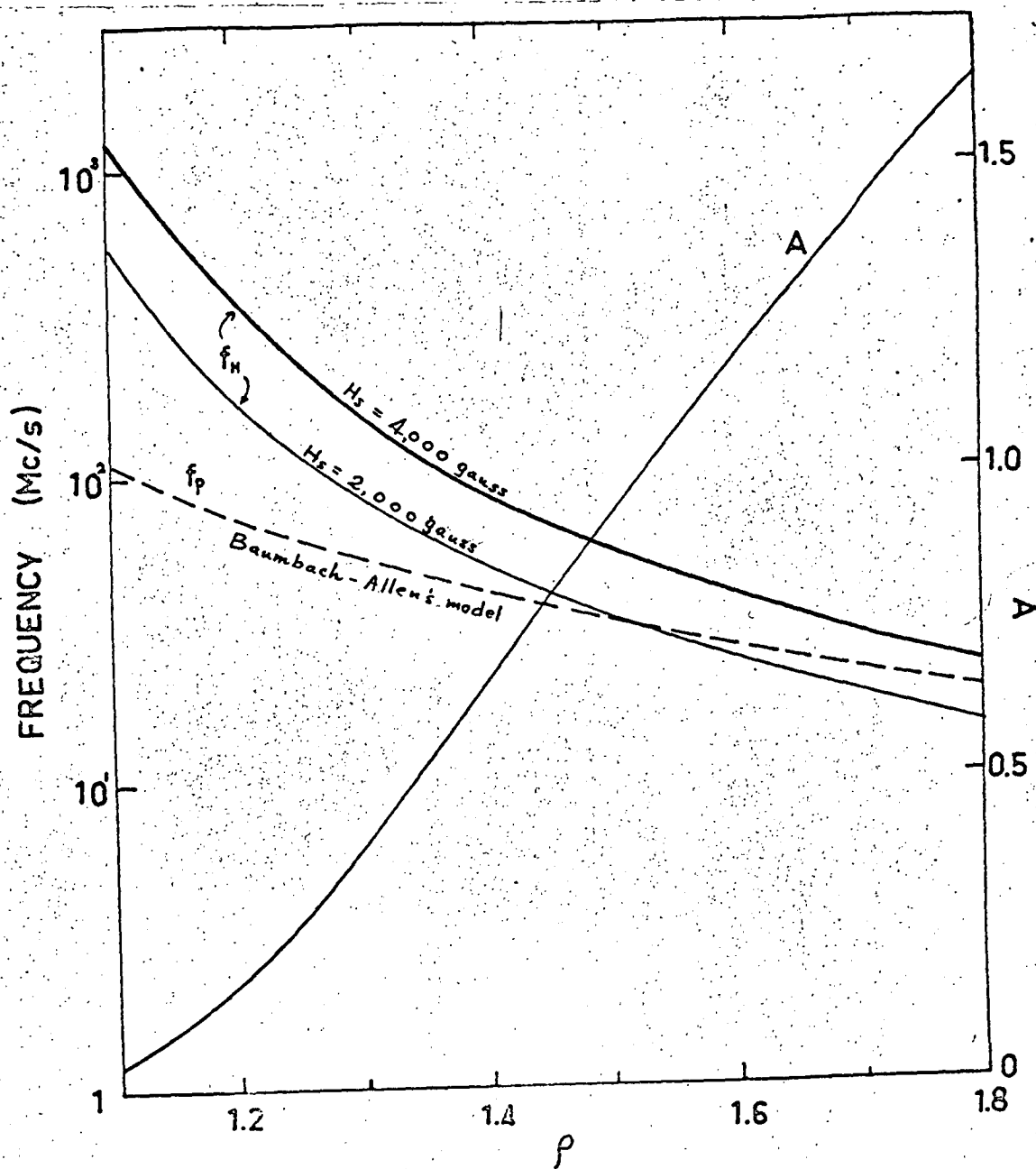


Fig. 6.4(a) Variation of the plasma frequency f_p (Baumbach-Allen's model), gyro-frequency f_H and A along the strongest field line of a unipolar spot with $H_s = 2,000$ gauss. The variation of f_H with ρ when $H_s = 4,000$ gauss is also plotted for comparison.

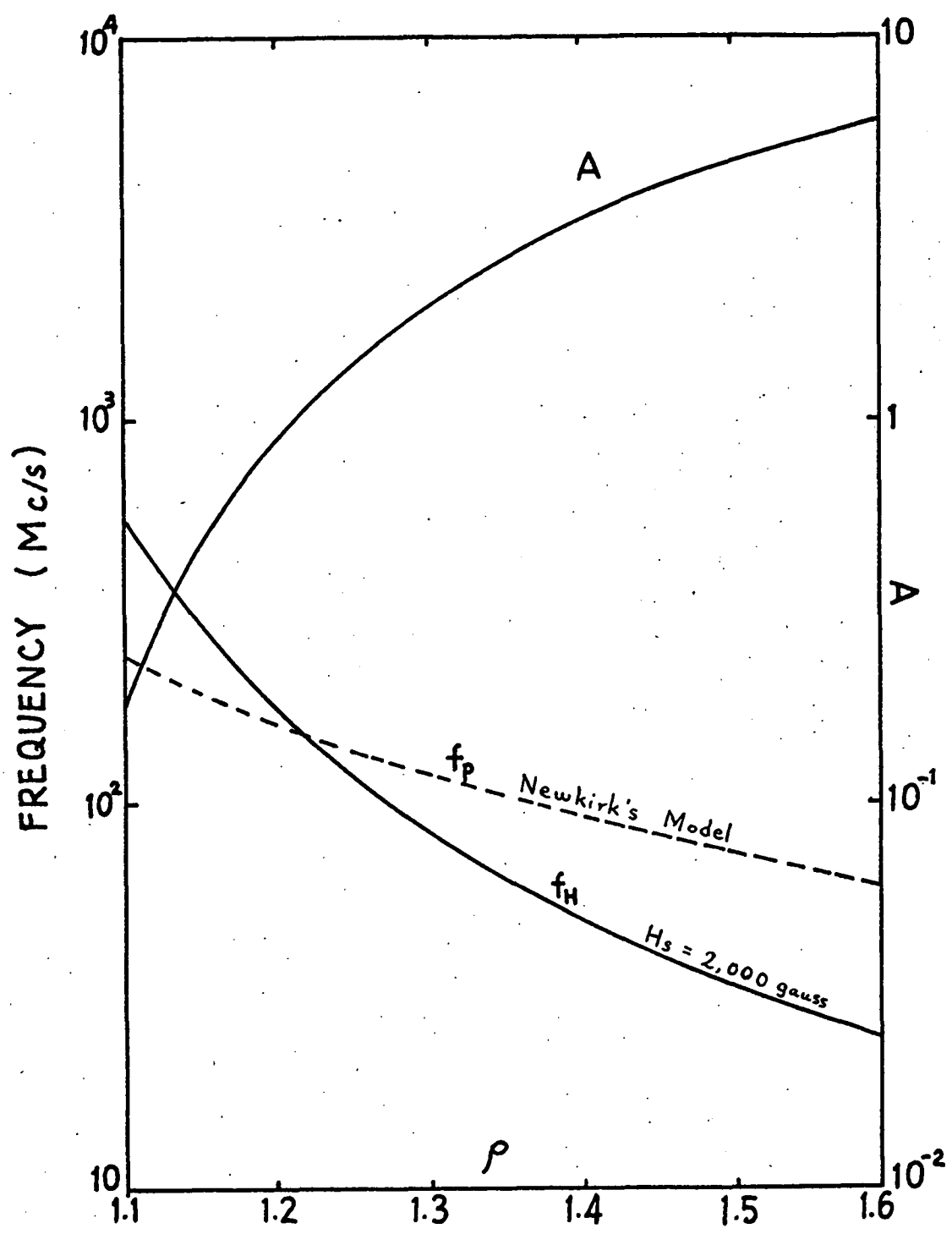


Fig. 6.4(b) Variation of the plasma frequency f_p (Newkirk's model), gyro-frequency f_H and A along the strongest field line of a unipolar spot specified by $H_s = 2,000$ gauss.

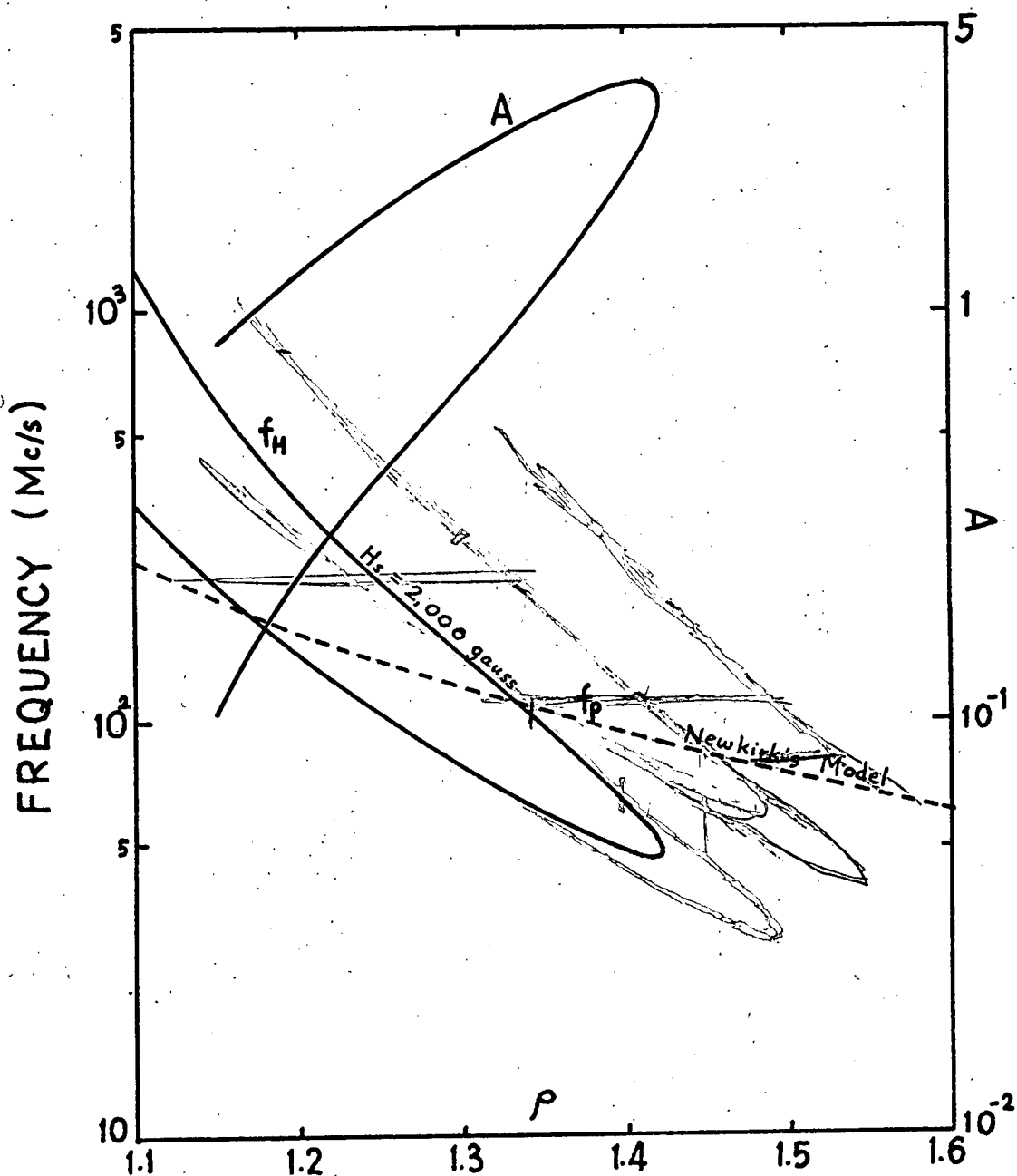


Fig. 6.4(c) Variation of the plasma frequency f_p (Newkirk's model), gyro-frequency f_H and A along the strongest field line of a bipolar spot-group specified by $H_s = 2,000$ gauss.

CHAPTER VII

COUPLING CONDITIONS IN THE SOLAR CORONA

(A) Introduction

In the type I noise storm source region where appreciable spot magnetic fields prevail, the two more plausible generating mechanisms are the cyclotron mechanism and the Cerenkov radiation process⁺, whereas the former process generates radio waves which can propagate through the corona and be received on the Earth, the latter mechanism generates plasma waves which are longitudinal or compression waves, which do not exist outside the plasma medium. Referring to Fig. 1.1(c), these Cerenkov plasma waves can only exist in modes number 3 and 4, and cannot propagate directly above the level $X = 1 - Y^{2++}$, where $X = f_p^2/f^2$, $Y = |f_H/f$. Consequently, if radiation from the Cerenkov plasma process

⁺We exclude the synchrotron mechanism since the bandwidth of this radiation is wide whereas the bandwidths of storm bursts are narrow.

⁺⁺This statement, of course, assumes no coupling occurs. It should be noted again that the physical nature of the waves propagating along mode 3 changes from longitudinal plasma waves ($n_j \gg 1$) to transverse electromagnetic waves ($n_j \geq 1$).

is to be received outside the corona, the plasma waves need to be transformed into radio waves through some coupling or transformation mechanisms. Two such mechanisms are known to exist; one is the transformation of plasma waves to radio waves through Rayleigh type of scattering and the other is the coupling or interaction of characteristic waves. Since for an electron gyrating along a magnetic field with a pitch angle which is not too small ($> 10^\circ$, say), the power radiated by the Cerenkov plasma mechanism is of the same order as that of cyclotron radiation (Ginzburg and Zheleznyakov, 1961), the efficiency of the coupling mechanisms will tell, as far as producing radio waves is concerned, whether the Cerenkov process will be as significant as the cyclotron radiation in the source region. It is, thus, the purpose of this chapter to discuss in a quantitative manner the two possible coupling mechanisms.

(B) Transformation of Plasma Waves to Radio Waves through Rayleigh Scattering and Combination Scattering (Ginzburg and Zheleznyakov, 1958, 1959 and 1961)

It has been pointed out by Ginzburg and Zheleznyakov (1958) that in a plasma specified by dielectric constant ϵ , plasma waves can be transformed into transverse

electromagnetic waves through scattering of the longitudinal plasma waves due to fluctuation of the dielectric constant $\delta \epsilon$. The fluctuation of the dielectric constant is induced by the variation of electron concentration δN which can be separated into two components:

$$\delta N = \delta N' + \delta N'' \quad (7.1)$$

where $\delta N'$ is associated with quasi-neutral plasma density fluctuation (mainly due to motion of electrons).

When a plasma wave is incident on a scattering volume, the amount of scattered signal is determined by the spectrum of the fluctuations. The spectrum of the scattered signal is obtained by the convolution of the incident spectrum with the fluctuation spectrum. The result of this convolution is that there is scattering both due to the density fluctuation ($\delta N'$) and the charge fluctuation ($\delta N''$). Since the variation of plasma density occurs quite slowly, scattering by $\delta N'$ does not result in any appreciable change of the incident frequency. This scattering process is called Rayleigh scattering. The scattering of a plasma wave with frequency ω_0 due to charge fluctuation results in a transverse electromagnetic wave of frequency $\approx 2\omega_0$. This scattering is called "combination scattering". The transformation coefficient, i.e. (intensity of transformed radio waves)/(intensity of incident plasma waves), has been found for both types of scattering to be of the order of 10^{-6} (e.g. Kundu, 1964).

(C) Coupling of Characteristic Waves in the Solar Corona

In general, there are four distinct modes of waves capable of propagating in a warm magnetoactive plasma (chapter I). In the cold-plasma, high-frequency approximations, the four modes are reduced into two — the o- and x-modes. Since each mode is represented by two branches of the refractive index curves (Fig. 1.1(c)), we will still adopt the 4-mode identification for convenience of discussion. The process of coupling between different branches of the o- and x-modes of electromagnetic waves is studied in this section for parameters appropriate to the background solar corona as well as active corona and frequencies appropriate to solar type I noise storms.

It has been found (Ratcliffe, 1959; Budden, 1961; Ginzburg, 1964) that under suitable conditions, coupling between the two characteristic modes can take place; these coupling conditions may be stated as: (i) The values of refractive index for the two modes coupled are close to each other. In other words, the coupled waves must travel at almost the same phase velocities. (ii) The values of the polarization constants $|R_o|$, $|R_x|$ of the two modes must be near to each other. To study the first condition of coupling, we will consider the behaviour of the refractive indices of the two modes in the corona; the computa-

tion will be based on the collisionless Appleton-Hartree equation, i.e. equation (3.1). Considering a unipolar spot field model with field intensity at the centre of the spot $H_g = 2,000$ gauss, we show in Fig. (7.1) the refractive index squared as a function of distance $\rho = R/R_0$ along the central field line for two frequencies ($f = 50, 100$ Mc/s) when the electron density distribution follows relation (6.1) (normal background corona model). When $H_g = 350$ gauss, other parameters being the same, we have Fig. 7.2. The electron density of the regions above sunspot groups and plages have been found from both optical and radio observations to be several to ten times the normal background coronal density (chapter VI). We will now take Newkirk's model (relation (6.2)) and investigate the behaviour of the refractive index in this case. For frequency = 100 and 150 Mc/s, these graphs are shown in Fig. 7.3 ($H_g = 2,000$ gauss) and Fig. 7.4 ($H_g = 500$ gauss).

The polarization constants for o- and x-waves in a magnetoactive plasma are given by (e.g. Budden, 1961):

$$R_o = -\frac{i}{Y \cos \theta} \left\{ \frac{Y^2 \sin^2 \theta}{2(1-X-iZ)} - \sqrt{\frac{Y^4 \sin^4 \theta}{4(1-X-iZ)^2} + Y^2 \cos^2 \theta} \right\}$$

$$R_x = -\frac{i}{Y \cos \theta} \left\{ \frac{Y^2 \sin^2 \theta}{2(1-X-iZ)} + \sqrt{\frac{Y^4 \sin^4 \theta}{4(1-X-iZ)^2} + Y^2 \cos^2 \theta} \right\} \quad (7.2)$$

where $Z = \nu/f$, ν = collision frequency & f = wave frequency

To specify the coupling region precisely, we need to calculate the polarizations of different modes along a field

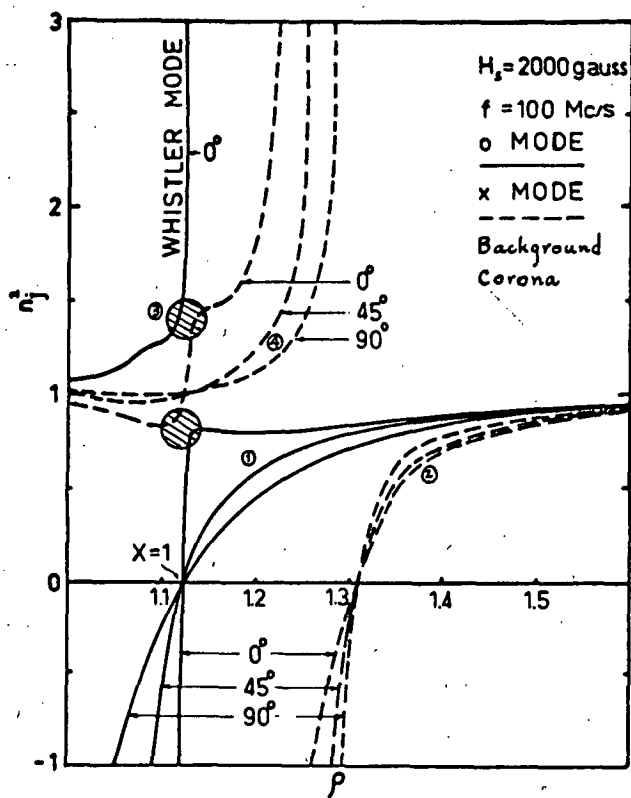
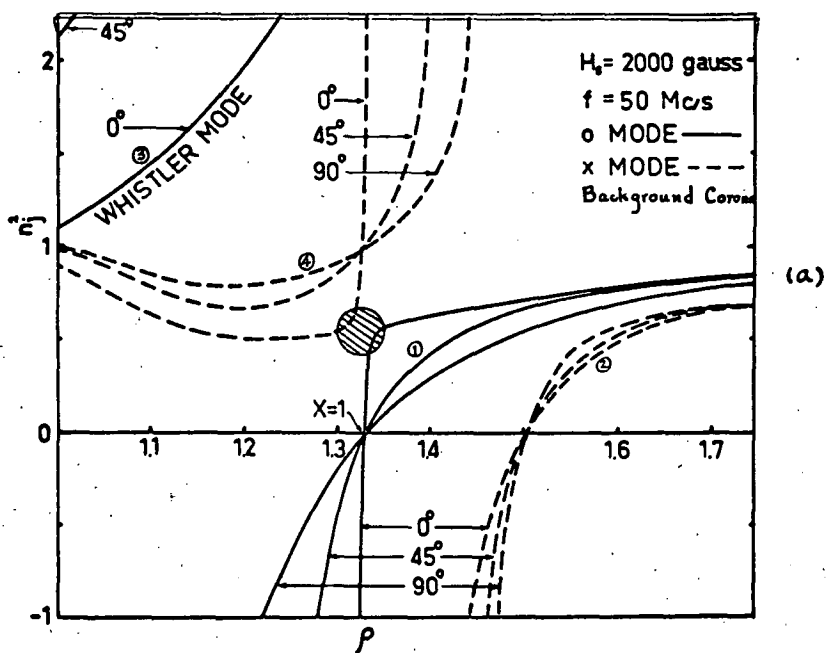


Fig. 7.1 The variation of refractive index squared n_j^2 along the radial line ρ passing through the centre of a strong uni-polar spot ($H_s = 2,000$ gauss) for

(a) $f = 50$ Mc/s

(b) $f = 100$ Mc/s

when the electron density follows Baumbach-Allen's model.

(b)

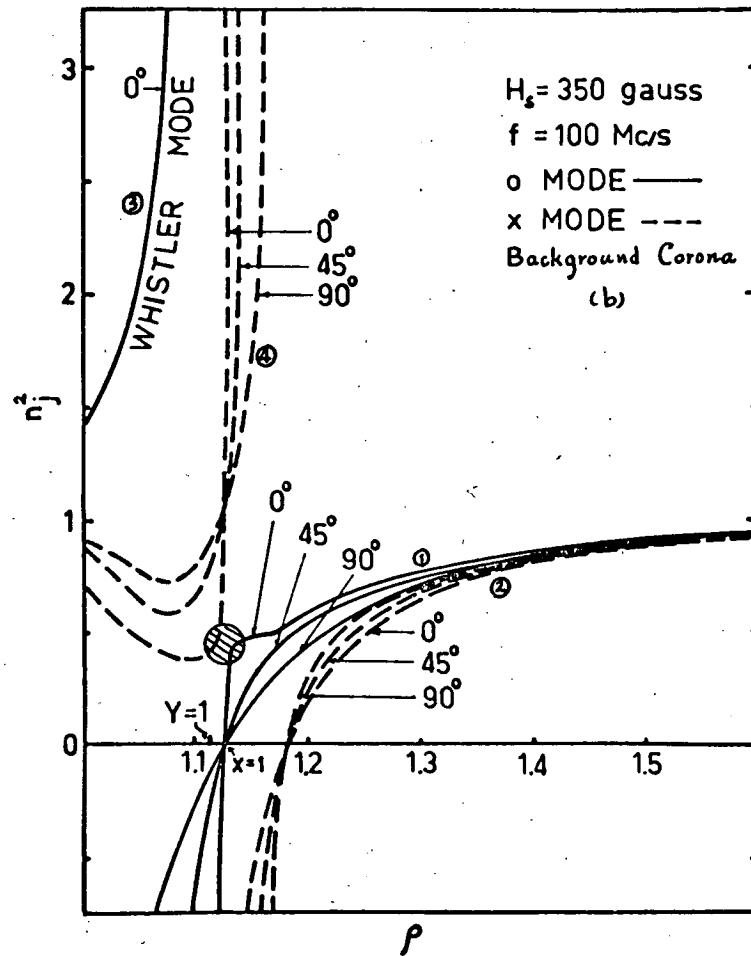
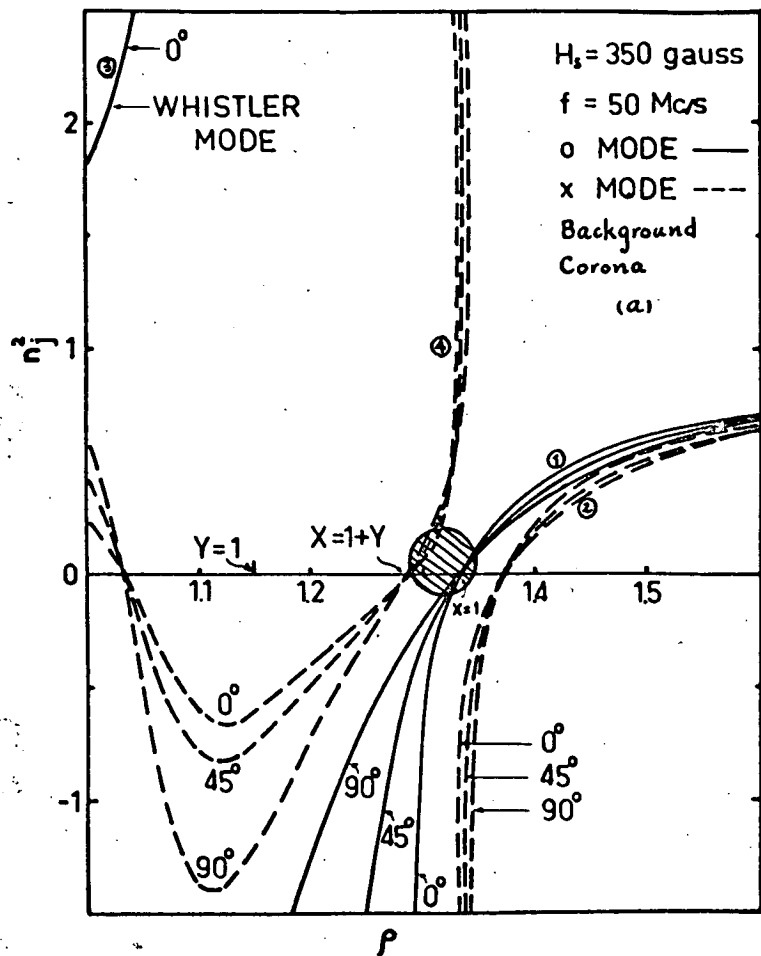


Fig. 7.2 The variation of refractive index squared n_j^2 along the radial line ρ passing through the centre of a weak unipolar spot ($H_s = 350$ gauss) for (a) $f = 50$ Mc/s (b) $f = 100$ Mc/s, when the electron density distribution follows Baumbach - Allen's model.

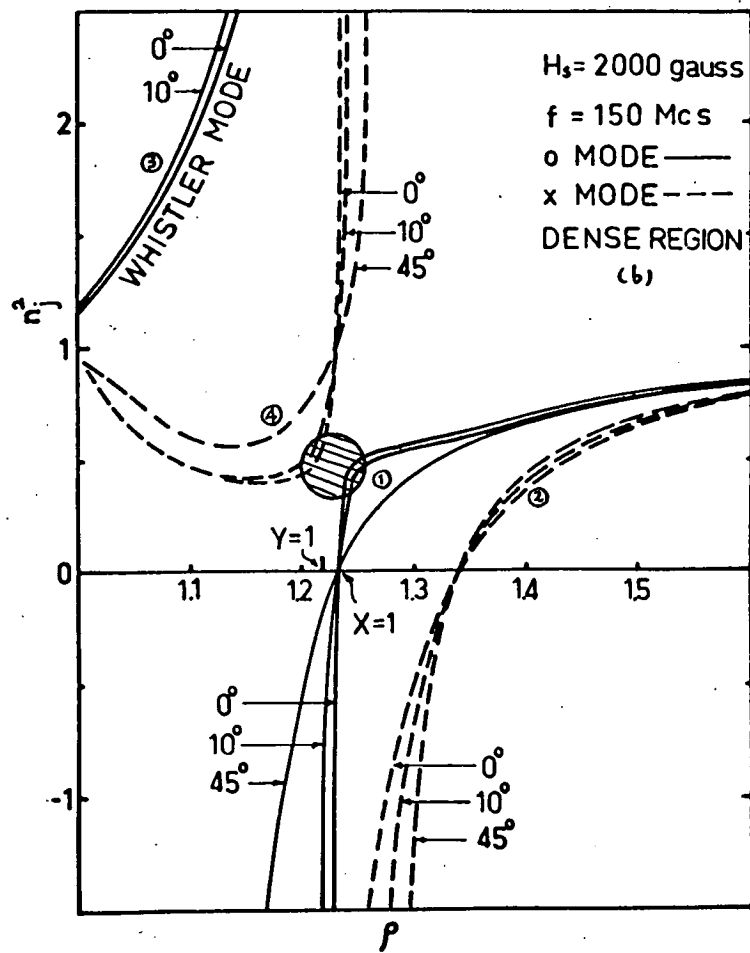
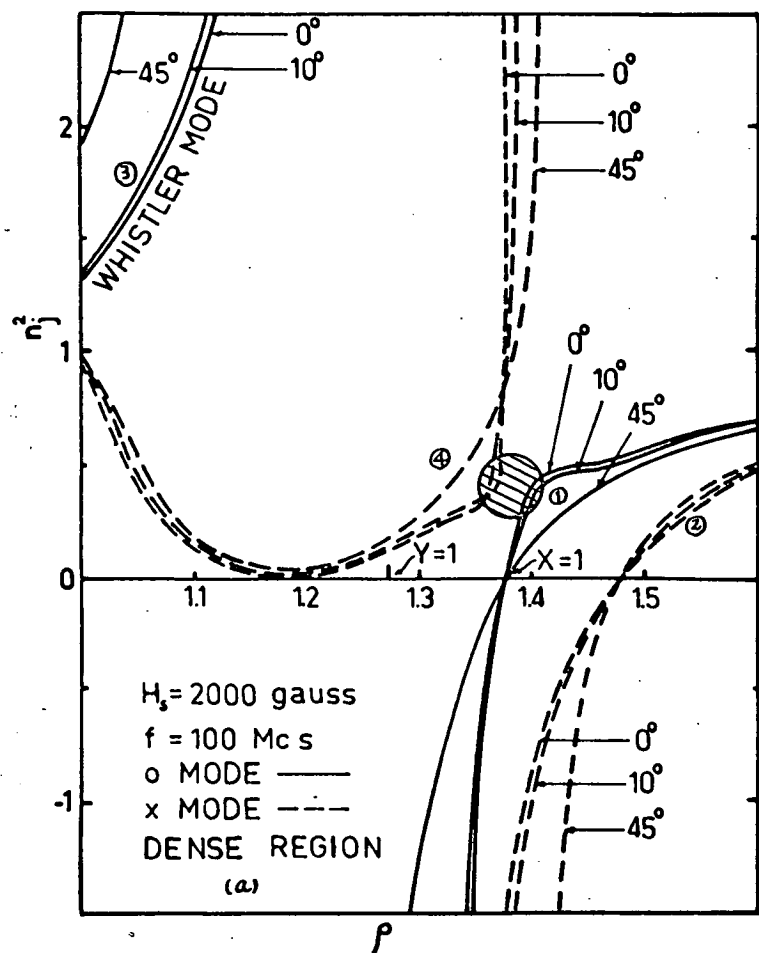


Fig. 7.3 The variation of refractive index squared n_j^2 along the radial line ρ passing through the centre of a strong unipolar spot ($H_s = 2,000$ gauss) for (a) $f = 100$ Mc/s (b) $f = 150$ Mc/s, when the electron density distribution follows Newkirk's model.

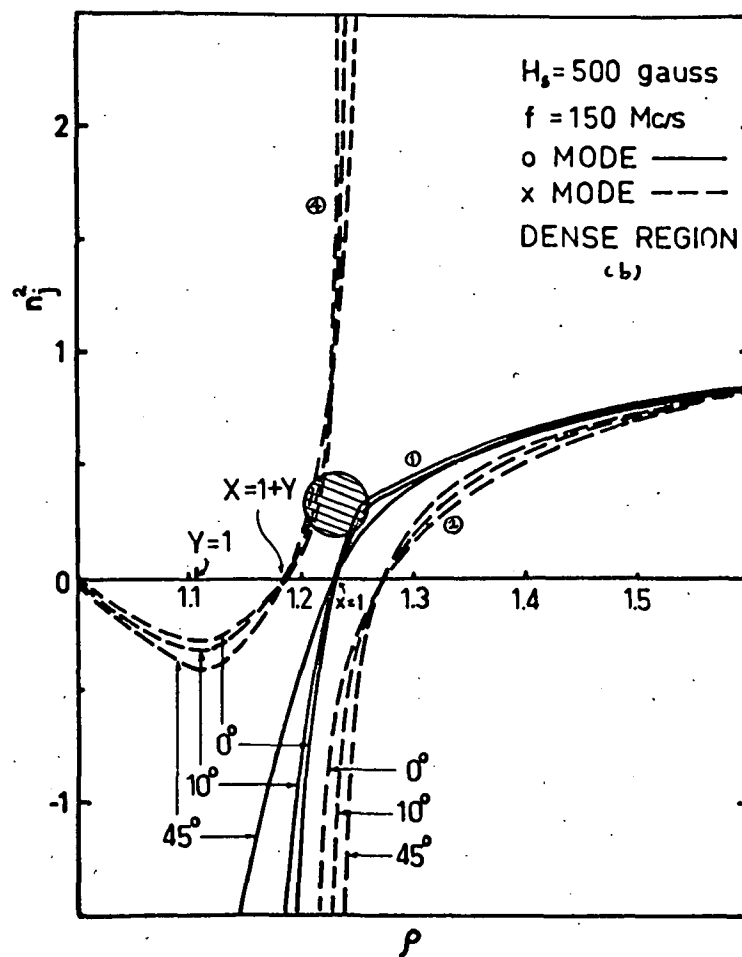
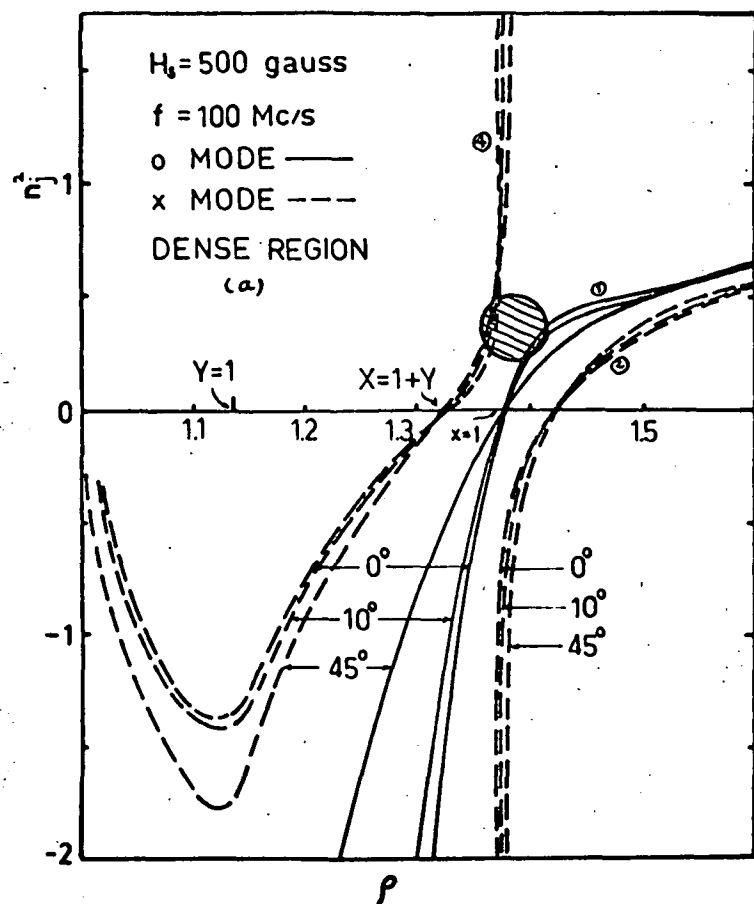


Fig. 7.4 The variation of refractive index squared n_j^2 along the radial line ρ passing through the centre of a weak unipolar spot ($H_s = 500$ gauss) for (a) $f = 100$ Mc/s (b) $f = 150$ Mc/s, when the electron density distribution follows Newkirk's model.

line in the corona; this is done for modes 1, 4 in Fig. 7.5 with parameters appropriate to that in Fig. 7.3. It can be seen in Fig. 7.5 that at the level $X = 1$, $|R_o| = |R_x| = 1$ for all θ . This does not mean that coupling condition (11) is satisfied at this point. In fact, coupling never occurs at exactly $X = 1$, but only in the neighbourhood of it. A x-mode wave, say, approaches near the point $X = 1$, will let some of its energy to "jump" over the o-mode branch and propagates along it thereon. This process is indeed a tunnelling effect in the terminology of Quantum Mechanics, and the level $X = 1$ is situated inside the layer where the wave has to tunnel through. It is, thus, meaningless to consider polarization at $X = 1$. In Fig. 7.5, we should draw vertical lines near to and on both sides of the dotted line $X = 1$, and consider the value of $|R_o|$, $|R_x|$ along these lines. It is readily observed that at a fixed value of ρ , the smaller the wave-normal angle, the closer the values $|R_o|$ and $|R_x|$ are to each other. Hence, coupling condition (11) is satisfied at small wave-normal angles only. Taking coupling condition (i) into consideration as well, it is easy to see that the coupling regions are those hatched in Fig. 7.1 - 7.4. The treatment in the above only gives the fact that coupling can take place in many circumstances, but we have to investigate whether the energy coupled is significant to be perceivable. The condition for strong or efficient coupling is given

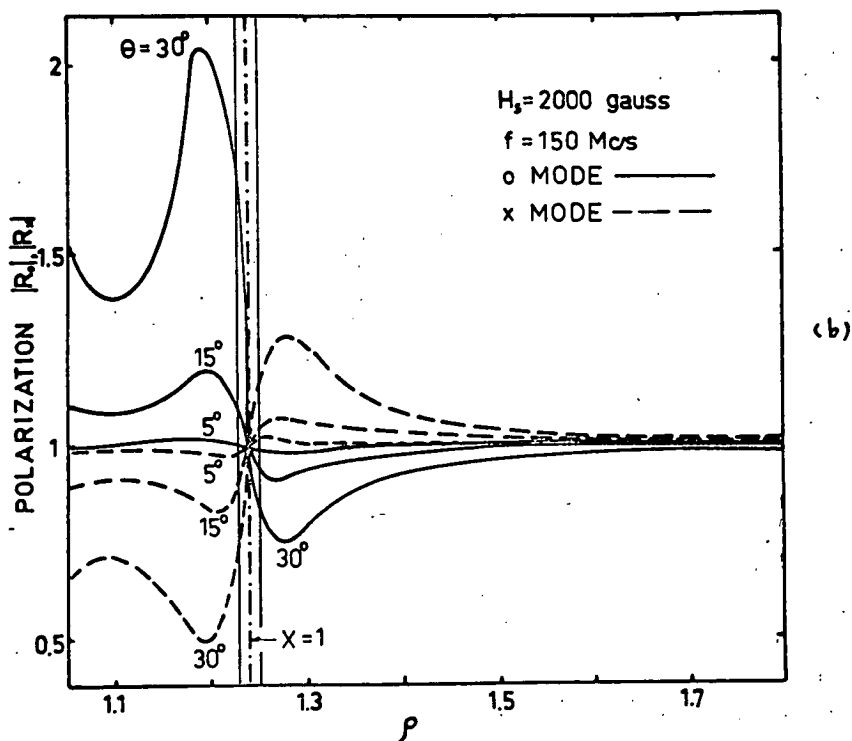
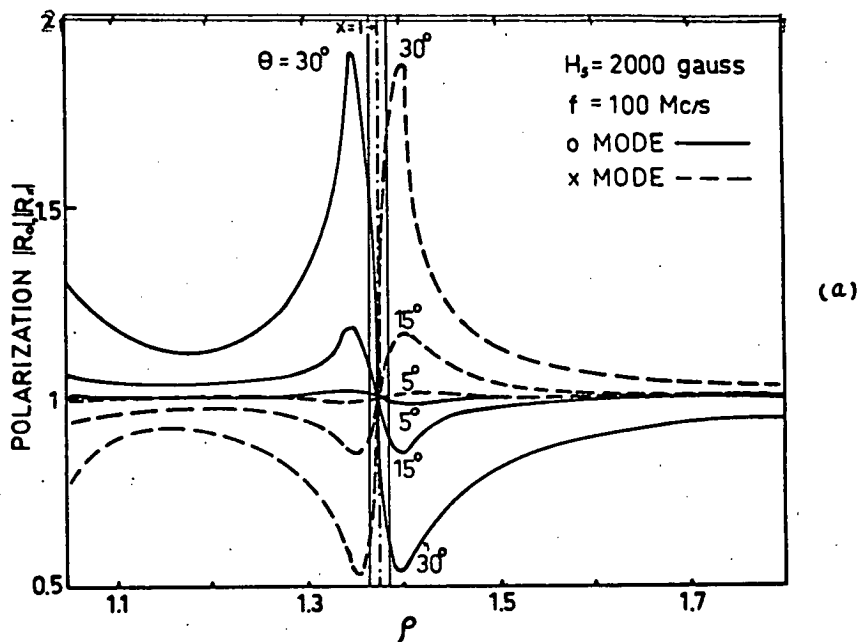


Fig. 7.5 The dependence of the polarization constants $|R_0|, |R_x|$ on normalized radial distance ρ is indicated for parameters as in Fig. 7.3 for two frequencies: (a) 100 Mc/s, (b) 150 Mc/s.

by (Ginzburg, 1964):

$$\nu = f_{cr} \quad (7.3)$$

where f_{cr} is the critical frequency, given by $\frac{f_H \sin^2 \theta}{2 \cos \theta}$.

In the solar corona where the plasma is highly ionized and the temperature high, the collision frequency ν can be calculated from (Ginzburg, 1964):

$$\nu = \frac{5.5}{T^{3/2}} N \ln \left(220 \frac{T}{N^{1/3}} \right) \quad (7.4)$$

It is found that ν is less than the order of c/s in most regions (both active region and background corona) in the corona and the condition for efficient coupling is satisfied only if the wave-normal angle θ is extremely small. This idea is illustrated in Fig. 7.6. We observed from Fig. 7.6 that the inequality

$$\nu \ll f_{cr} \quad (7.5)$$

holds if the wave-normal angle θ is not extremely small. If inequality (7.5) is satisfied for active region density, it must also be satisfied in the normal background plasma.

Under assumption (7.5), Ginzburg (p. 320, 1964) gives the coupling transmission coefficient for weak coupling from the o-mode (modes 1, 3) to x-mode (modes 2, 4) or vice versa for $\xi < 1$:

$$|D|_{o \leftrightarrow x}^2 = \exp \left\{ - \left| \frac{2\pi^2 f \sin^2 \theta}{2ca(1-\xi)^{3/2}} \right| \right\} \quad (7.6)$$

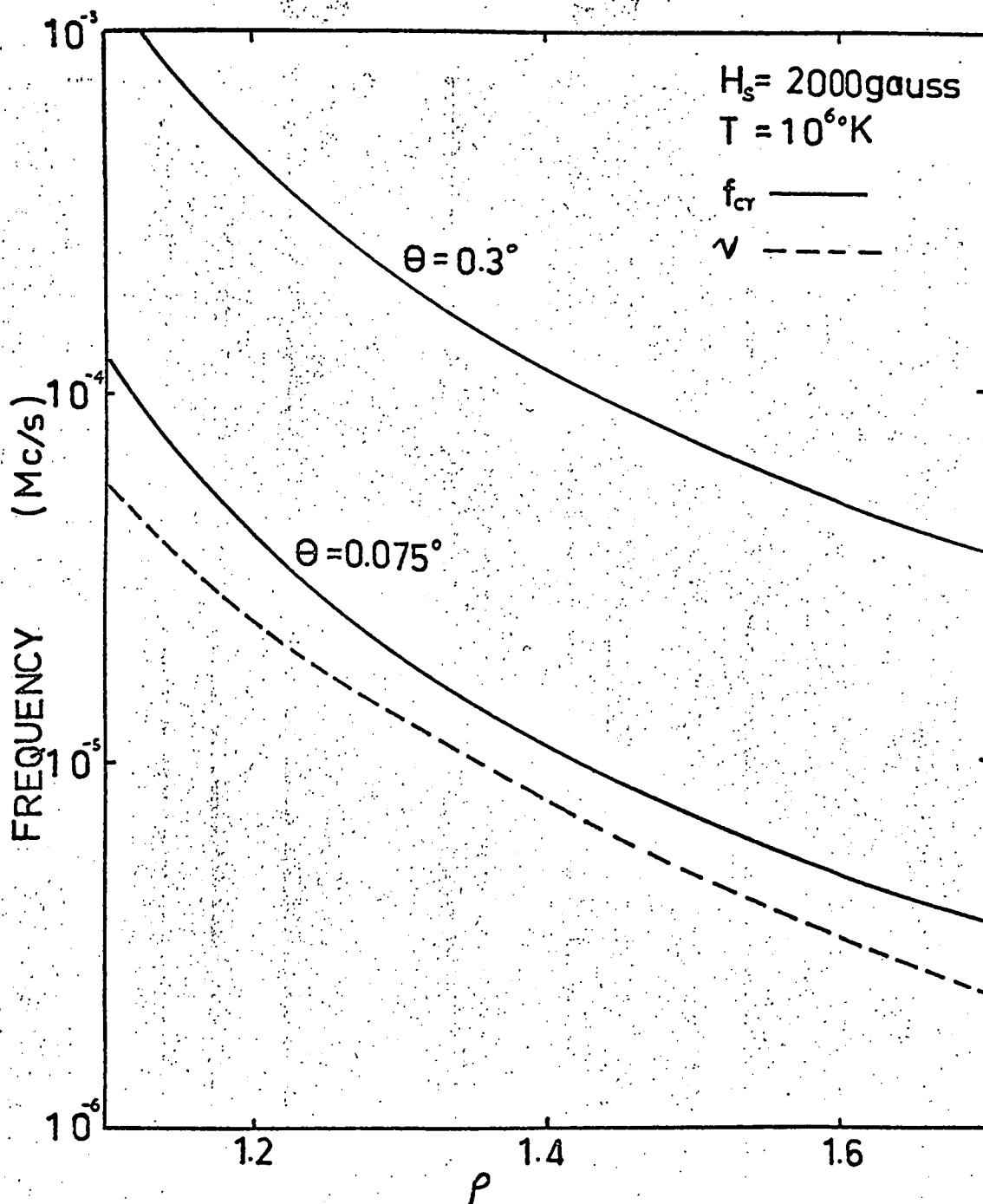


Fig. 7.6 Variation of the critical frequency $f_{cr} = \frac{f_H \sin^2 \theta}{2 \cos \theta}$ and collision frequency (expression (7.4)) along the radial line ρ passing through the centre of a strong unipolar spot. ($H_s = 2,000$ gauss). The electron density distribution is assumed to follow Newkirk's model.

and from the x-mode to o-mode or vice versa for $\xi > 1^*$:

$$|D|_{x \leftrightarrow 0}^2 = \exp \left\{ - \left| \frac{2\pi^2 f \sin^2 \theta}{2ca(1+\xi)^{3/2}} \right| \right\} \quad (7.7)$$

where $a = \left(\frac{1}{N} \cdot \frac{\partial N}{\partial \rho} \right)_{N=N_c}$ and N_c = electron density at the coupling region. Physically, $|D|^2$ represents the amplitude of the coupled wave when the amplitude of the "incident" wave is taken as 1.

If the electron density varies along the corona according to either the normal background model or the active region model undertaken, an estimation indicates that the coupling coefficient is hardly of any significance. However, it is reasonable to believe that irregularities of density distribution occur at times in the corona, particularly during highly disturbed periods, and some fluctuations in electron density can easily introduce a value of $\frac{\partial N}{\partial \rho}$ being 10^4 times that of the steady state. Taking this factor into account, we plot the coupling transmission coefficient $|D|^2$ as a function of wave-normal angle θ in Fig. 7.7 when $\left(\frac{\partial N}{\partial \rho} \right)_{N_c}$ is increased by 10^4 times. In Fig. 7.7(a), equivalent to the coupling regions in Fig. 7.3(b) and 7.4(b), the frequency of the wave considered (150 Mc/s) is greater than the gyro-frequency f_H at the coupling regions. Fig. 7.7(b) gives the coupling coefficient for the coupling processes shown in Fig. 7.1(a) and 7.1(b), where $\xi = f/f_H < 1$ at the coupling level.

*

Note that in this case only coupling between modes 1 & 4 is possible.

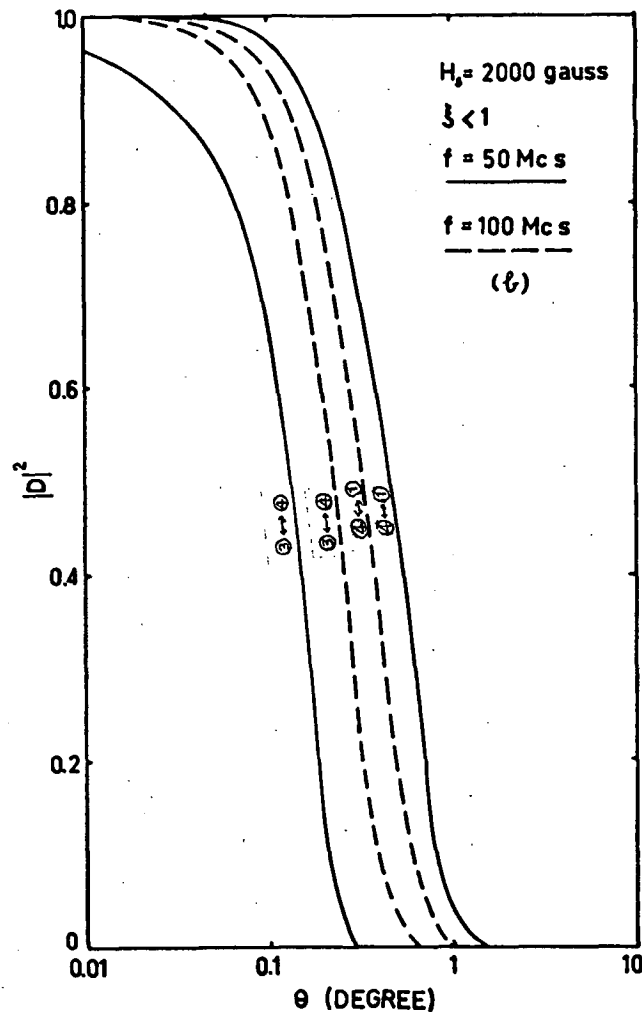
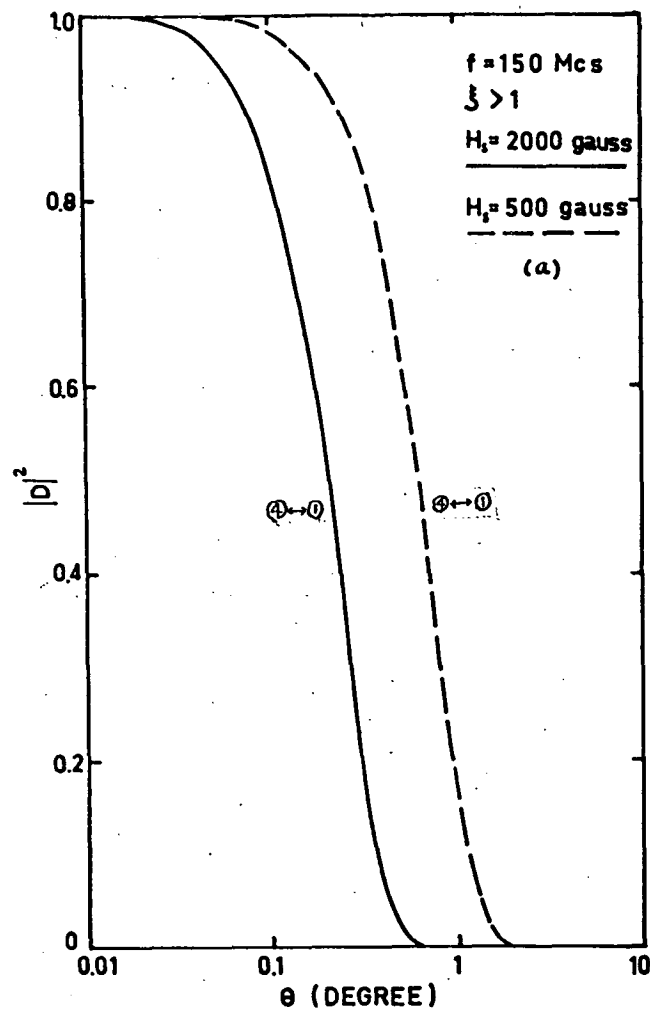


Fig. 7.7 The dependence of the transmission coupling coefficient $|D|^2$ on wave-normal angle θ for (a) $\xi > 1$, (b) $\xi < 1$.

Even with the assumption of large value of $\frac{\partial N}{\partial \rho}$, it is obvious from Fig. 7.7 that the coupling process is very inefficient in the corona; only waves (of one mode) propagating with wave-normal angle θ smaller than about 0.5° will be coupled to the other mode. If we assume the x-mode radiation power to be confined to one solid angle about the magnetic field line, then after coupling only $\sim 10^{-4}$ * of the power will be associated to the o-mode waves.

Since the incoherent radiation power of the Cerenkov process is of the same order as that of the cyclotron mechanism, we conclude from the results of sections (B) and (C) that in regions where strong magnetic fields prevail (as in the source regions of type I noise storms), the cyclotron radiation process is the much more significant one. We will, therefore, proceed to study the characteristics of the cyclotron radiation in the next chapter.

*This value will be less than 10^{-7} if $\frac{\partial N}{\partial \rho}$ assumes the normal value (fluctuation in density is absent).

CHAPTER VIII

CYCLOTRON RADIATION FROM ELECTRON STREAMS
GYTRATING IN SPOT-FIELD CONFIGURATIONS(A) Emitted Frequency Range from Electrons

We will, first of all, assume the existence of electrons spiralling along spot magnetic field lines in the source region[†]. When the spot-field configuration is of bipolar nature, electrons gyrating along a particular field line will be mirrored and trapped for some time before diffusing away. It is well known that each electron will radiate a range of frequency at an instant. If the electron acquires a kinetic energy of the order of Mev., synchrotron radiation results and the bandwidth of emission will be very wide, which is not observed. We will, therefore, assume that the energy of the radiating electron is of the order of 10 - 100 Kev. (cyclotron radiation will be emitted for this order of energy), and we will discuss the possible range of frequency emitted from such electrons.

In considering the cyclotron process, we will assume that the collisionless Appleton-Hartree equation is valid

[†]The question on the presence of such electrons will be discussed in chapter X.

in the solar corona, based on the fact that the mean thermal velocity β_T of electrons in the corona is very small, being $\sim 10^{-2}$ (Ginzburg, p. 121, 1964). The refractive index n_j for an electromagnetic wave in the corona alone is thus given by

$$n_j^2 = 1 - \frac{\frac{A}{\xi^2} \left(1 - \frac{A}{\xi^2}\right)}{1 - \frac{A}{\xi^2} - \frac{\sin^2 \theta}{2\xi^2} + \sqrt{\frac{\sin^4 \theta}{4\xi^4} + \left(1 - \frac{A}{\xi^2}\right)^2 \frac{\cos^2 \theta}{\xi^2}}} \quad (8.1)$$

All quantities have their usual meanings as defined in chapter II.

In the above dispersion equation the distribution of plasma density N and hence plasma frequency f_p follows relation (6.1) (background corona model) or (6.2) (Newkirk's model) in the corona, while the relation between the gyro-frequency f_H and position in the corona depends on the model and position of the spot-field undertaken.

Since majority of noise storms are observed to occur at altitudes between 0.2 and $0.5 R_\odot$ and a typical value of the maximum field intensity on the spot area is $H_g = 2,000$ gauss for a noise storm to occur, we can set up limits for the quantity A in the possible source region. Here, of course, we have to assume that in most cases, the apparent source positions are the real source positions. As to

electron density distribution in the source region, we will take both possibilities (relations (6.1) and (6.2)) into consideration. Within the regime of the above assumptions, from Fig. 6.4(a) and 6.4(b) A is found to range from about 0.2 to 5. To show a typical example of the form of equation (8.1), we plot the refractive index n_j as a function of normalized frequency $\xi = f/f_H$ for wave-normal angle $\theta = 10^\circ$ and 75° in case where $A = 1$, in Fig. 8.1. The lines marked x and o are refractive index curves for the x and o modes respectively.

It is easy to show from the refractive index expression that for all values of θ in the x -mode, when $n_j = 0$, ξ is given by

$$\xi_x = \frac{1 + \sqrt{1 + 4A}}{2} > 1 \quad (8.2)$$

In the o -mode, for all values of θ not equal to 0° , $\xi = \xi_o$ when $n_j = 0$:

$$\xi_o = \sqrt{A}^+ \quad (8.3)$$

For an observer in a reference system fixed to the background magnetactive plasma in which an electron is gyrating, the observed radiated frequency is given by the

⁺This expression is equivalent to stating $n_j = 0$ when $X = f_p^2 / f^2 = 1$.

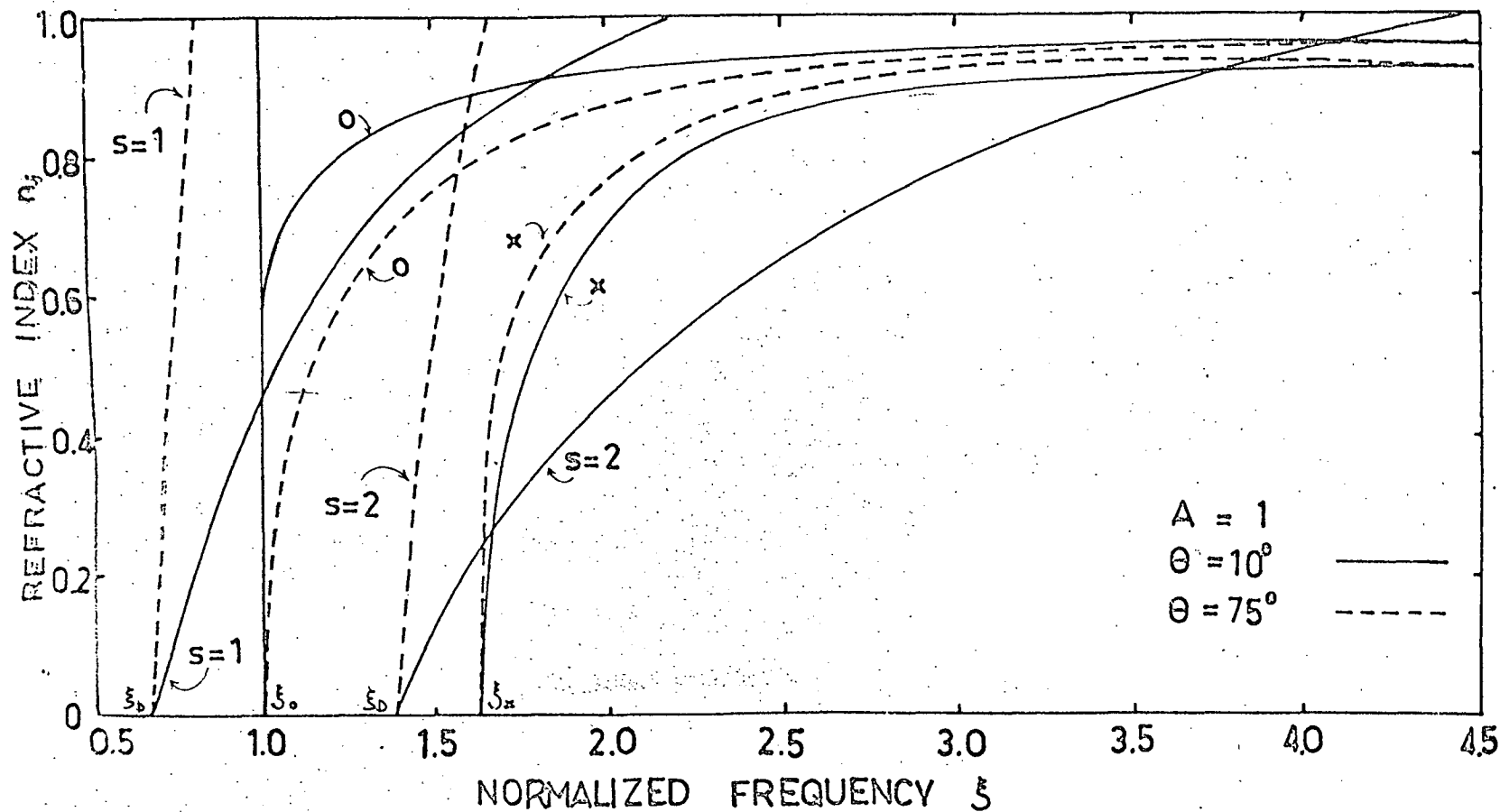


Fig. 8.1 Refractive index n for the o-mode and x-mode against normalized frequency ξ for $A = 1$, and $\theta = 10^\circ, 75^\circ$. The Doppler equation is also plotted as a function of ξ for $\beta_{\perp} = 0.3$, $\beta_{\parallel} = 0.7$ and harmonic $s = 1, 2$.

Doppler equation

$$\xi = \frac{s\gamma}{1 - n_j \beta_{||} \cos \theta} \quad (8.4)$$

where n_j must satisfy equation (8.1).

The frequency corresponding to $n_j = 0$ is independent of θ and is given by

$$\xi_D = s\gamma \quad (8.5)$$

The Doppler equation is plotted for the first two harmonics ($s = 1, 2$), taking $\theta = 10^\circ$ and 75° , $\beta_{\perp} = 0.3$, $\beta_{||} = 0.7$ in Fig. 8.1.

It is clear from Fig. 8.1 that there can be one or two simultaneous solutions (i.e. points of intersection) of the dispersion and Doppler equations depending on whether

$$\xi_D = s\gamma \geq \xi_{0,x} \quad (8.6a)$$

$$\text{or} \quad s\gamma < \xi_{0,x} \quad (8.6b)$$

We refer to these two cases as the Simple (8.6a) and Double (8.6b) frequency solutions respectively. These two different solutions show up clearly in Fig. 8.2 where simultaneous solutions of equations (8.1) and (8.4) are plotted for the o-mode (Fig. 8.2a) and the x-mode (Fig. 8.2b). The Double solutions have a limited θ -range. We denote the upper limit by the cut-off angle θ_0 which corresponds to the Doppler equation being a tangent to the dispersion

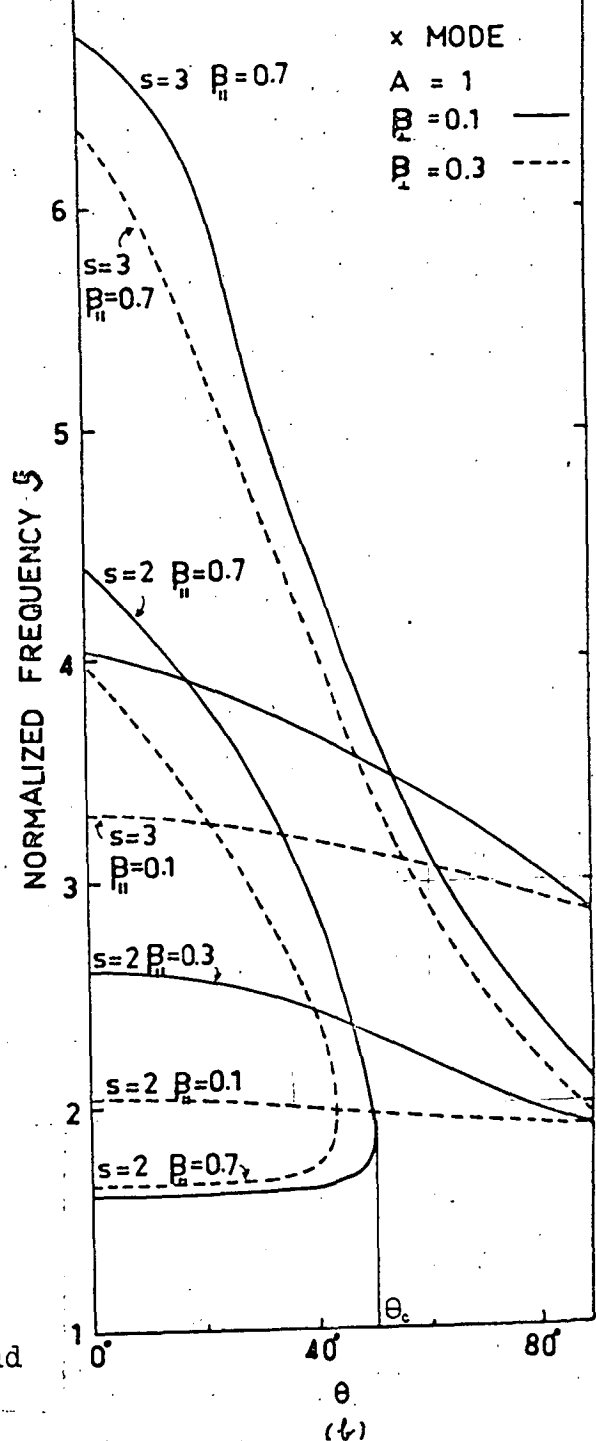
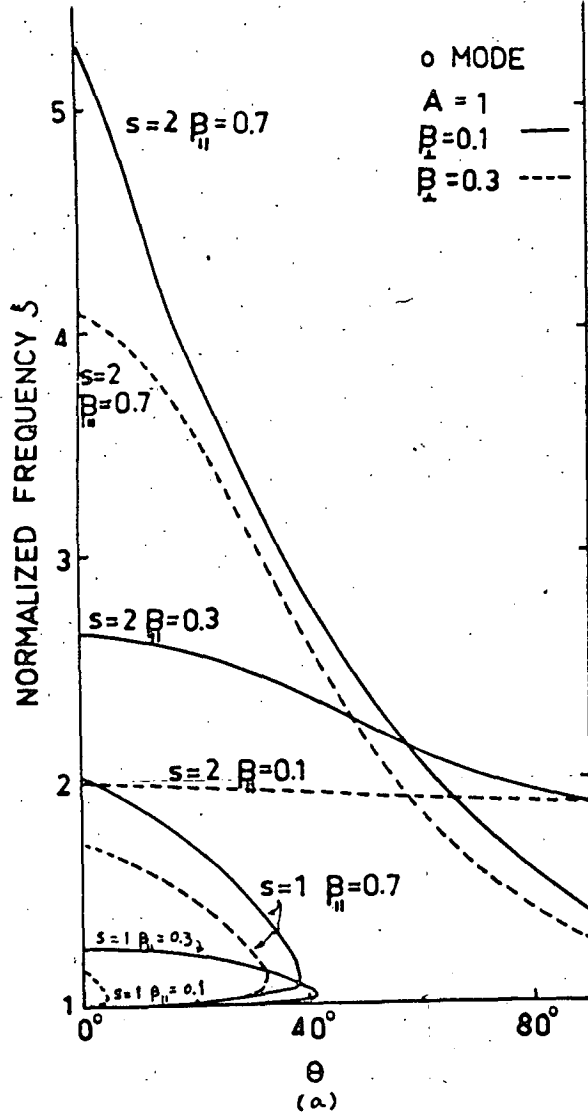


Fig. 8.2 The relation of the normalized frequency ξ and wave-normal angle θ for $A = 1$, different values of β_{\perp} , β_{\parallel} , s , and

- (a) o-mode wave;
- (b) x-mode wave.

An example of the cut-off angle θ_c is also indicated.

equation. These two types of solution for the normalized frequency ξ are very important in the explanation of bursts and continuous radiations and should always be kept in mind. It should be noted that for given β_{\perp} and β_{\parallel} , a Double solution for the x-mode usually occurs at a harmonic number which is one unit larger than that for the Double solution of the o-mode.

(B) Power Spectrum of a Single Electron

An electron emits cyclotron radiation in both ordinary and extraordinary modes. It is necessary to investigate whether only one of the two modes, or both carries significant energy and capable of escaping through the corona. With various values of β_{\perp} and β_{\parallel} for the radiating electron, the emitted characteristic normalized frequency ξ has been obtained as a function of the wave-normal angle θ in section (A) for three values of $A = 0.25, 1$ and 1.5 (we have shown an example of graph for the case $A = 1$ only). We will, first of all, evaluate the power spectra emitted by single electrons in the two modes for these cases. For an electron gyrating with pitch angle ϕ and with guiding centre along the z-direction (Fig. 8.3), the Eidman equation (Liemohn, 1965) gives the power radiated at θ per unit solid angle in the s^{th} harmonic:

$$P_s = \left(\frac{e^2}{2\pi c} \right) \left\{ \frac{\omega^2 n_j^2 K^2 \left[-\beta_{\perp} J_s'(X) + (\alpha_y s \beta_{\perp} / X + \alpha_z \beta_{\parallel}) J_s(X) \right]^2 \left(1 + \frac{\omega}{n_j} \frac{\partial n_j}{\partial \omega} \right)}{\left| 1 - \beta_{\parallel} n_j \cos \theta \left(1 + \frac{\omega}{n_j} \frac{\partial n_j}{\partial \omega} \right) \right|} \right\}$$

where $K = (1 + \alpha_{\theta}^2)^{-1/2}$ (8.7)

$$\alpha_y = \alpha_{\theta} \cos \theta + \alpha_K \sin \theta$$

$$\alpha_z = \alpha_K \cos \theta - \alpha_{\theta} \sin \theta$$

$$\alpha_{\theta} = - \frac{\xi \cos \theta}{\xi^2 + \frac{A}{n_j^2 - 1}}$$

$$\alpha_K = - \frac{(n_j^2 - 1) \xi \sin \theta}{A - \xi^2}$$

$$X = \beta_{\perp} \xi \sin \theta n_j / \gamma$$

$$\frac{\omega}{n_j} \frac{\partial n_j}{\partial \omega} = \frac{A}{2 n_j^2 \xi^2} \left\{ \frac{2(1 - 2A/\xi^2)D + (1 - A/\xi^2) \left(2A/\xi^2 + \sin^2 \theta / \xi^2 \pm \frac{1}{2} B^{-1/2} E \right)}{D^2} \right\}$$

(8.7a)

here the positive sign corresponds to o-mode and the negative corresponds the x-mode.

$$D = 1 - \frac{A}{\xi^2} - \frac{\sin^2 \theta}{2 \xi^2} - B^{1/2}$$

$$E = - \frac{\sin^4 \theta}{\xi^4} - \frac{2 \cos^2 \theta}{\xi^2} \left(1 - \frac{2A}{\xi^2} \right) \left(1 - \frac{3A}{\xi^2} \right)$$

$$B = \frac{\sin^4 \theta}{4 \xi^4} + \frac{\cos^2 \theta}{\xi^2} \left(1 - \frac{A}{\xi^2} \right)^2$$

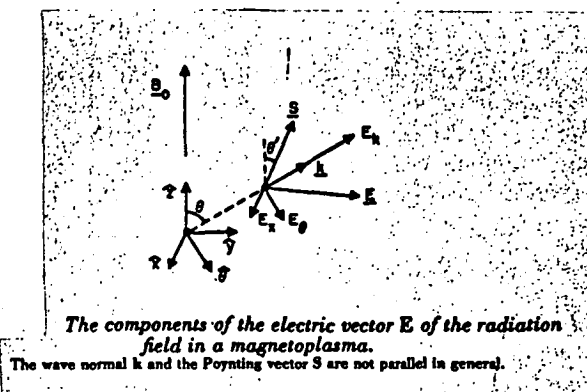
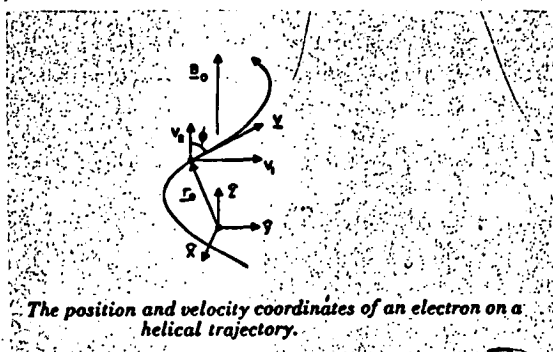


Fig. 8.3

With coordinate system (k, x, θ) as specified by Fig. 8.3, the polarization coefficient are defined by

$$\frac{E_\theta}{E_x} = i\alpha_\theta(\omega, \theta) \quad (8.8)$$

$$\frac{E_k}{E_x} = i\alpha_k(\omega, \theta)$$

when $E_\theta/E_x = 1$, or $E_k/E_x = 0$, the electromagnetic wave is circularly polarized. If $E_\theta/E = 0$ the wave is linearly polarized. ~~The polarization of cyclotron waves at the generation locality is discussed in Appendix .~~

The result of the computations for the two lowest harmonics ($s = 1, 2$) and for various values of electron energy and pitch angles (specified by $\beta_\perp = 0.1, \beta_\parallel = 0.3, 0.5, 0.7$ and $\beta_\perp = 0.3, \beta_\parallel = 0.1, 0.3, 0.5, 0.7$) and for different background plasmas specified by $A = 0.25, 1, 1.5$

are presented for the o-mode in Fig. 8.4, 8.6, 8.8 and for the x-mode in Fig. 8.5, 8.7, 8.9. From these diagrams, we realize that for such ranges of energy and pitch angle of the radiator, we have the following properties:

- (i) For Single frequency solution, the power of x-mode maximizes at θ ranging from 15° to 45° , while an o-mode wave carries most power at θ ranging from 40° to 70° .
- (ii) For Double frequency solution, energy of the wave maximizes at a direction very close to the cut-off angle θ_c for both x- and o-modes. Much more power is radiated by an electron whenever Double frequency solution exists.
- (iii) When β_\perp , β_\parallel and harmonic number s are kept constant, the maximum power carried by the x-mode wave exceeds that of o-mode wave by about 1 to 2 orders of magnitude.
- (iv) With increasing harmonic number, the radiated power decreases at the rate of several times to two orders of magnitudes per unit increase of s .
- (v) As it has been mentioned that in order to have Double frequency solution, the harmonic number for the x-mode wave will usually be one unit larger than that of o-mode wave, hence, from points (iii) and (iv), we observe that

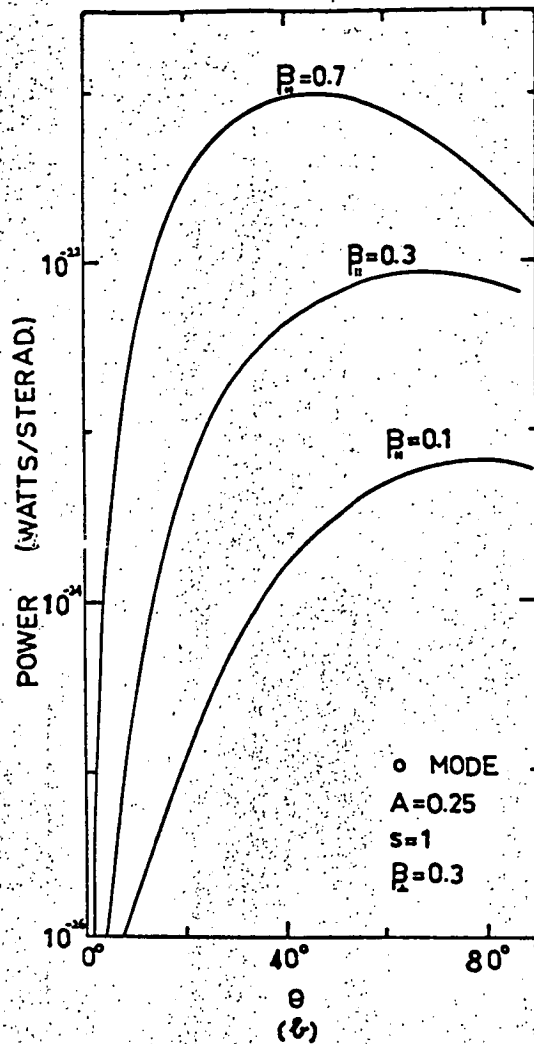
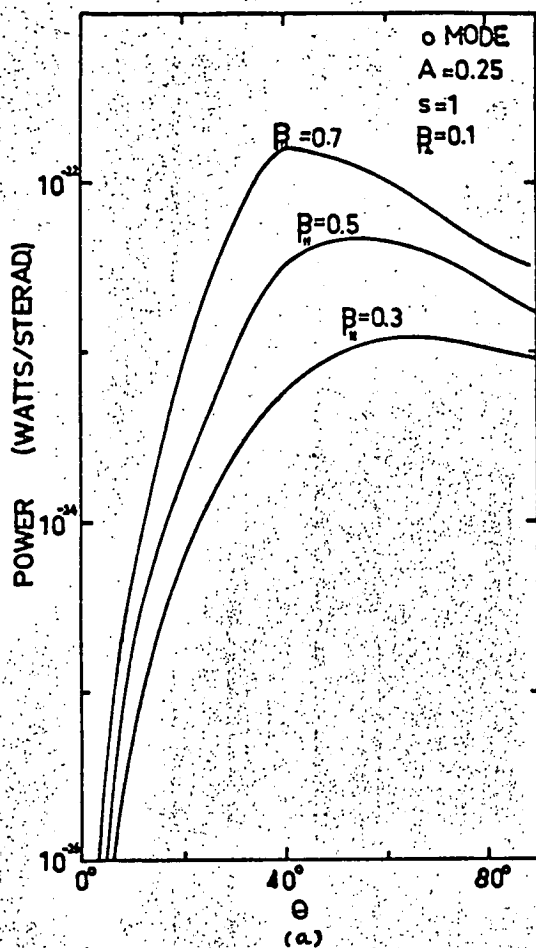


Fig. 8.4 Power spectrum radiated by a single electron, in the o-mode for $A = 0.25$, $f_H = 100$ Mc/s, and
 (a) $s = 1$, $\beta_{\perp} = 0.1$, $\beta_{\parallel} = 0.3, 0.5, 0.7$;
 (b) $s = 1$, $\beta_{\perp} = 0.3$, $\beta_{\parallel} = 0.1, 0.3, 0.7$.

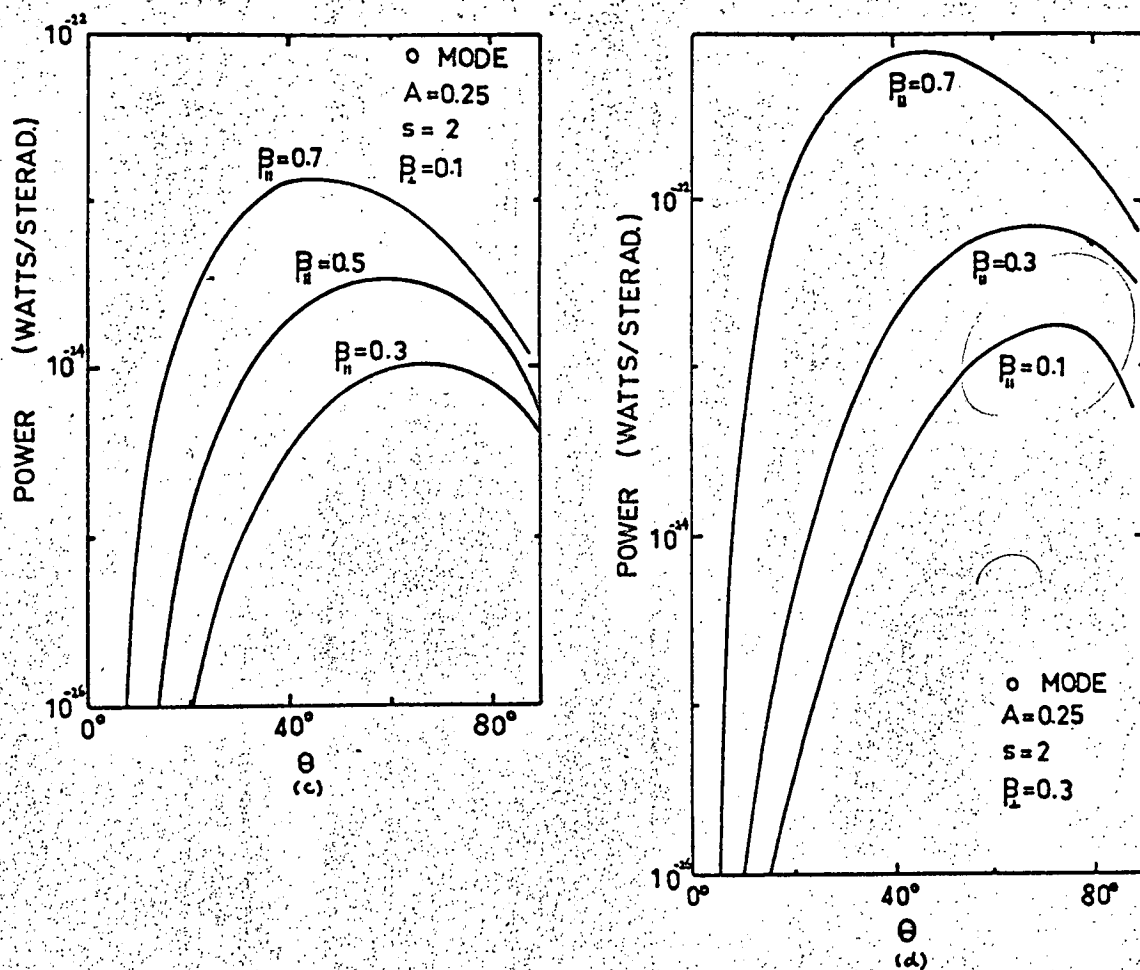


Fig. 8.4 Power spectrum radiated by a single electron in the o-mode for $A = 0.25$, $f_H = 100$ Mc/s, and
 (c) $s = 2$, $\beta_{\perp} = 0.1$, $\beta_{\parallel} = 0.3, 0.5, 0.7$;
 (d) $s = 2$, $\beta_{\perp} = 0.3$, $\beta_{\parallel} = 0.1, 0.3, 0.7$.

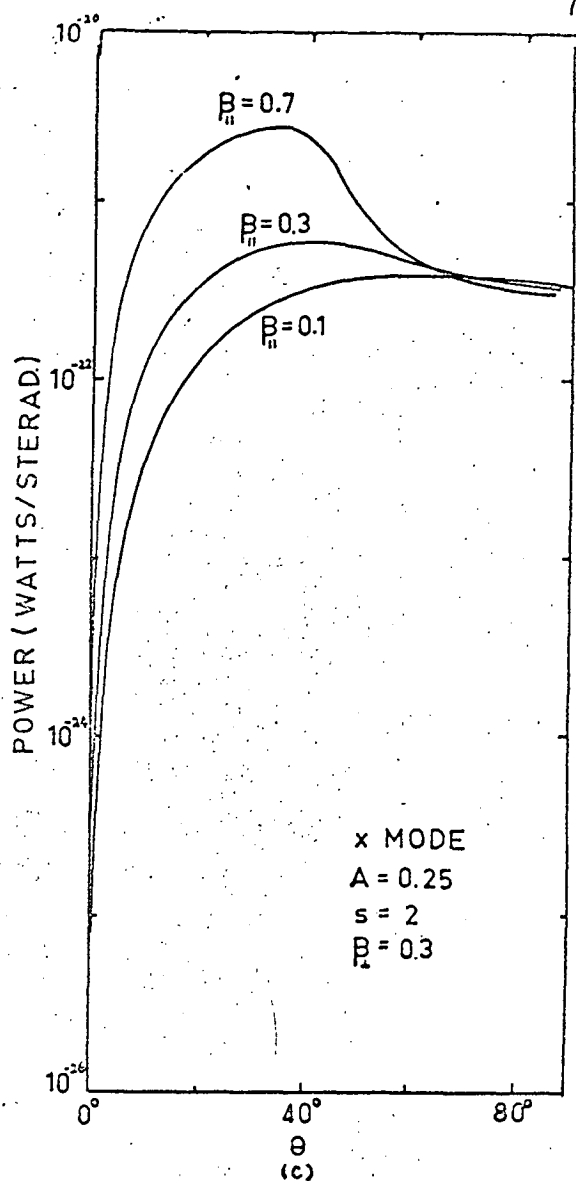
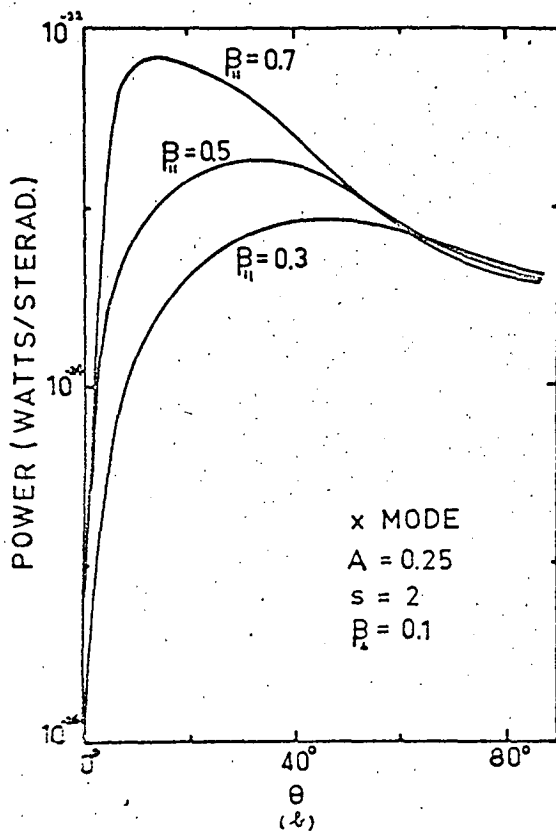
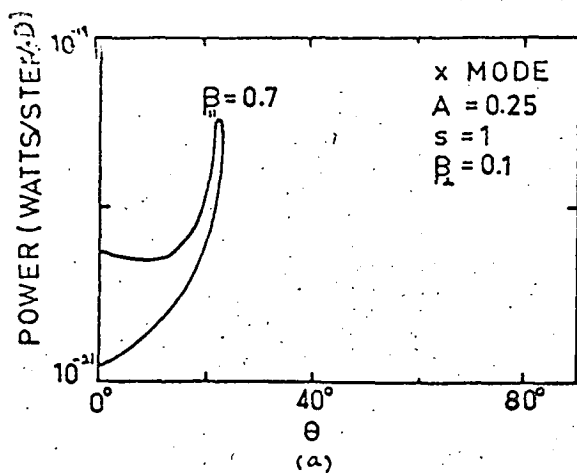


Fig. 8.5 Power spectrum radiated by a single electron in the x-mode for $A = 0.25$, $\bar{\nu}_H = 100$ Mc/s, and
 (a) $s = 1$, $\beta_{\perp} = 0.1$, $\beta_{\parallel} = 0.7$;
 (b) $s = 2$, $\beta_{\perp} = 0.1$, $\beta_{\parallel} = 0.3, 0.5, 0.7$;
 (c) $s = 2$, $\beta_{\perp} = 0.3$, $\beta_{\parallel} = 0.1, 0.3, 0.7$.

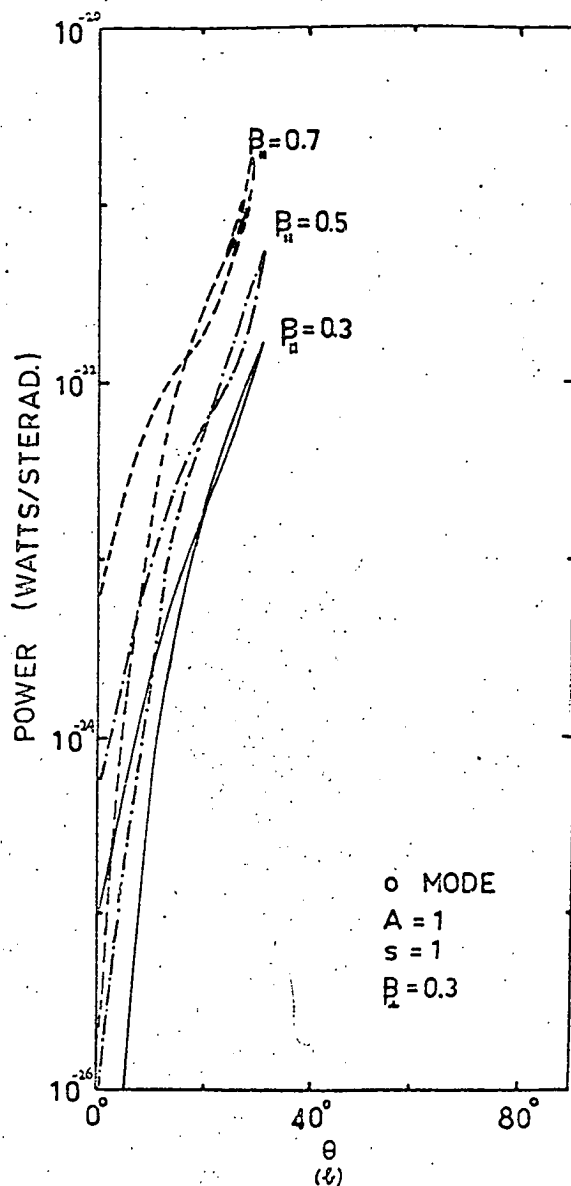
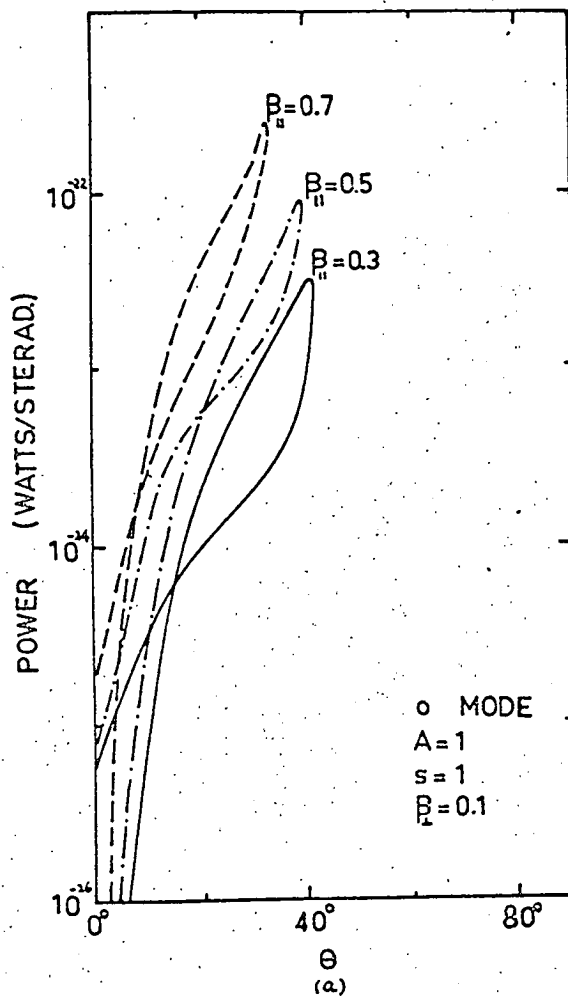


Fig. 8.6 Power spectrum radiated by a single electron in the o-mode for $A = 1$, $f_H = 100$ Mc/s, and
 (a) $s = 1$, $\beta_{\perp} = 0.1$, $\beta_{||} = 0.3, 0.5, 0.7$;
 (b) $s = 1$, $\beta_{\perp} = 0.3$, $\beta_{||} = 0.3, 0.5, 0.7$.

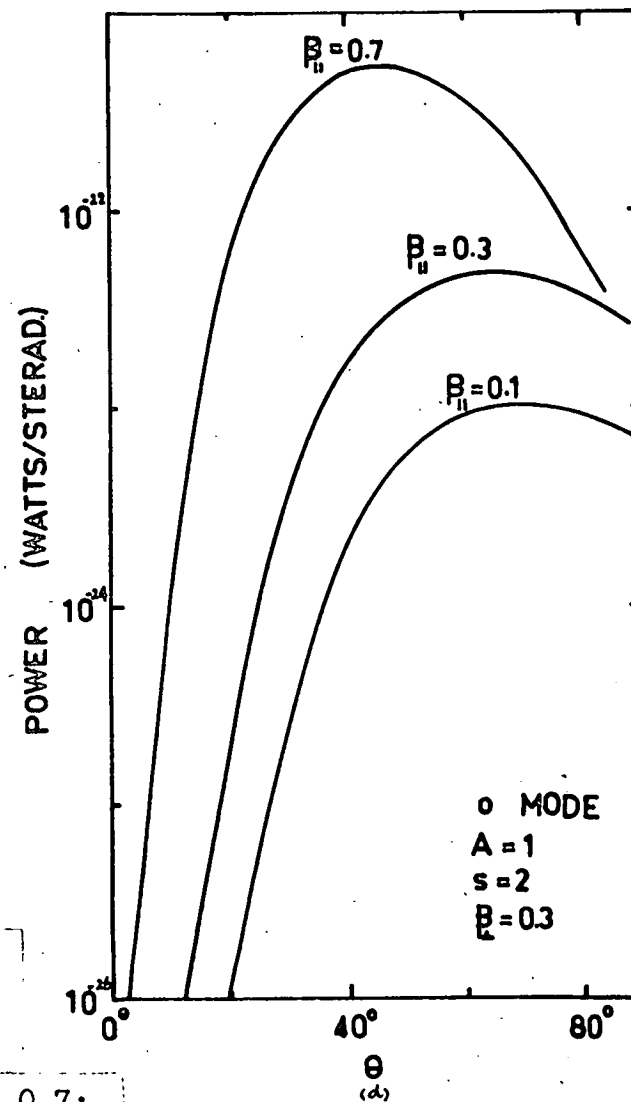
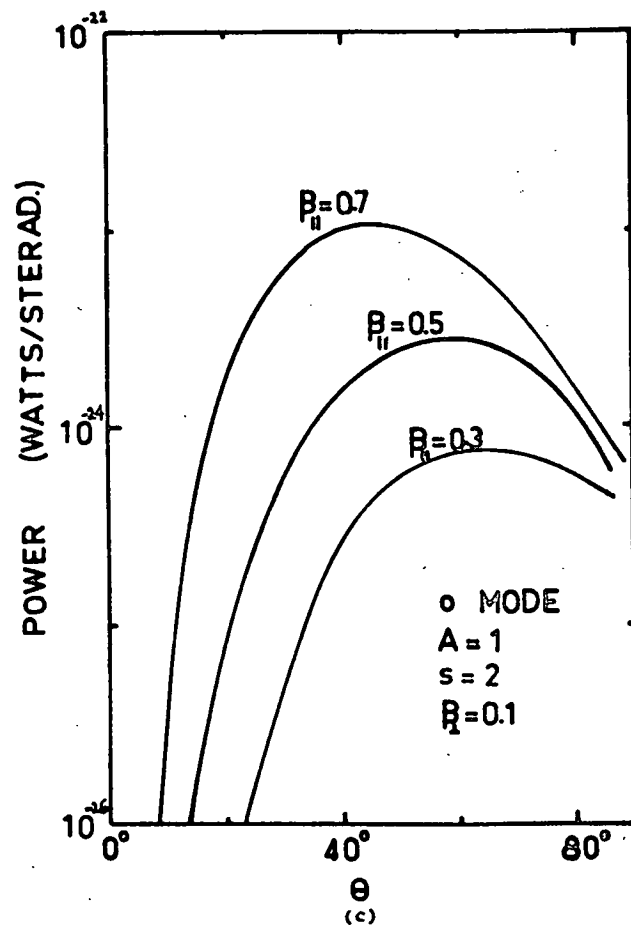


Fig. 8.6 Power spectrum radiated by a single electron in the o-mode for $A = 1$, $f_H = 100$ Mc/s, and

- (c) $s = 2$, $\beta_{\perp} = 0.1$, $\beta_{\parallel} = 0.3, 0.5, 0.7$;
 (d) $s = 2$, $\beta_{\perp} = 0.3$, $\beta_{\parallel} = 0.1, 0.3, 0.7$.

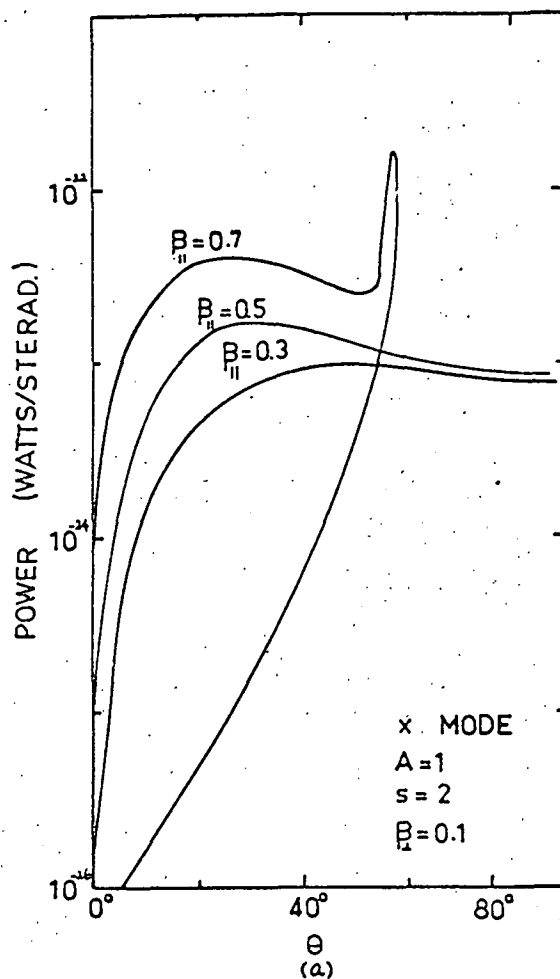
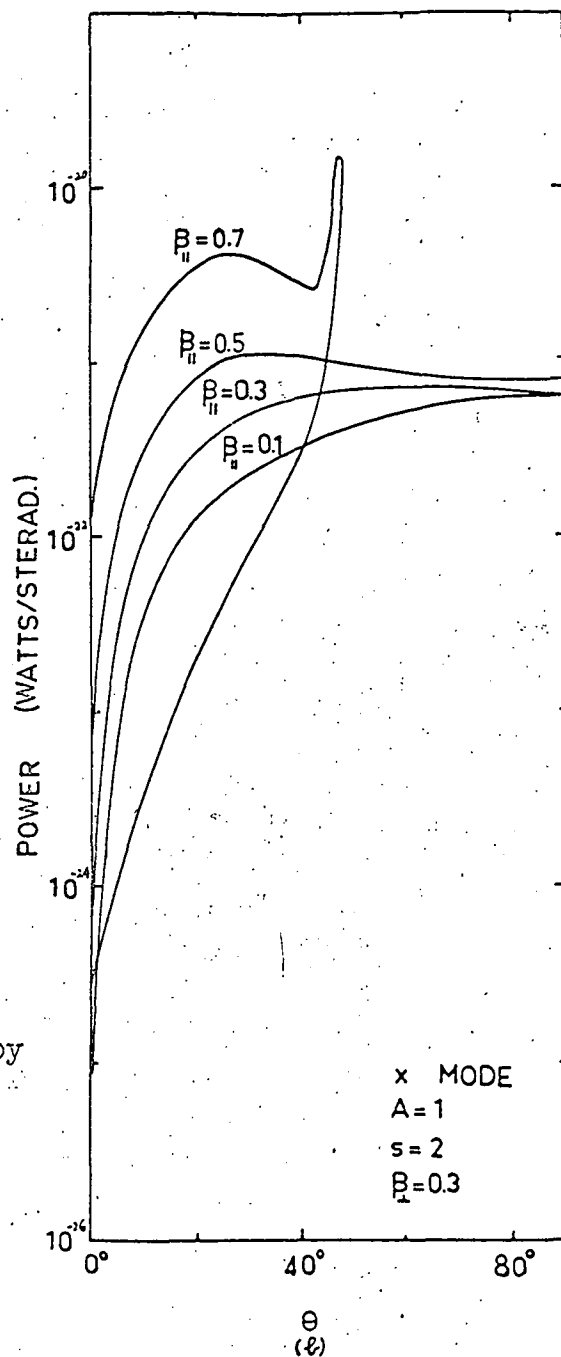


Fig. 8.1 Power spectrum radiated by a single electron in the x-mode for $A = 1$, $f_H = 100$ Mc/s, and

(a) $s = 2$, $\beta_{\perp} = 0.1$,
 $\beta_{\parallel} = 0.3, 0.5, 0.7$;



(b), $s = 2$, $\beta_{\perp} = 0.3$, $\beta_{\parallel} = 0.1, 0.3, 0.5, 0.7$.

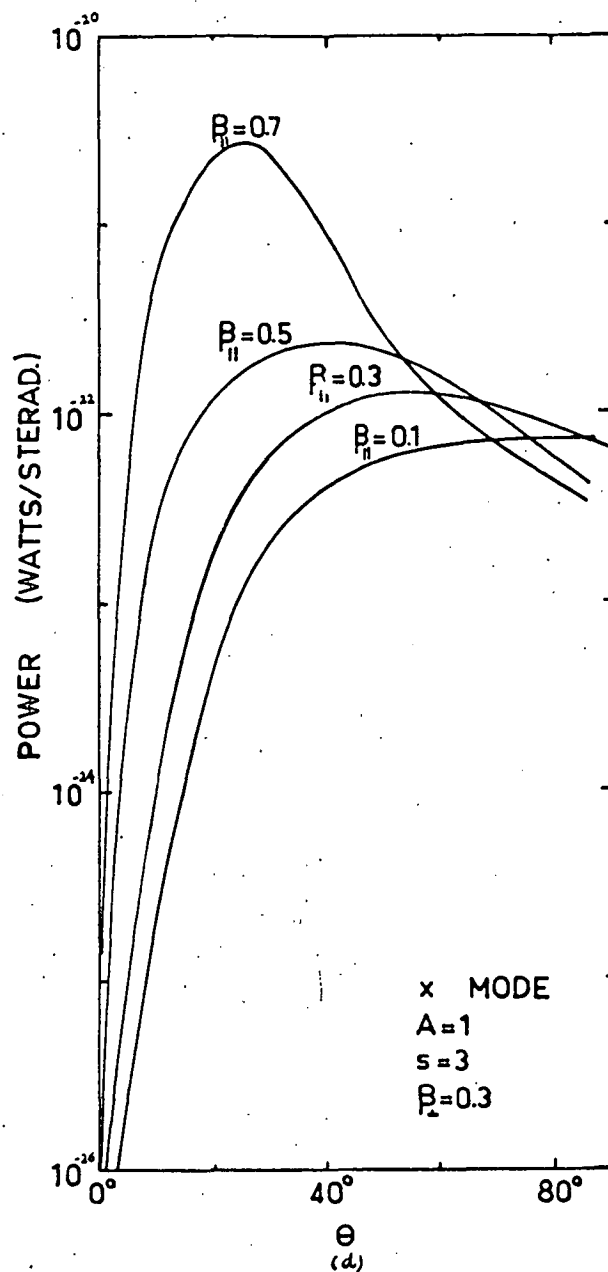
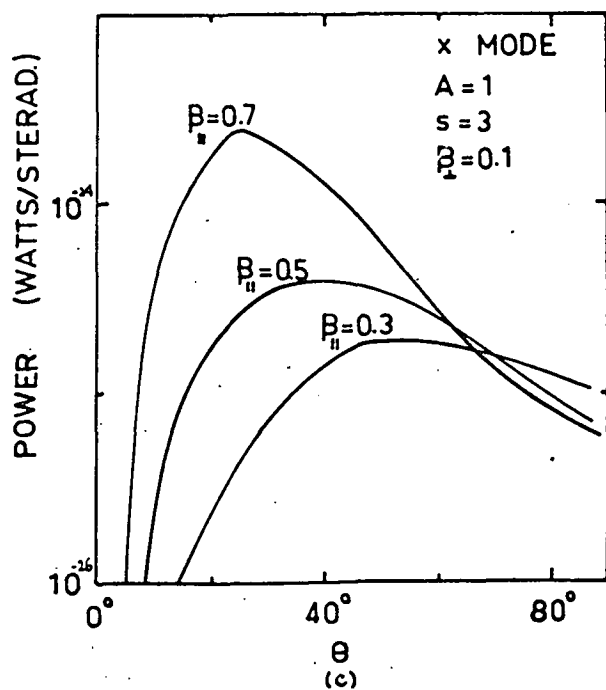


Fig. 8.7 Power spectrum radiated by a single electron in the x-mode for $A = 1$, $f_H = 100$ Mc/s, and
 (c) $s = 3$, $\beta_{\perp} = 0.1$, $\beta_{||} = 0.3, 0.5, 0.7$;
 (d) $s = 3$, $\beta_{\perp} = 0.3$, $\beta_{||} = 0.1, 0.3, 0.5, 0.7$.

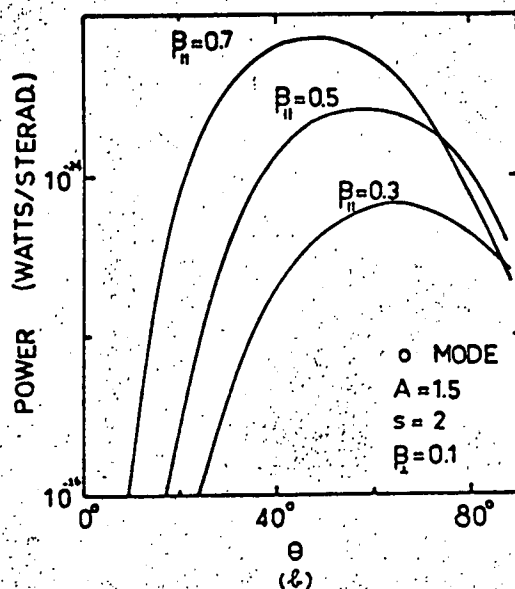
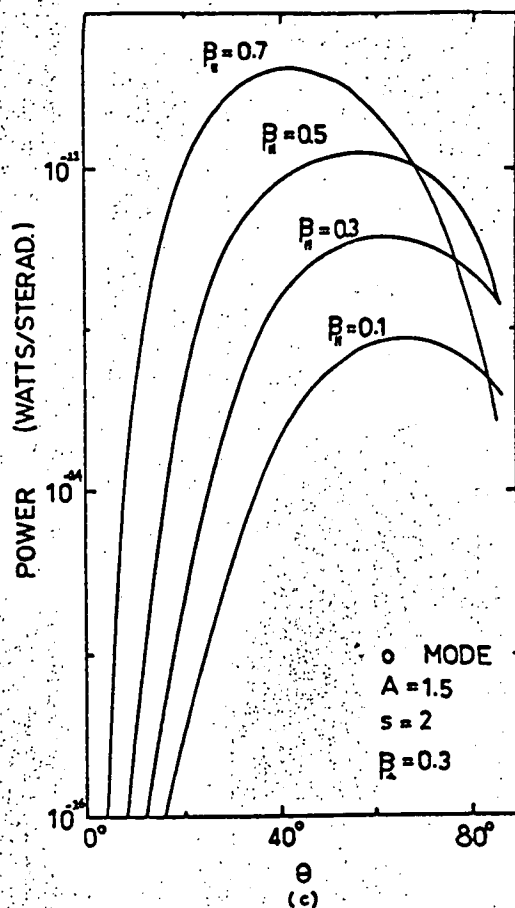
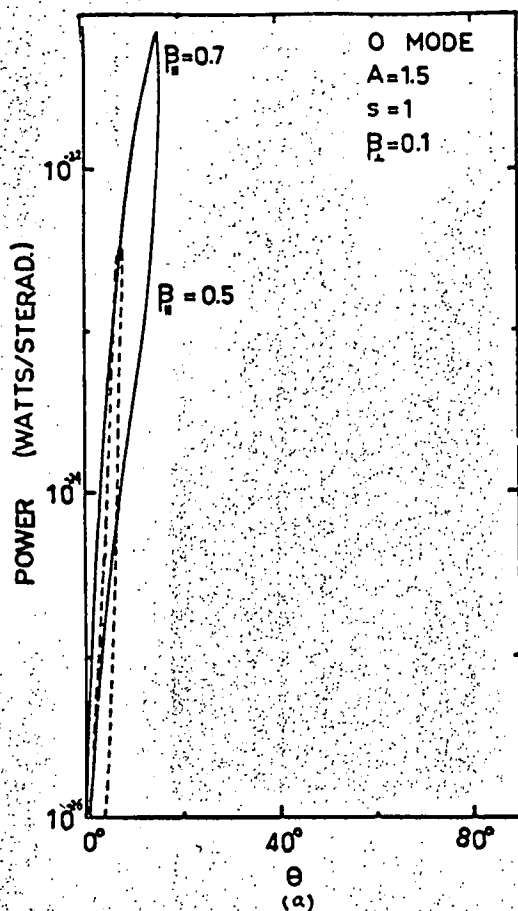


Fig.8.8 Power spectrum radiated by a single electron in the o-mode for $A = 1.5$, $f_H = 100\text{Mc/s}$, and

- (a) $s = 1$, $\beta_{\perp} = 0.1$, $\beta_{\parallel} = 0.5, 0.7$;
 (b) $s = 2$, $\beta_{\perp} = 0.1$, $\beta_{\parallel} = 0.3, 0.5, 0.7$;
 (c) $s = 2$, $\beta_{\perp} = 0.3$, $\beta_{\parallel} = 0.1, 0.3, 0.5, 0.7$.

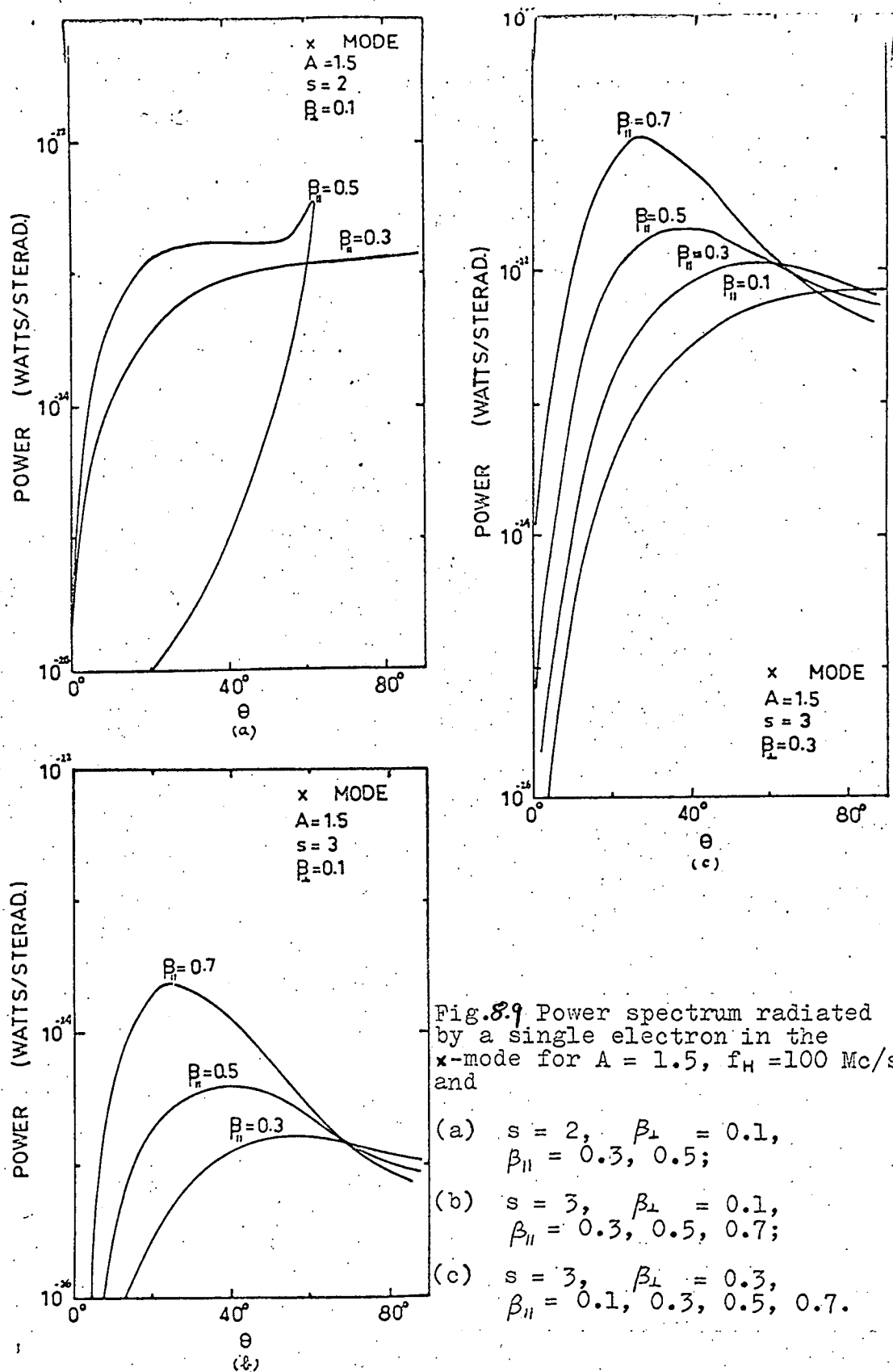


Fig. 8.9 Power spectrum radiated by a single electron in the x-mode for $A = 1.5$, $f_H = 100$ Mc/s, and

- (a) $s = 2$, $\beta_{\perp} = 0.1$, $\beta_{\parallel} = 0.3, 0.5$;
 (b) $s = 3$, $\beta_{\perp} = 0.1$, $\beta_{\parallel} = 0.3, 0.5, 0.7$;
 (c) $s = 3$, $\beta_{\perp} = 0.3$, $\beta_{\parallel} = 0.1, 0.3, 0.5, 0.7$.

the power radiated by both characteristic modes can be of the same order of magnitude for cases with Double frequency solution.

(C) Amplification of Electromagnetic Waves in a Stream-plasma System

So far we have considered radiation spectra from single electrons only. When the radiating electrons form a stream, the stream-plasma system can be radiatively unstable; an electromagnetic wave will grow as a function of time. We will assume here that gyrating electron streams prevail in the source region⁺. Since the bandwidth of a burst radiation is very narrow ($\Delta f/f \sim 0.04$), the spread in momentum distribution of the radiating stream must be very small for many cases. In another terminology, we say that such an electron stream has a finite temperature which is a measure of the momentum spread. The instability problem of such a stream-plasma system (when the temperature effect is taken into account) has been discussed in chapter II. On account of the complexity in mathematics for such a system, we will assume here that the temperature of the electron stream is zero, i.e. every electron in the stream has the same

⁺Discussion on this point will be given in chapter X.

values of $P_{\perp} = P_{\perp}^{\circ}$ and $P_{\parallel} = P_{\parallel}^{\circ}$ and the stream is called "helical". Even though such a stream is the limiting case of a realistic one, the instability theory gives the same general behaviour of the growth rate as in the case when temperature is included^{*}. We will, therefore, without loss of generality in the outcome of the result, assume that the stream is helical, and the distribution function of the stream will then be given by relation (2.4)

$$f_0(\vec{p}) d\vec{p} = \frac{1}{2\pi p_{\perp}^{\circ}} \delta(p_{\perp} - p_{\perp}^{\circ}) \delta(p_{\parallel} - p_{\parallel}^{\circ}) d\vec{p} \quad (8.9)$$

Assuming the particle density of the stream to be small compared with that of the ambient plasma, the growth rate of an electromagnetic wave in the stream-plasma system is given by equation (3.5):

$$\mathcal{G}_m\left(\frac{\delta}{\omega}\right) = \pm \frac{\sqrt{3}}{2} (M^{1/3} - C^{1/3}) \quad (8.10)$$

where $M = -\frac{d}{2} + \left(\frac{d^2}{4} + \frac{l^3}{27}\right)^{1/2}$ and $C = -\frac{d}{2} - \left(\frac{d^2}{4} + \frac{l^3}{27}\right)^{1/2}$

$$l = -\sigma A J_s^2 \left[\frac{(s\gamma - \xi)^2}{\beta_{\parallel}^2 \xi^2} - 1 \right] \frac{\beta_{\parallel}^2 \cos^2 \theta}{(\xi - s\gamma)^2}$$

$$d = \sigma A \left[\frac{(s\gamma - \xi)^2}{\beta_{\parallel}^2 \xi^2} - 1 \right] \frac{\left[J_s'^2 \beta_{\perp}^2 + J_s^2 \beta_{\parallel}^2 \frac{(s\gamma - \sin^2 \theta \xi)^2}{\sin^2 \theta (s\gamma - \xi)^2} \right]}{(AL - 2\xi^2)}$$

^{*}This statement is true only when the temperature of the stream is low; when the momentum spread is wide, the bandwidth of emission will be broad and the harmonics may not be resolved.

$$L = \frac{\frac{2AD}{\xi^2} - \left(1 - \frac{A}{\xi^2}\right) \left\{ \frac{2A}{\xi^2} + \frac{\sin^2 \theta}{\xi^2} - \bar{B}^{1/2} \left[-\frac{\sin^4 \theta}{\xi^4} + \frac{4A \cos^2 \theta}{\xi^4} \left(1 - \frac{A}{\xi^2}\right) - \frac{2 \cos^2 \theta}{\xi^2} \left(1 - \frac{A}{\xi^2}\right)^2 \right] \right\}}{b^2}$$

In expression (8.10), for thin stream such that $\sigma < 10^{-2}$, we have

$$\frac{d^2}{4} \gg \frac{|b^3|}{27}$$

and we can then specify the growth rate in the following form:

$$\left| \frac{\mathcal{I}_m \delta}{\omega_H \sigma^{1/3}} \right| = \frac{\sqrt{3}}{2} \xi \quad (8.11)$$

Fixing the energy and pitch angle of the helicon stream, the emitted characteristic normalized frequency ξ has been obtained as a function of the wave-normal angle θ in section (A) for three values of $A = 0.25, 1, 1.5$. The dependence of the growth rate (specified by $\left| \frac{\mathcal{I}_m \delta}{\omega_H \sigma^{1/3}} \right|$) on wave-normal angle θ is shown in Fig. 8.10 - 8.15 (Fig. 8.10, 8.12, 8.14 for o-mode and Fig. 8.11, 8.13, 8.15 for x-mode) for frequencies and other parameters as in Fig. 8.4 - 8.9. These graphs show the following features:

- (i) For Single frequency solution, the growth rate for the o-mode has a broad maximum around $\theta = \theta_m$ varying from 35° to 60° while the growth rate for the x-mode also shows a broad maximum around θ_m which ranges from 40° to 80° , for various values of β_\perp , β_\parallel and A as specified.

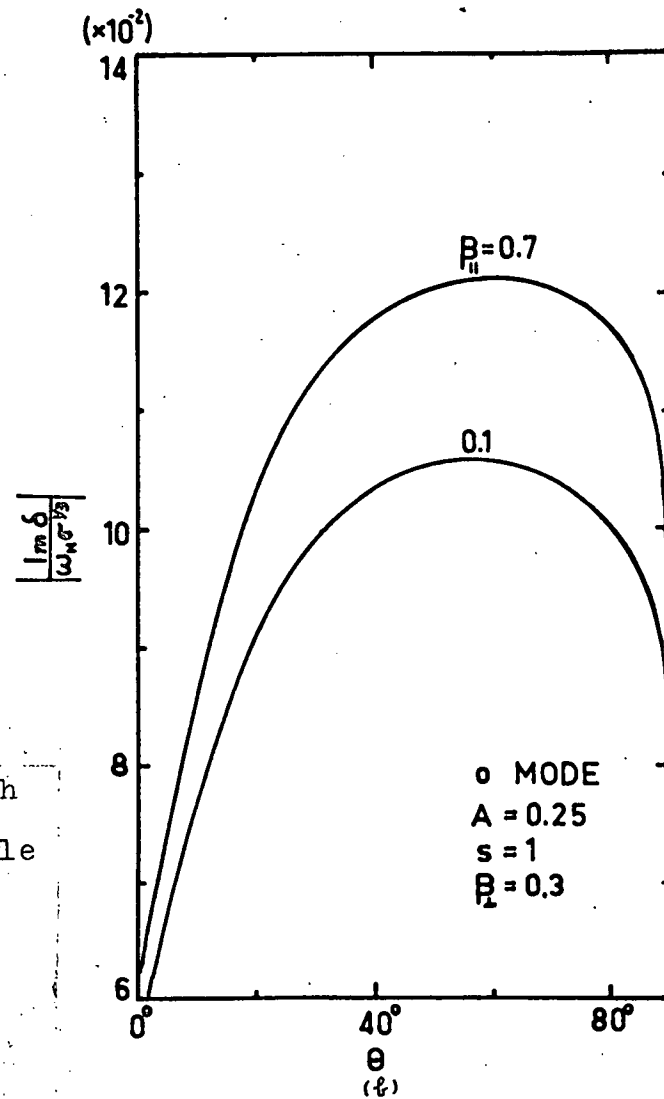
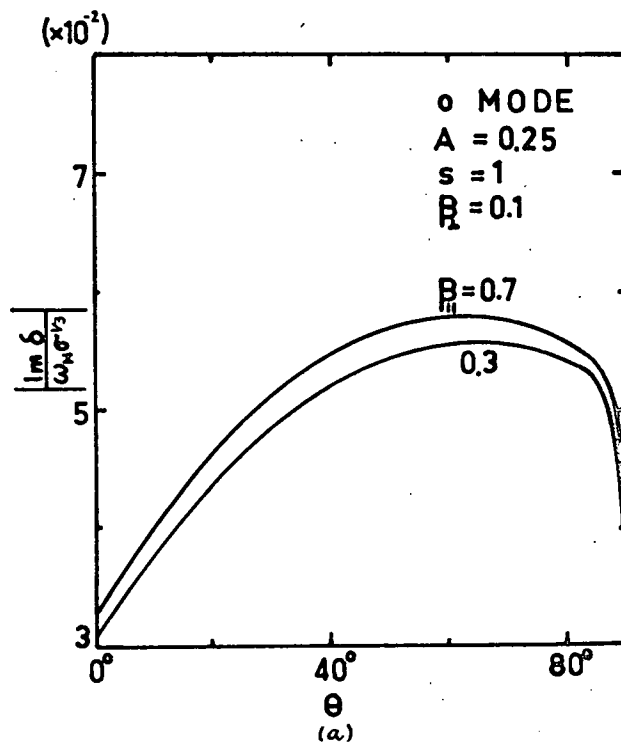


Fig. 8.10 The dependence of the growth rate $\frac{\text{Im } \delta}{\omega_H \sigma^{1/3}}$ on wave-normal angle θ in the o-mode for $A = 0.25$, and

(a) $s = 1$, $\beta_{\perp} = 0.1$, $\beta_{\parallel} = 0.3, 0.7$;

(b) $s = 1$, $\beta_{\perp} = 0.3$, $\beta_{\parallel} = 0.1, 0.7$.

(12)

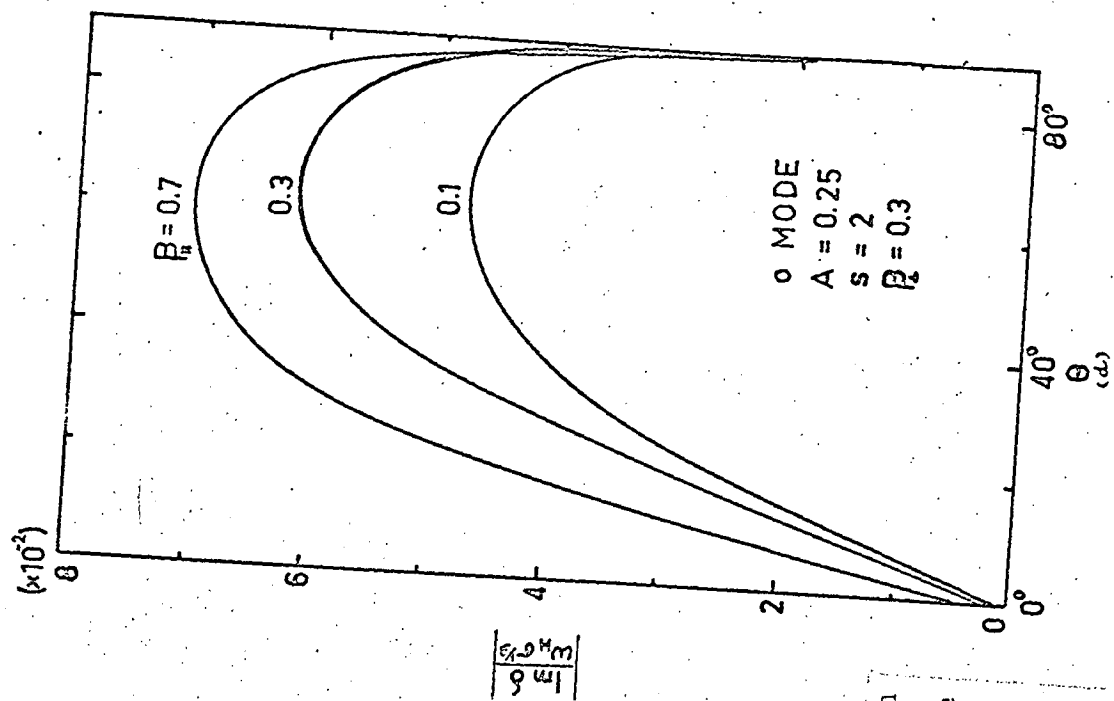
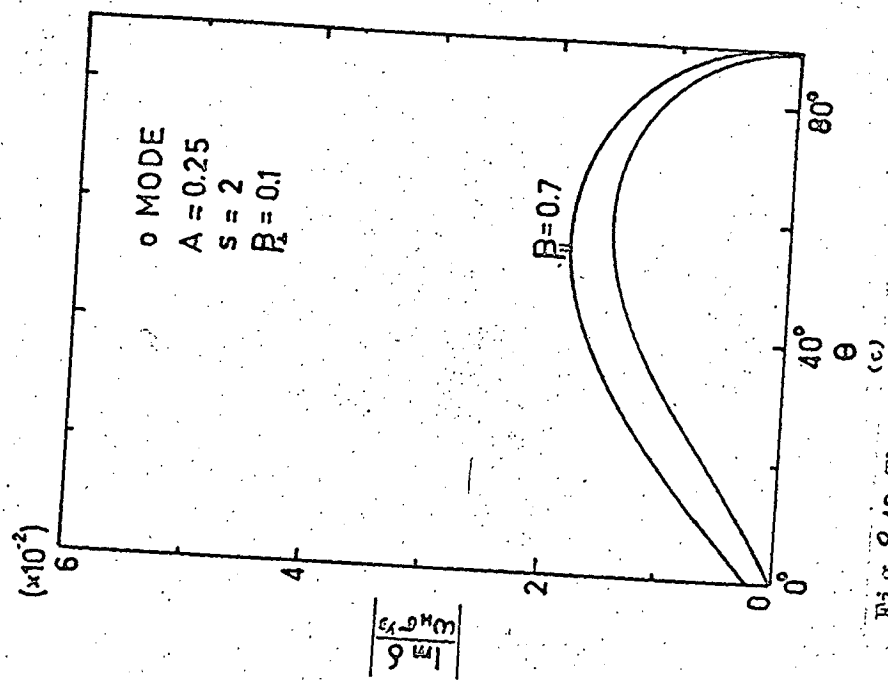


Fig. 8.10 The dependence of the growth rate $\left| \frac{\gamma_m \delta}{\omega_H \sigma^{1/2}} \right|$ on wave-normal angle θ in the o-mode for $A = 0.25$, and

(c) $s = 2$, $\beta_{\perp} = 0.1$,
 $\beta_{\parallel} = 0.3, 0.7$;

(d) $s = 2$, $\beta_{\perp} = 0.3$,
 $\beta_{\parallel} = 0.1, 0.3, 0.7$.

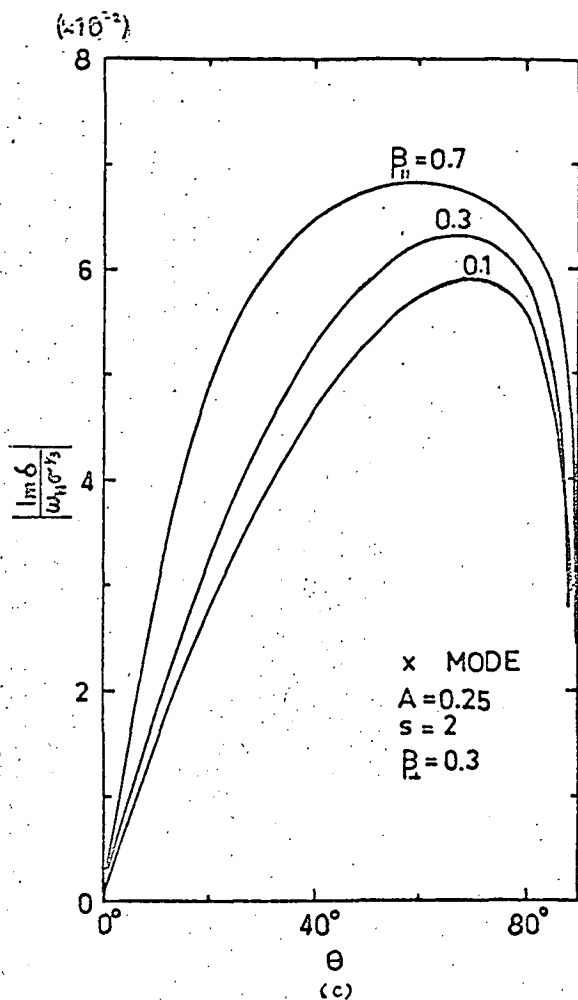
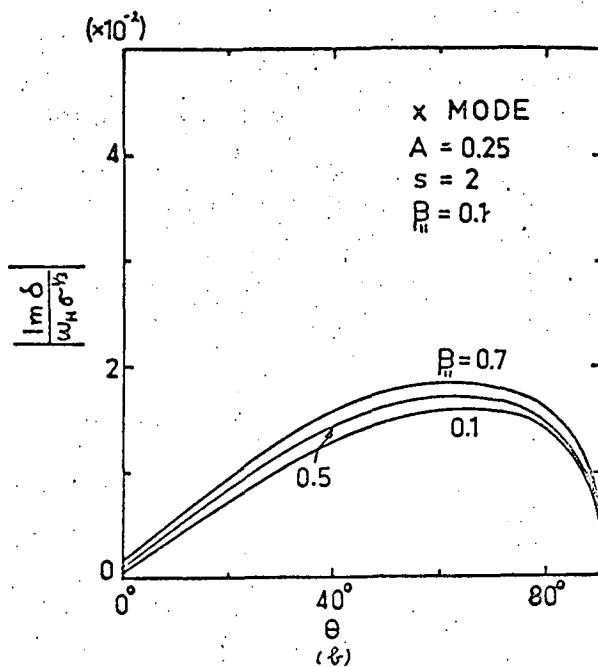
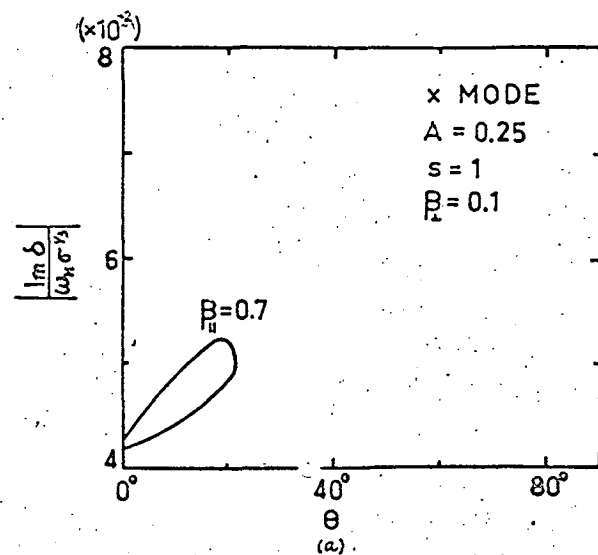


Fig. 8.11 The dependence of the growth rate $\frac{|\text{Im } \delta|}{\omega_H \sigma^{1/3}}$ on wave-normal angle θ in the x-mode for $A = 0.25$, and

- (a) $s = 1, \beta_{\perp} = 0.1, \beta_{||} = 0.7$;
 (b) $s = 2, \beta_{\perp} = 0.1, \beta_{||} = 0.1, 0.5, 0.7$;
 (c) $s = 2, \beta_{\perp} = 0.3, \beta_{||} = 0.1, 0.3, 0.7$.

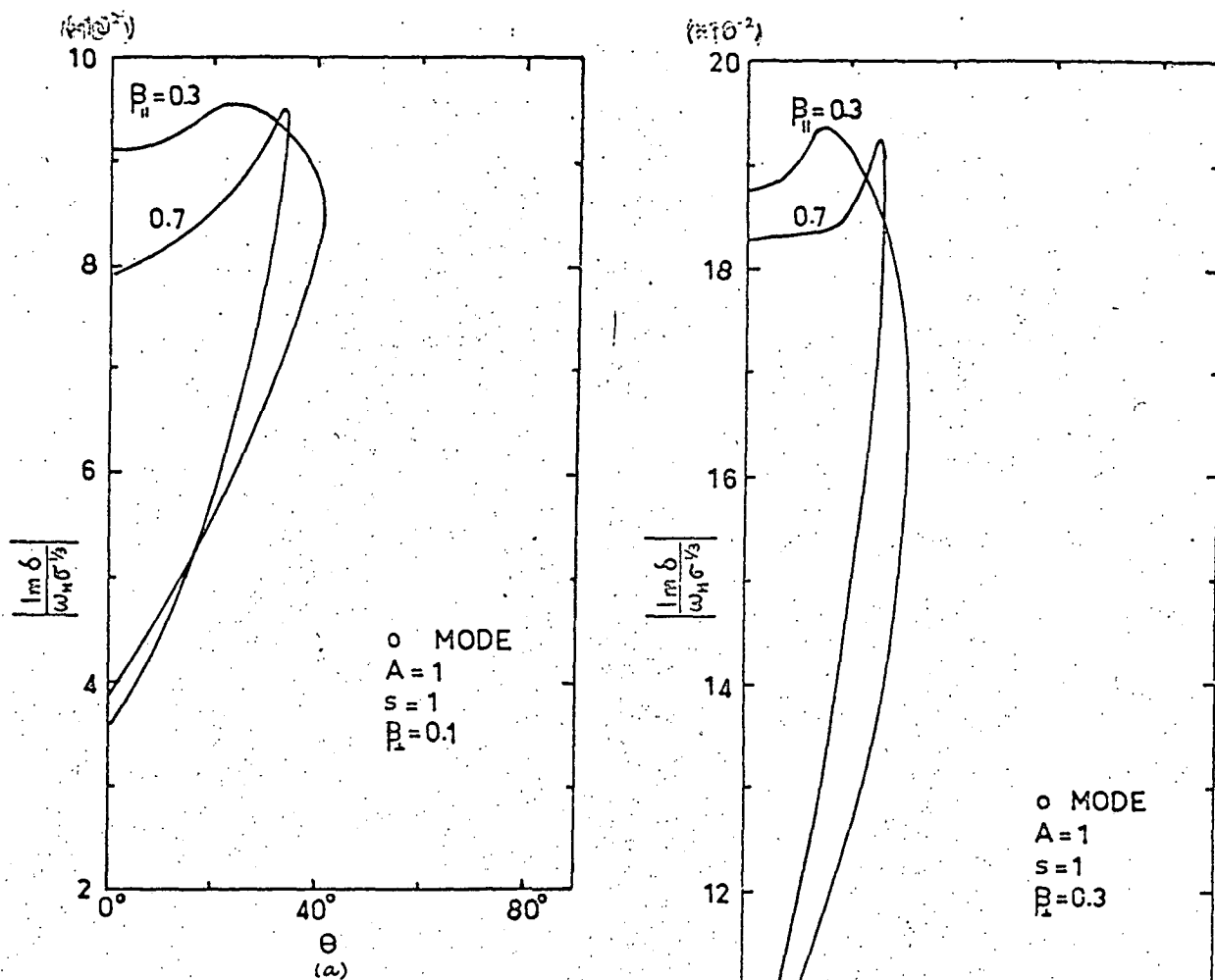


Fig. 8.12 The dependence of the growth rate $\frac{|\text{Im } \delta|}{\omega_H \sigma^{1/3}}$ on wave-normal angle θ in the o-mode for $A = 1$, and

- (a) $s = 1$, $\beta_{\perp} = 0.1$, $\beta_{\parallel} = 0.3, 0.7$;
 (b) $s = 1$, $\beta_{\perp} = 0.3$, $\beta_{\parallel} = 0.3, 0.7$.

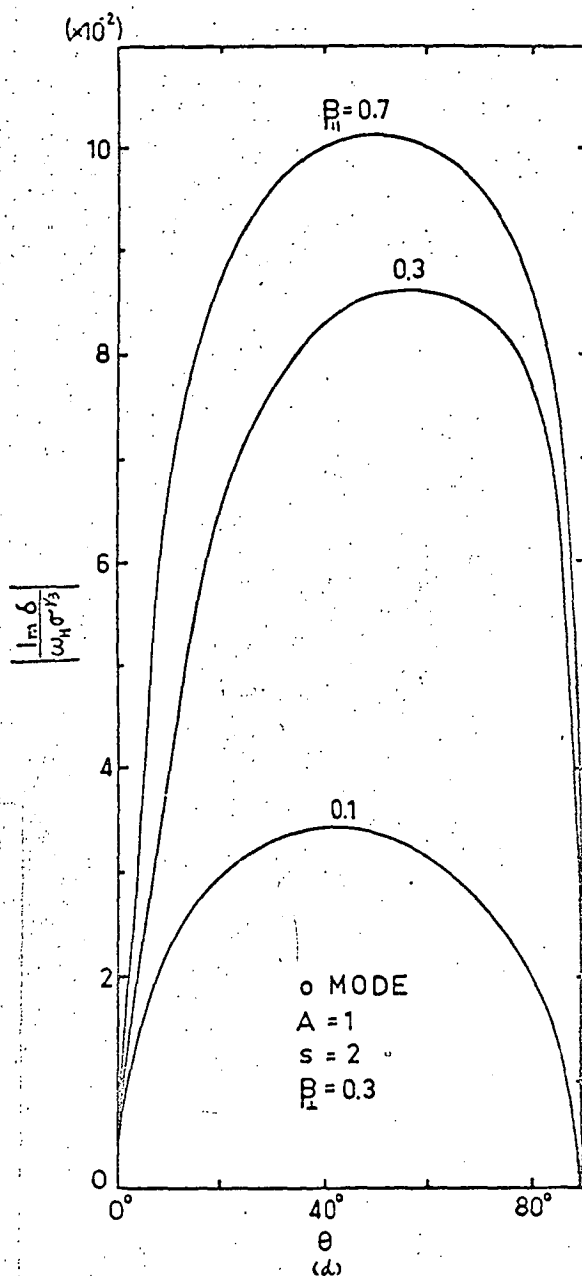
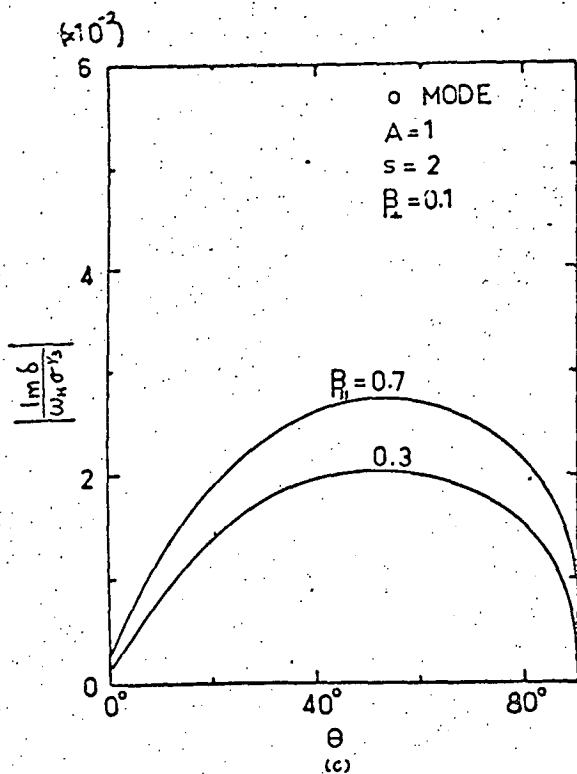


Fig. 8.12 The dependence of the growth rate $\frac{|\text{Im } \delta|}{\omega_H \sigma^{1/3}}$ on wave-normal angle θ in the o-mode for $A = 1$, and

- (c) $s = 2$, $\beta_{\perp} = 0.1$,
 $\beta_{\parallel} = 0.3, 0.7$;
 (d) $s = 2$, $\beta_{\perp} = 0.3$,
 $\beta_{\parallel} = 0.1, 0.3, 0.7$.

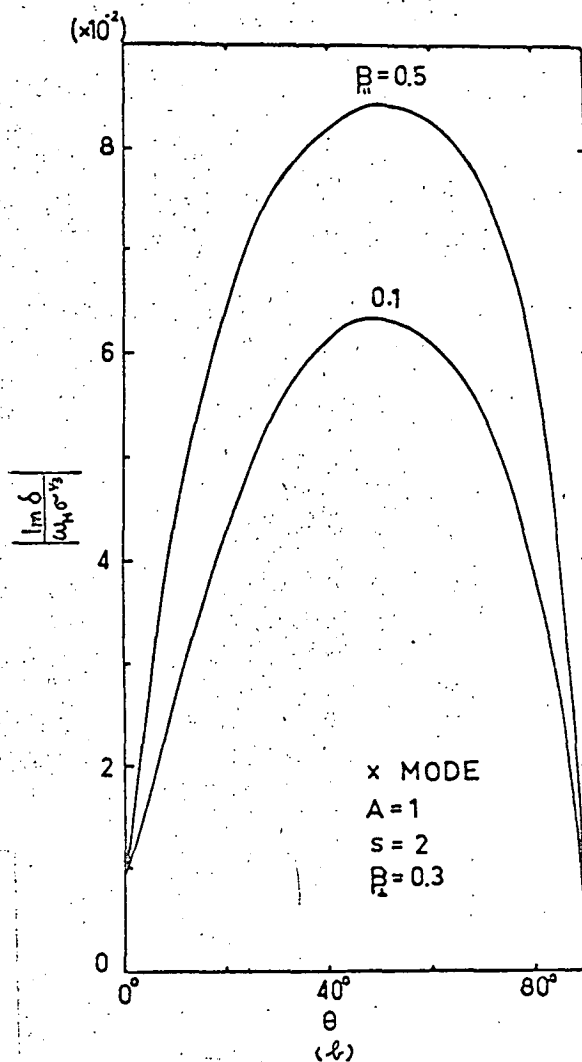
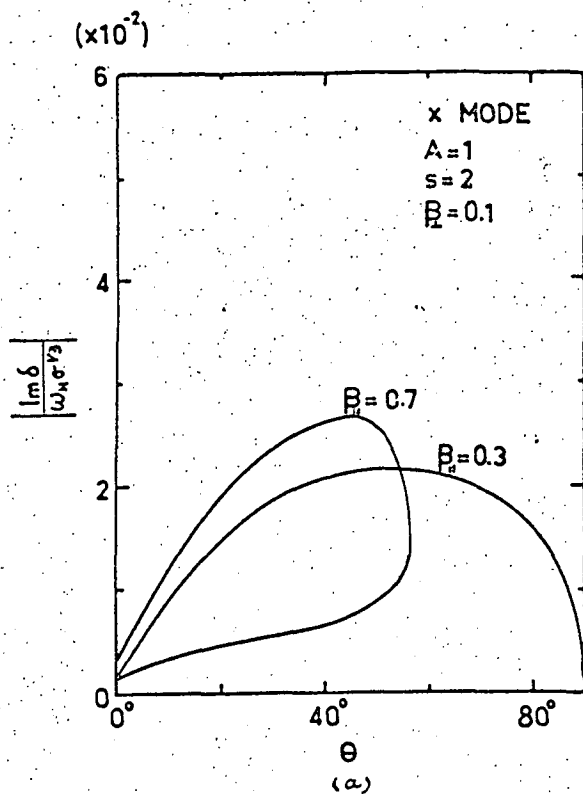


Fig. 8.13 The dependence of the growth rate $\left| \frac{\text{Im } \delta}{\omega_H \sigma^{1/3}} \right|$ on wave-normal angle θ in the x-mode for $A = 1$, and

(a) $s = 2$, $\beta_{\perp} = 0.1$, $\beta_{||} = 0.3, 0.7$;

(b) $s = 2$, $\beta_{\perp} = 0.3$, $\beta_{||} = 0.1, 0.5$.

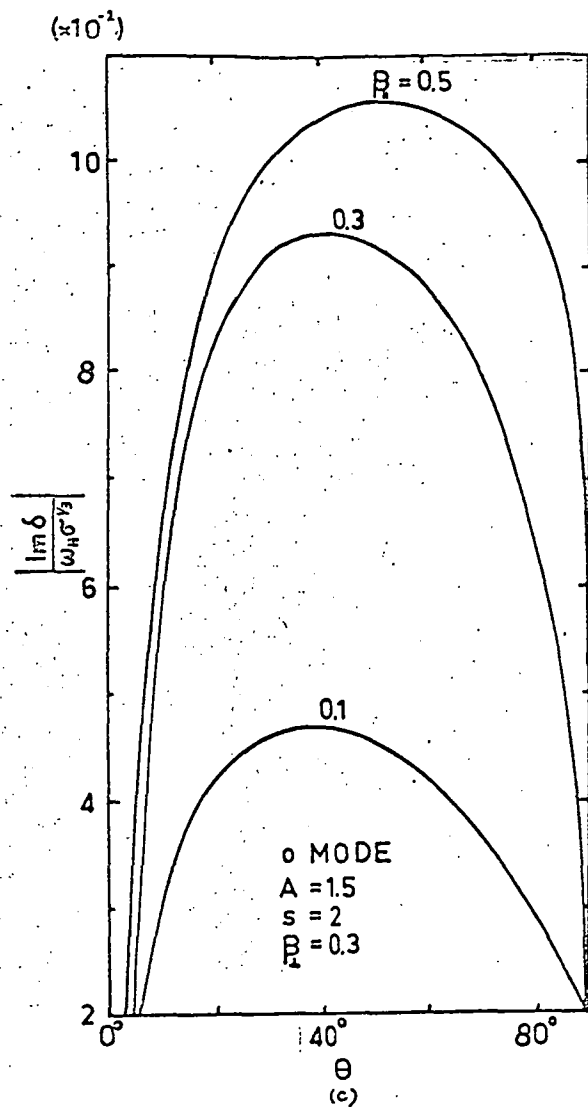
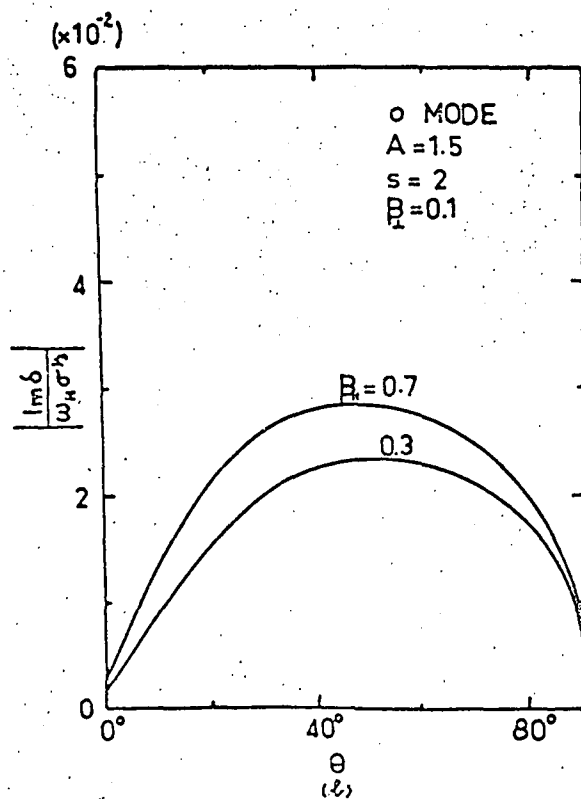
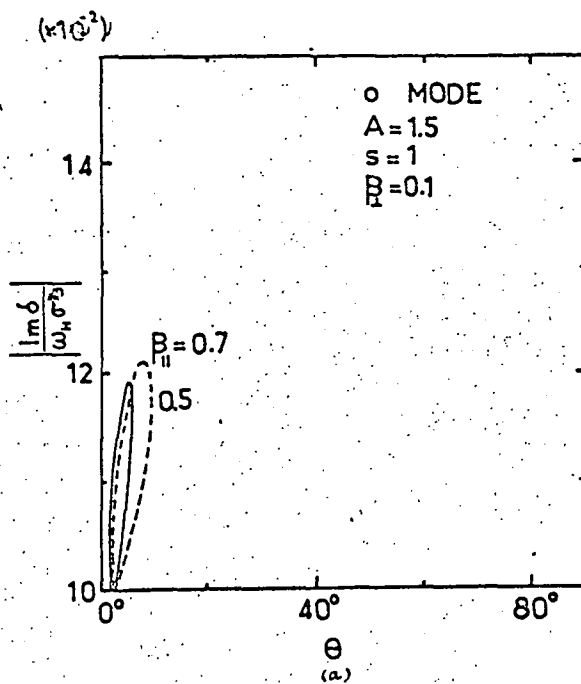


Fig.8.14 The dependence of the growth rate $\frac{\text{Im} \delta}{\omega_H \sigma^{1/2}}$ on wave-normal angle θ in the o-mode for $A = 1.5$, and
 (a) $s = 1$, $\beta_{\perp} = 0.1$, $\beta_{\parallel} = 0.5, 0.7$;
 (b) $s = 2$, $\beta_{\perp} = 0.1$, $\beta_{\parallel} = 0.3, 0.7$;
 (c) $s = 2$, $\beta_{\perp} = 0.3$, $\beta_{\parallel} = 0.1, 0.3, 0.5$.

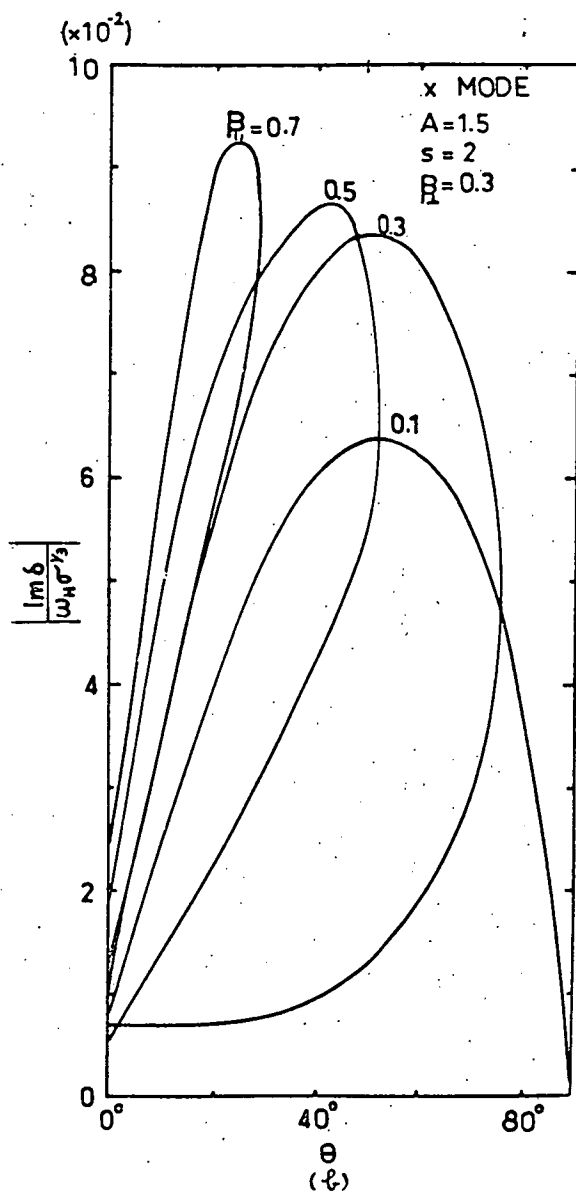
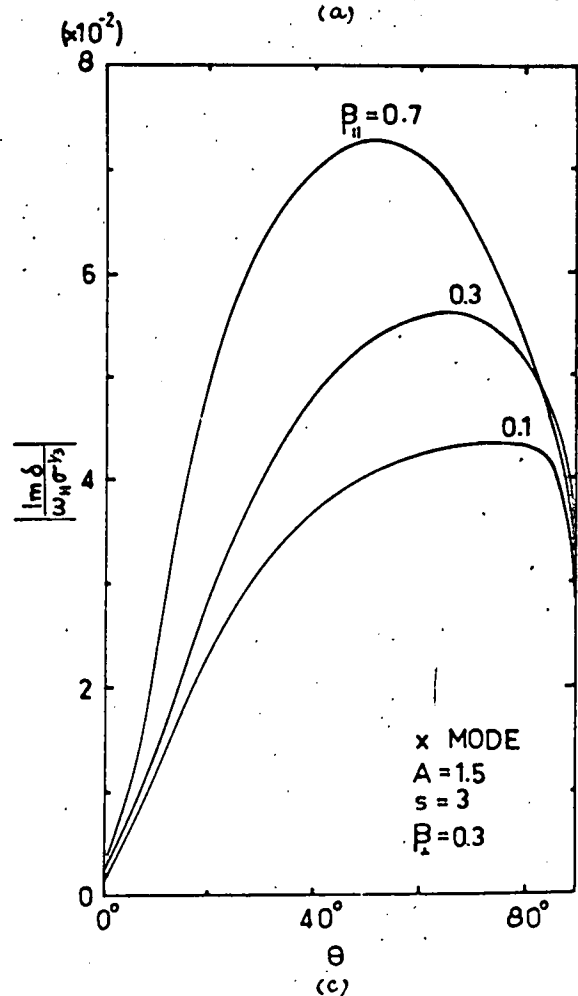
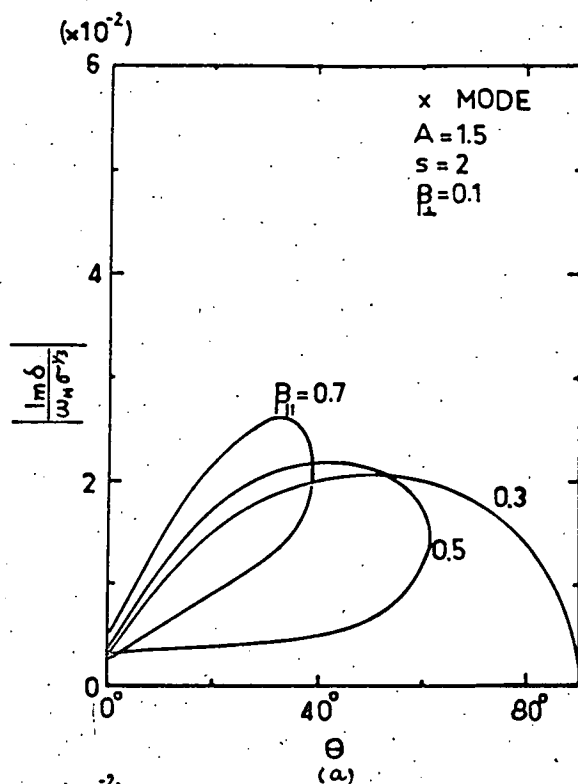


Fig. 8.15 The dependence of the growth rate $\left| \frac{\text{Im } \delta}{\omega_H \sigma^{1/2}} \right|$ on wave-normal angle θ in the x-mode for $A = 1.5$, and

- (a) $s = 2$, $\beta_{\perp} = 0.1$, $\beta_{\parallel} = 0.3, 0.5, 0.7$.
- (b) $s = 2$, $\beta_{\perp} = 0.3$, $\beta_{\parallel} = 0.1, 0.3, 0.5, 0.7$;
- (c) $s = 3$, $\beta_{\perp} = 0.3$, $\beta_{\parallel} = 0.1, 0.3, 0.7$.

- (ii) For both modes, whenever the Double frequency solution exists, the growth rate is large and θ_m occurs near the cut-off angle θ_c . For a constant value of β_\perp , θ_m approaches towards θ_c as the pitch angle of the stream decreases (i.e. increasing β_\parallel). Moreover, when β_\perp is fixed, the value of maximum growth rate increases with increasing β_\parallel up to an optimum value of β_\parallel ; then the maximum growth decreases with still increasing β_\parallel .
- (iii) With the range of value for A as assigned (0.25 - 1.5), the growth rates for both modes are of the same order of magnitude.
- (iv) The growth rate decreases rapidly with increasing harmonic number for electron energy of the order of 10 - 100 Kev.

In this stream-plasma system, the electromagnetic wave grows exponentially as a function of time. If we take that the wave interacts for 10^{-2} msec. (or 5×10^{-3} msec.) with the stream, and that the gyro-frequency $f_H = \omega_H/2\pi = 100$ Mc/s, $\sigma = \text{density of stream/density of ambient plasma} = 10^{-3}$ (or 10^{-6}), we can calculate the power gain after this short period of interaction. We show some examples of the relation between the power gain in db and the wave-normal angle θ in Fig. 8.16. To show how the power gain behaves with respect to change of frequency, and thus, to estimate the bandwidth of emission, we have Fig. 8.17 corresponding to Fig. 8.16. Note that in Fig. 8.17 the range of frequency amplified

corresponds to different directions. However, if we consider a half-power or quarter-power emission cone and let the range of frequencies radiated within this cone to be the estimated bandwidth, then this estimated bandwidth is the maximum bandwidth which can be received on Earth, since the emission cone may be too wide and only part of the radiation will "strike" the Earth on account of geometrical factor⁺.

Fig. 8.17 shows that:

- (i) For both Single and Double types of frequency solution, the bandwidth is small when the pitch angle is large.
- (ii) When β_{\perp} and β_{\parallel} are fixed, the bandwidth for Double frequency solution is much narrower than that for Single frequency solution. Obviously, in this case, the harmonic number for the Single frequency solution is one unit higher.
- (iii) A bandwidth as narrow as $\Delta \xi \sim 0.09$ is possible.⁺⁺

⁺In this argument, we have assumed that the wave is refracted only slightly in the corona.

⁺⁺Note that in Fig. 17(c), the pitch angle is 45° ; if the pitch angle is increased to greater than 60° , a half-power bandwidth of $\Delta \xi < 0.03$ is possible. Note also that the theoretical bandwidth decreases when the power gain is increased, i.e. allowing a longer interaction time or denser stream.

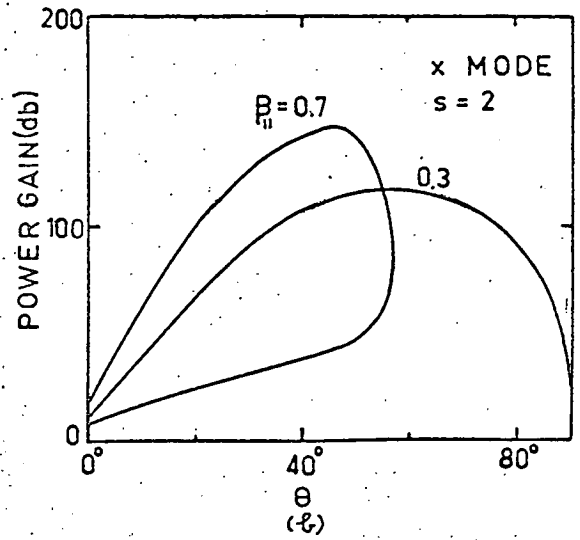
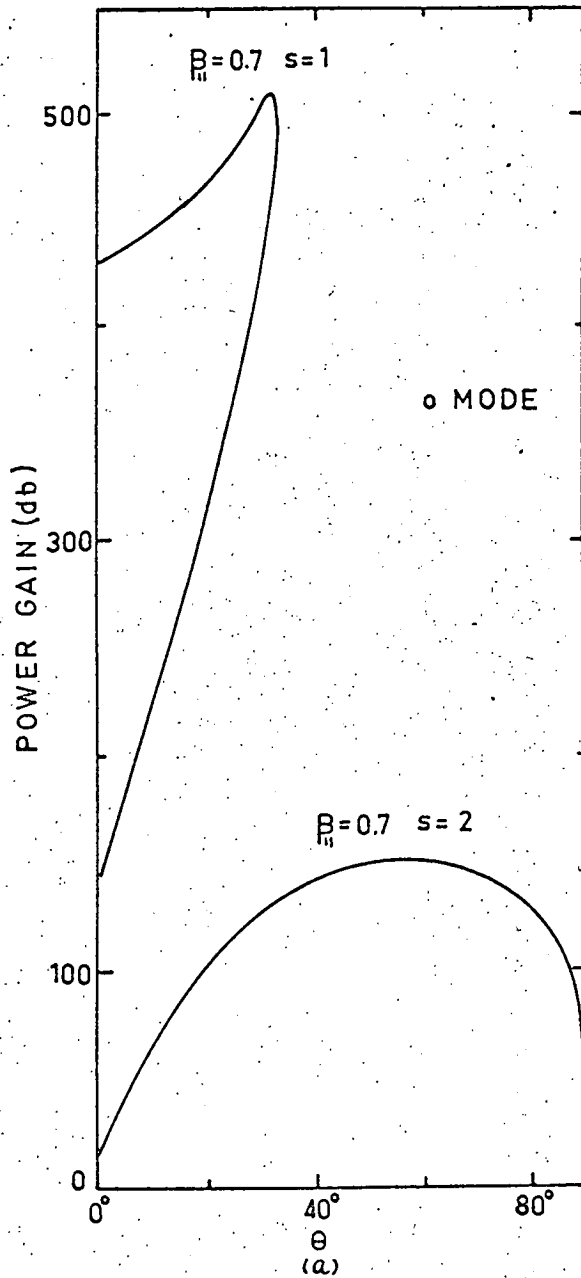


Fig. 8.16 The relation of the power gain (db) after 10^{-5} sec. and the wave-normal angle θ for $\sigma = \omega_o^2/\omega_p^2 = 10^{-3}$, $f_H = 100$ Mc/s, $A = 1$, $\beta_{\perp} = 0.1$ and

- (a) o-mode, $\beta_{||} = 0.7$,
 $s = 1, 2$;
- (b) x-mode, $\beta_{||} = 0.3, 0.7$,
 $s = 2$.

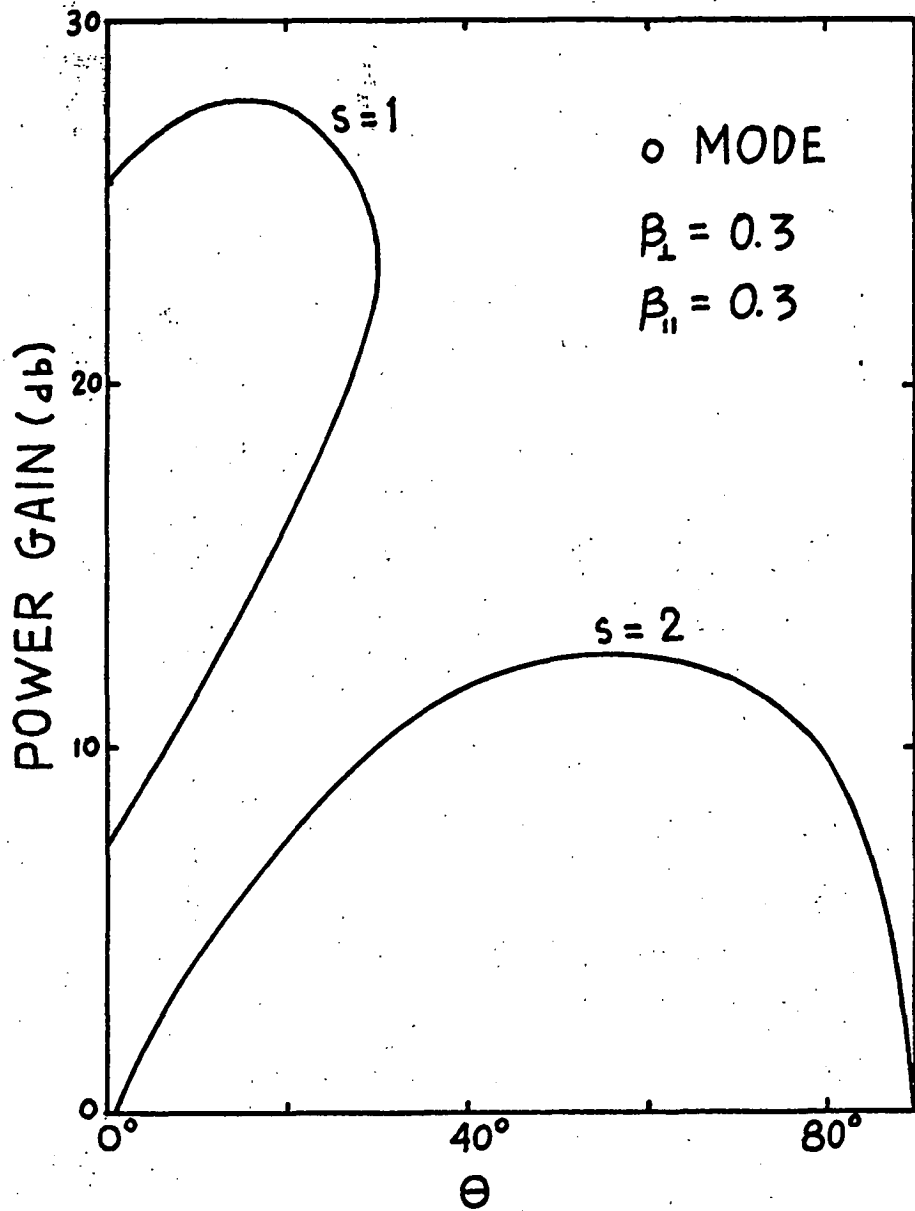


Fig. 8.16(c) The relation of the power gain (db) after 5×10^{-6} sec. and the wave normal angle Θ for $\sigma = \omega_0^2/\omega_p^2 = 10^{-6}$, $f_H = 100$ Mc/s, $A = 1$, $\beta_{\perp} = 0.3$, $\beta_{\parallel} = 0.3$ and $s = 1, 2$.

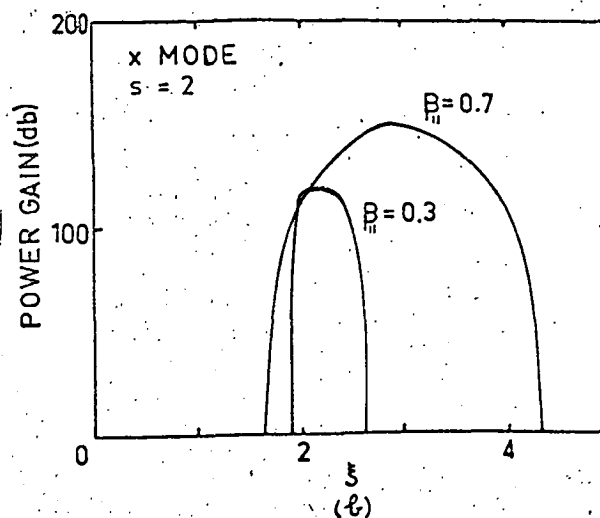
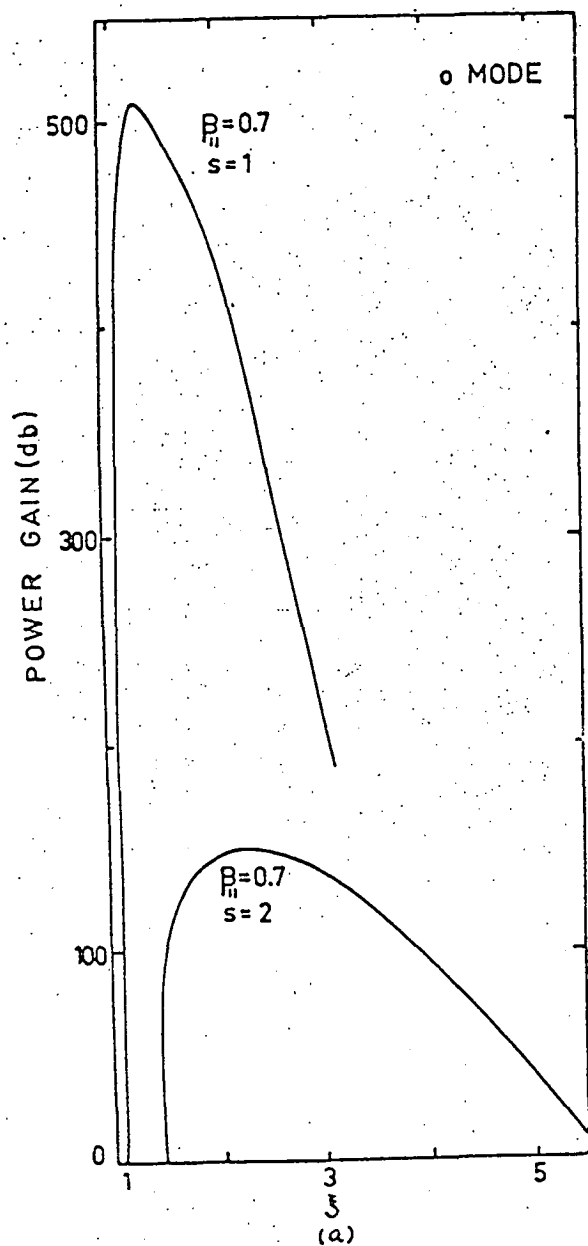


Fig. 8.17 The relation of the power gain (db) after 10^{-5} sec. and the normalized frequency ξ for $\sigma = \omega_0^2/\omega_p^2 = 10^{-3}$, $f_H = 100$ Mc/s, $A = 1$, $\beta_{\perp} = 0.1$, and

(a) o-mode, $\beta_{||} = 0.7$, $s = 1, 2$;

(b) x-mode, $\beta_{||} = 0.3, 0.7$, $s = 2$.

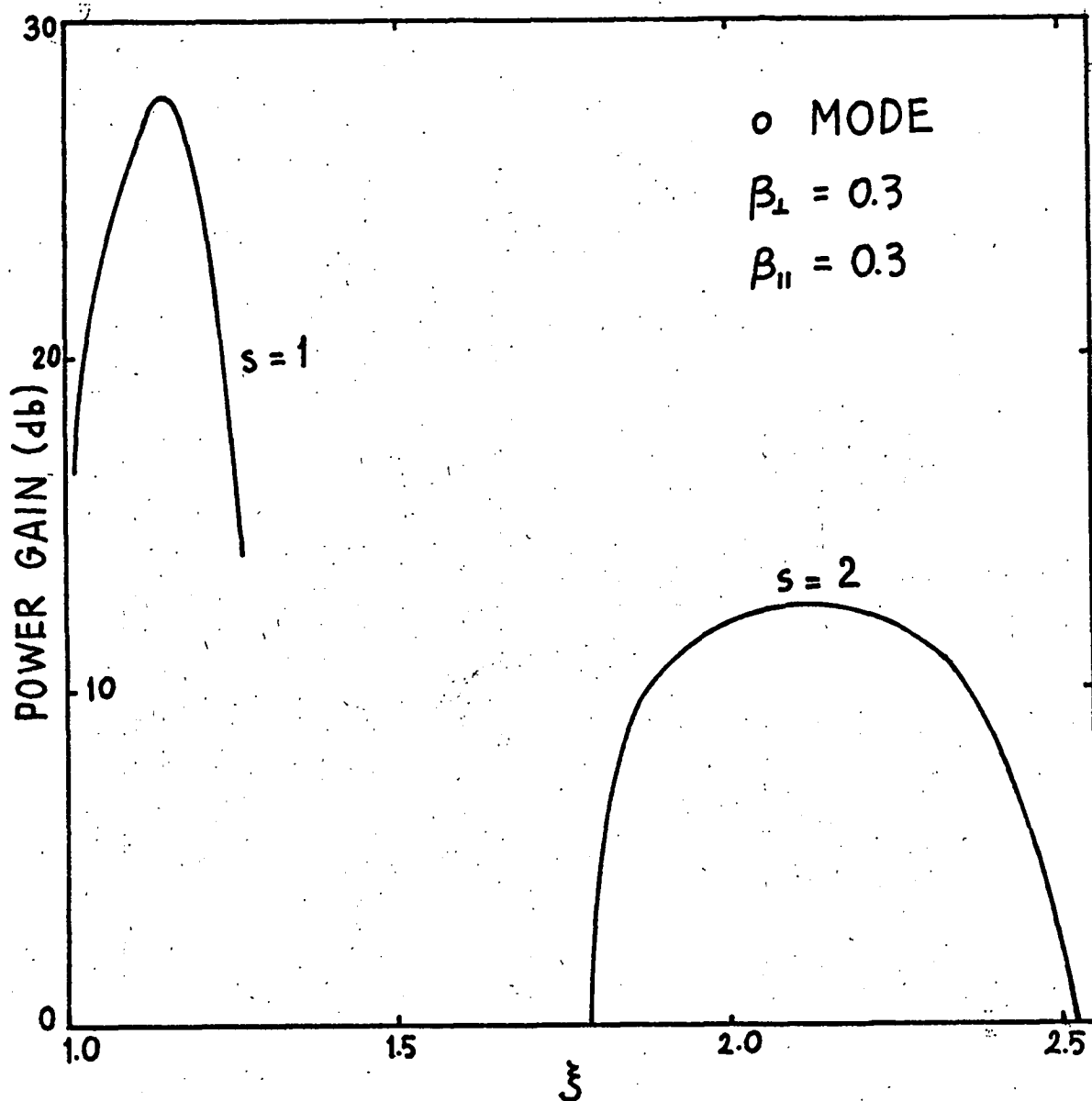


Fig. 8.17(c) The relation of the power gain (db) after 5×10^{-6} sec. and the normalized frequency ξ for $\sigma = \omega_o^2 / \omega_p^2 = 10^{-6}$, $f_H = 100$ Mc/s, $A = 1$, $\beta_{\perp} = 0.3$, $\beta_{\parallel} = 0.3$ and $s = 1, 2$.

(D) Resonance Absorption at the First Three Harmonics

It is well known from both classical and quantum theories that when an electron emits cyclotron radiation at some particular frequency, it can also absorb radiation of the same frequency (e.g. Ginzburg, 1964). When an electromagnetic wave passes through a magnetoactive plasma, some electrons "feel" the wave gyrating at their own frequency and either excitation or damping can take place depending on the energy distribution of the electrons as discussed in chapter II. Hence, whereas electromagnetic waves satisfying the resonance condition $\tilde{\omega} - k_{\parallel} v_{\parallel} - s \gamma \omega_H = 0$ will grow in a stream-plasma system (section (C)), they will be damped in a background plasma of "slow" electrons and ions (the resonance condition is now approximated to $\tilde{\omega} - s \omega_H \approx 0$). Consequently, absorption will take place when an electromagnetic wave of angular frequency $\tilde{\omega}$, propagating in the active corona with varying magnetic fields in space, encounters angular gyro-frequency ω_H such that

$$\tilde{\omega} \doteq s \omega_H \quad (8.12)$$

where $s = 1, 2, 3 \dots$

This type of collisionless absorption is called resonance absorption. It has been pointed out by Gershman (1960)

that since the collision frequency in the corona is very small ($\nu \sim 10^{-3}$, chapter VII), the only important absorption for transverse electromagnetic waves is the resonance absorption.

Let an electromagnetic wave be specified by $e^{i(kz - \omega t)}$, where z is distance along which the phase velocity is travelling. If we assume the frequency to be real and wave vector complex so as to look for a damping in space, we can write

$$k = -iq + \tilde{k}$$

and the damping factor will be e^{-qz} . According to Gershman (1960), the rate of the first harmonic absorption ($\omega \approx \omega_H$) is given by

$$\left(\frac{q}{\tilde{k}}\right)_{\text{res}} = \frac{\sqrt{2}\pi [\beta_T / (n_j X)] \cos \theta}{2X - 2 - \sin^2 \theta + 2n_j^2 \sin^2 \theta} \left\{ \left[1 - \left(1 - \frac{7}{4} \sin^2 \theta\right) X \right] n_j^4 - \left[2 + X \left(-\frac{5}{2} + \frac{7}{4} \sin^2 \theta\right) + \frac{X^2}{4} (2 \cos 2\theta - \tan^2 \theta) \right] n_j^2 + \left[1 - \frac{3X}{2} + \frac{X^2}{2} (1 - \tan^2 \theta) + \frac{X^3 \tan^2 \theta}{4} \right] \right\} \quad (8.13)$$

where $\beta_T = (X T / (m_0 c^2))^{1/2}$ is normalized thermal velocity.

The width of the line $\omega \approx \omega_H$ is of the order of

$$\Delta \omega \sim \omega \beta_T n_j \cos \theta = \omega \sqrt{\frac{X T}{m_0}} \cdot c n_j \cos \theta \quad (8.14)$$

In studying the first harmonic absorption, we consider

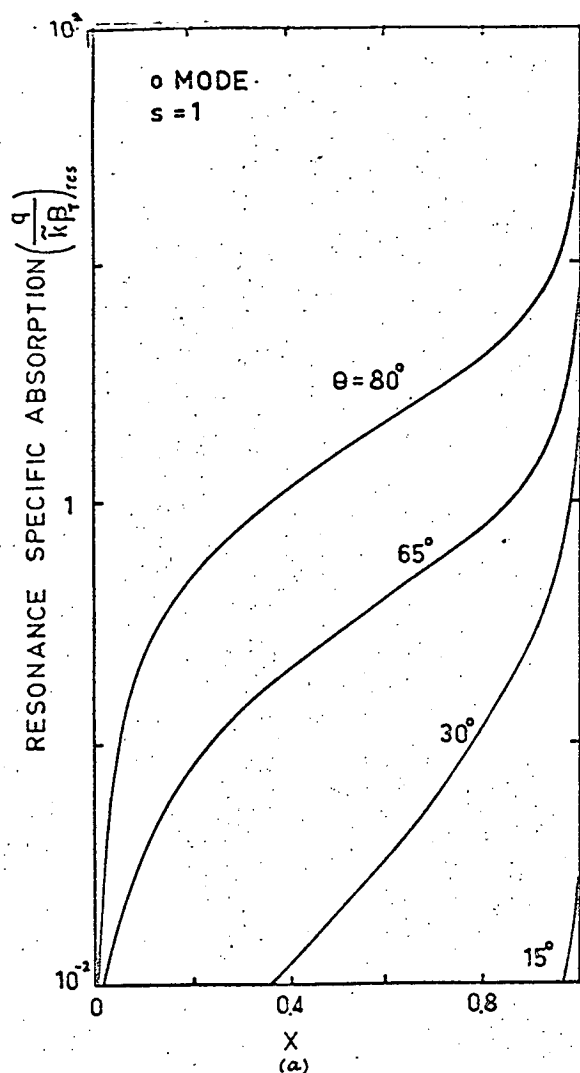


Fig. 8.18(a) Variation of the resonance specific absorption with $X = \omega_p^2/\omega^2$ for the first harmonic in the o-mode and different values of the wave-normal angle θ .

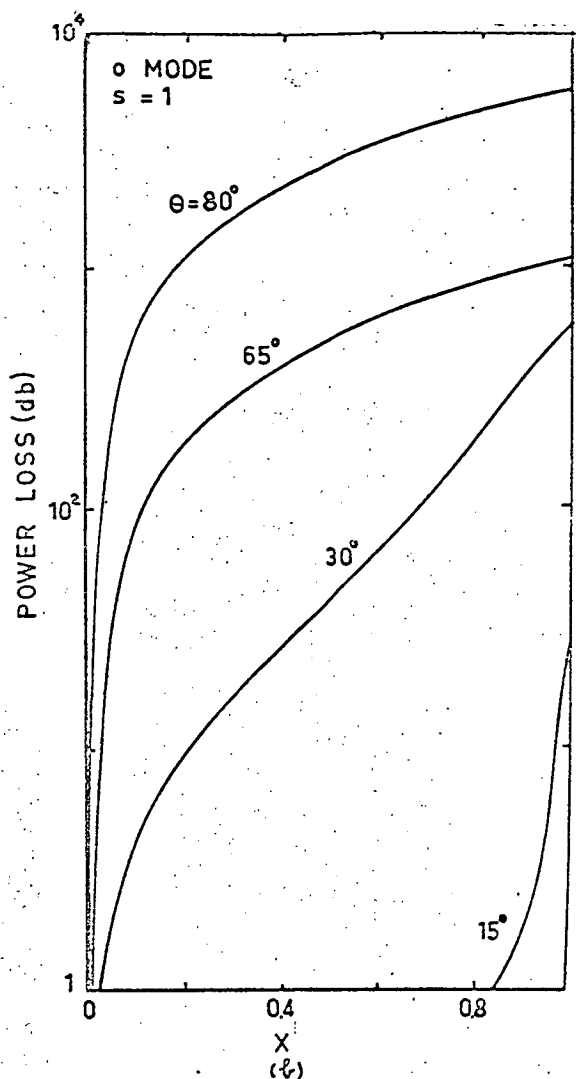


Fig. 8.18(b) Variation of the power loss (db) with $X = \omega_p^2/\omega^2$ for the first harmonic in the o-mode, taking the thickness of the absorption layer to be 10 Km, $\beta_r = 10^{-2}$, for different values of the wave-normal angle θ .

the absorption for the o-mode wave only since an x-mode wave cannot escape through the level $X = 1 - Y$ if it passes through the level $Y = 1$ (here Y is defined by $Y = 1/\xi$). The dependence of the resonance specific absorption (specified by $q/k\beta_T$) for the first harmonic on the quantity X is shown in Fig. 8.18(a) and the corresponding power loss in db is indicated in Fig. 8.18(b), assuming the thickness of the absorption level $\Delta z = 10$ Km. In the graphs for power loss the value of β_T is taken to be 10^{-2} (Gershman, 1960) and the wave-normal angle θ is taken to be the parameter for each line. From these diagrams, we observe that the absorption increases from increasing value of X and increasing wave-normal angle θ . We have seen in section (C) that for cyclotron radiation caused by gyrating electron stream with energy of the order of 10 - 100 Kev. per electron, a typical value of θ for maximum power (θ_m) in case of Double frequency solution is 35° . With this value of θ , the resonance absorption is not large except when X is small (say, < 0.2 , Fig. 8.18(b)). This means that the source region for o-mode radiation is limited to the region above the level $Y \approx 1$.

The resonance specific absorption for the second and third harmonics are given by (Gershman, 1960; Ginzburg, 1964):

$$\left(\frac{q}{k}\right)_{s=2} = \sqrt{\frac{\pi}{2}} V \exp \left[-\frac{(1 - 2/\xi)^2}{2\beta_T^2 \eta_j^2 \cos^2 \theta} \right] \quad (8.15)$$

$$\left(\frac{q}{k}\right)_{s=3} = \sqrt{\frac{\pi}{2}} \sqrt{\frac{3\beta_T^2 n_j^2 \sin^2 \theta}{8X}} \exp\left[-\frac{(1-3/\xi)^2}{2\beta_T^2 n_j^2 \cos^2 \theta}\right] \quad (8.16)$$

where
$$V = \frac{\left[\left(\frac{1}{\xi}-1\right)/n_j^2\right] X \sin^2 \theta \beta_T n_j \xi}{2 \cos \theta \left\{2\left(1-\frac{1}{\xi}-X+\frac{X}{\xi} \cos^2 \theta\right) n_j^2 - \left[2(1-X)^2 + (1+\cos^2 \theta)\frac{X}{\xi} - \frac{2}{\xi}\right]\right\}}$$

$$\left\{\frac{n_j^4 \sin^2 \theta}{2} + \left[X\left(\frac{1}{2} + \frac{\cos^2 \theta}{2} + \frac{\sin^2 \theta}{1+1/\xi}\right) - \frac{\sin^2 \theta}{2} - 1\right] n_j^2 + \left[\frac{X^2}{1+1/\xi} - X\left(\frac{1}{1+1/\xi} + 1\right) + 1\right]\right\}$$

In calculating the second harmonic resonance absorption, we put $\xi = \frac{1}{b_H} = 2$ in (8.15) and we substitute $\xi = 3$ in (8.16) for the third harmonic. Assuming $\theta \neq 0$, $\theta \neq \frac{\pi}{2}$, $n_j \sim 1$, we have the following rough estimation:

$$\left(\frac{q}{k}\right)_{s=1} \sim X \beta_T \quad \text{for o-mode}$$

$$\left(\frac{q}{k}\right)_{s=2} \sim X \beta_T \quad \text{for x-mode} \quad (8.17)$$

$$\left(\frac{q}{k}\right)_{s=3} \sim X \beta_T^3 \quad \text{for x-mode}$$

For accurate calculation, we can use $(q/(\tilde{k} \beta_T))$ and $(q/(\tilde{k} \beta_T^3))$ to describe the second and third harmonic resonance specific absorption respectively. The relation between $(q/(\tilde{k} \beta_T))$ and $X = \omega_p^2 / \omega^2$ is shown in Fig. 8.19(a) and 8.19(b) for the second harmonic of the o-mode wave and the x-mode wave respectively. The corresponding graphs for the third harmonic $((q/(\tilde{k} \beta_T^3))$ vs X) are given in Fig. 8.20(a) and 8.20(b).

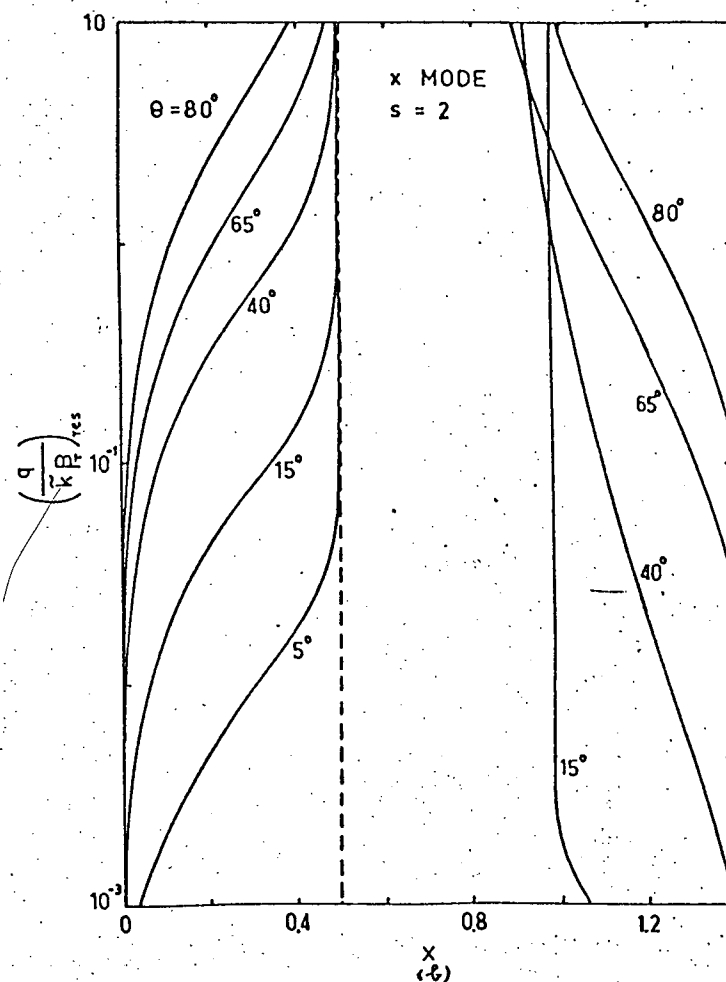
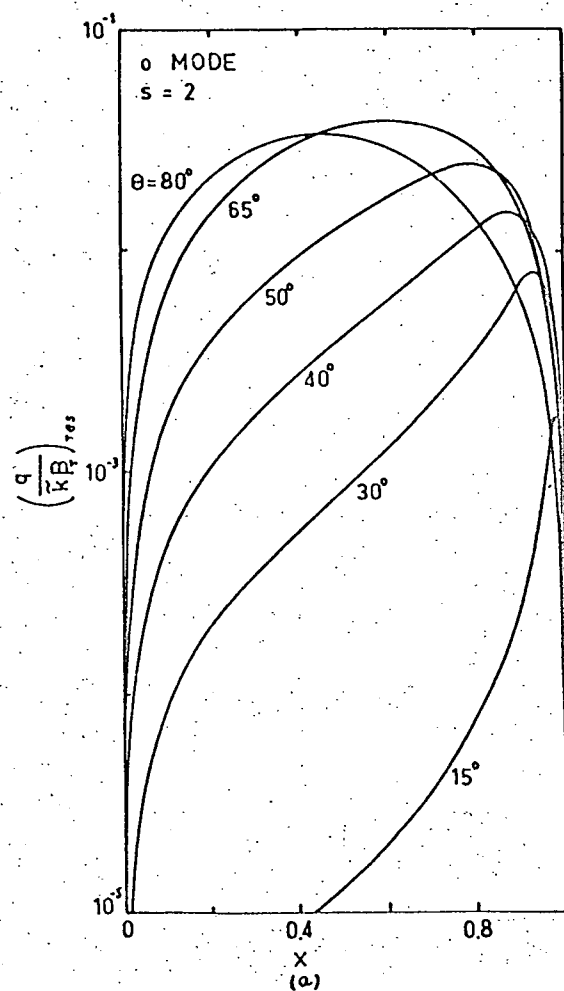


Fig. 8.19 Variation of the resonance specific absorption with $X = \omega_p^2 / \omega^2$ for the second harmonic, different values of the wave-normal angle θ , and
(a) o-mode wave; (b) x-mode wave.

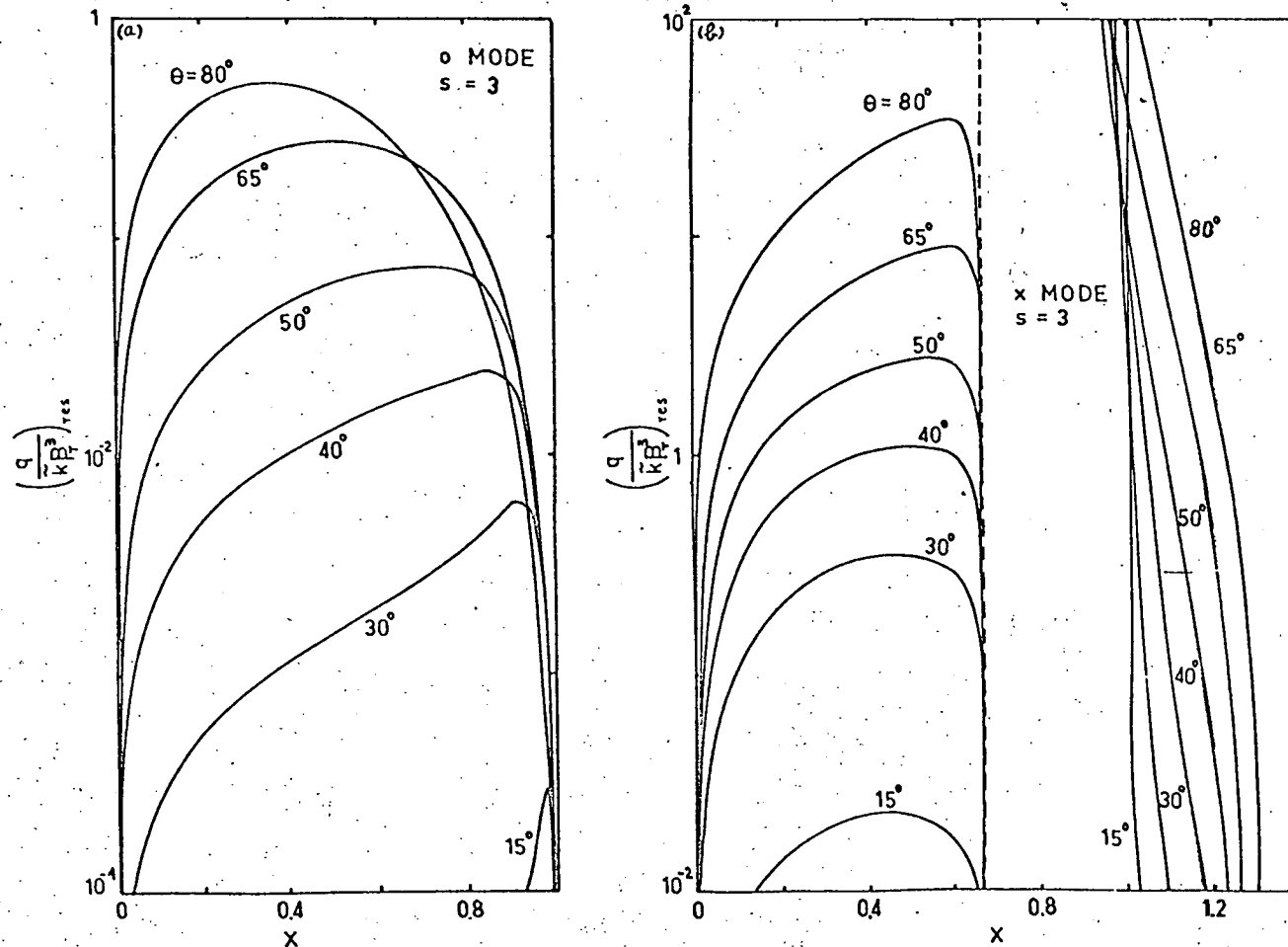


Fig. 8.20 Variation of the resonance specific absorption with $X = \omega_p^2/\omega^2$ for the third harmonic, different values of the wave-normal angle θ , and
 (a) o-mode wave; (b) x-mode wave.

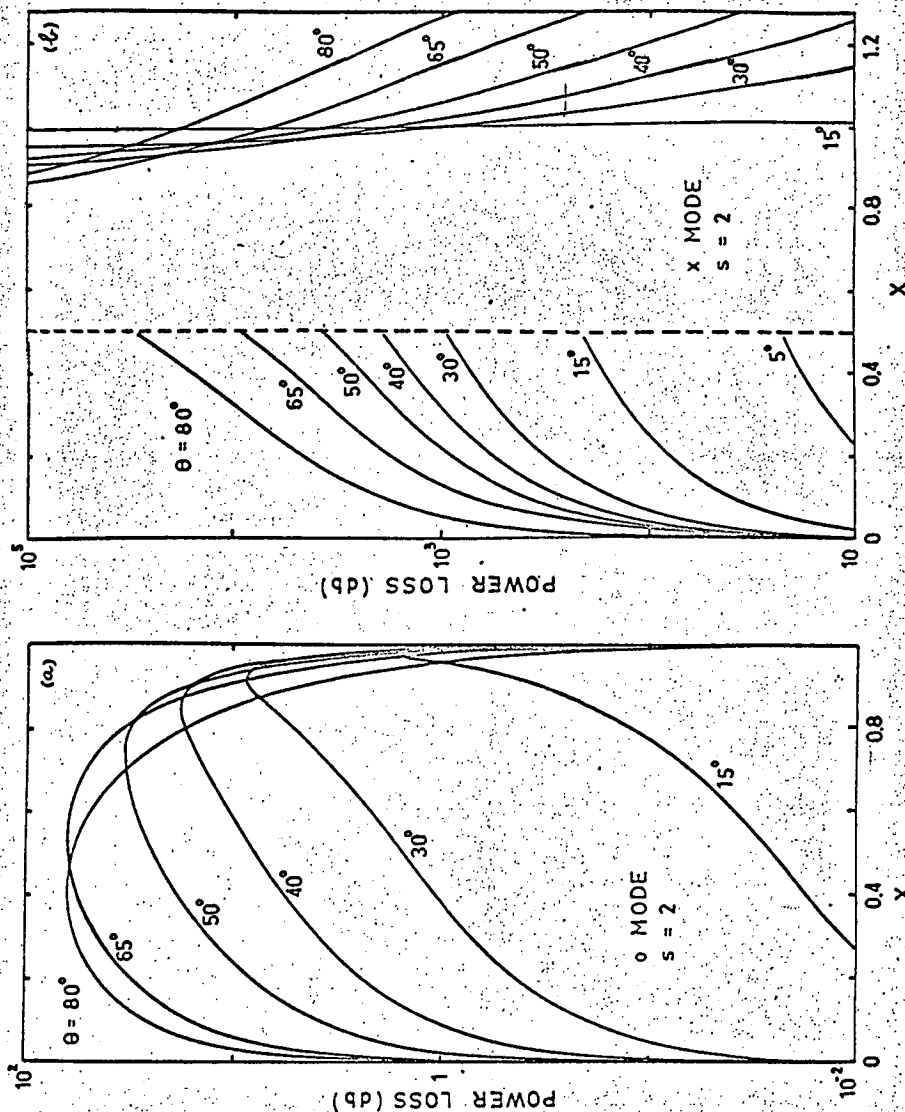


Fig. 8.21 Variation of the power loss (db) with $X = \omega_p^2/\omega^2$ for the second harmonic, taking the thickness of the absorption layer to be 10 km, $\beta_r = 10^{-2}$, for different values of the wave-normal angle θ , and

(a) o-mode wave;

(b) x-mode wave.

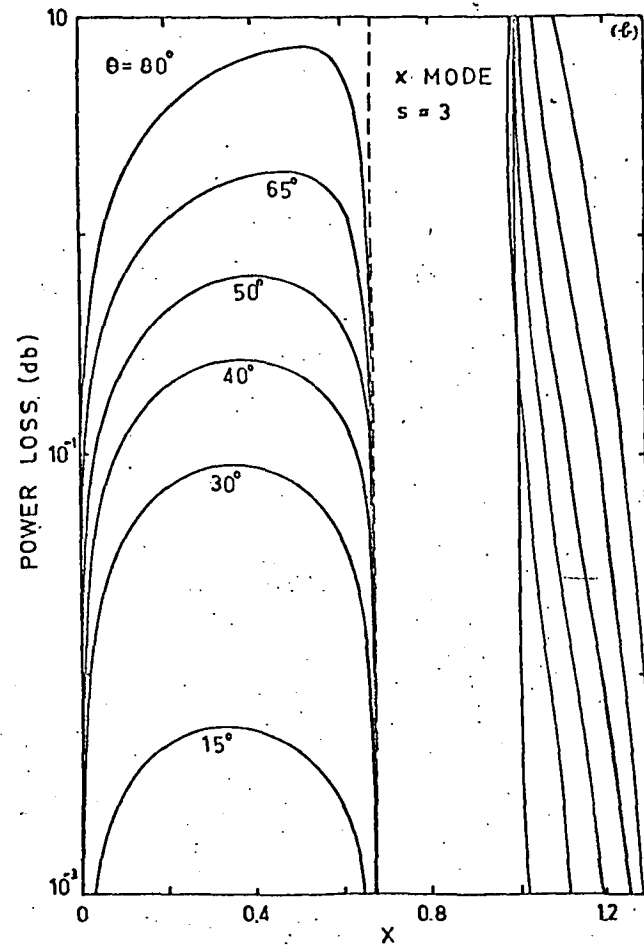
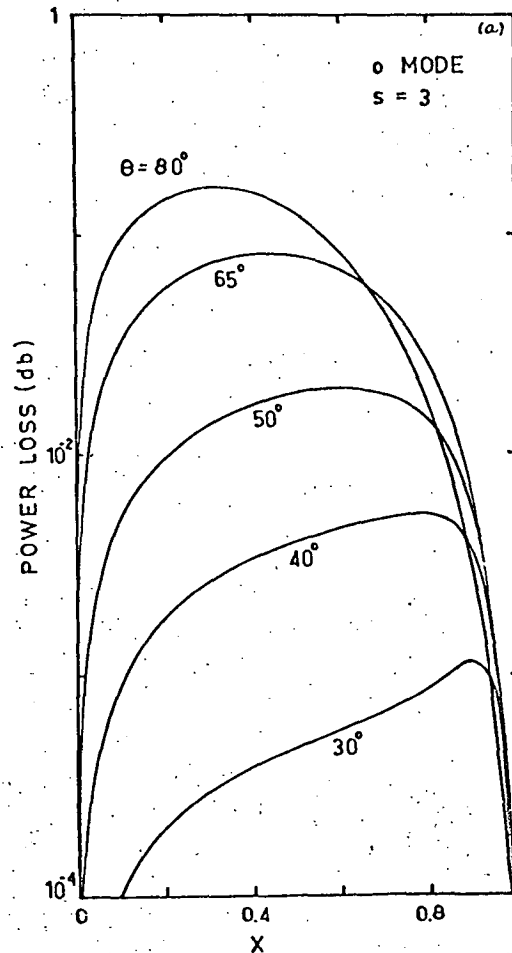


Fig.8.22 Variation of the power loss (db) with $X = \omega_p^2/\omega^2$ for the third harmonic, taking the thickness of the absorption layer to be 10 Km, $\beta_r = 10^{-2}$, for different values of the wave-normal angle θ , and

(a) o-mode wave;

(b) x-mode wave.

Taking $\beta_r = 10^{-2}$ which is a typical number in the corona, $z = 10$ Km as thickness of the absorption layer, one can calculate the power loss of an electromagnetic wave passing through the absorption level; these graphs are given in Fig. 8.21 and 8.22. In all these graphs, the parameter of each line is the wave-normal angle θ . An inspection of Fig. 8.19 - 8.22 indicates that the resonance specific absorption for the x-mode is at least two orders of magnitude higher than that of o-mode and the corresponding power loss in db for the x-mode exceeds that of o-mode by several orders of magnitude (Ginzburg and Zheleznyakov (1961) have already mentioned this result in a qualitative way). This is a very important fact concerning the escape conditions for the two modes and will be referred to later on.

(E) Reflection Levels and Escape Conditions for the Two Characteristic Waves

It is well known from the magnetoionic theory that the refractive index $n_j = 0$ at the level $X = 1 - Y$ for the x-mode for all θ and at the level $X = 1$ for the o-mode for all values of θ except $\theta = 0^\circ$. One usually refers to the levels $X = 1 - Y$ and $X = 1$ as the reflection levels in a magnetoactive plasma. However, the last statement is not always true. Jaeger and Westfold

(1950) have shown that only when a ray entering normally to the $X = 1$ level is reflected from this level and rays not normal to the stratification of refractive index are deviated according to Snell's law. In the solar atmosphere where the electron density decreases radially and gradually, the reflection levels for large ray incident angles (with respect to the radius vector) will be shifted to higher altitudes where n_j is not equal to zero. For a particular frequency, the reflection levels for both modes are, therefore, higher at the limb than near the centre of the solar disc. This situation for the o-mode is shown clearly in Fig. 8.23. However, for wave-normal direction not greater than 35° with respect to the radius vector, the levels corresponding $n_j = 0$ can be assumed as the true reflection levels and this assumption, unless otherwise stated, will be taken in the discussion of the rest of this chapter.

To study the escape conditions in the corona for the two characteristic waves, a conventional method is to relate, for a particular wave frequency, the quantities X and Y in graphical form (e.g. Pawsey and Bracewell, 1955). We will discuss one such example below.

*It will be seen later that in most cases the ray direction differs from the wave direction only by a few degrees (chapter IX); we can, therefore, assume the two directions to be the same for such estimation.

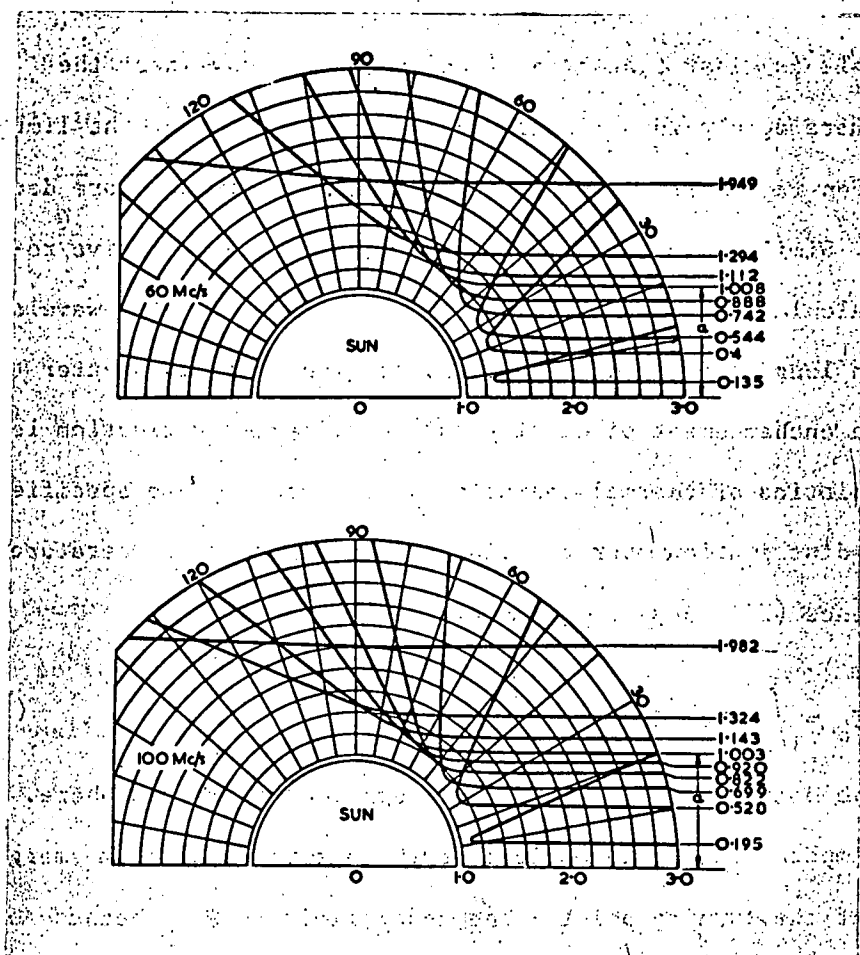


Fig. 8.23 Ray trajectories in the solar corona for 60 and 100 Mc/s. The radial scale is in units of 705,000 Km (= photospheric radius + 7650 Km).

(Jaeger and Westfold, 1950)

Suppose we take the maximum field intensity of the centre point on the spot surface of a unipolar spot field to be $H_s = 2,000$ gauss, and we define the radial line passing through the said point to be the r-line. The magnetic field intensity of any point along this r-line will be given by (6.6). The radial variation of the plasma frequency is assumed to satisfy either relation (6.1) (represented by Fig. 8.24(a)) or relation (6.2) (represented by Fig. 8.24(b)). If we now consider a particular electromagnetic wave with certain wave frequency f , the values of X and Y along the r-line can be calculated with the help of Fig. 6.4. In Fig. 8.24 the solid curves give the variation of X and Y along the r-line for four values of wave frequency: $f = 50, 100, 150, 200$ Mc/s. Each number on a curve indicates the value of $\rho = R/R_0$ at that particular point. The identity $Y^2 = X/A$ is shown in Fig. 8.24 for three values of $A(0.25, 1, 1.5)$. The first three harmonic levels ($Y = 1, \frac{1}{2}, \frac{1}{3}$) and the reflection levels ($X = 1, X = 1-Y$) are also shown in the figure. We observe from this figure that as an electromagnetic wave of a particular frequency travels along the r-line, it will first meet the o-mode reflection level and the first harmonic absorption level, the reflection level for x-mode and the second harmonic absorption level, and then the third harmonic absorption level. As this wave propagates it encounters an increasing value of A . Considering propagation along the r-line, we can thus estimate the possible source

Fig. 8.24 The relation of $Y = \omega_H / \tilde{\omega}$ and $X = \omega_p^2 / \tilde{\omega}^2$ along the r-line of a unipolar spot specified by $H_0 = 2,000$ gauss for four frequencies as indicated when the electron density distribution follows (a) Baumback-Allen's model and (b) Newkirk's model. The dotted lines represent the three harmonic resonance levels and the line $---$ represents the identity $Y^2 = X/A$. The numbers on the solid lines show the positions in units of solar radii.

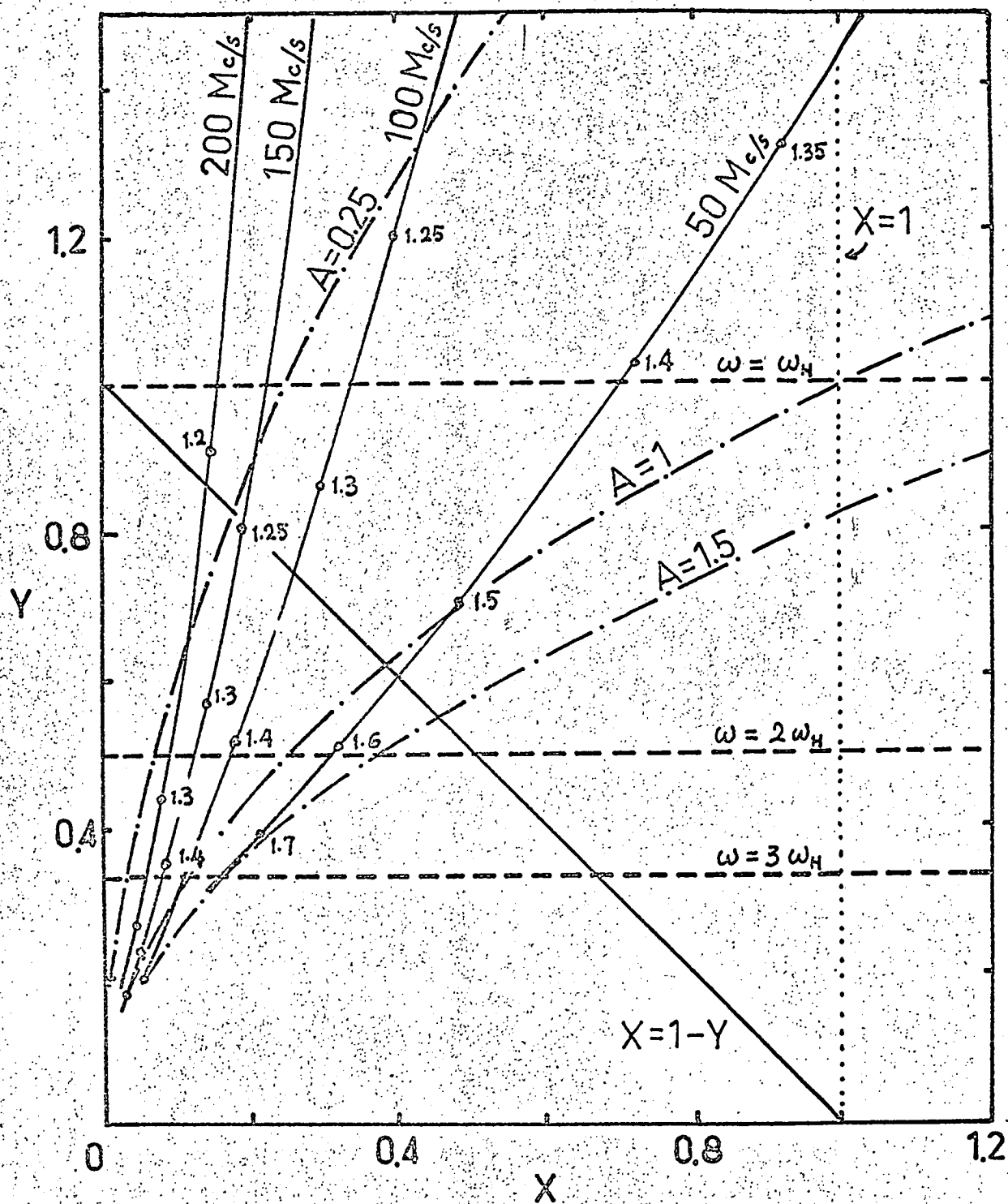


Fig. 8.24(a)

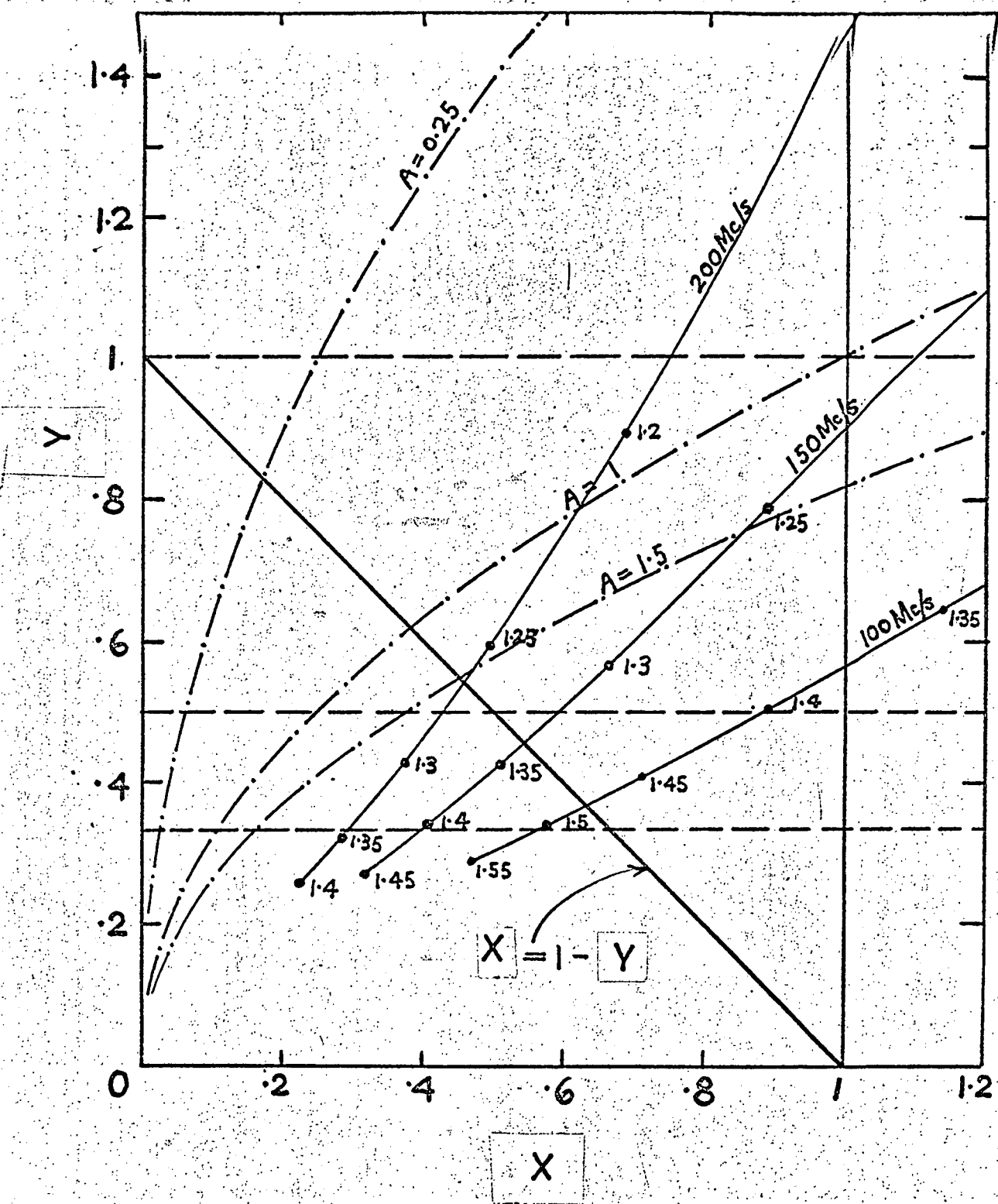


Fig. 8.24 (b)

positions for x- and o-mode waves from which the radio waves can escape. From Fig. 8.24, we realize that there is a much larger possible source region (in the square bounded by $X = 1$ and $Y = 1$) from which an o-mode can escape without meeting the first harmonic absorption level and the reflection level, while an x-mode wave must be generated at a much higher level in order to escape from being reflected. In most cases, an escaping x wave will have to encounter the second and third harmonic absorption levels, where the loss of energy is in general high..

So far, we have considered briefly the propagation along a field line of a unipolar spot only. It has been found in section (C) that the emission angle θ where maximum power occurs is not at $\theta = 0^\circ$, but ranging from 5° to 50° . A two-dimensional picture of the various reflection and absorption levels is needed when we consider radiation at the surface of a cone. Therefore, a more detailed discussion on the escape conditions for the two characteristic waves in two dimensions will be given below. We will take the example of a bipolar spot field; the argument is similar and simpler when a unipolar field is used instead.

After some tedious calculations, we show various levels of reflection and absorption for frequencies = 100, 150, 200 Mc/s in Fig. 8.25 (Baumbach-Allen's model of electron density distribution) and in Fig. 8.26 (Newkirk's model and 10 times

Baumbach-Allen's model of electron density distribution) when the value of H_g is taken to be 2,500 gauss. The solid field line shown in each of these diagrams is the strongest field line of the associated spot pair, and need not be the line passing through the centre of the spot area where H_g is specified.

The result of investigation in section (A) indicates that when $A \approx 1$, Double frequency solution always exists for the first harmonic which carries more energy than any other harmonic in cyclotron radiation. It has been pointed out that when Double frequency solution occurs, the emission is in general narrow-band and the radiation power is intense. We may, therefore, consider the location specified by $A \approx 1^+$ to be the best position where intense noise bursts are emitted. Moreover, the radiated frequency corresponding to maximum power for Double solution is always close to but greater than $f_H \sqrt{A} \approx f_H$ (i.e. $f_m \geq \sqrt{A}$; section (A) and section (C)). Hence, the gyro-frequency at the source position must be

*When A is greater than 1, Double frequency solution may still exist for a higher harmonic. In this case, the radiation power will be less. We should, therefore, keep in mind that the level at which $A \approx 1$ is not the only possible location where bursts are radiated.

Fig. 8.25 Assuming $H_0 = 2,500$ gauss for the stronger spot of the associated pair, different levels of interest are shown in two dimensions for

(a) $f = 100$ Mc/s

(b) $f = 150$ Mc/s

(c) $f = 200$ Mc/s.

$Y = 1/3$ ———— $Y = 1/2$ ———— $Y = 1$ ————

$X = 1$ ———— $X = 1 - Y$ ———— , as marked.

The strongest field line is represented by the solid thick line and the thick dotted line is another field line of the associated pair. The points \otimes indicate some localities where $A = 1$. The coronal electron density is assumed to follow Saumbach-Allen's model.

$f = 100 \text{ Mc/s}$

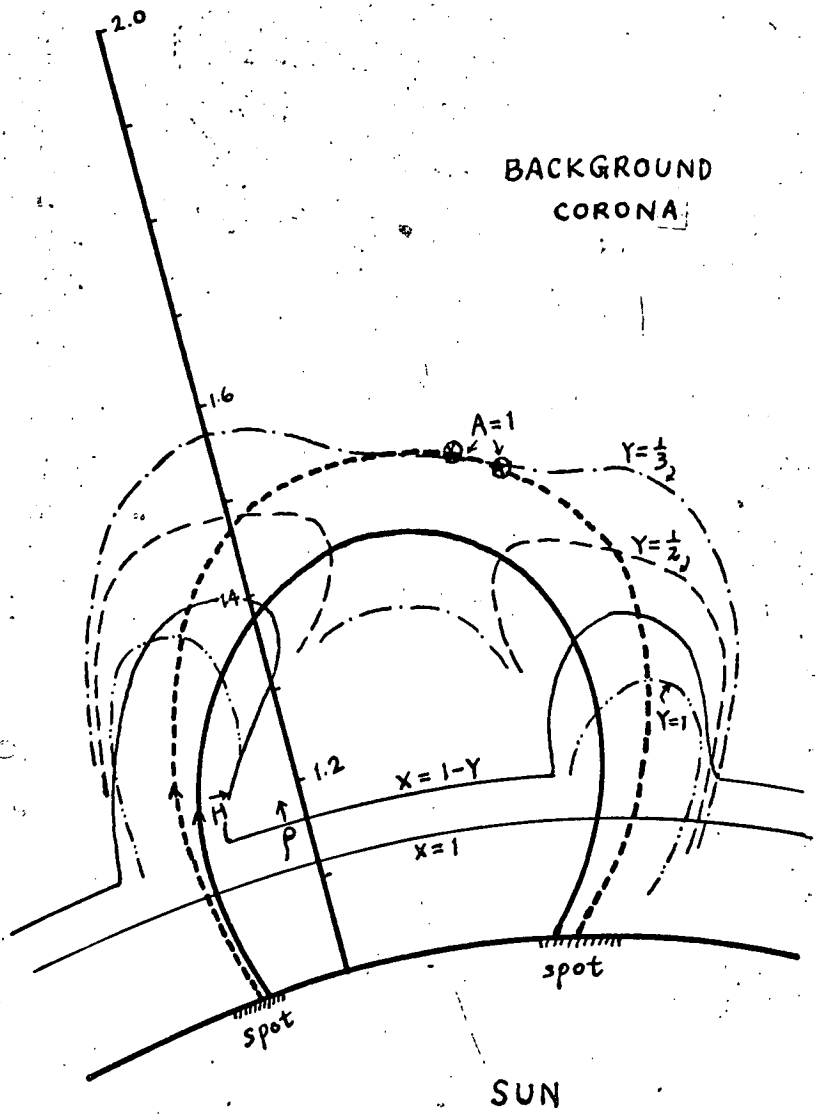


Fig. 8. 25(a)

$$f = 150 \text{ M/s}$$

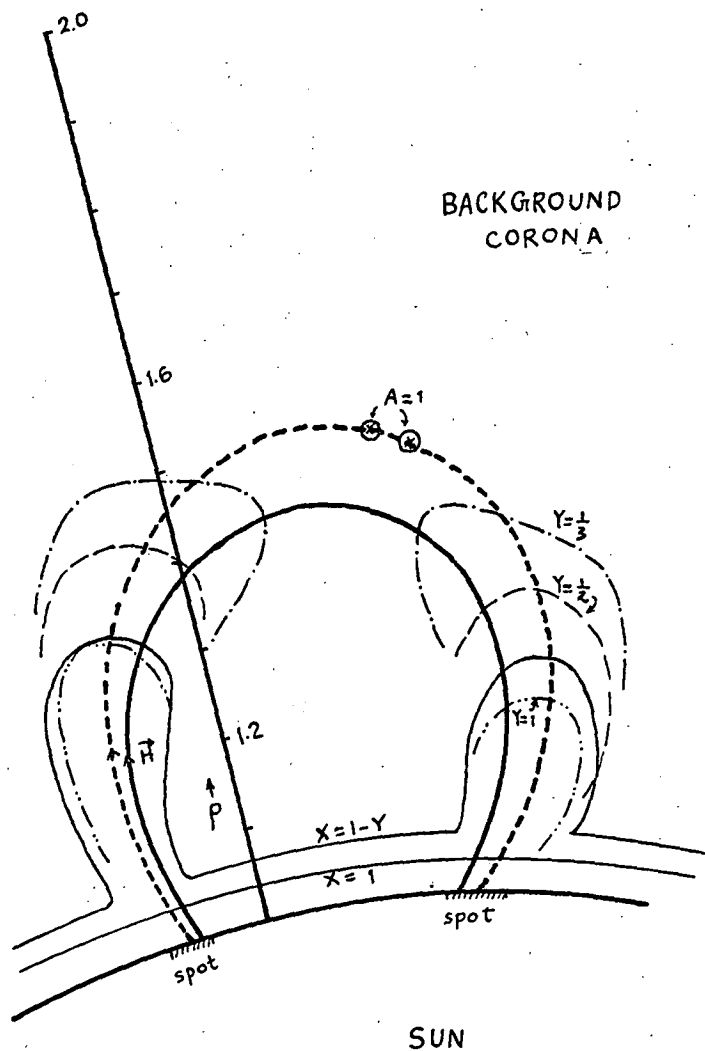


Fig. 8. 25(b)

$$f = 200 \text{ Mc/s}$$

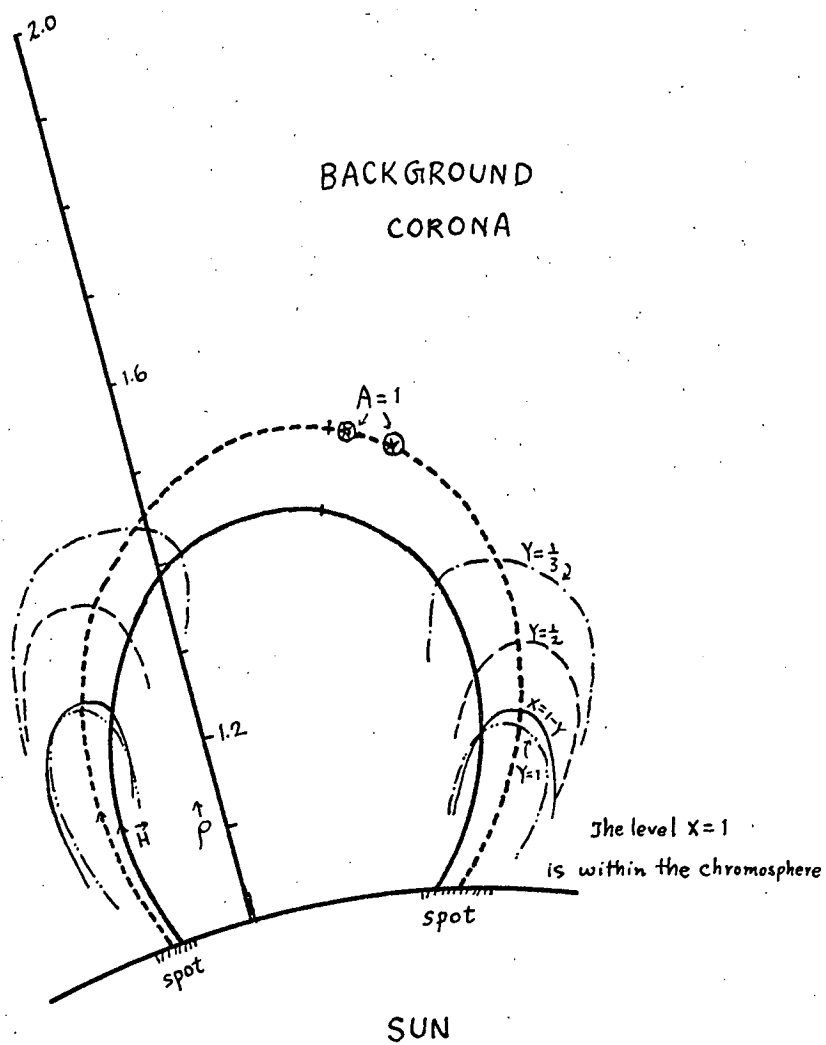


Fig. 8.25 (c)

Fig. 8.26 Assuming $H_g = 2,500$ gauss for the stronger spot of the associated pair, different levels of interest are shown in two dimensions for

(a) $f = 100$ Mc/s

(b) $f = 150$ Mc/s

(c) $f = 200$ Mc/s

$Y = 1/3$ — — — — — $Y = 1/2$ — — — — — $Y = 1$ — — — — —

For Newkirk's model of active region:

$X = 1$ — — — — — $X = 1 - Y$ — — — — — , as
marked and $\Delta = 1$: \odot

For 10 Baumbach-Allen's model (or 2 Newkirk's model) of electron density in the active region:

$X = 1$ — — — — — $X = 1 - Y$ — — — — — , as
marked and $\Delta = 1$: \times

The field lines are represented by the thick curves with arrows; the complete loop indicates the strongest field line. Points S_1 , S_2 , S_3 and S_4 are possible source positions where the "intense burst radiation conditions" are satisfied. The thin straight lines with arrows show the possible wave paths.

$$f = 100 \text{ Mc/s}$$

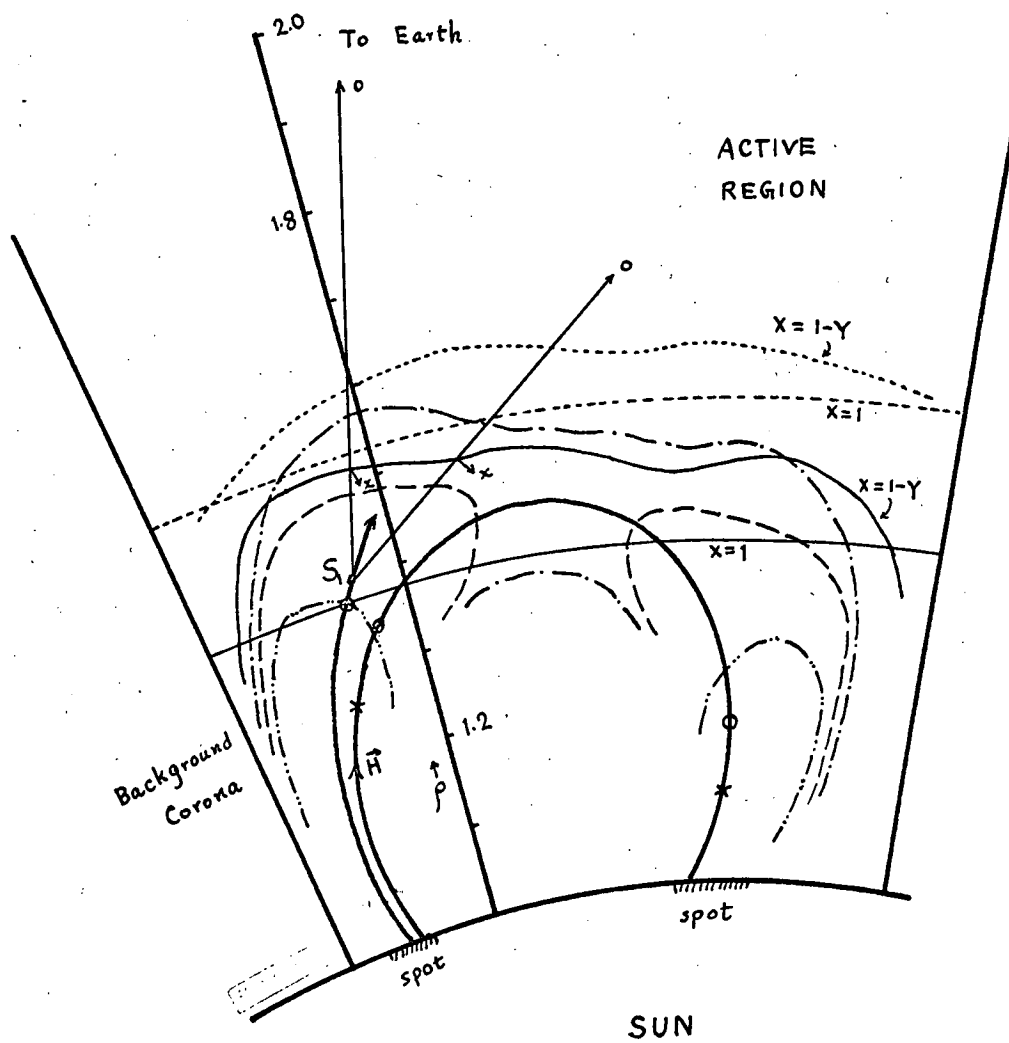


Fig. 8.26 (a)

$$f = 150 \text{ Mc/s}$$

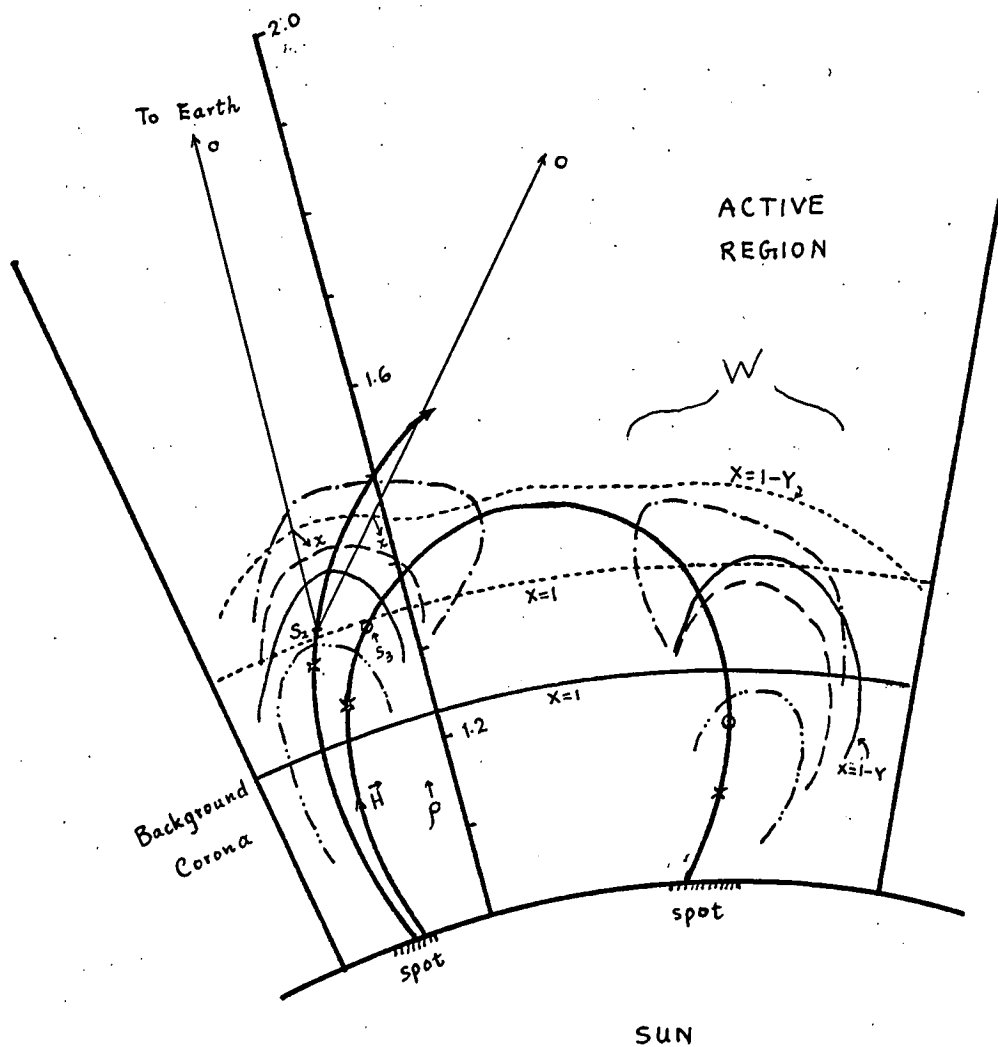


Fig. 8.26 (b)

$$f = 200 \text{ Mc/s}$$

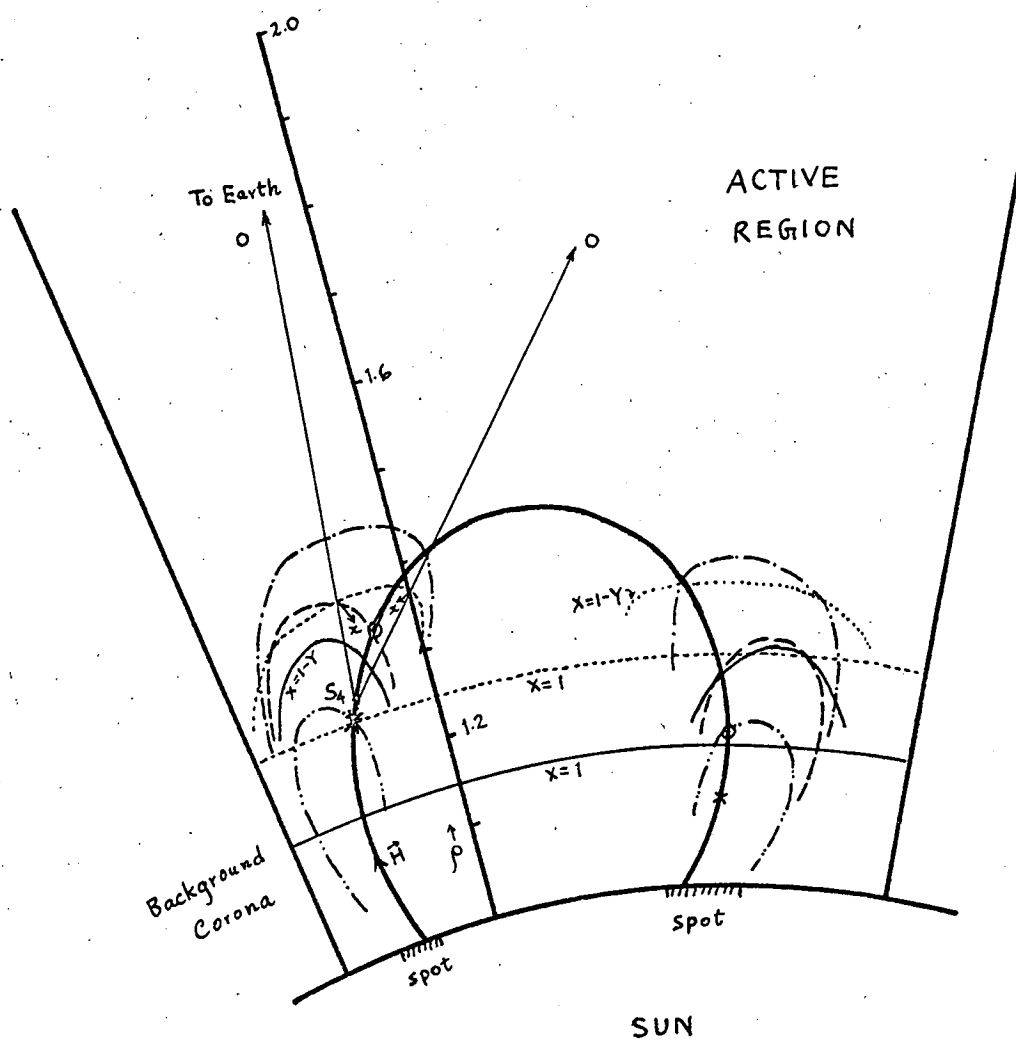


Fig. 8.26 (c)

slightly smaller than the assumed radiated frequency f (so that the normalized radiated frequency ξ which is slightly greater than 1, when multiplied by the local f_H which is slightly smaller than f , will give exactly the value of f assumed). Note that for $A = f_p^2/f_H^2 \approx 1$, $\xi = f/f_H \geq 1$, we have $f \lesssim f_p$ at the source. The source for intense burst radiation should, therefore, be situated slightly above the plasma level of f . We will call these three conditions the "intense burst radiation conditions". Consequently, to look for a source position for intense burst radiation at frequency f three conditions must be satisfied:

- (i) A must be close to 1.
- (ii) The source position must be near and above the level $|f_H| = f$.
- (iii) The source position must be situated above the reflection level $X = 1$.

An inspection on Fig. 8.25 shows that with our model of spot field configuration, there is hardly any location where the three mentioned conditions are satisfied.

When we examine Fig. 8.26(a), we will notice that for Newkirk's model, a point like S, will satisfy all the intense burst radiation conditions and the o-mode radiating, suffering little loss at the second and third harmonic levels, will escape, while the x-mode will be reflected at the level $X = 1 - Y$. Referring to Fig. 8.26(b) and taking 10 x Baumbach-Allen's

model of electron density distribution, an electron stream gyrates through the point S_2 can readily radiate an intense noise burst of centre frequency 150 Mc/s. Using Newkirk's model, S_3 could well be another possible source. In Fig. 8.26(c), the intense burst radiation conditions are satisfied at a point like S_4 for $10 \times$ Baumbach-Allen's model. We remark that with $H_s = 2,500$ gauss as taken in this case, the source position is always below the x-mode reflection level, implying that the x-mode radiation can never escape through the corona.

Consider the region (marked W in Fig. 8.26^(c)) above the weaker spot of the bipolar group. Using $10 \times$ Baumbach-Allen's model of electron density distribution, since the level corresponding to $A = 1$ is well below both reflection levels, no significant radiation (for frequency 100 - 200 Mc/s) of any mode will escape the region above the weaker spot.

The implications of all the important results discovered in this chapter will be summarized in the following section.

(F) Predictions of the Theory

When all theories, properties and variables are taken into consideration in the study of escape conditions and the possible source positions for particular frequencies,

the study and hence the discussion is extremely complicated. In the above discussion we have only demonstrated one method by which the problem is analysed. Investigation on many cases like the one just considered give the following predictions subsequent to the theory of cyclotron radiation from electron streams:

- (1) In cases when the source is not too high, the x-mode wave radiated is either reflected at the level $X = 1 - Y$ or suffering heavy loss of energy due to second and third harmonics resonance absorption; this result holds for any of the electron density models taken in the investigation. The o-mode radiation, on the other hand, can be excited readily by an electron stream gyrating at heights greater than the levels $X = 1$ and $Y = 1$. When the source is high enough, however, radiation in both modes may escape. But in this circumstance the harmonic of radiation will be high (due to large value of A) and the radiation power small. Hence, in general, only the o-mode radiation will assume significant power.
- (2) From sections (A) and (C), the radiation power associated with Double frequency solution is much greater than the power of radiation for Single frequency solution. We suggest that radiation in the former case, in the o-mode, is the origin of the storm burst phenomenon.
- (3) If Single frequency solution is satisfied for the generating

process, the bandwidth and emission cone are broad, if the pitch angle of the stream is not too large. Since this case is always met with (whenever there is Double frequency solution there is always Single frequency solution with a greater harmonic number whereas the reverse may not be true), many such events will occur simultaneously and all these broad-band emissions will superimpose to form a long-lived, broad-band radiation (type I background continuum). Fluctuations in plasma density and magnetic field will not result in any significant change in the superimposed radiation. Based on (1), the background continuum radiation is also in the o-mode.

- (4) In order to have intense storm bursts radiated near the centre of the solar disc, the electron density distribution needs to follow Newkirk's model or $10 \times$ Baumbach-Allen's model; in particular, the latter model is more favourable and all the following discussions will be based on this model.
- (5). No significant radiation will escape through the region above the weaker spot of the bipolar group when H_s (associated with the stronger spot) is less than about 3,500 gauss. This result indicates that in majority of cases the received radiation will be polarized in

the o-mode with respect to the polarity of the stronger spot in the sunspot group.

- (6) From points (2) and (3) above, the background continuum radiation may not be able to survive through absorption along the corona and be observed on earth. On the other hand, Double frequency solution is not always met with. As a result, storm bursts may be observed alone while at times continuum radiation may not be accompanied by storm bursts.
- (7) From section (E), we observe that for source near the centre of the disc, the source position of intense storm burst radiation at frequency f is always near and above the plasma level of the frequency f .

It has been mentioned that when the source (for a particular frequency f) is near the limb, the true reflection level (for rays to reach the Earth) is situated above the level $X = 1$. Except when the value H_g is extraordinary large ($> 3,500$ gauss), the intense burst radiation conditions, in general, will not be satisfied above the true reflection level. Now consider the space above the true reflection level (where A is greater than 1) for a particular frequency f . Since the value of A increases with height and (for a particular gyrating electron stream) the lowest possible harmonic

radiation increases with Λ (equations (8.3), (8.5) and (8.6)), the radiation at lower heights will be more significant than that at greater heights[†]. The lowest possible altitude for the source (radiating frequency f) is, obviously, just above the critical or true reflection level for f . Hence, according to our theory, we have the following important prediction:

At an instant, the source position of a burst radiation with instantaneous centre frequency f is situated slightly above the true reflection level of the frequency f , no matter the source is near the centre of the disc or near the limb.

- (8) Based on the discussion given in (7), the radiation power of bursts coming from the centre of the disc should be greater than that from the limb.
- (9) For burst radiation in a particular spot field configuration, the higher the emitted frequency (corresponding to maximum power) the lower the source position (Fig. 8.26). When the source region is near the centre of the solar disc, the source height for 200 Mc/s burst radiation ranges from about $0.25 R_0$ to $0.35 R_0$ for H_0 ranging from 1,500 gauss to 3,500 gauss. The altitude of a limb source for 200 Mc/s is about $0.5 R_0$.

[†]The reason being that for cyclotron radiation, the radiation power decreases with increasing harmonic number.

- (10) For spot sizes ranging from 1,500 gauss to 3,500 gauss and energy of electron in the stream of the order of 10 - 100 Kev., the limits of emitting frequency are about 10 Mc/s and several hundred Mc/s.
- (11) The bandwidth of the superimposed broad-band radiation can be as high as several hundred Mc/s while the bandwidth of a narrow-banded event can be as low as several Mc/s.
- (12) In general, the source position is not exactly on the radial line passing through the associated spot, but it should not be far away.

CHAPTER IX

THEORETICAL DYNAMIC SPECTRA OF STORM BURSTS

A genuine theory must be able to produce theoretical dynamic spectra which agree with that observed. Since storm bursts are considered to be individual events⁺, we will attempt to produce some typical theoretical dynamic spectra of storm bursts in this chapter. To start off, we need to consider the geometry of the ray path along which energy and thus information is travelling. This, in its essence, is the problem of ray tracing.

(A) Ray Tracing in the Corona

Firstly, we will consider the tracing of ray paths from the emission radiated by a point source along a unipolar field. The active region associated with this sunspot is assumed to consist of a conical region of apex angle 6° (Newkirk, 1959), with the axis of the cone passing through the centre of the spot. The distribution of magnetic intensity inside the sunspot is supposed to take the form as observed by von Klüber

⁺Meaning that one storm burst is produced by one stream or bunch of electrons.

(Fig. 5.2) and the variation of magnetic intensity along any field line is assumed to obey relation (6.4). The maximum field intensity of the spot area is taken to be 2,000 gauss. The radial distribution of electron density in the active region is assumed to follow Newkirk's model (relation (6.2)) while that in the background corona is supposed to satisfy relation (6.1). The effects of the general magnetic field of the Sun will be neglected in the calculations.

We will begin with the ray tracing inside the active region. Referring to Fig. (9.1), let $Q(\rho_0, l_0)$, the point source, be situated at a point along the central field line; the subscript "o" indicates initial quantities and l is the solar longitude angle. Suppose a wave of frequency f is radiated with wave-normal angle θ_0 at Q (Fig. 9.1). For gradual variation of electron density and magnetic field intensity, the phase or wave path can be approximated to be straight over a short distance; let QP be such a short path length. Now consider area $QP'PQ$ bounded by two radial lines OP' , OP (of longitudes l_0 and l respectively) and two arcs QQ' and $P'P$ (of radii ρ_0 and ρ_1 respectively). Within this small area, the magnetic field intensity is assumed to be constant along each of these two arcs. Under the assumptions stated, both electron density distribution and magnetic field intensity distribution are then spherically symmetrical within

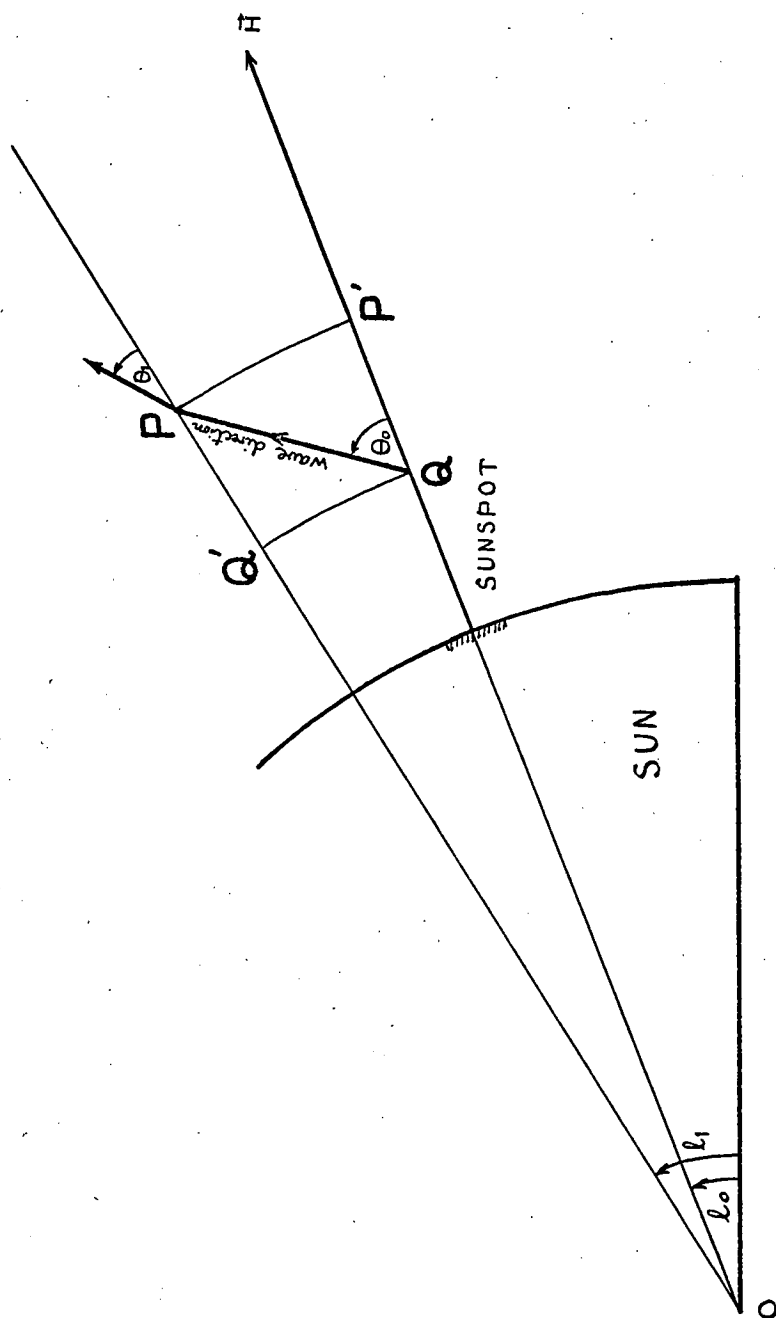


Fig. 9.1 Illustrating wave tracing technique. $Q'P'Q$ is enlarged about ten times.

QP'PQ' and Snell's law can be applied:

$$n_0 \rho_0 \sin \theta_0 = n \rho \sin \theta = a \quad (9.1)$$

where n is wave refractive index and a is a constant.

Fixing ρ_0 and knowing the variation of magnetic field and electron density in space, n_0 can be calculated by means of Appleton-Hartree⁺ equation (equation(8.1)).

Let subscript 1 to represent quantities associated to the point P. From (9.1), we have

$$n_1 = \frac{a}{\rho_1 \sin \theta_1} \quad (9.2)$$

Note that since P is chosen at our wish, ρ_1 and hence f_p and f_H are known quantities. Fixing the wave frequency f , from (9.2), n_1 is thus a function of θ_1 which is not yet found. On the other hand, n_1 is also given by the Appleton-Hartree equation:

$$n_1 = n_1(\theta_1) \quad (9.3)$$

Solving the two simultaneous equations (9.2) and (9.3) graphically, the two unknowns n_1 and θ_1 can be found. The value of θ_1 is then taken to be the initial wave normal angle in another small region like QP'PQ'. Repeating the same

⁺The effects of collisions are neglected.

process, the phase path can be traced inside the active region readily.

Outside the active region, the refractive index can be written as

$$n^2 = 1 - \frac{81 \times 10^6 N}{f^2} \quad (9.4)$$

where N , the electron density expressed in units of electrons/cm³, is a function of ρ only. Snell's law becomes

$$\theta = \arcsin \left(\frac{a}{n \rho} \right)$$

and θ is a function of ρ only. In this case tracking is done much more easily.

To show some examples of the dependence of the incident wave-normal angle θ on ρ (for both inside and outside the active region) for different values of the constant a , we have Fig. (9.2).

In a magnetoactive plasma, the ray direction is in general different from the phase direction. From magneto-ionic theory, at a point where the phase direction is specified by wave-normal angle θ_k , the angle between the ray and phase directions is given by (Budden, 1961):

$$\begin{aligned} \tan \psi &= \left(\frac{1}{n_j} \frac{\partial n_j}{\partial \theta} \right)_{\theta=\theta_k} \\ &= \left(\frac{1 - n_j^2}{\frac{2(1-\chi)}{Y^2 \sin \theta \cos \theta} \sqrt{\frac{Y^4 \sin^4 \theta}{4(1-\chi)^2} + Y^2 \cos^2 \theta}} \right)_{\theta=\theta_k} \quad (9.5) \end{aligned}$$

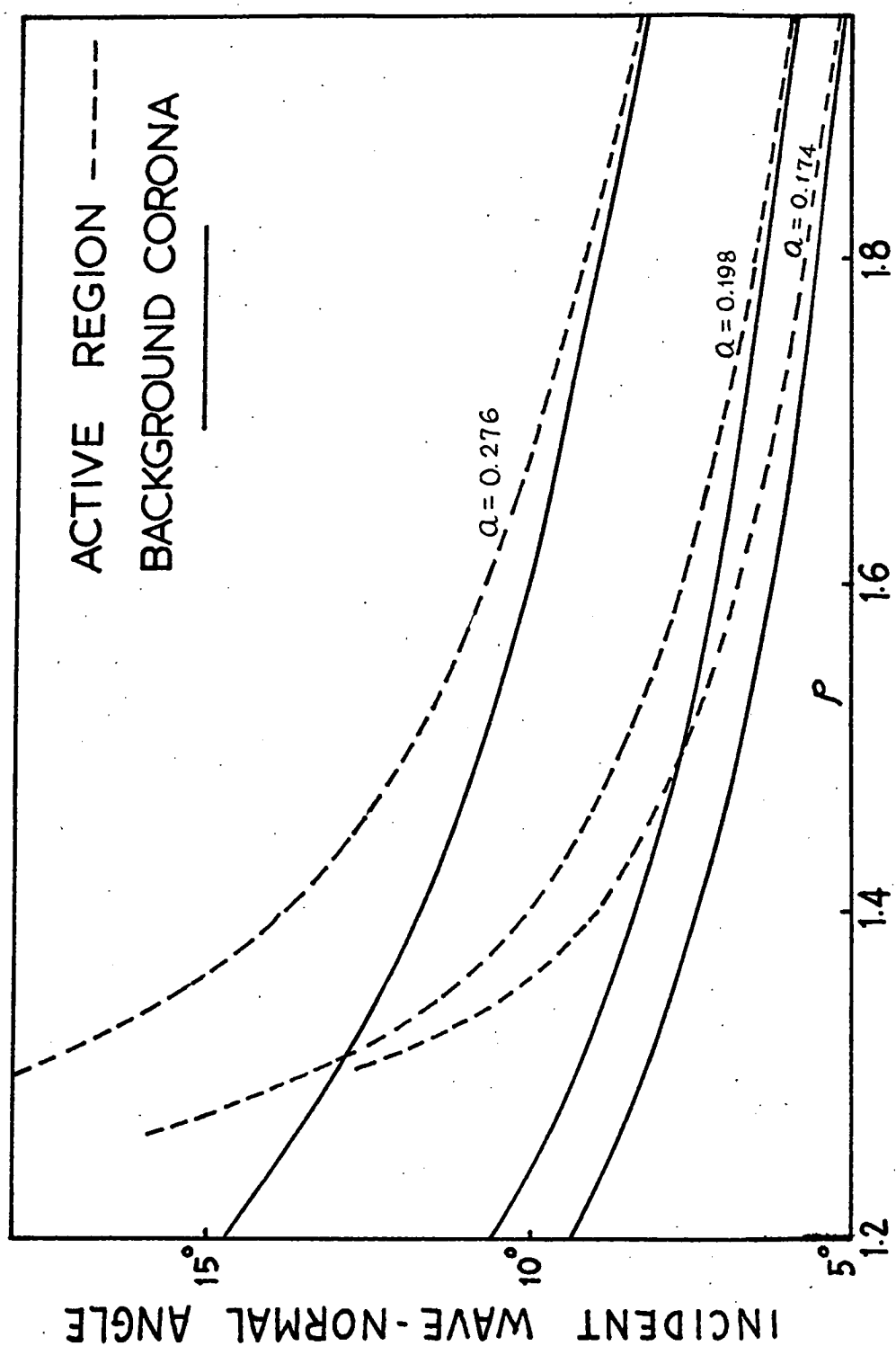


Fig. 9.2 Relation between incident wave-normal angle and radius vector for various values of initial constant a .

Using (9.5), the ray path corresponding to a known phase path can be traced. In the background corona, we have $Y = 0$ and it is clear from (9.5) that both the phase and ray directions coincide.

(B) Theoretical Dynamic Spectra of Storm Bursts

We will, first of all, assume a helical bunch of electrons gyrating along the strongest field line of a unipolar spot. The magnetic field intensity along the length of the bunch is assumed constant, so that, the radiation characteristics of the bunch may be described in terms of a single electron. Let ϕ_0 and f_H be the initial pitch angle and gyro-frequency of the electron respectively. On account of the property of constancy in magnetic moment, the pitch angle ϕ at any point with gyro-frequency f_H is given by (e.g. Gold, 1959):

$$\sin^2 \phi = \sin^2 \phi_0 \frac{f_{H_0}}{f_H} \quad (9.6)$$

here the velocity β of the electron is assumed constant. From (9.6) we can write the longitudinal velocity of the electron $\beta_{||}$ as:

$$\beta_{||}^2 = \beta^2 \left(1 - \sin^2 \phi_0 \frac{f_H}{f_{H_0}} \right) \quad (9.7)$$

The travelling time for the electron from point S_0 to

point S^+ is then

$$t_e = \frac{1}{c} \int_{S_0}^S \frac{ds}{\beta_{||}} = \frac{1}{\beta c} \int_{S_0}^S \frac{ds}{(1 - \sin^2 \phi_0 f_H / f_{H_0})^{1/2}} \quad (9.8)$$

where ds is elementary path length along the magnetic field line of force.

The time taken by a wave packet to travel from a point r_0 to another point r is

$$t_g = \int_{r_0}^r \frac{dr}{v_{gp}} \quad (9.9)$$

where dr is an element of ray path, and the group or ray velocity is given by (Ginzburg, 1964):

$$v_{gp} = c \left(n_j + f \frac{dn_j}{df} \right)^{-1} \quad (9.10)$$

where in this case $f \frac{dn_j}{df} = f \frac{\partial n_j}{\partial f} = n_j \left(\frac{\omega}{n_j} \frac{\partial n_j}{\partial \omega} \right)$ and $\frac{\omega}{n_j} \frac{\partial n_j}{\partial \omega}$ is given by relation (8.7(a)). Once a ray is traced, the group velocity at any point on the ray trajectory can be calculated numerically by means of (9.10) and the

*Here S_0 and S are points on the magnetic field line along which the electron is spirally.

group travelling time between the source and the observer can be evaluated by numerical integration (equation (9.9)).

At any point on the electron bunch's trajectory, we have a set of known parameters β_1 , $\beta_{||}$ and $A = f_p^2 / f_H^2$. With these values, the emitted frequency range is calculated as in section (A) of chapter VIII. From the ξ vs θ graph we select the values of ξ_m and θ_m at which the growth rate is maximum (section (C), chapter VIII). Employing the technique discussed in section (A), a ray of frequency $f_0 = \xi_m f_H$ and with initial phase angle $\theta_0 = \theta_m$ can then be traced. This ray of frequency f_0 , when received on the Earth (if geometry permits), corresponds to the centre frequency at an instant of a burst event*. We repeat the same procedure for other points along the electron bunch's trajectory. The electron travelling time between two such points plus the group delay time for the two corresponding rays (of frequencies f_0 , f_1 , say) gives the total delay time for the two frequencies f_0 and f_1 .

Assuming a helical electron bunch starts radiating at $p = 1.21$, with $\beta_1 = 0.3$, $\beta_{||} = 0.157$, the rays (corresponding to wave-normal angle θ_m) will form the surface of a cone.

*We choose such a location that A is around 1, so that, Double frequency solution exists — a burst can be radiated.

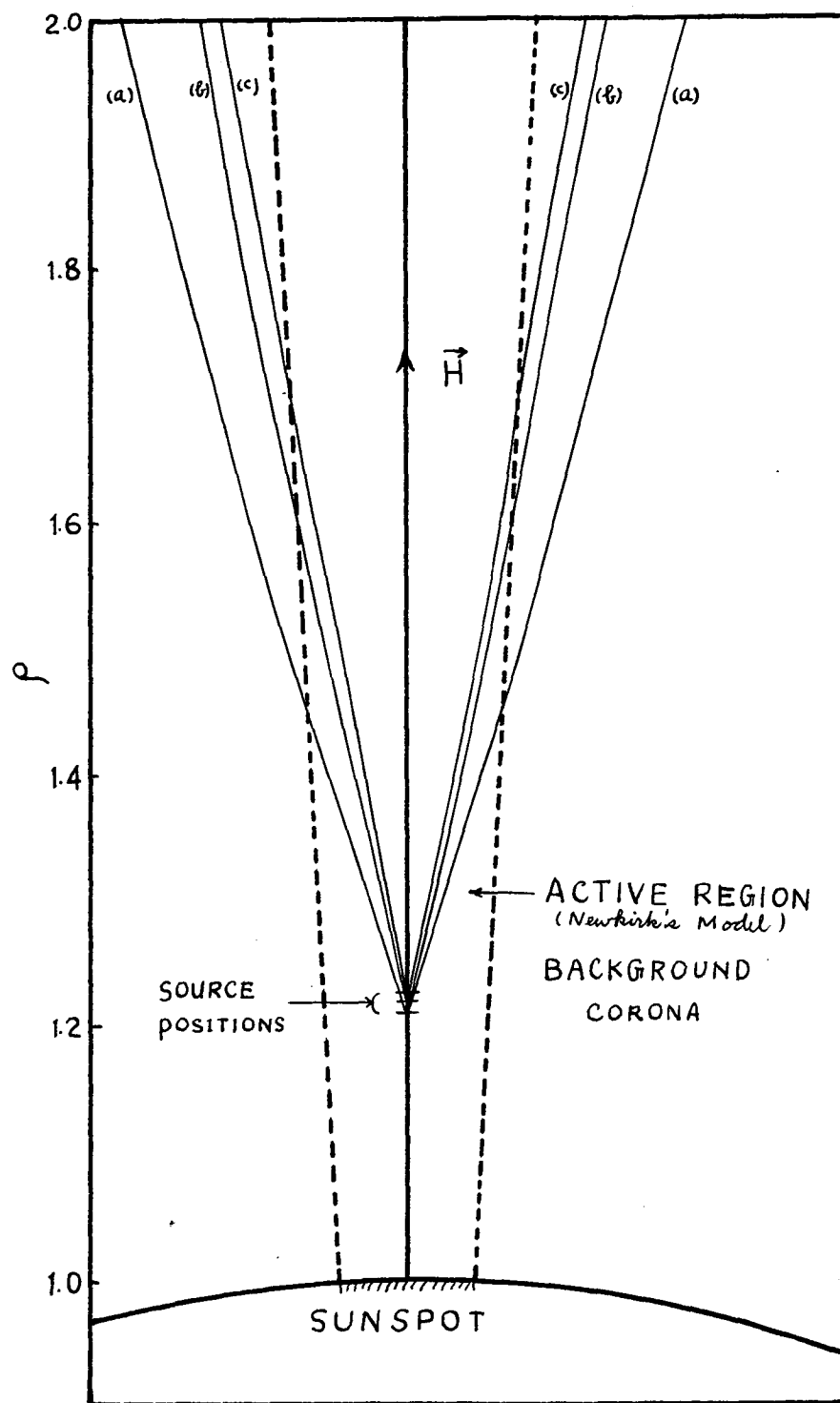


Fig. 9.3 Ray paths in the solar corona:

(a) $f = 168 \text{ Mc/s}$

(b) $f = 159 \text{ Mc/s}$

(c) $f = 153 \text{ Mc/s}$.

Table 9.1

| Source Position | $\beta_{ }$ | f Mc/s | A | Σ_m | θ_m (Degrees) | f Mc/s | t_e sec. | t_g sec. | $t =$ $t_e + t_g$ |
|--------------------|--------------|-------------|-----|------------|-------------------------|-----------|---------------|---------------|----------------------|
| Burst I | 1.21 | 0.157 | 158 | 1.00 | 1.07 | 10 | 168 | 0 | 0 |
| | 1.22 | 0.175 | 146 | 1.08 | 1.086 | 5.5 | 159 | 0.14 | 0.068 |
| | 1.226 | 0.183 | 140 | 1.13 | 1.096 | 4.2 | 153 | 0.078 | 0.15 |
| Burst II | 1.21 | 0.7 | 158 | 1.00 | 1.225 | 32 | 194 | 0 | 0 |
| | 1.24 | 0.701 | 126 | 1.27 | 1.37 | 23 | 173 | 0.1 | 0.027 |
| | 1.265 | 0.702 | 105 | 1.56 | 1.435 | 10.5 | 151 | 0.087 | 0.089 |
| | | | | | | | | | 0.127 |
| | | | | | | | | | 0.176 |

Fig. 9.3 shows in two dimensions three sets of ray paths as the electron bunch gyrates along. If all the three rays are received on the Earth, the theoretic dynamic spectrum will have the shape marked burst 1 in Fig. 9.4. When β_{\perp} and β_{\parallel} of the bunch take the values 0.3, 0.7 respectively, the theoretical dynamic spectrum takes the form as labelled burst 2 in Fig. 9.4⁺. Table 9.1 summarizes the significant numbers in deducing the theoretical spectra of these two hypothetical storm bursts.

If the spot-field configuration is of bipolar nature, the tracing of ray paths⁺⁺ and calculation of group velocities are much more tedious. In Fig. 9.5 we show three sets of rays radiated by an electron bunch at three points along a bipolar field line of force. Note that in this case the rays will travel most of the time inside the active region and the rays a', b' and c' are almost parallel. The theoretical dynamic spectrum corresponding to the rays a', b' and c' is also shown in Fig. 9.4 (burst 3).

Over a short distance S ($\sim 0.05 R_0$, say) along a magnetic field line, the pitch angle of the bunch changes by a few per cent, while the parameter A changes by ever

⁺Here, of course, we assume that all the three rays will reach the Earth.

⁺⁺We use the same technique as described before for the unipolar case.

Fig. 9.4 Theoretical dynamic spectra of storm bursts. The characteristic numbers for bursts 1 and 2 are given in Table 9.1. Burst 3 corresponds to the rays a' and b' (radiated by a bunch) in Fig. 9.5 and burst 4 is radiated by a long stream (length = 1.35×10^5 km) gyrating through the point B₁ of Fig. 9.5.

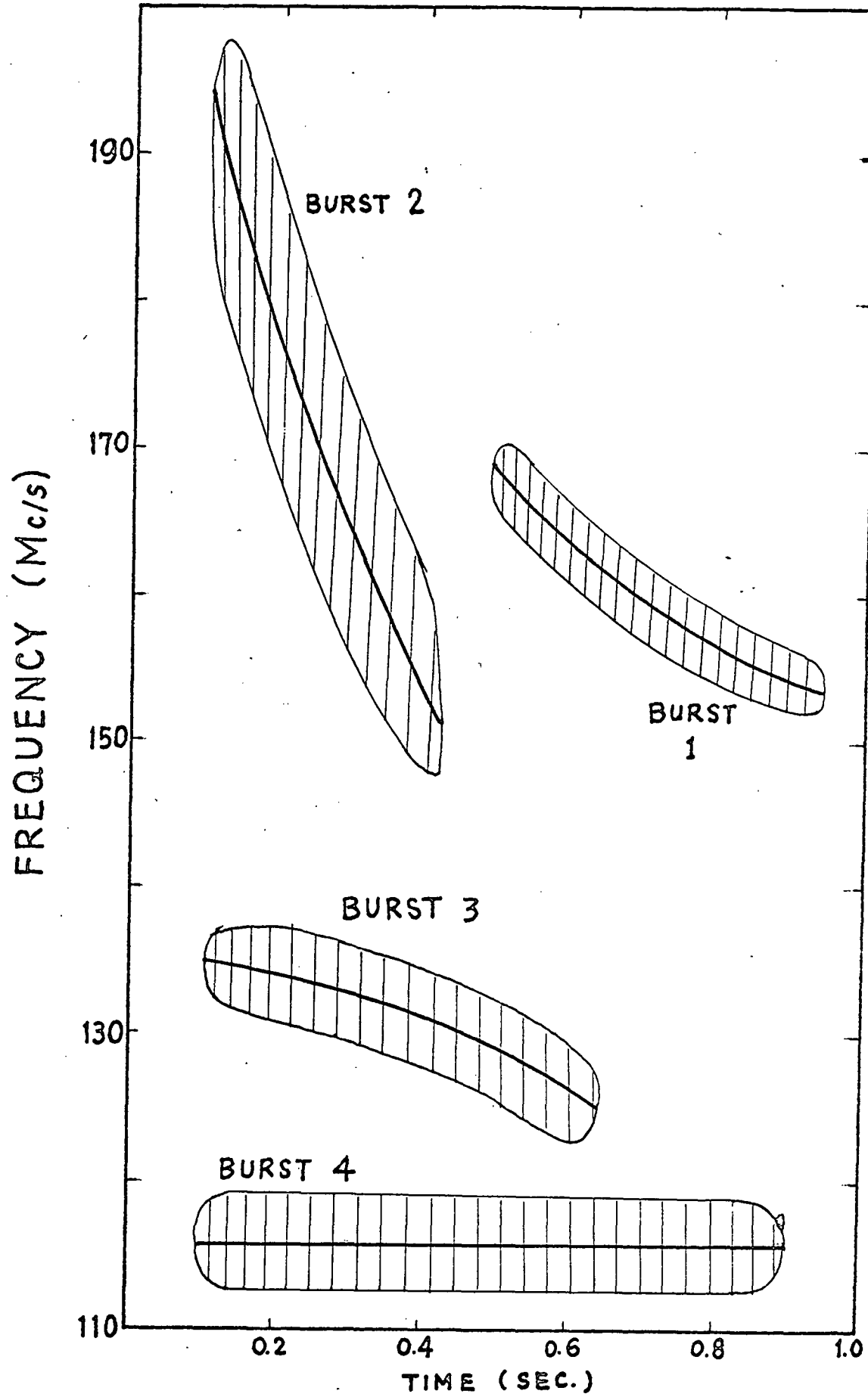


Fig. 9.4

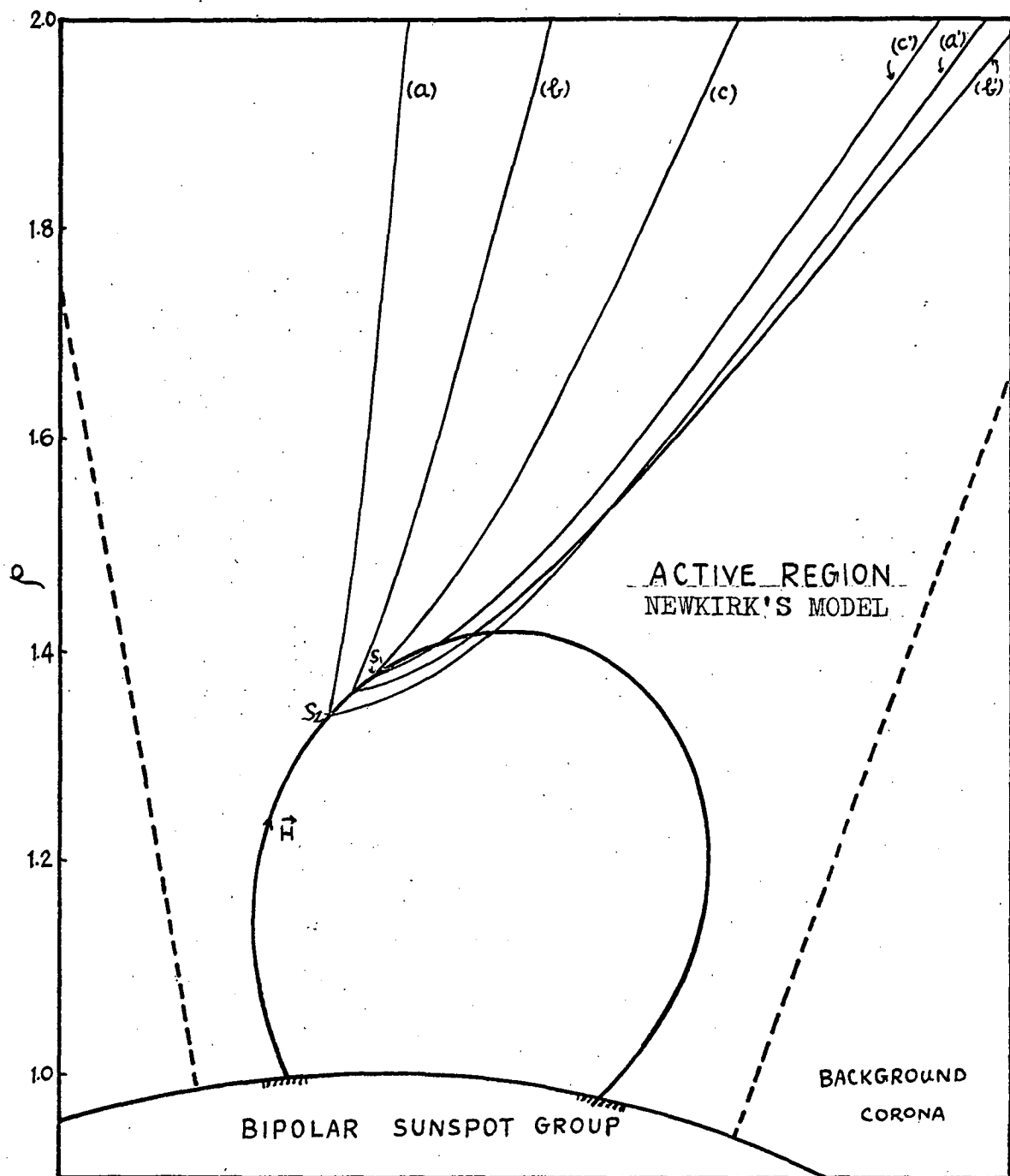


Fig. 9.5 Ray paths in the solar corona:

(a) $f = 135$ Mc/s (b) $f = 129$ Mc/s (c) $f = 116$ Mc/s.

At S_2 , $\beta_{\perp} = 0.3$, $\beta_{\parallel} = 0.5$ for the electron stream.

ten per cent. This change of A will cause a great change in the value of θ_m and hence the ray direction, with the result that the rays may diverge from the source region S (Fig. 9.3 and rays a, b, c of Fig. 9.5). This means that, on account of geometry, only the rays emitted within an extremely short length ΔS along S can reach the Earth. Consequently, if the radiating system is a bunch, a storm burst as observed will show an extremely short duration, being < 0.05 sec., which is inconsistent with the observed duration of most bursts (~ 1 sec.). We, thus, conclude that in the case where the rays from the source region diverge, a storm burst cannot be radiated by an electron bunch. However, if a helical electron stream gyrates through S , then radiation by the electrons as they pass through ΔS will be of the same frequency (this is true when ΔS can be approximated to a point) and same direction. According to this theory, no frequency drift will appear in the dynamic spectrum of a burst — this, in fact, is observed in most cases. In such a circumstance, the durations of a burst t can be related to the length of the stream L and the longitudinal velocity $v_{||}$ of the electrons at ΔS :

$$t = \frac{L}{v_{||}} \quad (9.11)$$

If we take $t = 1$ sec., the lengths of the radiating stream

corresponding to $v_{||} = 0.1c$ and $0.7c$ are $\approx 0.04 R_0$ and $0.3 R_0$ respectively. It is suggested that the value of $v_{||}$ can hardly be as high as $0.7c$, but $0.1c$ or $0.2c$ are more likely. The theoretical dynamic spectrum of a burst radiated by a helical stream is given in Fig. 9.4 (burst 4).

When the rays do not diverge in the source region (e.g. rays a', b', c' in Fig. 9.5) and the radiating electrons form a bunch⁺, they may all be observed and there will be frequency shift in the spectrum of the burst. Our estimated drift rates for this case (17 Mc/s per sec. to 32 Mc/s per sec. for $\beta_{||}$ ranging from about 0.15 to 0.7) agree with the observation of Vitkevich (1961). It should be noted that when the radiating system is moving away from the Sun as we have assumed so far, the noise burst will have a frequency drift given by $\frac{\Delta f}{\Delta t} < 0$. However, when an electron stream or bunch encounters increasing gyro-frequency in its motion, the rays under suitable geometrical conditions may reach the Earth after reflecting from the critical levels; in this case the frequency drift will be: $\frac{\Delta f}{\Delta t} > 0$. Both types of frequency drift have been observed (Fig. 5.5).

⁺If a stream is radiating in this case, the bandwidth of emission will be broad, instead of being narrow for most storm bursts.

CHAPTER X

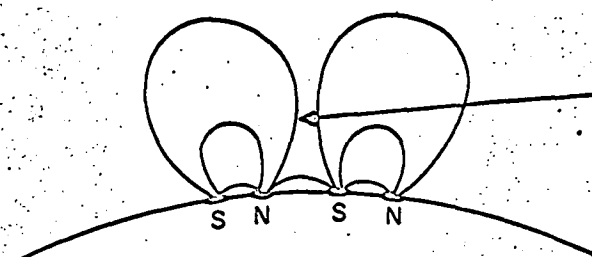
CONCLUDING REMARKS ON THE INTERPRETATION
OF SOLAR TYPE I NOISE STORMS

In this chapter we will give a general picture of the proposed cyclotron theory and some concluding remarks on the explanation of the noise storm phenomenon.

On the basis of the currently accepted theories (e.g. De Jager, 1963; Wild, 1963), a flare, which results from the annihilation of large volume of intense magnetic fields in the chromosphere or lower corona, gives rise to the production of high energy electrons and protons in different stages. At the first stage the explosion ejects charged particles in all directions, but majority of the electrons (with energy of the order of 10 - 100 Kev.) are ejected along the neutral plane of a sunspot group (Fig. 10.1). They travel in a radial direction and excite type III bursts. Some of the energetic electrons are trapped in the nearby magnetic fields and those particles arriving at a field line in about the same direction and with almost equal velocities will form an electron stream (or bunch) with a narrow momentum spread. When such a stream gyrates through the corona and whenever Double frequency solution is satisfied, a storm burst is radiated. The radiation power is strongest when the stream spirals through a region where the "intense burst radiation conditions" are

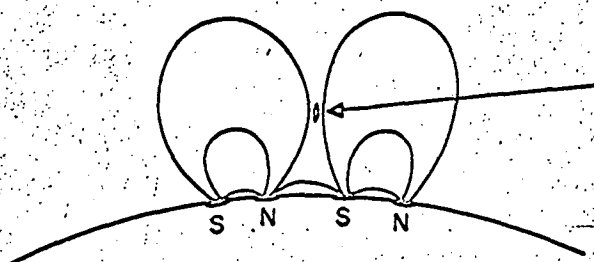
Fig. 10.1 An evolutionary model of the active region and the flare event as a whole. The model corresponds to the magnetic field configuration described by Sweet (1958)

(Kundu, 1964, with addition of type I event)

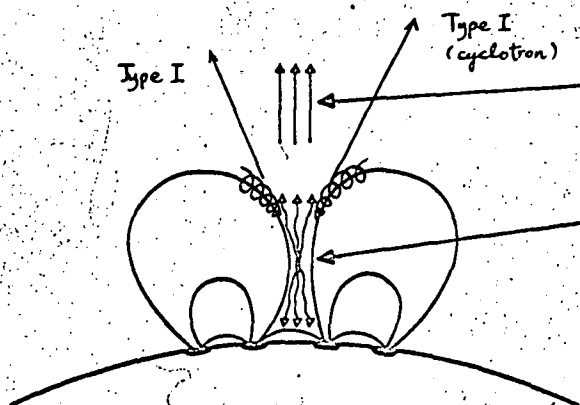


(a) Several hours earlier

Gyro-resonance absorption
Big increase in intensity and polarization
of the pre-existing cm- λ source

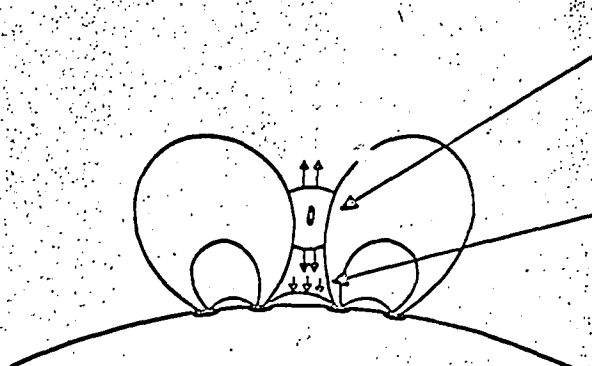
(b) $t=0$

Start of the H α flare
Thermal Bremsstrahlung (local heating)
cm- λ bursts - "gradual rise and fall"
Low energy X-ray bursts (<20 Kev)

(c) $t \sim 10 \text{ sec} - 30 \text{ sec}$

Outgoing electrons ($\sim 100 \text{ Kev} - 1 \text{ Mev}$)
Type III bursts (plasma waves)
Type V bursts

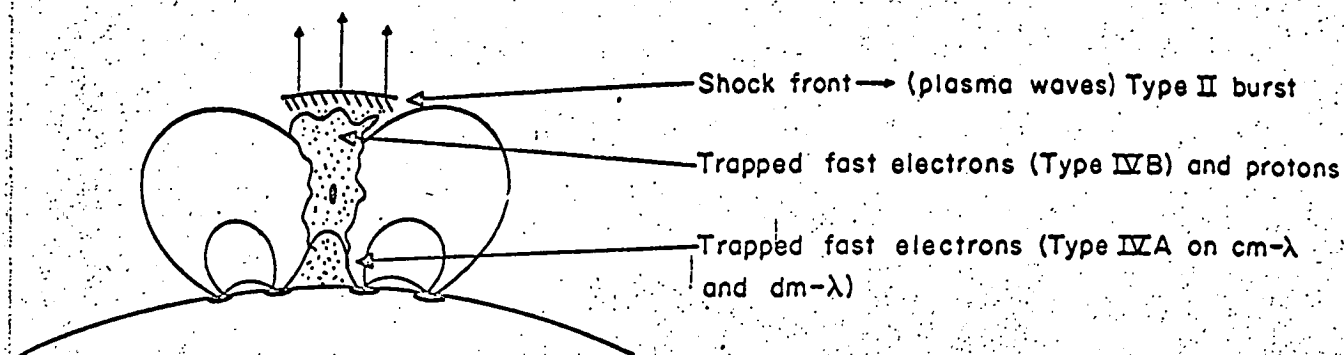
Electrical discharge in overdense plasma
Explosive phase of H α flare

(d) $t \sim 30 \text{ sec} - 1 \text{ min}$

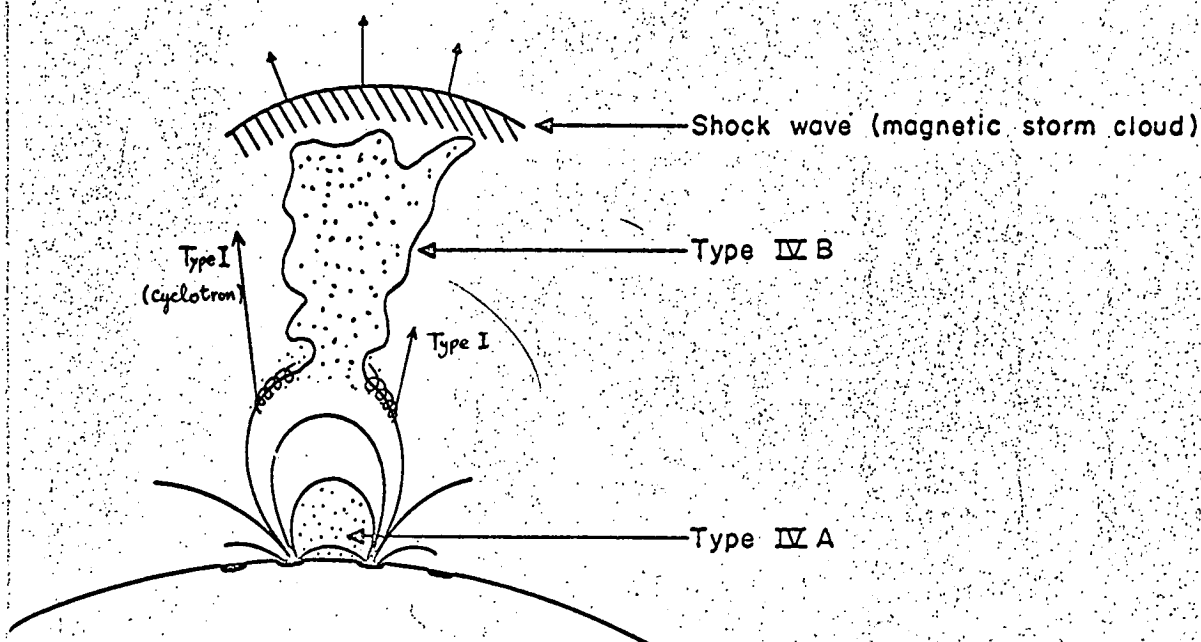
Expanding cloud of ionized gas

Downcoming electrons (100 Kev-Mev)
Non-thermal Bremsstrahlung and Synchrotron
Impulsive cm- λ burst
Generalized fast-drift bursts on dm- λ (prob. plasma)
High energy X-ray burst (>20 Kev)
Fermi-acceleration of electrons and protons
(solar cosmic rays 100 Mev \sim several Bev)

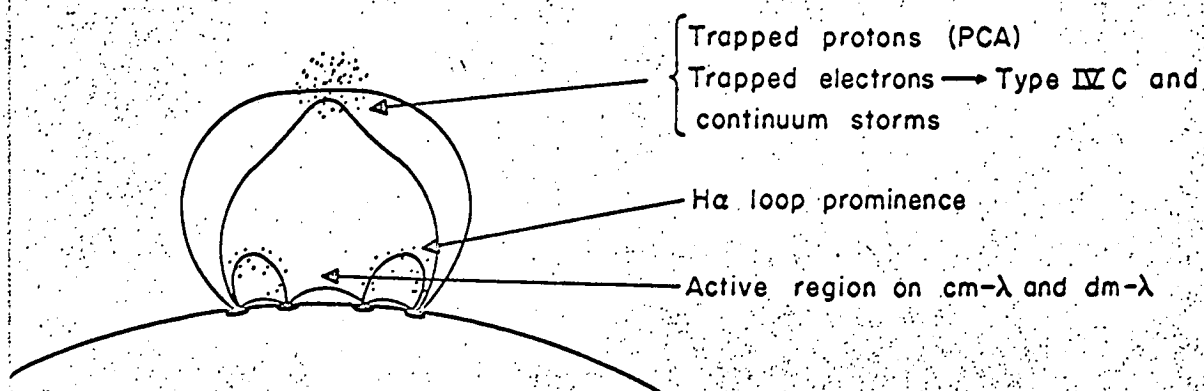
Fig. 10.1



(e) $t \sim 5 \text{ min} - 10 \text{ min}$



(f) $t \sim 10 \text{ min} - 1 \text{ hour}$



(g) $t \sim 1 \text{ to several hours}$

Fig. 10.1

satisfied. All the radiation from a number of streams satisfying the single frequency solution will superimpose to form a weak intensity, wide-band, continuous radiation—the background continuum. With suitable geometry conditions, the rays of the radiation will be observed on the Earth as a flare-related solar type I noise storm. In the radiation of a burst, when the rays from a relatively small source region diverge, the detected spectrum will show no frequency drift, which is often the case. When the rays propagate in almost parallel directions, the dynamic spectrum of a burst may indicate upward or downward frequency drift as discussed in chapter IX.

As it has been mentioned before that most noise storms are preceded by flares and the most probable delay time is 30 minutes. It seems, therefore, that there is a lapse of time ~ 30 minutes during which either source electrons are as yet unavailable, or that propagation conditions do not allow the radiated waves to escape. The flare phenomenon is very complex and is not well understood yet. From the more popular proposed theories of the flare evolution, it seems that the existence of trapped electrons with energy $\sim 10 - 100$ Kev. in the source region after ~ 30 minutes of the initial explosive phase of the flare is possible. This idea is illustrated in Fig. 10.1 which is self-explanatory. Noise storms will be radiated in this case in the same manner as

described above.

As a noise storm may go on for hours or days, either the radiating electron streams remain trapped in the spot-field configurations all the time or that there is a continuous supply of nonthermal electrons to keep the emission process in progress. The first possibility is opposed by the fact that an electron stream with narrow momentum spread cannot remain in the same state for such a long time on account of diffusion, gradient drift and curvature drift. Apart from direct ejection of high energy electrons (energy > 10 Kev.) in the flare phenomenon, a number of mechanisms have been proposed for the production of high energy charged particles. The high energy corpuscles may be emitted through the action of an electric field arising as a result of unipolar induction and creating high voltages (Alfven, 1937), as a consequence of thermo-nuclear reactions taking place near the photosphere (Wild, Roberts and Murray, 1954), or as a result of certain processes which originate in regions of intense turbulence in the solar atmosphere (Ginzvurg, 1953). Besides the mentioned theories, Kolpakov (1957, 1959) has shown that if the magnetic fields of a unipolar spot increase with time $\left(\frac{\partial H}{\partial t} > 0 \right)$ and if there exists a pressure gradient and an magnetic intensity gradient directed towards the axis of the unipolar spot field configuration, a net transverse (with respect to magnetic field direction) induced electric field E_{\perp} will exist.

Due to the action of this induced field E_{\perp} , the particles at the tail of the Maxwellian distribution of the chromosphere background plasma will be accelerated to energies up to the order of 1 Mev. It seems therefore that high energy electrons are produced from time to time by various processes and a flare may be the triggering mechanism to bring these operations to high efficiency.

The investigation in section (F) of chapter VIII indicates that the intense burst radiation conditions are quite easily satisfied in the source region if the electron density is ten times the normal corona background density. Working independently, this result on magnitude of electron density agrees with the type II and type III radio observations of Weiss and others (chapter VI).

A comparison on the predictions of the cyclotron theory (chapter VIII) with the observational data (chapter V) will show that the mode of radiation, the observed frequency range, the narrow-band structure of storm bursts, the relation between the background continuum and storm bursts, the source positions, the association of noise storms with sunspots and the relative angular sizes of storm burst and background continuum are all well accounted for with our presented theory. The dynamic spectra of storm bursts have been explained in chapter IX. Based on the very limited knowledge of the flare phenomenon, the flare association property has been discussed in this chapter.

There remains, however, two features which have not yet been discussed: These are the polarization properties and the estimation of electron density in the stream needed in order to account for the radio flux density received. We will consider these two features below.

For longitudinal propagation of radio waves in a magnetoactive plasma, the polarizations of both modes are circular and the polarization constants $|R_o|$ and $|R_x|$ are both equal to 1. For transverse propagation, $|R_o| = 0$ and $|R_x| = \infty$ and the waves are linearly polarized. Piddington and Minnett(1951) have shown that the polarization of radio waves tends to be circular as the quantity $Y/(1 - X)$ tends towards zero except for θ very close to 90° . In the solar atmosphere, both X and Y and hence $Y/(1 - X)$ decrease with height. Consequently, for θ not very close to 90° at the boundary where $Y/(1 - X) \rightarrow 0$, the limiting polarization of the emergent wave (either mode) is circular, the sense being depending upon whether the value of θ is greater than or smaller than 90° in the boundary level. The above situation is clearly shown in Fig. 10.2 where R_o is plotted against θ for various values of $Y/(1 - X)$. Consider the circumstance when the source is near the centre of the disc. Referring to Fig. 10.3, it is not difficult to see that except when the source is very near the top of a bipolar field line, the wave-normal angle of the wave will not take

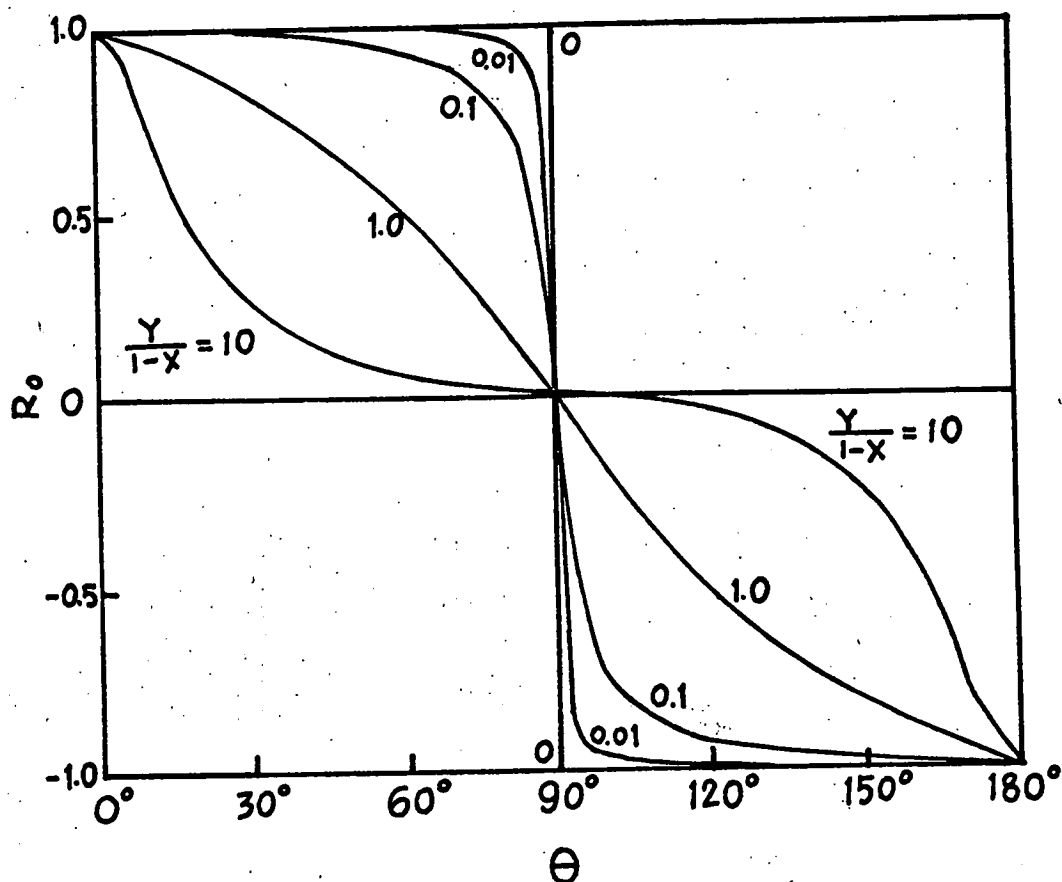


Fig. 10.2 Variation of the ordinary mode polarization R_0 as a function of wave-normal angle θ for various values of the parameter $\frac{Y}{1-X}$.

(Piddington and Minnett, 1951)

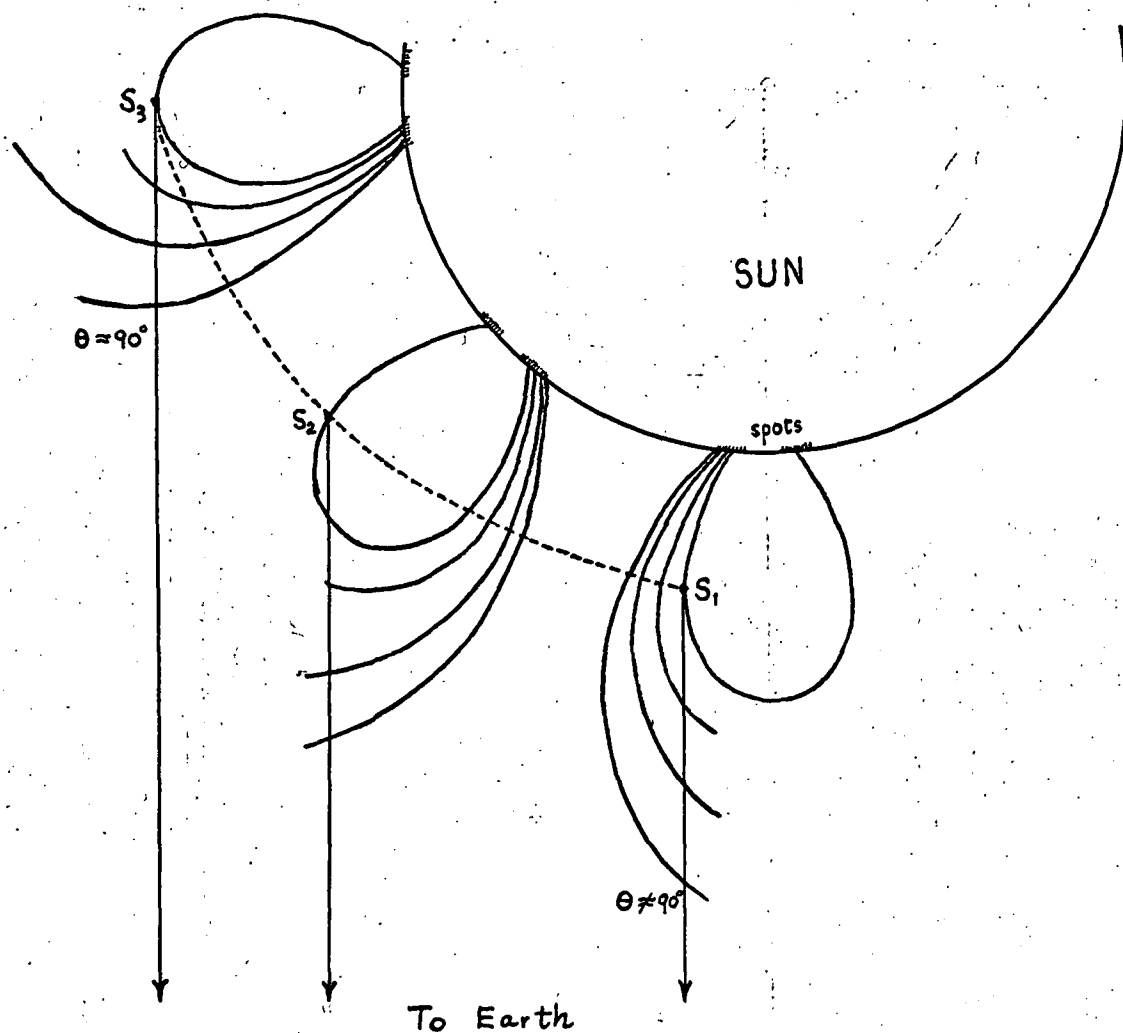


Fig. 10.3 Geometry showing wave paths (represented by arrows) which would reach the Earth. S_1 , S_2 & S_3 are possible source positions and the wave-normal angle is 10° at generation in each case.

the value of 90° as it propagates through the corona (here we assume the wave path to be straight). The polarization detected in general will be circular. For a limb source, the probability that θ will assume 90° at the boundary level (where $Y/(1 - X) \rightarrow 0$) is very much higher. The emergent wave will be linearly polarized in many cases. The linearly polarized waves from a finite source will be depolarized due to the Faraday rotation effect and we will receive unpolarized noise storms from the limb. Moreover, when the received radiation comes from two sources, we may receive mixed polarized waves (as observed by Fokker, 1961) or unpolarized waves due to the difference in polarity of the spots associated with the sources or due to the fact that the values of θ for waves from one source are smaller than 90° while that from the other source are greater than 90° at the boundary levels. With these views in mind, the polarization properties of different noise storms may well be explained.

Finally, to estimate roughly the density of stream and the interaction time needed in order to account for the observed maximum flux density, we perform the following calculation. Assume that electrons in a volume of 100 m^3 of the streams radiate a particular frequency. Let N_0 be the density of the stream. The maximum power radiated by a single electron in the σ -mode is about 10^{-21} watts/sterad.

Then the total power associated with a particular frequency is about $10^{-19} N_0 G$ watts/sterad., where G is the power gain in the stream-plasma system. The theoretical flux density received on the Earth for frequency of 100 Mc/s would then be $5 \times 10^{-50} N_0 G$ watts $m^{-2}/(c/s)$. Assuming the active region density to be $10^9/cm^3$ and $\sigma = 10^{-6}$, giving $N_0 = 10^3/cm^3$, we have theoretical flux density $\sim 5 \times 10^{-41} G$. Equating this value to the observed maximum flux density (10^{-20} watts $m^{-2}/(c/s)$), we need a power gain of $G \sim 2 \times 10^{21}$ (~ 21 db). We observe from Fig. 8.16(c) that the interaction time needed is only about 5×10^{-6} sec. Note that if the stream density is much smaller, we can still explain the observed flux density by allowing a longer interaction time. The above estimation is very crude, but it seems that all the numbers involved are physically realizable.

CHAPTER XI

CONCLUSIONS

(A) General Concluding Remarks

Employing the kinetic approach as firstly suggested by Zheleznyakov for longitudinal propagation, the linearized dispersion equation for a stream-magnetoactive-plasma system for general θ has been derived for two distribution functions of the stream: (i) A helical stream, (ii) a stream with bi-Maxwellian distribution function associated with both ρ_{\perp} and ρ_{\parallel} . The corresponding expressions for the growth rate have been obtained.

The instability theory has been applied successfully to explain the two existing problems (chapter I) in some emissions of Jupiter, the Earth and the Sun: (i) Narrow band structure, and (ii) extraordinary higher power associated with these emissions. Some doubts in the radiation characteristics of terrestrial VLF discrete emissions (triggered and non-triggered) are clarified and the reason for the existence of emission cone in Jupiter's decametric burst radiation is clearly accounted for. The origin of solar type I noise storm, which has been in doubt for more than twenty years, is explained in detail.

Studying the cyclotron radiation process by an electron stream in the atmospheres of Jupiter, the Earth and the Sun shows that under different background plasma conditions (specified by the quantity A), the cyclotron radiation characteristics have different forms according to a distant observer. For example, in the Jovian magnetosphere where A is very much smaller than 1 ($0.09 - 0.0016$), the forward radiation is predominant in the x-mode since the harmonic resonance absorption is small ^{for both o and x modes} and the x-mode electromagnetic power is generally one to two orders of magnitude larger. For $A < 1$, it is elementary to show from the Appleton-Hartree equation that for the whistler mode, $n_j \rightarrow \infty$ as $\xi \rightarrow \sqrt{A}$. It is easy to see that for $A \ll 1$, there is generally no simultaneous solution for the backward Doppler equation ($180^\circ \geq \theta > 90^\circ$) and the corresponding Appleton-Hartree equation. Consequently, with the model of Jovian exosphere as proposed by Ellis, radiation of whistler mode waves is hardly possible. Hence, the forward cyclotron radiation in the x-mode (being observed as Jupiter's decametric burst emission) by a gyrating electron stream is the only significant form of cyclotron radiation in the Jovian magnetosphere.

When $A \gg 1$ as in the terrestrial exosphere, the lowest possible harmonic number of radiation for both characteristic modes in the forward radiation is large

(chapter VIII) and the cyclotron radiation power will be small. Thus, the Earth is not a good external radiator⁺. This property has been pointed out by Ellis (1964). Cyclotron radiation in the backward direction, however, can easily be significant. Whereas the "backward waves" propagating along mode 4 cannot penetrate the ionosphere (Liemohn, 1965), the waves propagating in the whistler mode can reach the Earth, being detected as VLF emissions.

When $A \approx 1$ as in some parts of the active solar coronal regions, the harmonic resonance absorption for the x-mode is very large and the x-mode reflection level for fundamental harmonic radiation is high, so that, the forward radiation in the o-mode will be predominant (chapter VIII). Backward shifted cyclotron radiation is also significant for $A \approx 1$ and we should expect strong whistler waves reaching the chromosphere or the photosphere. Since the coupling mechanism in the solar corona is very inefficient, the whistler mode wave can hardly transfer significant electromagnetic energy to the o-mode branch. As a result, the o-mode cyclotron wave radiated in the forward

⁺Meaning radiating waves into the outer space.

direction is the only type of cyclotron waves that will carry significant power and propagate to the outer space ——— we receive the radiation as solar type I noise storm.

We can, thus, see that knowing the value of A in the possible source region, the general cyclotron radiation characteristics from a plasma can be predicted, with the knowledge of the investigation in this thesis. These properties will give a guide to future research on cyclotron radiation in the atmospheres of heavenly objects or thermal nuclear reactor plasmas.

(B) Suggestions for Further Research

Based on the results of this investigation, we may suggest the following items for further research:

- (i) Concerning the instability problem of a stream-plasma system, study the correspondence between the kinetic approach and the negative absorption approach as suggested in chapter II. Following either approach, investigate the non-linear theory.
- (ii) The origin of hiss is not yet fully understood. We may seek a solution in the form of cyclotron radiation by electron streams, having smaller pitch angles and different distribution functions from

that associated with discrete emissions. Attention should be focussed on the continuous supply of the energetic electrons, since a "Hiss storm" lasts for hours. The dynamic spectra of other types of VLF discrete emissions have not been explained quantitatively; this deserves some attention.

- (iii) Since solar type IV emission is in many cases strongly polarized and the radiation is also in the o-mode, the origin may be similar to that of type I radiation. A detailed study of the radiation characteristics in the possible source region of type IV radiation, following the same line as described in chapter VIII, would be fruitful.
- (iv) Carry out laboratory experiment to study the radiative behaviour of a stream-plasma system.

Appendix A

Derivation of the Vlasov Equation (Delcroix, 1963; Smerd, 1965; Vlasov, 1938)

(a) The Distribution Functions

Strictly speaking, in a many-body problem where there are N particles of one species --- electrons, say, one should work with a N -particle distribution function F_N , where at time t , $F_N d\bar{r}_1 d\bar{r}_2 \dots d\bar{r}_N d\bar{v}_1 d\bar{v}_2 \dots d\bar{v}_N$ is the probability of finding particle 1 in the volume element $d\bar{r}_1 = d\bar{x}_1 d\bar{y}_1 d\bar{z}_1$ centred at \bar{r}_1 with velocity in the range $d\bar{v}_1 = dv_{x1} dv_{y1} dv_{z1}$ centred at \bar{v}_1 , particle 2 in $d\bar{r}_2$ at \bar{r}_2 with velocity range $d\bar{v}_2$ at $\bar{v}_2 \dots$ up to the N th particle. Since the number N is usually very large, we have to use a coarser description of the plasma in practice. The distribution function usually used in kinetic theory is the one particle distribution $f_1(\bar{r}, \bar{v}, t)$.

Now the probability that particle 1 will occupy the volume element $d\bar{r}_1$ at \bar{r}_1 , with velocity in the range $d\bar{v}_1$ at \bar{v}_1 , while at that time all the other $(N - 1)$ particles may be anywhere in the phase space of the system is

$$d\bar{r}_1 d\bar{v}_1 \int F_N d\bar{r}_2 d\bar{v}_2 \dots d\bar{r}_N d\bar{v}_N \quad (\text{A.1})$$

Since all N particles are of the same type, this probability is also the probability that any other one particle will occupy the volume element $\overline{dr}_1 \overline{dv}_1$ in phase space. Therefore, the probable number of particles in volume element $\overline{dr}_1 \overline{dv}_1$, i.e. $f_1 \overline{dr}_1 \overline{dv}_1$, is N times the probability (A.1) and we then have

$$f_1 = N \int F_N \overline{dr}_2 \overline{dv}_2 \dots \overline{dr}_N \overline{dv}_N \quad (\text{A.2})$$

Similarly, from the probability of finding particle 1 in the volume element $\overline{dr}_1 \overline{dv}_1$ and, at the same time, particle 2 in the volume element $\overline{dr}_2 \overline{dv}_2$, while all the other $N-2$ particles being anywhere in the available phase space, we can find the probable number of pairs of particles in the volume element $\overline{dr}_1 \overline{dv}_1$ and $\overline{dr}_2 \overline{dv}_2$ respectively. We will now have a 2-particle distribution function $f_{12}(\vec{r}, \vec{v}, t)$ which can be shown to relate the N -particle distribution function in the form

$$f_{12} = N(N-1) \int F_N \overline{dr}_3 \overline{dv}_3 \dots \overline{dr}_N \overline{dv}_N \quad (\text{A.3})$$

This process can be continued for three particle distribution function f_{123} and so on. We note here that the 2-particle distribution function f_{12} will already enable us to determine the macroscopic effects such as the internal fields and pressures due to the interaction forces between the particles.

Such distribution functions describe the state of the plasma at time t to varying degrees of accuracy. We need now to describe the microscopic state of the plasma in the course of time in terms of the microscopic distribution functions.

(b) The Kinetic Equation

In the system under consideration, assuming all forces are conservative and independent of velocity, the Liouville theorem describes the changes of F_N as a function of time in phase space (c. f. Delcroix, chapter 7, 1963):

$$\frac{\partial F_N}{\partial t} + \sum_{i=1}^N \bar{v}_i \frac{\partial F_N}{\partial \bar{r}_i} + \sum_{i=1}^N \left(\frac{\bar{X}_i + \sum_{j \neq i} \bar{X}_{ij}}{m} \right) \frac{\partial F_N}{\partial \bar{v}_j} = 0 \quad (\text{A.4})$$

where the total force acting on the i th particle consists of the external force \bar{X}_i and the forces \bar{X}_{ij} ($i \neq j$) due to the interaction of the i th particle with each of the other $(N - 1)$ particles.

In order to simplify calculation which becomes impossible when N is large, a regression method has been developed to describe the evolution of the plasma in terms of successive pairs $f_1, f_{12}; f_{12}, f_{123}; f_{123}, f_{1234}; \dots$ of the one-particle and multiple-particle distribution functions. Thus, one has to know f_{12} in order to determine f_1 , to know f_{123} to determine f_{12} so on. This method

is called the BBGKY-method which bears the initials of its originators

The first and the simplest of these Liouville-type equations is (Delcroix, chapter 7, 1963):

$$\frac{\partial f_1}{\partial t} + \bar{v}_1 \frac{\partial f_1}{\partial \bar{r}_1} + \frac{\bar{X}_1}{m} \cdot \frac{\partial f_1}{\partial \bar{v}_1} + \int \frac{\bar{X}_{12}}{m} \cdot \frac{\partial f_{12}}{\partial \bar{v}_1} d\bar{r}_2 d\bar{v}_2 = 0 \quad (\text{A.5})$$

In most problems, only the first BBGKY -equation i.e. equation (A.5) is employed.

Neglecting the interactions between particles, equation (A.5) becomes

$$\frac{\partial f_1}{\partial t} + \bar{v}_1 \frac{\partial f_1}{\partial \bar{r}_1} + \frac{\bar{X}_1}{m} \cdot \frac{\partial f_1}{\partial \bar{v}_1} = 0 \quad (\text{A.6})$$

and one sees that this is in fact the collision-free Boltzman equation.

(c) Correlation between Particles

In above, we arrive at a kinetic equation (A5) which is the approximated form of the complete one. To obtain the Vlasov equation, a few more approximations have to be taken. Before we consider these approximations, we need to define the concept of "correlation" between particles. (c.f. Delcroix, chapter 6, 1963).

The N particles of a species are said not to be correlated or independent if the N -particle distribution

function can be written as the product of N single-particle distribution functions:

$$F_N = F_0(\bar{r}_1, \bar{v}_1, t) F_0(\bar{r}_2, \bar{v}_2, t) \dots F_0(\bar{r}_N, \bar{v}_N, t) \quad (A7)$$

These functions are functionally identical since all particles of one kind are quite the equivalent of each other. The probability of finding the plasma to be in some state of phase space is 1:

$$\int F_0(\bar{r}, \bar{v}, t) d\bar{r} d\bar{v} = 1 \quad (A8)$$

From equations (A2), (A7) and (A8), one finds that for the one-particle distribution function,

$$f_1 = N F_0 \quad (A9)$$

From (A7) and (A9), one realizes that if $f_2 = f_1(\bar{r}_2, \bar{v}_2, t)$, $f_3 = f_1(\bar{r}_3, \bar{v}_3, t) \dots$ then

$$F_N = \frac{1}{N^N} f_1 f_2 f_3 \dots f_N$$

In the case of the 2-particle distribution function, we have from equations (A3), (A7), (A8) and (A9) that for no correlation

$$\begin{aligned} f_{12} &= \frac{(N-1)}{N} f_1 f_2 \\ &\approx f_1 f_2 \quad \text{for } N \gg 1 \end{aligned} \quad (A10)$$

(d) The Vlasov Equation

If we assume that there is interaction but no correlation between the particles in a plasma subject to electromagnetic disturbance, relation (A10) holds and the last term of equation (A5) becomes

$$\int \frac{\bar{X}_{12}}{m} \cdot \frac{\partial f_{12}}{\partial \bar{v}_1} d\bar{r}_2 d\bar{v}_2 = \frac{\partial f_1}{\partial \bar{v}_1} \int \frac{\bar{X}_{12}}{m} f_2 d\bar{r}_2 d\bar{v}_2 \quad (A.11)$$

With \bar{X}_{12} independent of velocity, we can carry out the integration with respect to $d\bar{v}_2$ to get the density n_2 :

$$n_2 = \int f_2 d\bar{v}_2 \quad (A12)$$

In other words, the probable number of particles with any velocity in the volume element $d\bar{r}_2$ is $n_2 d\bar{r}_2$, and relation (A11) becomes

$$\frac{\partial f_1}{\partial \bar{v}_1} \int n_2 \frac{\bar{X}_{12}}{m} d\bar{r}_2 = \frac{\bar{X}_1'}{m} \cdot \frac{\partial f_1}{\partial \bar{v}_1} \quad (A.13)$$

where \bar{X}_1' is the electrostatic force due to space charge (Delcroix, equation (6.49) of chapter 6, 1963) and is equivalent to the term $e_j \bar{E}$ of relation (1.3). With (A13), equation (A5) reads

$$\frac{\partial f_1}{\partial t} + \bar{v}_1 \cdot \frac{\partial f_1}{\partial \bar{r}_1} + \frac{\bar{X}_1 + \bar{X}_1'}{m} \cdot \frac{\partial f_1}{\partial \bar{v}_1} = 0 \quad (A.14)$$

This is the Vlasov equation with an external force \bar{X}_1 and an electrostatic force \bar{X}_1' due to space charge. Including

a magnetic force $\frac{e_j}{c} \vec{v} \times (\vec{B}_0 + \vec{B})$ as in (1.3) requires a relativistic treatment of the Liouville equation and will not be dealt here.

In the derivation of the Vlasov equation, we have assumed that there is interaction but no correlation between particles. This means that the interaction is of a collective or macroscopic nature and acts continuously and equally on all particles like an external force. It is worth remarked here that when we assume that the interaction occurs only in binary collisions with no interaction force acting on the particles between the period of such collisions, equation (A5) is approximated to the well known Boltzman equation.

Appendix B

The Transport Equations in the Macroscopic Approach
of Describing Wave Propagation in a Plasma
(Denisse and Delcroix, 1963; Delcroix, 1963)

In the macroscopic treatment, the mean value of a particle property $a(\vec{r}, \vec{v}, t)$ is defined as

$$\bar{a}(\vec{r}, t) = \frac{1}{n} \int a(\vec{r}, \vec{v}, t) f(\vec{r}, \vec{v}, t) d\vec{v} \quad (\text{B.1})$$

where n is the macroscopic density given by

$$n(\vec{r}, t) = \int f d\vec{v} \quad (\text{B.2})$$

The transport equations can be obtained as successive moments of the first BBGKY-equation, i.e. equation (A.5); this equation may be referred to as the first kinetic equation.

For particle property $a = 1$, we have from (B.1) the definition of mean density n (i.e. equation (B.2)). Using the mean velocity $\vec{v} = \frac{1}{n} \int \vec{v} f d\vec{v}$, integration of the first kinetic equation over velocity space gives

$$\frac{\partial n}{\partial t} + \nabla \cdot \vec{n} \vec{v} = 0 \quad (\text{B.3})$$

Equation (B.3) remains valid if the particle interactions do not change the number of particles of a species.

For particle property $\bar{a} = m\bar{v}$, integration of equation (A5) with respect to velocity gives

$$nm \left(\frac{\partial}{\partial t} + \bar{v} \cdot \nabla \right) \bar{v} = n\bar{X} - \nabla \cdot \bar{\bar{\tau}} + \bar{P} \quad (B.4)$$

where $\bar{P} = \int m \bar{v}' \left(\frac{\partial f}{\partial t} \right)_{\text{interaction}} d\bar{v}'$

$\bar{\bar{\tau}}$ is the kinetic pressure tensor and it is usually assumed that $\bar{\bar{\tau}}$ can be reduced to an isotropic scalar pressure $p = n\kappa T$.

\bar{X} is the external force.

\bar{P} is the interaction force divided by the mean density and it consists of two parts: (i) a collective interaction which is added to the external force \bar{X} ; (ii) a collision interaction which adds, in part, to the pressure tensor $\bar{\bar{\tau}}$ due to collisions between like particles, while the remaining term $\sum_{b \neq a} P'_{ab}$ represents the momentum transfer due to collisions between particles of different species. In deriving the Vlasov equation, all collision effects are neglected.

Equations (B3) and (B4) are two transport equations. From these two equations and the Maxwell equations, the dispersion equation can be derived.

Appendix C

Dispersion Equation of Plane Waves Propagating in a Warm, Collisionless, Magnetoactive Plasma

Using the macroscopic approach, Denisse and Belcroix give the dispersion equation for plane waves propagating in a warm, collisionless, magnetoactive plasma:

$$\Delta_T \Delta_L + B + C + D + E = 0 \quad (C1)$$

$$\text{where } \Delta_T = \Delta_1^2 + \frac{\omega_L^2 \Omega_L^2}{\omega^4} (\eta_j^2 - 1)^2 - \frac{\omega_L^2}{\omega^2} \left(\eta_j^2 - 1 + \frac{\Omega_P^2}{\omega^2} \right)^2 - \frac{\Omega_L^2}{\omega^2} \left(\eta_j^2 - 1 + \frac{\omega_P^2}{\omega^2} \right)^2 + \frac{2 \omega_L \Omega_L \omega_P^2 \Omega_P^2}{\omega^6}$$

$$\Delta_L = \left(1 - \frac{\eta_j^2}{\epsilon_e} \right) \left(1 - \frac{\eta_j^2}{\epsilon_i} \right) - X \left(1 - \frac{\eta_j^2}{\epsilon_s} \right)$$

$$B = \frac{\omega_T^2}{\omega^2} \left(\frac{\eta_j^2}{\epsilon_i} - 1 + \frac{\Omega_P^2}{\omega^2} \right) \left[\Delta_1 \left(\eta_j^2 - 1 + \frac{\Omega_P^2}{\omega^2} \right) - \frac{\Omega_L^2}{\omega^2} (\eta_j^2 - 1) \left(\eta_j^2 - 1 + \frac{\omega_P^2}{\omega^2} \right) \right]$$

$$C = \frac{\Omega_T^2}{\omega^2} \left(\frac{\eta_j^2}{\epsilon_e} - 1 + \frac{\omega_P^2}{\omega^2} \right) \left[\Delta_1 \left(\eta_j^2 - 1 + \frac{\omega_P^2}{\omega^2} \right) - \frac{\omega_L^2}{\omega^2} (\eta_j^2 - 1) \left(\eta_j^2 - 1 + \frac{\Omega_P^2}{\omega^2} \right) \right]$$

$$D = 2 \frac{\omega_T \Omega_T \omega_P^2 \Omega_P^2}{\omega^6} \left[-\Delta_1 + (\eta_j^2 - 1) \frac{\omega_L \Omega_L}{\omega^2} \right]$$

$$E = \frac{\omega_T^2 \Omega_T^2}{\omega^4} (\eta_j^2 - 1) \Delta_1$$

$$\Delta_1 = \eta_j - 1 + X$$

$$\omega_L = \omega_H \cos \theta \quad \omega_T = \omega_H \sin \theta$$

$$\Omega_L = \Omega_H \cos \theta \quad \Omega_T = \Omega_H \sin \theta$$

$$\omega_H = \frac{e H_0}{m_e c}$$

$$\Omega_H = \frac{e_i H_0}{m_i c}$$

e, e_i = charge of electron, ion respectively.

m_e, m_i = mass of electron, ion respectively.

c = speed of light in vacuum.

H_0 = static magnetic field strength in gauss.

θ = angle between static magnetic field (which is on y - z plane)

and wave vector $\vec{k} = k \hat{z}$.

n_j = refractive index.

$$\omega_p^2 = 4\pi \bar{n}_e e^2 c^2 / m_e$$

$$\Omega_p^2 = 4\pi \bar{n}_i e_i^2 c^2 / m_i$$

\bar{n}_e and \bar{n}_i are average particle densities of electron and ion in the plasma respectively.

$$\epsilon_e = c^2 / V_e^2$$

$$\epsilon_i = c^2 / V_i^2$$

$$\epsilon_s = c^2 / V_s^2$$

with V_e, V_i are the average thermal velocity for electron and ion respectively.

$$V_s^2 = \frac{\Omega_p^2 V_e^2 + \omega_p^2 V_i^2}{\omega_p^2 + \Omega_p^2}$$

$$X = \omega_0^2 / \omega^2$$

$$\omega_0^2 = \omega_p^2 + \Omega_p^2$$

The above dispersion can be arranged into an equation of

the fourth degree in n_j and hence for one value of angular frequency there corresponds in general four values of the refractive index squared. In other words, this medium is quadruply refracting — four distinct modes of waves can therefore propagate through this medium.

Appendix D

Two Methods of Solving the Radiative Instability Problem of a Stream-Plasma System within the Kinetic Regime

To attack a radiative instability problem of a stream-plasma system, two methods are generally used within the classical kinetic regime: (i) assuming the wave vector to be real and solve the dispersion equation of the system for complex frequency, considering the dielectric tensor of the system to be made up of two parts — one due to the ambient magnetoactive plasma and the other due to the presence of the stream (e.g. Stepanov and Kitsenko, 1961) (ii) assuming the wave vector to be real, derive the dispersion equation for an electromagnetic wave in a system of a stream travelling in vacuum in the presence of a static magnetic field, and then include the presence of the ambient plasma by assuming

$$n^2 = n_j^2 + n_s^2 - 1 \quad (D.1)$$

where n = overall refractive index for the combined system

n_j = refractive index for the ambient plasma alone,

and

n_s = refractive index for the stream alone (in the presence of the static magnetic field).

The presence of the term "1" in relation (D.1) comes from

the fact that each of the refractive indices n_j , n_s has included the effect of a vacuum (the refractive index for an electromagnetic wave in vacuum is 1). This approach was firstly introduced by Zheleznyakov (1960a).

It is interesting to find out whether the two approaches are exactly equivalent, or one being the approximated form of the other. We investigate the case when the stream is a helical electron stream, i.e. each electron in the stream moves with the same non-zero transverse velocity $\beta_{\perp} = v_{\perp}/c$ and the same longitudinal velocity $\beta_{\parallel} = v_{\parallel}/c$, c being the velocity of light in vacuum. The particle density in the stream is assumed to be very small compared with that in the background plasma and the stream-plasma system is assumed to be electrically neutral. The collisionless Appleton-Hartree equation is assumed to be applicable to the propagation of electromagnetic waves in the background plasma alone. To simplify calculation, we consider longitudinal propagation only i.e. the wave-normal angle θ is either 0° or 180° , with respect to the static magnetic field. The electromagnetic wave is assumed to vary according to $e^{-i\omega t}$ and we consider the first harmonic only. The refractive index for the electromagnetic in a system of helical stream and static magnetic field is ($\theta = 0^\circ$ or 180°) (Zheleznyakov, 1960a)

$$n_s^2 = \epsilon_{xx}' \pm \sqrt{-\epsilon_{xy}'^2} \quad (D.2)$$

where ϵ_{xx}' and ϵ_{xy}' are dielectric tensor components for this system and are given by

$$\epsilon_{xx}' = 1 - \epsilon \quad \epsilon_{xy}' = i\epsilon$$

with

$$\epsilon = \frac{\omega_o^2 \beta_{\perp}^2 (c^2 k_{\parallel}^2 / \tilde{\omega}^2 - 1)}{4\delta^2}$$

$$\omega_o^2 = \frac{4\pi N'e^2}{m_o} \quad \text{is angular plasma frequency of the electron stream}$$

N' = particle density of electron stream

$\tilde{\omega}$ = "characteristic frequency" of the emitted complex wave angular frequency, given by

$$\omega = \tilde{\omega} + \delta, \quad \tilde{\omega} \text{ real and } \delta \text{ complex} \quad (\text{D.3})$$

assuming $|\omega| \gg |\delta|$ (D.3a)

Taking negative sign in equation (D.2), we have

$$n_g^2 = 1 - 2\epsilon \quad (\text{D.4})$$

Taking into account the effect of the background plasma as specified by relation (D.1), the second approach gives the overall refractive index:

$$n^2 = n_j^2 - 2\epsilon \quad (\text{D.5})$$

Taking the first approach, we must know the dielectric tensor components for the electromagnetic in the ambient

plasma alone (Stepanov and Kitsenko, 1961):

$$\epsilon_{xx}^0 = 1 - H = \epsilon_{yy}^0$$

$$\epsilon_{xy}^0 = i \frac{H}{\xi}$$

where

$$H = \frac{\omega_p^2}{\tilde{\omega}^2 - \omega_H^2}$$

$$\xi = \frac{\tilde{\omega}}{|\omega_H|}, \quad \omega_p^2 = \frac{4\pi N e^2}{m_0}$$

N = particle density of ambient plasma

The overall dielectric tensor components for the whole stream-plasma system are then*

$$\epsilon_{xx} = \epsilon_{xx}^0 + \epsilon_{xx}' = 1 - H - \epsilon = \epsilon_{yy}$$

$$\epsilon_{xy} = i \left(\frac{H}{\xi} + \epsilon \right) \quad (D.7)$$

The overall refractive index is then given by

$$\begin{aligned} n^2 &= \epsilon_{xx} \pm \sqrt{-\epsilon_{xy}^2} \\ &= 1 - H - \epsilon \pm \sqrt{\frac{H^2}{\xi^2} + \epsilon^2 + \frac{2H\epsilon}{\xi}} \\ &= 1 - H - \epsilon \pm \frac{H}{\xi} \left(1 + \frac{\xi\epsilon}{H} \right) \end{aligned} \quad (D.8)$$

here we have taken into account the fact that we are considering a thin stream and thus

*We have written down three dielectric tensor components only because the dispersion equation does not involve any other component for case of $\theta = 0^\circ, 180^\circ$

$$\xi^2 \ll \left| \frac{2\xi\epsilon}{H} \right| \quad (\text{D.9})$$

and
$$\left| \frac{2\xi\epsilon}{H} \right| \ll 1 \quad (\text{D.9a})$$

Taking negative sign, relation (D.9) gives:

$$\begin{aligned} n^2 &= 1 + \frac{\omega_p^2}{\omega(\omega_H - \omega)} - 2\xi \\ &= n_j^2 - 2\xi \end{aligned} \quad (\text{D.10})$$

Mathematically, we have seen that with a thin stream such that inequalities (D.9) and (D.9a) are valid, the two approaches give the same dispersion equation for the case of longitudinal propagation. Once the dispersion is derived, the growth rate can be calculated readily. Formulating the radiative instability problem with the second method means that we assume that the refractive indices n_s and n_j of the two interpenetrating media, i.e. the stream and the ambient plasma, are non-interacting and this is valid only when the density of the stream is small compared to that of the background plasma such that the presence of the stream is represented by a small perturbation term (-2ξ) in the dispersion equation of the whole system. When we investigate the radiative instability problem of more complicated systems (e.g. including temperature effect of the stream, considering a general wave-normal angle θ) the second method has the great advantage of being simple in mathematics. It has been found numerically that both

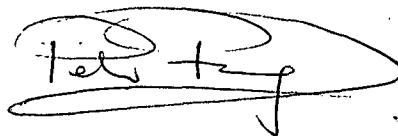
methods give the same general behaviour of the growth spectrum for both backward shifted and forward shifted normal cyclotron radiation.

ACKNOWLEDGEMENTS

I am indebted to my supervisors Professor G.R.A. Ellis (during my whole period of research - April, 1964 to April, 1966) and Dr. R.L. Dowden (April, 1964 to December, 1965) for their encouragement, criticisms and advice. I also wish to express my sincere gratitude to Dr. S.F. Smerd, Radiophysics, C.S.I.R.O., Sydney, for his stimulating discussions and criticisms on the instability theory and solar work. Parts of the numerical computation in the theoretical study of solar type I noise storm were carried out jointly with Mr. W. K. Yip.

Apart from those acknowledged above and in the body of the thesis, all the ideas and calculations are my own.

During the period of these investigations, I have been awarded the University Postgraduate Scholarship.

A handwritten signature in dark ink, appearing to read 'Peter Fung', enclosed within a large, loopy oval stroke.

(Peter Fung)

April, 1966.

PUBLICATION

Some parts of this thesis have been set in paper forms and have been accepted by appropriate journals for publication:

- (1) P.C.W. Fung "Excitation of Backward Doppler-Shifted Cyclotron Radiation in a Magnetoactive Plasma by an Electron Stream", Planetary & Space Science (in press).
- (2) P.C.W. Fung "Excitation of Cyclotron Radiation in the Forward Subluminous Mode and its Application to Jupiter's Decametric Emissions", Planetary & Space Science (in press),
- (3) P.C.W. Fung "Excitation of Cyclotron Electromagnetic Waves in a Magnetoactive Plasma by a Stream of Charged Particles including Temperature Effects in the Stream", Australian Journal of Physics, (in press).

Other papers being prepared for publication are:

- (4) P.C.W. Fung "On Two Methods of Solving the Radiative Instability Theory of a Stream-Plasma System".

- (5) P.C.W. Fung & W.K. Yip "Cyclotron Radiation from Electron Streams as the Origin of Solar Type I Noise Storm".
- (6) P.C.W. Fung & W.K. Yip "Theoretical Dynamic Spectra of Solar Storm Bursts".
- (7) P.C.W. Fung "The Role of Cyclotron Radiation in Radio Astronomy".

REFERENCES

1. Astrom, E. - Arkiv f. Fysik, 2, 443, 1950.
2. Akhiezer, A.J. & Fainberg, Ya.B. - Doklady, Akad. Nauk, S.S.S.R., 64, 555, 1949.
3. Allen, C.W. - Monthly Notices Roy Astron. Soc., 107, 386, 1947.
4. Alfven, H.-Z. - Physik, 105, 633, 1937.
5. Bell, T.F. & Buneman, O. - Phy. Review, 133, A1300, 1964.
6. Beck, A.H.W. - "Space-charge Waves", Pergamon Press Ltd., London, 1958.
7. Barrow, C.H. - Astrophys. J., 135, 847, 1962.
8. Brice, N. - J. Geophys. Res., 68, 4626, 1963.
9. Brice, N. - J. Geophys. Res., 69, 4515, 1964.
10. Baumbach, S. - Astronomische Nachrichten, 263, 121, 1937.
11. Bray, R.J. & Loughhead, R.E. - Australian J. Phys., 15, 482, 1962.
12. Bray, R.J. & Loughhead, R.E. - "Sunspots", chap. 5, sect. 4, Chapman & Hall Ltd., 1964.
13. Budden, K.G. - "Radio Waves in the Ionosphere", Cambridge Press, 1961.
14. Cohen, M.H. - Phys. Rev., 123, 711, 1961.
15. Carr, T.D., Smith, A.G., Bollhagen, H., Six, N.F., Jr. & Chatterton, N.E. - Astrophys. J., 134, 105, 1961.

16. Denisse, J.F. & Delcroix, J.L. - "Theorie des Ondes dans les Plasmas", Dunod, Paris, 1960. English translation: "Plasma Waves", Interscience Publishers, N.Y., 1963.
17. Delcroix, J.L. - "Physique des Plasmas", Dunod, Paris, 1963.
18. Dowden, R.L. - J. Geophys. Res., 67, 1745, 1962a.
19. Dowden, R.L. - Nature, 195, 1085, 1962b.
20. Denisse, J.F. - Inf. Bull. Europ. Solar Radio Obs., No. 4, 1960a.
21. Denisse, J.F. - XIII U.R.S.I. General Assembly, London, 1960b.
22. Dowden, R.L. - Australian J. Phys., 15, 114, 1962c.
23. Dowden, R.L. - Australian J. Phys., 15, 490, 1962d.
24. De Jager, C. - Space Science Reviews, 1, 487, 1963.
25. Ellis, G.R.A. - Planet. Space Sci. 1, 253, 1959.
26. Ellis, G.R.A. - Radio Science, 690, No. 12, 1513, 1965.
27. Eidman, V.Ya. - Soviet Phys., J.E.T.P., 34, 91, 1958.
28. Eidman, V.Ya. - Soviet Phys., J.E.T.P., 36, 947, 1959.
29. Engel, R.D. - The Phys. Fluids, 8, 939, 1965.
30. Ellis, G.R.A. - Nature, 194, 667, 1962a.

31. Ellis, G.R.A. - Australian J. Phys., 15, 344, 1962b.
32. Ellis, G.R.A. - Australian J. Phys., 16, 74, 1963.
33. Ellis, G.R.A. & McCulloch, P.H. - Australian J. Phys., 16, 380, 1963.
34. Ellis, G.R.A. - J. Geophys. Res., 65, 1705, 1960.
35. Elgaroy, O. - Astrophysica Norvegia, 7, 123, 1961.
36. Ellis, G.R.A. - Australian J. Phys., 17, 63, 1964.
37. Painberg, Ya.B. & Shapiro, V.D. - Sov. Phys., J.E.T.P., 20, 937, 1965.
38. Pokker, A.D., Jr. - Studies of Enhanced Solar Radio Emission at Frequencies, Netherlands Ptt, Section Ionosphere and Radio Astronomy, 1961.
39. Ginzburg, V.L., Zheleznyakov, V.V. & Eidman, V. Ya. - Phil. Mag., 7, 451, 1962.
40. Ginzburg, V.L. - "The Propagation of Electromagnetic Waves in Plasma", Pergamon Press, 1964.
41. Gardner, F.F. & Shain, C.A. - Australian J. Phys., 11, 55, 1958.
42. Gershman, B.B. - Soviet Phys., J.E.T.P., 11, 657, 1960.
43. Gallet, R.H. - Proc. IRE, 47, 211, 1959.
44. Goldstein, Jr., S.J. - Astrophys. J., 130, 393, 1959.
45. Ginzburg, V.L. & Zheleznyakov, V.V. - Sov. Astron., AJ, 3, 235, 1959.

46. Ginzburg, V.L. & Zheleznyakov, V.V. - Soviet
Astronomy, AJ, 5, 1, 1961.
47. Ginzburg, V.L. & Zheleznyakov, V.V. - Soviet
Astronomy, AJ, 2, 653, 1958.
48. Ginzburg, V.L. & Zheleznyakov, V.V. - Paris
Symposium on Radio Astronomy, Stanford
University Press, p. 574, 1959b.
49. Gold, T. - Nature, 183, 355, 1959.
50. Ginzburg, V.L. & Frank, J.N. - C.R. Acad. Sci.,
U.S.S.R., 56, 583, 1947.
51. Ginzburg, V.L. - Doklady Akad. Nauk., S.S.S.R., 92,
727, 1953.
52. Helliiwell, R.A. & Carpenter, D.L. - "Whistlers-
West IGY-IGC synoptic program," SEL
Final Report, Stanford University,
Mar. 20, 1961.
53. Harang, L. & Larsen, R. - J.A.T.P., 27, 481, 1965.
54. Hansen, S.P. - J. Geophys. Res., 68, 5925, 1963.
55. Helliiwell, R.A. - J. Geophys. Res., 68, 5387, 1963.
56. Helliiwell, R.H. - J. Geophys. Res., 69, 2391, 1964.
57. Hey, J.S. - Nature, 157, 47, 1946.
58. Hale, G.E. & Nicholson, S.B. - Pub. Carnegie Inst.,
No. 498, 1938.
59. Jelley, J.V. - "Cerenkov Radiation and Its
Applications," Pergamon Press, London,
1958.

60. Jaeger, J.C. & Westfold, K.C. - Aust. J. of Phys.
Sci. Res., A3, 376, 1950.
61. Jackson, J.D. - "Classical Electrodynamics",
Wiley, 1962.
62. Kovner, H.S. - News of higher educational
institutions, U.S.S.R. Radiophysics
series, 4, 118, 1961a.
63. Kovner, H.S. - News of higher educational
institutions, U.S.S.R. Radiophysics
series, 4, 97, 1961b.
64. Kundu, H.R. - "Solar Radio Astronomy", Report
no. 64 - 4, The University of
Michigan, Radio, Astronomy observatory,
1964.
65. Kiepenheuer, K.O. - Nature, 158, 340, 1946.
66. Kruse, U.W., Marshall, L. & Platt, J.R. - Astrophys.
J., 124, 601, 1956.
67. Kolpakov, P.E. - Soviet Astronomy, AJ, 1, 218, 1957.
68. Kolpakov, P.E. - Soviet Astronomy, AJ, 3, 69, 1959.
69. Kai, K. - Publ. Astron. Soc. Japan, 14, 1, 1962.
70. Liemohn, H.B. - Radio Science, 690, 741, 1965.
71. Mainstone, J.S. & McNicol, R.W. - Proc. Ionosphere
Conf., p. 163, The Physical Society,
London, 1962.
72. Makhan'kov, V.G. - Sov. Phys., Tech. Phys., 8, 673,
1964.

73. Hartyn, D.F. - Nature, 158, 632, 1946.
74. Morimoto, M. & Kai, K. - Publ. Astron. Soc. Japan,
13, 294, 1961.
75. Malinge, A.M. - Ann. d' Astrophys., 26, 97, 1963.
76. Morimoto, M. & Kai, K. - J. Phys. Soc. Japan,
Supplement A - 11, 17, 220, 1962.
77. Newfield, J. & Wright, H. - Phys. Review, 135,
A1175, 1964a.
78. Newfield, J. & Wright, H. - Phys. Fluids, 7, 1527,
1964b.
79. Newkirk, G. - Paris Symposium on Radio Astronomy
(ed. R.N. Bracewell, Standford
University, Standford), p. 149, 1959.
80. Piddington, J.H. - Phil. Mag., 46, 1037, 1955.
81. Pierce, J.R. - "Travelling-wave Tubes", D. Van
Nostrand Company, Inc., Princeton,
N.J., 1950.
82. Pawsey, J.L. - Proc. I.R.E., London, Part III, 97,
290, 1950.
83. Payne-Scott, R., Yabsley, D.E. & Bolton, J.G. -
Nature, 160, 256, 1947.
84. Payne-Scott, R. & Little, A.G. - Australian J. Sci.
Res., A4, 508, 1951.
85. Pawsey, J.L. & Bracewell, R.N. - "Radio Astronomy,
Clarendon Press, N.Y., 1955.

86. Piddington, J.H. & Minnett, H.G. - Australian
J. Sci. Res., A4, 131, 1951.
87. Ratcliffe, J.A. - The Magneto-Ionic Theory and its
Applications to the Ionosphere,
Cambridge, 1959.
88. Roberts, J.A. - Planet. Space Sci., 11, 221, 1963.
89. Ryle, M. & Vonberg, D.D. - Nature, 158, 339, 1946.
90. Ryle, M. & Vonberg, D.D. - Proc. Roy. Soc., A193,
98, 1948.
91. Roberts, J.A. - Australian J. Phys., 11, 215, 1958.
92. Smerd, S.F. - Private communication, 1965.
93. Scheuer, P.A.G. - Mon. Not. Roy. Astron. Soc.,
120, 231, 1960.
94. Schwinger, J. - Phys. Rev., 75, 1912, 1949.
95. Stepanov, K.N. & Kitsenko, A.D. - Sov. Phys. Tech.
Phys., 6, 120, 1961.
96. Smerd, S.F. - AAS-Symposium on "The Physics of Solar
Flares", NASA SP-50, p. 349, 1963.
97. Sturrock, P.A. - Phys. Rev., 112, 1488, 1958.
98. Shapiro, V.D. & Shevchenko, V.I. - Sov. Phys.,
J.E.T.P., 15, No. 4, p. 731, 1962.
99. Shapiro, V.D. - Sov. Phys., J.E.T.P., 17, No. 2, 416,
1963.
100. Shain, C.A. - Australian J. Phys., 2, 61, 1956.

101. Shain, C.A. & Higgins, C.S. - Australian J. Phys.,
12, 357, 1959.
102. Smith, H.J. & Douglas, J.N. - "Paris Symposium
on Radio Astronomy", p. 53 (ed. R.N.
Bracewell), Stanford University Press,
Stanford, Calif., 1959.
103. Suzuki, S. - Annals of the Tokyo Astronomical
Observatory, University of Tokyo,
sec. series, VII, No. 2, 75, 1961.
104. Sweet, R.A. - I.A.U. Symposium No. 6 on "Electro-
magnetic Phenomena in Cosmical
Physics", ed. Lehnert, B.P., Cambridge
University Press, p.123, 1958.
105. Twiss, R.Q. - Australian J. Phys., 11, 564, 1958.
106. Twiss, R.Q. - Phys. Rev., 88, 1392, 1952.
107. Tchickachev, B.M. - 5th Colloquium on Cosmogony,
Moscow, p. 245, 1956.
108. Takakura, T. - Publ. Astron. Soc. Japan, 8, 182, 1956.
109. Twiss, R.Q. & Roberts, J.A. - Australian J. Phys.,
11, 424, 1958.
110. Takakura, T. - Astron. Soc. Japan, Publ., 15, 462,
1963.
111. Takakura, T. - Publ. Astron. Soc. Japan, 13, 166,
1961.
112. Vlasov, A.A. - Zh. Eksp. and Teor. Fiz., 8, 291,
1938.

113. Vitkevich, V.V. & Gorelova, M.V. - *Sov. Astron.*,
4, 595, 1961.
114. von Klüber, H. - *Z. Astrophys.*, 24, 121, 1948.
115. Wild, J.P., Smerd, S.P. & Weiss, A.A. - "Solar
Bursts", *Annual Review of Astronomy and
Astrophysics*, 1, 291, 1963.
116. Warwick, J.W. - *Astrophys. J.*, 137, 41, 1963.
117. Warwick, J.W. - *Ann. N.Y. Acad. Sci.*, 95, 39, 1961.
118. Watts, J.H. - *J. Geophys. Res.*, 62, 199, 1957.
119. Wild, J.P. - *Australian J. Sci. Res.*, 4, 36, 1951.
120. Wild, J.P., Sheridan, K.V. & Neylan, A.A. - *Austra-
lian J. Phys.*, 12, 369, 1959.
121. Weiss, A.A. - Unpublished data, 1965.
122. Weiss, A.A. - *Australian J. Phys.*, 16, 240, 1963.
123. Wild, J.P. & Sheridan, K.V. - *Proc. I.R.S.*, 46,
160, 1958.
124. Wild, J.P. & Sirin, H. - *Australian J. Phys.*, 2,
315, 1956.
125. Wild, J.P. - "The Radio Emission from Solar Flares",
J. Physical Soc. Japan, 17, Supple-
ment A - II, p. 249, 1962.
126. Wild, J.P. - "The Solar Corona", ed. Evans, J.W.,
Academic Press, p. 115, 1963.
127. Wild, J.P., Roberts, S.A. & Murray, J.D. - *Nature*,
173, p. 532, 1954.

- 128. Zheleznyakov, V.V. - Radiofizika, 3, 57, 1960a.
- 129. Zheleznyakov, V.V. - Soviet Astron., AJ, 2, 206,
1958.
- 130. Zheleznyakov, V.V. - Radiofizika, 3, 180, 1960b.

SYMBOLS

All symbols are defined in the body of the thesis when they first occur. Those which are used more extensively and which may appear somewhere apart from their definitions are listed below:

$$a_{\perp}^2 = 2m_0 \kappa T_{\perp}$$

$$a_{\parallel}^2 = 2m_0 \kappa T_{\parallel}$$

$$A = \omega_p^2 / \omega_H^2$$

c = speed of light in vacuum

e = charge of an electron

$$f_p = \omega_p / 2\pi = (Ne^2 / m_0 \Pi)^{1/2} = \text{electron plasma frequency}$$

$$f_H = \omega_H / 2\pi = eH_0 / (2\pi m_0 c) = \text{electron gyro-frequency}$$

H_0 = static magnetic field intensity

H_s = magnetic field intensity at the centre of a sunspot

k = complex wave number

k_{\perp}, k_{\parallel} = transverse and longitudinal components of
wave vector \vec{k} respectively

\tilde{k} = characteristic wave number, is real

m_0 = rest mass of an electron

Π = electron particle density

n_j = refractive index

P = power of electromagnetic wave

p_{\perp}, p_{\parallel} = transverse and longitudinal components of
momentum \vec{p} respectively

$$q = (k - \tilde{k})/i$$

$$R_0 = \text{solar radius}$$

$$s = \text{harmonic number}$$

$$T = \text{temperature in degrees Kelvin}$$

$$v_{\perp}, v_{\parallel} = \text{transverse and longitudinal velocities respectively}$$

$$X = \omega_p^2 / \tilde{\omega}^2$$

$$Y = |\omega_H| / \tilde{\omega}$$

$$\beta_{\perp} = v_{\perp} / c$$

$$\beta_{\parallel} = v_{\parallel} / c$$

$$\gamma = (1 - \beta_{\perp}^2 - \beta_{\parallel}^2)^{-\frac{1}{2}}$$

$$\delta = \omega - \tilde{\omega}$$

$$\delta' = \delta / \tilde{\omega}$$

$$\epsilon_{ik} = \text{dielectric tensor of a system}$$

$$\xi = \tilde{\omega} / |\omega_H|$$

$$\xi' = (p_{\parallel} - p_{\parallel}^0) / a_{\parallel}$$

$$\xi_0 = \sqrt{A}$$

$$\xi_x = (1 + \sqrt{1 + 4A}) / 2$$

$$\xi_p = s\gamma$$

$$\phi = \arctan \beta_{\perp} / \beta_{\parallel} = \text{pitch angle of gyrating particle}$$

$$\theta = \text{wave-normal angle, i.e. angle between static magnetic field and wave vector}$$

$$\theta_m = \text{wave-normal angle at which the growth rate for the stream-plasma system is maximum}$$

$$\theta_c = \text{cutoff angle}$$

ω_0 = angular electron plasma frequency of the stream

$\rho = R/R_0$ = radial distance from centre of the Sun

$\zeta = p_{\perp} / a_{\perp}$

$\zeta_0 = p_{\perp}^0 / a_{\perp}$

ν = electron-ion collision frequency

χ = Boltzman's constant

$\tilde{\omega} = 2\pi f$ = angular characteristic wave frequency